Establishing the sensitivity of Synthetic Aperture Radar to above-ground biomass in wooded savannas

Karin Marijke Viergever

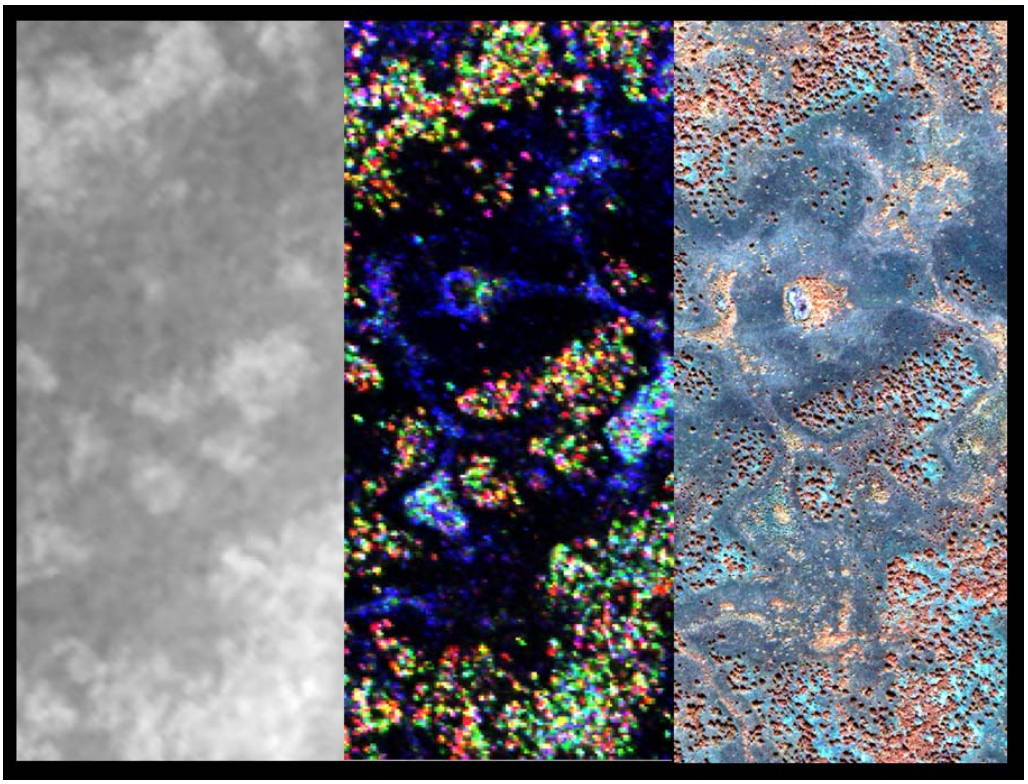

Submitted for Doctor of Philosophy
The University of Edinburgh
June 2008

Establishing the sensitivity of Synthetic Aperture Radar to above-ground biomass in wooded savannas

Karin Marijke Viergever

Supervised by:
Dr. Iain H. Woodhouse
Dr. Neil Stuart

Examined by:
Prof John Grace
Prof Richard M. Lucas
Dr Mark E.J. Cutler
August 2008

Submitted for Doctor of Philosophy
The University of Edinburgh
June 2008

Declaration of originality

I declare that the work contained in this thesis is my own, unless indicated otherwise. The thesis has been composed by myself and has not (in whole or in part) been previously submitted or accepted for a degree or professional qualification.

Signed:

.....

Karin Marijke Viergever

7 June 2008

Abstract

Radar for biomass estimation has been widely investigated for temperate, boreal and tropical forests, yet tropical savanna woodlands, which generally form non-continuous cover canopies or sparse woodlands, have been largely neglected in biomass studies. This thesis evaluates the capability of Synthetic Aperture Radar (SAR) for estimating the above-ground biomass of the woody vegetation in a savanna in Belize, Central America. This is achieved by evaluating (i) polarimetric Synthetic Aperture Radar (SAR) backscatter and (ii) single-pass shortwave interferometric SAR (InSAR) as indicators of above-ground biomass. Specifically, the effect on SAR backscatter of woody vegetation structure such as canopy cover, basal area, vegetation height and above-ground biomass is evaluated. Since vegetation height is often correlated to above-ground biomass, the effectiveness of vegetation height retrieval from InSAR is evaluated as an indicator of above-ground biomass.

The study area, situated in Belize, is representative of Central American savannas. Radar data used are AIRSAR fully polarimetric L- and P-band SAR, and AIRSAR C-band InSAR, Intermap Technologies STAR-3i X-band InSAR, and Shuttle Radar Topography Mission (SRTM) C-band InSAR. The field data comprise accurately georeferenced three-dimensional measurements for 1,133 trees and shrubs and 75 palmetto clumps and thickets in a transect of 800 m x 60 m which spans the main savanna vegetation strata of the study area. An additional 2,464 ground points were observed.

Results show that savanna woodlands present a challenge for radar remote sensing methods due to the sparse and heterogeneous nature of savanna woodlands. Long-wave SAR backscatter is dominated not only by high biomass areas, but also by areas of leafy palmetto which have low vegetative biomass. Retrieved woodland canopy heights from X- and C-band InSAR are indicative of the general patterns of tree height, although retrieved heights are underestimated. The amount of underestimation is variable across the different canopy conditions. Of these two methods, the shortwave InSAR data give a better indication of the spatial distribution

of the above-ground biomass of the woody vegetation in the savannas than SAR backscatter. These results have implications for new and planned future global biomass estimation missions, such as ALOS PALSAR, ESA's planned P-band BIOMASS and TanDEM-X. Without appropriate mediation, SAR backscatter methods might overestimate above-ground biomass of the woody vegetation of savannas while InSAR height retrieval methods might underestimate biomass estimates. Some possible mediating approaches are discussed.

Acknowledgements

There are so many people to whom I am extremely grateful for their intellectual, moral and practical support during the course of my PhD. First of all I would like to thank both my supervisors, Iain Woodhouse and Neil Stuart, for their continuous support and encouragement. I've learnt a great many skills from both of you. Thanks Iain for, amongst others, introducing me to the wonderful world of SAR and for teaching me to think about trees and how they interact with microwaves. I've only just seen the tip of the iceberg, and would love to learn more! Neil, your Belize expertise and contagious enthusiasm have been a great help. Thank you both for helpful comments during the writing of this thesis. Peter Furley has been a tremendous source of information on savannas, especially the biogeography of Belizean savannas and was always willing to set aside time for an informative chat. Other useful advice has been provided by Genevieve Patenaude, Chris Place, Armando Marino and Michal Petr during various stages of processing and writing.

Duncan Moss has been extremely helpful during fieldwork planning in sharing his knowledge on surveying, but also during post-processing of the field data. His assistance during the set-up of the transect area in the first week of the first fieldwork campaign saved valuable time which ultimately enabled the collection of a larger dataset than originally planned. On the topic of fieldwork, the time and assistance of the following people should not go unmentioned: Ed Wallington, who having been to Hill Bank on a similar expedition before, made the arrangements for the first fieldwork expedition in 2005 run smoothly and helped collect data in the field for 3 weeks. Carol Hay collected data in the field for 5 weeks. Neil Stuart also spent 2 weeks braving the heat and humidity to help map and measure the savanna woodlands. Thanks to all of you for working very hard, with only a few breaks in very hot conditions – on 26 April 2005 Carol, Ed and I measured 50 ºC in the spot of shade under the total station! Although the second fieldwork campaign in 2007 focused mainly on acquiring field data for Tom Jaas's MSc dissertation, I was able to obtain additional data. For this I would like to thank Zoe Goodwin who helped find, permanently mark and re-measure trees in the original fieldwork transect and Iain Woodhouse who risked vicious plants and lurking beasties to help measure the height of several gallery forests in the savanna. Pre- and post fieldwork advice and assistance on equipment and all associated practical matters was provided by Anthony Newton and Iain Cameron. Thanks to the IT support staff, Steve Dowers, Gavin Parks and Chris Place, who have helped in a few computing crisis situations.

Other invaluable support during fieldwork was provided by the staff at Hill Bank research station and in particular Rudolph Williams, the manager in 2005, who always thoughtfully managed the rangers' activities so that help was available when we needed it. It was also through his support that entry into the savanna was made much easier by clearing a footpath through the wetland to the savanna. During the second fieldwork campaign, management had been taken over by Efrain Cocom, who was equally supportive. He was eager to learn from what we were doing and spent some time assisting with fieldwork. Various Hill Bank rangers were a great help in the field and were happy to share their knowledge of the savanna. The Hill

Bank cooks, in particular Patricia (Miss Patsy) Lanza and Christina (Miss Chris) Fermin, ensured that we stayed fit by providing three healthy meals a day and always managed to hit the spot with a great meal at the end of the day. Rick Mena, the forester at Hill Bank, provided information on current and planned Programme for Belize (PfB) forestry operations. The staff in the PfB office, in particular Edilberto Romero, Dareece Chuc and Wilber Sabido were always helpful in providing information or assisting with logistics. Percival Cho from the Belize Forest Department provided advice on tree growth.

Sandra Brown and Timothy Pearson of Winrock International have been extremely generous with their time and have provided information and allometric equations for biomass calculations of the savanna woodland vegetation of the study area. They have also provided us with high resolution aerial photography of the study area, which has since been used by several MSc students for their dissertation work. Silvia Petrova has been especially helpful in sending the aerial photography.

Without funding support, this research would not have been possible. I would like to thank the School of GeoSciences for funding my PhD research through a teaching studentship. Extra funding for fieldwork was provided by the Carnegie Trust for the Universities of Scotland, Earth and Space Foundation, Edinburgh Earth Observatory, International Federation of Surveyors, Royal Geographical Society, Royal Scottish Geographical Society and Royal Institution of Chartered Surveyors. A Panasonic toughbook computer was provided by NERC FSF for both fieldwork campaigns. Extra funding for attending several conferences has been provided by IEEE Travel support funding (twice), Remote Sensing and Photogrammetry Society (twice), Royal Scottish Geographical Society and Iain Woodhouse.

Thanks to NASA JPL and Intermap Technologies for donating the SAR data. Both these organisations have also been helpful in providing information on the data. Dave Bautts went to extra trouble to pinpoint the acquisition dates for the Intermap data over the study area and Bryan Mercer was always helpful and informative when asked about the data. Scott Hensley at JPL has been helpful in my attempts to correct the multipath error in the AIRSAR C-band data. Unfortunately this was not completed before the thesis was written but, with ongoing attempts to correct the data, I hope to thank Scott for this in the near future. Thanks also go to Richard Lucas of Aberystwyth University for additional advice on how to have the data corrected and for allowing me to get a feel for their AIRSAR C-band data for the woodlands of Injune in Australia.

My close colleagues and friends in the School of GeoSciences have made my time here very enjoyable. Thanks especially to my office mates in the Barra Suite (Nick, Omair, Iain, Sebastien), my later neighbours (Jimmy and Vicki) in the rooms of ‘solitary confinement’ and all the other friendly faces (students, staff, cleaners) in the building who have provided ample opportunity for stress relief. Thanks also to all my other friends, near and far, whom I have neglected over the past months.

Finally, I would like to extend a very warm and sincere thank you to my parents, Ben and Dia Viergever, for moral support throughout and for always showing genuine interest in my progress. Last but not least, thank you Ilona Kemeling, for a daily dose of enthusiastic encouragement and support, for feeding me and for keeping me on the right side of the brink of sanity towards the end!

Table of Contents

List of Figures

List of Tables

CHAPTER 1:
Introduction

1.1. Problem definition

With the increasing importance of forestry-based carbon sequestration initiatives and global forest monitoring, there is a need for accurate information, at regional and national scales, on the spatial extent, condition, biomass and growth potential of forests and woodlands with a canopy cover[1] as low as 10%. Earth observation (EO) techniques are better suited to these information needs than traditional *in situ* methods for biomass estimation. The latter involve laborious fieldwork, often based on destructive sampling (Overman *et al.*, 1994) and produce regional biomass estimates based mainly on extrapolation. However, regional biomass estimates based on EO data more accurately represent the spatial heterogeneity of the landscape and are, in most cases, frequently updatable. Depending on the spatial and temporal resolution, EO can detect differences in the spatial distribution of biomass density such as the occurrence of forest gaps and land cover changes, offers systematic observations at scales ranging from local to global and improve the monitoring of inaccessible areas (Rosenqvist *et al.*, 2003).

Various EO techniques exist, providing different ways to estimate AG biomass. Synthetic Aperture Radar (SAR) is especially useful in the tropics since it is not affected by cloud cover. SAR backscatter has been statistically correlated with forest biomass up to a certain level[2], depending on the radar wavelength and polarisation (Le Toan *et al.*, 1992, Imhoff 1995). It is therefore widely assumed that backscatter intensity at long wavelengths will be sufficient to estimate biomass in forest areas at the low end of the biomass scale (e.g. savanna woodlands) but this has not been sufficiently investigated. Other SAR EO methods such as Synthetic Aperture Radar

[1] Canopy cover is defined as the proportion (in percentage) of a unit area of ground covered by a vertical projection of the outermost perimeter of tree crowns (Philip, 1994).
[2] Typical saturation levels for the different SAR wavelengths are given in 3.3.3.1.

(SAR) interferometry (InSAR) have been used for canopy height retrieval in closed-canopy forests. Retrieved heights are then used in conjunction with allometric equations to estimate AG biomass (Askne *et al*., 1997) since vegetation tree height is often correlated to biomass. A degree of underestimation is expected due to the penetration of microwaves into the forest canopy, the accuracy of which is dependent on a combination of radar characteristics (e.g. wavelength and polarisation) and forest characteristics (e.g. density and uniformity). This method has had success in closed-canopy, mostly homogeneous forests but has not been sufficiently tested in sparse heterogeneous forests such as savanna woodlands.

1.2. Aim and objectives

Neither the use of InSAR for canopy height retrieval nor SAR backscatter-biomass correlations have been sufficiently tested at the lower end of the biomass scale such as in sparse heterogeneous forests (having non-continuous or sparse canopy cover). The aim of this research is to evaluate the capability of SAR for estimating the above-ground (AG) biomass of the woody vegetation in a savanna by evaluating:

- the effect of woody vegetation structure (AG biomass, canopy cover, basal area and height) on SAR backscatter, and
- the effectiveness of vegetation height retrieval from SAR interferometry.

The chosen study area is situated in Belize and is representative of Central American savannas. Single-pass shortwave InSAR data from AIRSAR (C-band), Intermap Technologies (X-band) and SRTM (C-band) were used and longer wavelength fully polarimetric SAR backscatter data from AIRSAR (L- and P-band) are also employed.

1.3. Context and relevance

Research has shown that the gradual rise in average temperature of the Earth's surface is linked to human-induced increasing atmospheric concentrations of greenhouse gases, of which carbon dioxide (CO_2) has the greatest warming potential. Although it occurs in a relatively low concentration (0.035% of the troposphere), the

increase in atmospheric CO_2 since pre-industrial times has caused a radiative forcing of +1.66 ± 0.17 W/m^2; a much larger contribution than any other radiative forcing agent considered in the 2007 IPCC report (Solomon *et al.*, 2007). Climate change is expected to have a profound effect on the living environment with repercussions for natural ecosystems and cultural issues such as food security and environmental hazards.

The Kyoto Protocol, which originated from the United Nations Framework Convention on Climate Change (UNFCCC), sets legally binding targets for industrialised countries to reduce greenhouse gas emissions or to remove them from the atmosphere. The Protocol was adopted in 1997 and finally came into force in February 2005. In the face of mounting concern that national CO_2 emission reduction targets cannot be met solely by emission reduction strategies, industrialised countries are keen to find alternative ways to lower atmospheric CO_2 concentrations.

A significant mechanism for removing CO_2 from the atmosphere is through carbon sequestration in growing vegetation. However, the viability of carbon sequestration programmes such as forestry projects relies on both a scientific understanding of how CO_2 is captured and stored as vegetative biomass and the development of operational techniques for measuring standing biomass globally.

The largest impact on the global carbon cycle is caused by human activities through the burning of biomass and fossil fuels and the removal of vegetation cover, especially forests (Bolin and Sukumar, 2000). It is estimated that approximately 75% of CO_2 emissions to the atmosphere are caused by burning, while the rest is contributed by land use change (Prentice *et al.*, 2001), through removal of carbon sinks. The UN Climate Change Conference in Bali (COP 13, December 2007), has included a call for future inclusion of Reduced Emissions from Deforestation in Developing countries (referred to as REDD[3]) (UNFCCC, 2008). Thus, apart from estimating global forest biomass, there is a need for forest monitoring by quantifying

[3] Although the general use of the acronymn REDD now refers to Reduced Emissions from Deforestation and Degradation, UNFCCC sources refer to it as Reduced Emissions from Deforestation in Developing Countries. As the larger part of this thesis was written before REDD was announced, the latter term is used throughout the thesis.

deforestation and other potential sources of atmospheric CO_2 emissions such as fire damage from forest areas.

To date, the definition of *forest* for the purposes of carbon sequestration projects is loosely based on the FAO definition (FAO, 2006) which defines *forest* based on minimum canopy cover (10-30%), minimum surface area (500-10,000 m^2) and minimum tree height at maturity (2-5 m) (Schulze *et al.*, 2002). This definition includes most woodlands within savanna areas. Traditionally thought of as mainly grassland, the term *savanna* now encompasses a dynamic mosaic of continuous herbaceous cover (grassland) and non-continuous cover woodland, the latter consisting of scattered to dense trees, shrub and palm. Savannas are the most common vegetation type in the tropics and subtropics (Mistry, 2000), covering approximately 20% of the global land surface. The net primary productivity and carbon stocks for savannas vary widely according to the amount and extent of tree cover. On average they have been found to have previously unappreciated high net primary productivity rates, third only to tropical rain forests (Grace *et al.*, 2001) and temperate forests (Saugier *et al.*, 2001). Savannas occur primarily in developing countries and support approximately 20% of world's human population (Mistry, 2000; House and Hall, 2001). Human-induced disturbance such as agricultural land use and fire therefore form major disturbances (Frost *et al.*, 1986), with effects ranging from mild woodland degradation to deforestation. As their importance in terms of carbon sequestration potential has until recently been largely overlooked, savannas are not routinely censused in the same way as forests (Grace *et al.*, 2006), and it is therefore difficult to assess change in their extent, structure and biomass.

Earth observation (EO) techniques offer the potential for systematic observations at scales ranging from local to global, thereby enabling the monitoring of inaccessible areas. Examples relevant to savannas are the estimation of biomass, land cover change monitoring and mapping of fire damage. This research evaluates the capability of radar EO data, such as SAR and InSAR, to estimate the AG biomass of the woody vegetation in a savanna in Belize, Central America. The results of this research are expected to have an impact on carbon accounting under Kyoto Protocol and possible future woodland monitoring under REDD and will have implications for

future EO satellites (such as ESA's proposed BIOMASS mission) for the purpose of global biomass estimation .

1.4. Thesis structure

Chapter 1 has placed this research in the context of international issues relating to the estimation of vegetative carbon in forests and woodlands globally. The importance of savannas and in particular of savanna woodlands, as a sink for carbon has been introduced and is further elaborated upon in Chapter 2. The savanna biome is defined and the global distribution is described. The ecological determinants and disturbances, which ultimately affect the unique morphology of savanna vegetation are then explained. An in-depth discussion is provided on the role of carbon in the global climate, including a description of forestry projects as a strategy for carbon emission reduction under the Clean Development Mechanism (CDM) and, in future, the reduction of deforestation in developing countries (REDD). Savannas are shown to have an important role to play in such carbon sequestration projects because of the occurrence of woodlands. The successful implementation of forestry-based carbon sequestration projects necessitate accurate, frequently updateable monitoring techniques which are best provided by Earth observation (EO) techniques, described in Chapter 3. *In situ* methods for the estimation of biomass are also discussed since these methods are used to validate the results given in Chapter 6. Chapter 4 describes the location of the study area and various physical characteristics such as climatic conditions, landscape and vegetation structure that affect SAR backscatter response. The occurrence of fire is a common savanna disturbance and is therefore discussed specifically for the study area.

Chapter 5 describes the EO and field data as well as all pre-processing required for the main data analyses and interpretation later described in Chapter 6. This includes further processing of field data to obtain a ground surface DEM, calculation of palmetto stem number density, estimation of tree crown diameters for trees that were not included in the initial tree crown measurements and an analysis of tree growth in the study area. A description of EO processing for the extraction of woodland canopy density for the study area is also given. An assessment of the data quality is given in terms of spatial alignment (co-registration) of the different datasets. The occurrence

of multipath error in the AIRSAR C-band InSAR data and its implications for further analyses is also discussed. Chapter 6 deals with the processing and results of data analyses and interpretation that answer to the main aim of this thesis (i.e. SAR backscatter analysis and InSAR height retrieval for estimating biomass). Chapter 7 concludes with a summary of the results and a discussion on the implications of the results for global biomass mapping. Finally, recommendations are made for further research.

CHAPTER 2:
Global significance of the biomass of the savanna biome

2.1. Introduction

Research has shown that the gradual rise in average temperature of the Earth's surface is linked to human-induced increasing atmospheric concentrations of greenhouse gases, of which carbon dioxide (CO_2) is the most important (UNFCCC, 2007). Growing concern eventually led to international action in the form of the Kyoto Protocol, which sets legally binding targets for industrialised countries to limit or reduce their greenhouse gas emissions or to remove carbon from the atmosphere. Understanding the carbon cycle is therefore crucial to mitigation of the greenhouse effect and is discussed together with the Kyoto Protocol and its mechanisms for lowering atmospheric carbon emissions (see 2.2). Vegetation forms one of the largest terrestrial sinks for atmospheric carbon, by removing CO_2 from the atmosphere through photosynthesis and slowly releasing it through respiration and natural decay. This equilibrium is disturbed through processes such as biomass burning which sets free excess carbon into the atmosphere in a short time.

The Clean Development Mechanism initiative under the Kyoto Protocol provides for, amongst others, forestry projects for the sole purpose of carbon sequestration as a means for industrialised countries to offset their atmospheric carbon emissions. The definition of *forest* at the time of writing is based on a fairly low canopy cover (10%, see 2.2). This includes sparse woodlands such as those often occurring in savanna ecosystems. The savanna biome is extremely diverse (see 2.3), consisting of different savanna ecosystems, and is an abundant and vulnerable land cover in the tropics and subtropics. However, the savanna biome has been largely overlooked due to ambiguity in land cover definitions which often cause an overlap with forest definitions and to the greater emphasis on moist evergreen forest. The fact that savannas often contain areas of sparse woodland with a broken canopy has caused

them to be classified as forest or woodland by organisations such as the FAO. It is this presence of woodlands and their location mostly in developing nations that make savannas such important areas for carbon sequestration projects under the Kyoto Protocol. Up to now, the value of savannas in the global carbon cycle (see 2.4) has been largely underestimated and studies of savanna biomass have been scarce. Chapter 3 will discuss various methods for biomass estimation by means of *in situ* and Earth Observation, highlighting their use in savannas.

This chapter includes a discussion on savanna determinants and disturbance processes (see 2.3.3) in order to provide an increased understanding of the biome. A general description of savanna morphology (vegetation structure, see 2.3.4) is included as this is important for understanding Synthetic Aperture Radar (SAR, see 3.3.3) backscatter response to savanna vegetation. A description of the savanna morphology specific to the study site is given in Chapter 4. The chapter concludes with a section (2.4) illustrating the carbon sequestration potential of savannas and highlighting their significance in the global carbon cycle and their potential significance for climate change.

2.2. The role of carbon in the global climate

The average temperature of the Earth's surface has risen by 0.6 °C since the late 19th century (UNFCCC, 2007). The global climate is determined mainly by incoming energy from the Sun and the properties of the Earth's surface and the atmosphere. The balance of reflection, absorption and emission of the Sun's energy within the atmosphere and at the Earth's surface determine the global climate. Several gases, the so-called greenhouse gases (e.g., carbon dioxide (CO_2), methane (CH_4) and nitrous oxide (N_2O) increase the atmospheric absorption of outgoing radiation) trapping warmth within the atmosphere (Middleton, 1999). Of these gases, carbon dioxide (CO_2) has the greatest warming potential (Solomon, *et al.*, 2007). CO_2 makes up 0.035% of the troposphere, the lower portion of the atmosphere which consists of approximately 75% of the atmosphere's mass (Cunningham and Saigo, 2000). CO_2 is a long-lived greenhouse gas (i.e., it is chemically stable and therefore persists in the atmosphere up to several centuries) so that it has a long-term influence on climate. Although it occurs in a relatively low concentration, the increase in atmospheric CO_2

since pre-industrial times has caused a radiative forcing (warming effect) of +1.66 ± 0.17 W/m^2; a much larger contribution than any other radiative forcing agent considered in the 2007 IPCC report[1]. In the decade from 1995 to 2005, the increase of atmospheric CO_2 has led to a 20% increase in its radiative forcing (Solomon, *et al.*, 2007). Glacial ice core data has shown a correspondence between increased atmospheric CO_2 concentrations and the occurrence of inter-glacial warm periods over the past 650,000 years (Solomon, *et al.*, 2007). Currently it is believed that the unprecedented increase in greenhouse gases over the past 250 years is very likely the cause of temperature increases detected through observations taken at the Earth's surface, in the atmosphere and in the oceans. Global warming is expected to have a profound effect on the living environment: sea level rise, receding ice caps, glaciers and snow cover, changes in biogeochemical cycles such as the carbon cycle, and changes in the water cycle affecting cloud formation and precipitation which in turn, will increase incidences of flooding and drought in different parts of the world. These effects are expected to have repercussions for natural ecosystems and cultural issues such as food security and increased risk of environmental hazards (Miller, 1998).

2.2.1. The carbon cycle: human impacts and feedback mechanisms

Carbon is an element that is essential for life on Earth; it forms the building blocks of nucleic acids such as DNA and RNA, carbohydrates and other organic compounds. Carbon cycles through the ecosphere in the form of a gaseous cycle, the basis of which is carbon dioxide (CO_2) (Miller, 1998). The Earth's largest carbon reservoir is formed by storage in sedimentary rocks, such as limestone, on ocean floor sediments and on continents. Carbon is very gradually released from these reservoirs through a combination of geological and chemical processes, either releasing it directly into the atmosphere as CO_2 or dissolving carbon in water. Volcanic activity releases carbon more rapidly from rocks deep in the Earth's crust into the atmosphere. As CO_2 is

[1] CH_4 has the second highest radiative forcing effect at +0.48 ± 0.05 W/m^2.

readily soluble in water, the Earth's oceans form the second largest carbon reservoir, containing approximately 50 times more carbon than the atmosphere (Miller, 1998). Carbon is stored in the oceans either in dissolved state, or as carbonate ions (CO_3^{2-}) and bicarbonate ions (HCO_3^-), following chemical reactions with water. Due to the slow rate of ocean mixing, carbon exchange between the oceans and the atmosphere occurs on a time-scale of several hundred years (Prentice, *et al.*, 2001).

Through the process of photosynthesis, terrestrial and aquatic producers remove CO_2 from the atmosphere and from water, converting it into complex carbohydrates such as glucose ($C_6H_{12}O_6$). In return, living organisms release CO_2 into the atmosphere through the process of aerobic respiration, breaking down complex organic compounds back into CO_2 which is released directly into the atmosphere or dissolved in water. Decomposition of dead organisms releases carbon into the environment during a similar process (Miller, 1998). Due to photosynthetic producers' high demand for CO_2, atmospheric carbon cycles rapidly through air, water and biota, but carbon stored as woody biomass recycles much slower as it is released by decomposition (Miller, 1998). Carbon is stored for much longer periods as fossil fuels such as coal and oil, which are formed over millions of years by compression of buried organic matter. Burning of fossil fuels and biomass eventually releases carbon back into the atmosphere.

The net global carbon flux between the atmosphere and the terrestrial ecosystems is caused by a small imbalance between photosynthetic uptake and release processes; soil microbes, plants, animals and biochemical processes are a few causes of the latter. In contrast, the largest impact on the global carbon cycle is caused by human activities through the burning of fossil fuels and biomass and the removal of vegetation cover, especially forests (Bolin and Sukumar, 2000). Since the Industrial Revolution human activity has caused a rapid increase in fossil fuel burning and other activities such as land use change, causing a marked increase in atmospheric levels of CO_2. Atmospheric CO_2 concentration had been relatively stable at 280 ± 10 parts per million (ppm) for several thousands of years in the period preceding the Industrial Revolution. Since then, these levels have risen continuously, reaching 379 ppm in 2005 (Solomon, *et al.*, 2007). Such levels of atmospheric CO_2 concentrations have not been exceeded during the past 420,000 years, and it is thought unlikely to

have done so during the past 20 million years (Prentice, *et al.*, 2001). Apart from a small contribution from cement production, it is estimated that 75% of CO_2 emissions are caused by fossil fuel burning, while the rest is contributed by land use change (Prentice, *et al.*, 2001), through removal of carbon sinks.

Sedimentary rocks and the oceans have sufficient uptake capacity to incorporate 70-80% of projected anthropogenic CO_2 emissions to the atmosphere, but the effects of feedback mechanisms linked to increased atmospheric CO_2 levels and increasing temperatures are still uncertain. As the properties of the Earth's surface and the atmosphere are important determining factors for the global climate, changes in these due to climate change will cause further feedbacks. For example, the solubility of CO_2 in water is dependent on temperature (Prentice, *et al.*, 2001) so that an increase in water temperature reduces the oceanic uptake of CO_2 which makes this major sink a potential source of atmospheric CO_2 under positive feedback mechanisms caused by global warming. Expected negative effects of global warming include an increase in rain events in some areas of the world, while other areas are expected to experience increased drought. Savanna burning might increase with drought due to warming and drying where savanna replaces rain forest (Grace, *et al.*, 2006). This is likely to cause positive feedback by increasing atmospheric CO_2 levels. It has been found that an increase in atmospheric CO_2 concentration tends to increase the rate of photosynthesis up to a saturation point (Cox, *et al.*, 2000, Malhi, *et al.*, 2002). Bolin and Sukumar (2000), for example, report an increased global net uptake of CO_2 by the terrestrial biosphere although they are unsure of the reason for this. In contrast, increasing temperature tends to increase plant and soil respiration rates, which could ultimately cause a positive feedback (Cox, *et al.*, 2000).

Human-induced land cover changes, such as deforestation can remove the potential warming effect of trees caused by the greater absorption of incoming solar energy while at the same time increasing the global surface albedo. This could lead to a potential cooling effect (Gibbard, *et al.*, 2005, Bala, *et al.*, 2007, Solomon, *et al.*, 2007). However, in the tropics this cooling is outweighed by the loss of photosynthetic potential and the loss of the cooling effect caused by trees due to evapotranspiration and resulting cloud cover (Gibbard, *et al.*, 2005, Bala, *et al.*, 2007). To avoid the expected drastic impact on the global climate and the biosphere

due to increasing amounts of greenhouse gases, preventative response in the form of the reduction of atmospheric CO_2 emissions should be a priority. This requires drastic measures at international level.

2.2.2. International response to curb climate change

The Intergovernmental Panel on Climate Change (IPCC) finding that global climate was being significantly altered due to human influence led to the United Nations Framework Convention on Climate Change (UNFCCC) - an international environmental treaty adopted at the United Nations Conference on Environment and Development (UNCED), held in Rio de Janeiro in 1992. The treaty was aimed at reducing greenhouse gas emissions to counteract global warming. It is projected that stabilization of atmospheric CO_2 concentrations at 450 ppm would require global anthropogenic CO_2 emissions to drop below 1990 levels within a few decades and continuously decrease to the level of persistent natural land and ocean sinks (Prentice, *et al.*, 2001). The UNFCCC treaty did not include legally binding commitments for member countries but made provisions for updates (or "protocols") that would set mandatory emission limits for reducing greenhouse gas emissions. This gave rise to the Kyoto Protocol, a stand-alone international agreement linked to the UNFCCC. The Protocol sets legally binding targets for greenhouse gas emissions for Parties to the Convention that have also become Parties to the Protocol. The Protocol covers six greenhouse gases: CO_2, methane (CH_4), nitrous oxide (N_2O), hydrofluorocarbons (HFCs), perfluorocarbons (PFCs) and sulphur hexafluoride (SF_6), all measured in terms of CO_2 equivalents as a function of global warming potential (Rosenqvist, *et al.*, 2003).

The Protocol was adopted in 1997 and after a final Agreement was reached at the sixth and seventh Conference of Parties (COP 6 and 7) in The Hague, Bonn and Marrakesh (Schulze, *et al.*, 2002), finally came into force on 16 February 2005. At the time of writing, 174 countries plus the EEC had deposited instruments of

ratification, approval, acceptance or accession[2]. The member states are distinguished as follows:

- **Annex I Parties** are the industrialised countries and economies in transition listed in Annex I of the UNFCCC and later Annex B of the Kyoto Protocol (Aukland, *et al.*, 2002). Annex B lists each Party's legally binding emission reduction obligations by the first commitment period of the Protocol, 2008 - 2012.
- **Annex II Parties** are a subgroup of the Annex I Parties, excluding the economies in transition. They are required to pay for the costs of developing countries to undertake emissions reduction activities and to help them adapt to adverse effects of climate change.
- **Non-Annex I Parties** are developing countries that have ratified or acceded to the UNFCCC and are not included in Annex I. These countries might be vulnerable due to their natural conditions, such as low-lying coastal areas and proneness to desertification and drought or due to the potential economic impacts of climate change response measures on their economies because they rely heavily on fossil fuel production and commerce (UNFCCC, 2007).

The United Kingdom, listed as both Annex I and Annex II Party, signed the Protocol in 1998 and ratified it in 2002 whilst Belize, listed as non-Annex I Party, accessed in 2003. The total percentage of Annex I Parties greenhouse gas emissions is listed as 61.6%; the UK and Northern Ireland contribute 4.3% (UNFCCC, 2007). The Protocol aims to reduce the overall greenhouse gas emissions by at least 5% below existing 1990 levels in the commitment period 2008 to 2012. To achieve this overall target, Annex I Parties have set different binding targets for themselves ranging from -8% to +10% of 1990 emissions, requiring significant reductions in currently

[2] "Ratification", "acceptance", "approval" and "accession" of a treaty all have the same legal effect. Ratification defines the international act whereby a state indicates its consent to be bound to a treaty; "acceptance" or "approval" is in effect the same as "ratification" (except for minor administrative difference) as a state expresses the consent to be bound by a treaty; while "accession" is the act whereby a state accepts the offer or the opportunity to become a party to a treaty already negotiated and signed by other states (UNFCCC, 2007).

projected emissions. The EU has set a so-called “bubble” target of -8% by 2010 and -20% by 2020, which was redistributed based on EU agreement (UNFCCC, 2007). The UK’s reduction target was set particularly high at -20% of 1990 levels by 2010, while further legally binding reduction targets have been set at 26-32% below 1990 levels for 2020 with a planned 60% reduction in CO_2 emissions by 2050 (DEFRA, 2007). Currently, it seems as if the UK will only be able to achieve a projected greenhouse gas emissions reduction of 16.2% below 1990 levels (DEFRA, 2007).

2.2.3. Reducing carbon emissions by carbon sequestration

Targets stipulated in Annex B of the Kyoto Protocol can be met in various ways (i.e., by lowering emissions or by creating sinks to remove CO_2 from the atmosphere) either in a Party’s own territory or within another. These are regulated by the following mechanisms (UNFCCC, 2007) as set out in the Marrakesh Accords:

- **Emissions trading** provide for Annex I Parties to acquire tradeable carbon credits from other Annex I Parties for use towards meeting their emissions targets, thus enabling them to make use of lower cost opportunities to reduce emissions.
- **Joint Implementation (JI)** enables an Annex I Party to implement an emission reduction project or a project that creates a CO_2 sink in the territory of another Annex I Party in return for emission reduction units that count towards meeting their own Kyoto target (e.g., a coordinated forest management scheme).
- The **Clean Development Mechanism (CDM)** allows Annex I Parties to implement emission reduction projects or create CO_2 sinks in Non-Annex I Parties in return for emission reduction credits. This is different from JI as it strives to promote sustainable development in developing countries. While JI and emissions trading have not yet been practically applied at the time of writing, 781 CDM projects have already been registered, with expected total certified emission reductions (CERs) > 1,020,000,000 until the end of 2012.

A significant mechanism for removing CO_2 from the atmosphere is through carbon sequestration in growing vegetation. The notion of CDMs in the form of forestry

projects have been the subject of ongoing debate. Proponents see forests and woodlands as important potential carbon sinks that should be monitored at a global scale. However, opponents believe that carbon is only temporarily stored in vegetation and can be released at any time through natural and social processes such as natural decay, fire and deforestation, thus making forests non-permanent carbon sinks. Recent findings (e.g. Bala *et al.*, (2007) and Gibbard *et al.*, (2005)) that boreal and mid-latitude afforestation of grassland can have a warming effect due to a reduction in surface albedo has strengthened their argument. These studies, however, show an opposite effect in the tropics, which calls for further research and initial moderate application of afforestation projects outside the tropics.

Tropical deforestation releases large amounts of CO_2 into the atmosphere which can potentially exceed the effect of carbon sequestration through afforestation and reforestation activities (Gibbard, *et al.*, 2005, Grace, *et al.*, 2006). It is therefore regrettable that CDM currently excludes tropical forest conservation projects. Ongoing debate has culminated in a decision at the UN Climate Change Conference in Bali (COP 13, December 2007) to in future reduce emissions from deforestation in developing countries (REDD programme) (Heffernan, 2007, UNFCCC, 2008).

For the purposes of carbon sequestration projects, the Marrakesh Accords definition of *forest* is loosely based on the FAO (FAO, 2006) definition[3]. It was designed to give each Party flexibility to take into account differing national circumstances and defines *forest* based on minimum canopy cover (10-30%), minimum surface area (0.05-1 ha, or 500-10,000 m^2) and minimum tree height at maturity (2-5 m)[4] (Schulze, *et al.*, 2002). This definition would include most savanna woodlands as forest areas (see 2.3) under the mechanisms relating to carbon accounting. To enable the practical application of such legislation, there is a clear need for accurate mapping and monitoring of forests, including savanna woodlands.

---

[3] FAO defines *forest* based on canopy cover (> 10%), surface area (> 0.5 ha, or 5,000 m^2) and minimum tree height at maturity (5 m), whilst 'other wooded land' has identical surface area and minimum tree height characteristics with a canopy cover 5-10%.

[4] Young natural stands and all plantations which have not yet reached a canopy cover of 10-30% or tree height of 2-5 m are included under forest, as are areas normally forming part of the forest area which are temporarily unstocked as a result of human intervention such as harvesting or natural causes but which are expected to revert to forest.

2.3. The savanna biome

Savannas are the most common vegetation type in the tropics and subtropics (Mistry, 2000), with savanna woodlands accounting for 40% of the total tropical forest area (Grainger, 1999). Despite their abundance in the tropics, these ecosystems have been thought in the past to exist only due to the impoverishment of more ecologically rich neighbouring forest areas. However, they are now recognised for their rich biodiversity and significant proportions of biomass (Furley, 1999, Grainger, 1999). The definition of savannas has changed over time, now including a large diversity of landscapes containing a mix of both grass and woody vegetation. This continuously evolving definition coupled with the heterogeneous character of savannas has led to different interpretations by researchers and forestry organisations, both national and international. Wooded savanna areas have been classified in many cases as sparse forest or woodland. The importance of savannas in terms of biodiversity and biomass value has therefore been largely overlooked. Moreover, savannas are not routinely censused in the same way forests are (Grace, *et al.*, 2006), and it is therefore difficult to assess changes in their extent, structure and biomass. The environmental and economic value of savannas lies mostly in their carbon sequestration potential. The presence of non-timber forest products such as seeds give savannas important added economic and cultural value for local inhabitants (Schreckenberg, 1999). When savannas are exploited in an unsustainable way, degradation and land use change can take place, which have a significant effect on the savanna ecosystem.

The occurrence and morphology of savanna ecosystems are mainly determined by the availability of moisture and nutrients and disturbances such as the occurrence of fire and herbivory. A variety of human disturbances related to land use play a major role although the effects can vary from mild woodland degradation to deforestation. The remainder of this chapter provides discussions on the changing definition of savannas and how this has caused confusion about their global distribution since they are frequently classified as forest or woodland. The following sections then discuss the key savanna ecological determinants and disturbances, followed by a general description of savanna morphology. Finally, section 2.4 places the savanna biome

within the context of this research, by discussing its contribution to the global carbon cycle.

2.3.1. Defining savannas

The term *savanna* (sabana) originated in Haiti and Cuba to designate plains with tall herbaceous cover devoid of trees; in Brazil this was called *campo*. These terms denoted both the open landscape as well as the type of vegetation that characterised the landscape (Sarmiento, 1984). The term *savanna* evolved over time to include grasslands with trees and was used in scientific literature to convey an increasingly broader meaning, mainly defining savannas based on physiognomy or climatic conditions (Sarmiento, 1984, Mistry, 2000). The vast range of savanna definitions, and indeed the large degree of diversity in both biotic and abiotic characteristics present in savannas worldwide (Solbrig, 1996), has hindered savanna research by making it difficult to relate observations and results of one savanna to another. Moreover, several studies concluded that the classification of savannas based on a deterministic relationship between climate and vegetation was inappropriate (Kellman and Tackaberry, 1997). This further underlined the need to focus the definition of savannas.

Current use of the term views savannas as a biome with several constituent and varying ecosystems, rather than a unit of vegetation. Although a number of constituent savanna ecosystem types can be distinguished, it is possible to broadly define the savanna biome so that it encompasses all ecosystem subtypes. Based on this premise, Sarmiento (1984) and Furley and Newey (1983) define savannas as ecosystems of the warm (lowland) tropics that commonly experience alternating wet and dry seasons. The herbaceous layer is continuous and a woody layer may exist, consisting of scattered to dense tree, shrub and palm. The herbaceous cover is partially drought-resistant and shows clear seasonal phenological trends, especially characterised by a period of low activity related to water stress. Fire caused by natural occurrences or human activities is a common disturbance. It is clear that the definition of savannas encompasses a large diversity of landscapes, including a variety of rainfall regimes, levels of soil fertility and grass-tree mixtures (Solbrig,

1993). Other savanna definitions exist, but common similarities include the importance of a grassy or herbaceous stratum and the presence of a generally discontinuous layer of trees and shrubs of varying height and density (Solbrig, *et al.*, 1996, Kellman and Tackaberry, 1997, Mistry, 2000, Grace, *et al.*, 2006). Of particular interest is the savanna type distinction of Scholes and Hall, cited by House and Hall (2001) that distinguishes between savanna subtypes based on woody canopy cover, ranging from 10% to 100%. All these savanna definitions exclude forested formations with a continuous canopy cover where a herbaceous understorey cover is not co-dominant, either perennially or seasonally (Furley and Newey, 1983, Sarmiento, 1984).

The changing definition and the heterogeneous character of savannas have caused an overlap in savanna/forest classification systems due to different interpretations of wooded savanna areas, or savanna woodlands. In many cases, these have been classified as sparse forest or woodland by researchers and forestry organisations for forestry purposes (Grainger, 1999, Homewood and Brockington, 1999, House and Hall, 2001, FAO, 2006). For example, the FAO definition of *forest* is based on a canopy cover of 10% or more, which includes many savanna woodlands. To add confusion, FAO defines woodland with a canopy cover of 5-10% as *other wooded land*. Based on these definitions, the savanna of the study area in Belize (see Chapter 4) would be classified as *forest*, because the savanna woodlands generally have a canopy cover of 30-40% (see 4.5.3 and 5.6.2). Similarly, these definitions include many other savannas into the FAO *forest* or *other wooded land* classes. An important consequence is that the abundance of savannas and the importance of savanna woodlands in the global carbon cycle are commonly underappreciated.

The term *savanna* used throughout this thesis refers to the dynamic mosaic of wooded grassland and non-continuous cover woodland, as determined by factors discussed in 2.3.3 and having a morphology as described in 2.3.4. The study site that is described in Chapter 4 is an example of a savanna ecosystem subtype.

2.3.2. Global distribution of savannas

A consequence of the diversity of savanna definitions discussed above is that the global extent of the savanna biome is uncertain. Estimates vary between different authors. For example, House and Hall (2001) list five different estimates ranging from 15 to 37.3 Mkm^2, forming between ~10 and ~25 % of the global land surface. It should be noted that these estimates were published between 1973 and 2001 and that the estimates do not show a trend. Other estimates in literature are 15% of the global land surface (representing ~40% of the tropics) (Cole, 1986), ~17% (Grace, *et al.*, 2006), 20%, including half the African continent (Osborne, 2000, Malhi, *et al.*, 2002), and ~33% (Mistry, 2000). Despite the different estimates of their absolute extent, it is generally agreed that savannas occur primarily in developing countries and provide support to ~20% of the world population (Mistry, 2000, House and Hall, 2001).

Several global land cover products exist, often derived from coarse spatial resolution multi-temporal optical Earth Observation (EO) data. These products represent savannas to varying degrees. An example that represents savannas as a separate land cover class is the Global Land Cover Characterization (GLCC, USGS (2007)), which consists of a set of derived thematic maps produced through the aggregation of seasonal land cover regions. Several of the thematic maps contain *savanna* or *wooded savanna* classes, depending on the classification scheme applied. Fig. 2.1 shows the GLCC based on the International Geosphere Biosphere Programme (IGBP) land cover classification scheme. A regional Central American ecosystem map (Vreugdenhil, *et al.*, 2002) based on an adaptation of the UNESCO classification system specifically includes *savanna* because it had received too little attention in previous mapping exercises (Meerman and Sabido, 2001). Fig. 4.1 shows savanna distribution in Belize from this mapping exercise. An example that does not distinguish savanna as a separate land cover class is the Global Land Cover 2000 Project (GLC 2000, JRC (2006)). It does, however, offer various forest classes based on canopy cover in combination with distinctions between broad-leaved/needles and evergreen/ deciduous.

Savannas have, in many cases, been classified as forests due to the occurrence of woodlands of varying canopy cover within savannas. According to the latest FAO Global Forest Resources Assessment (FRA 2005, FAO (2006)), the world's forests cover ~40 Mkm^2, or ~30% of the global land surface. This includes all forest and woodland with a canopy cover > 5%. Whereas FRA 2000 (FAO, 2001) enabled distinction of forest classes based on canopy cover[5], FRA 2005 (see Fig. 2.2) has only two forest classes, *other wooded land* (5-10% canopy cover) and *forest* (>10% canopy cover). FRA 2005 indicates that ~33% of the total forest resource consists of *other wooded land* while at the other end of the scale, primary forests with dense canopy cover and abundant native species that show no clear signs of human activity, make up ~36% of the total forest resource. Fig. 2.2 shows the global distribution of *forest* and *other wooded land* according to FRA 2005. Figs. 2.1, 2.2 and partly Fig. 4.1 show examples of global and regional land cover mapping projects that have considerable overlap in their respective savanna and forest classes.

2.3.3. Ecological determinants and disturbances

In places it has proved difficult to explain the existence of non-forest formations based on physical conditions in the wet and seasonally wet tropics (Sarmiento, 1984). A common misconception existed that savannas were derived through human disturbance of forest (Mistry, 2000). While it is impossible to attribute the global distribution of savannas based on a single environmental factor; most authors (Sarmiento, 1984, Frost, *et al.*, 1986, Kellman and Tackaberry, 1997, Mistry, 2000) agree that climatic and edaphic conditions are the main determinants of savanna ecosystems. This section identifies and discusses the four main ecological determinants of savanna in the form of resources and disturbances (i.e., plant-available moisture (PAM), plant-available nutrients (PAN), fire and herbivory).

---

[5] FRA 2000 forest classes:

- 'Closed forest' (>40% canopy cover), area estimated at 19.4% of the global land surface
- 'Open or fragmented forest' (10-40% canopy cover), area estimated at 10.4% of the global land surface
- 'Other wooded land' (5-10% canopy cover), area estimated at 7.9% of the global land surface

Furthermore, human activity is discussed as a major influence on savanna structure (Sarmiento, 1984, Frost, *et al.*, 1986, Sankaran, *et al.*, 2005). Additionally,

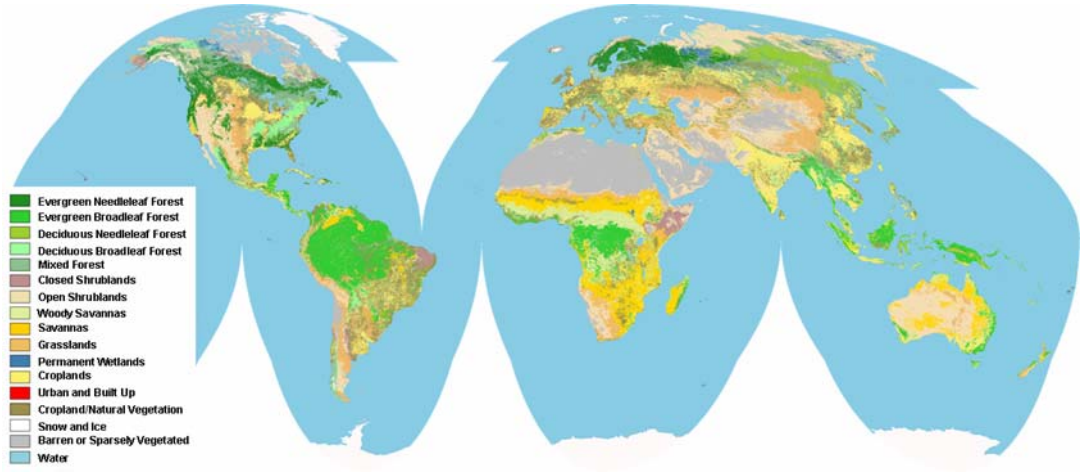

Figure 2.1: The Global Land Cover Characterization (GLCC) map based on the International Geosphere Biosphere Programme (IGBP) land cover classification scheme (© USGS (2007))

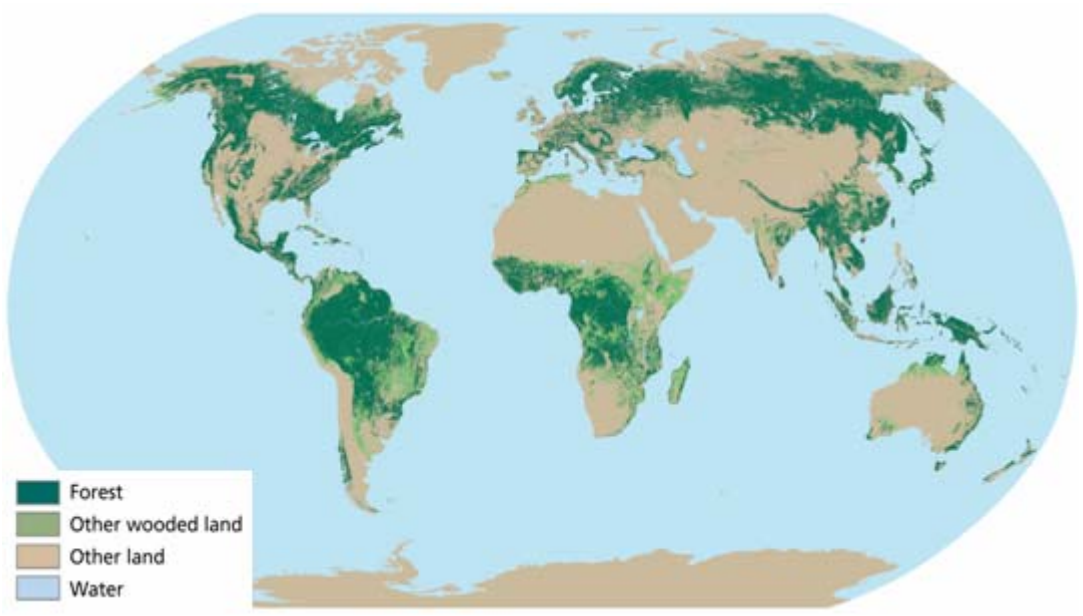

Figure 2.2: Global distribution of the forest resource according to the Global Forest Resources Assessment of 2005 (© FAO (2006))

topography related to drainage (Kellman and Tackaberry, 1997) and long-term biogeochemical cycles (Sarmiento, 1984) can be seen as main broad-scale habitat conditions for the existence of savannas. It should be noted that environments with the climatic, edaphic and topographic conditions associated with savannas often

support other ecosystems such as forest, but savannas seldom occur naturally in areas that do not contain at least one of these characteristic environmental conditions. The fact that most savannas naturally occur on extensive flat landscapes with few topographic interruptions does not necessarily prove this to be a determinant for savanna conditions; it is more likely due to the common correlation between flat landscapes, strong wind and problematic soil conditions and the ease with which fire spreads on such terrain (Kellman and Tackaberry, 1997).

The following subsections discuss in more detail the main savanna ecological determinants and disturbances. PAM, PAN, fire, herbivory and human pressure will be shown to influence the morphology or vegetation structure of the savanna in different and varying interrelated ways. When planning and executing the mapping and monitoring of savanna land cover by means of earth observation (EO) methods, knowledge about the heterogeneity and complexity of savanna ecosystems and the vegetation structure is important (Observation of savannas by means of EO is further discussed in Chapter 3). PAM and PAN are regarded as the main determinants of savanna functioning, affecting the balance between grasses and woody vegetation, vegetation quality and patterns of primary production. However, all the determinants are interrelated to varying degrees. For example, through their influence on the vegetation quality and balance, PAM and PAN influence the frequency and intensity of fire and the type of herbivory and its associated impacts. In turn, the effects of fire and herbivory influence the availability of moisture and nutrients. Fire is an important factor as it not only affects savanna morphology, but also impacts on climate change by setting free vegetative carbon into the atmosphere, consequently causing further feedbacks with climate change (see 2.2). Depending on the frequency, intensity and timing of these interactions, the cumulative effect of the interactions can be significant (Frost, *et al.*, 1986).

2.3.3.1. Plant-available Moisture (PAM)

Savanna soil moisture regimes are influenced by several main factors (i.e., annual precipitation, the proportion of precipitation that enters the soil combined with the water holding capacity of the soil, and the amount of evapotranspiration).

Mean annual precipitation in savanna areas ranges between approximately 300 mm and > 1,600 mm, most of which falls in one or, in equatorial regions, two clear wet seasons. The dry season can last between 3 and 9 months (Frost, *et al.*, 1986). The spatial and temporal distribution of the rainfall can be highly variable within the wet season as well as between years (Mistry, 2000). The effectiveness of the precipitation is determined by temperatures and the length of the dry season (Solbrig, 1996). Annual precipitation is a major determinant of the savanna morphology, or vegetation types, that prevail; woody cover tends to increase with precipitation (Solbrig, 1996, Sankaran, *et al.*, 2005).

Soil permeability and moisture retention properties related to soil texture, structure, profile and depth (Solbrig, 1993) determine the water holding capacity of the soil and the amount of precipitation that enters the soil. The redistribution and concentration of water by surface run-off has important local effects on soil moisture regimes. The amount of surface run-off depends on plant cover, soil surface conditions, topography, amount and intensity of rainfall and antecedent soil moisture conditions. In the drier savannas, more than half the precipitation can be lost in the form of surface run-off (Frost, *et al.*, 1986).

The amount of evapotranspiration is complexly related to climate, soil texture, surface characteristics and vegetation type. Temperatures are related to latitudinal position, so that savannas situated further from the subtropics experience more distinct seasonality in temperatures (Solbrig, 1993), while altitude is also a determining factor for temperature (Solbrig, 1996). Savannas characteristically experience a positive water regime (precipitation greater than evapotranspiration) during the rainy season and a negative water regime during the dry season (Mistry, 2000).

Sarmiento 1983 (cited by Solbrig (1993)) divides tropical savannas into four distinct functional types, based mainly on PAM and fire:

- Semi-seasonal savannas, which have low levels of water stress conditions and plant dormancy and little adaptation to fire.
- Seasonal savannas, the most widespread type of savanna, which have distinct wet and dry seasons. Fire is a common disturbance during the dry season.

- Hyperseasonal savannas, which also have distinct wet and dry seasons but experience flooding during the wet season which creates plant stress related to poor drainage. The study has hyperseasonal savannas.
- Esteros, which are not considered to be typical savannas, have no clear dry season and experience excess soil water for most of the year.

2.3.3.2. Plant-Available Nutrients (PAN)

Most savannas occur on soil conditions that inhibit vegetation growth in some way, either by extreme low fertility, aluminium toxicity or by physical constraints on root development due to impenetrable soil horizons and depth or seasonal waterlogging (Solbrig, 1993, Kellman and Tackaberry, 1997). Savannas are therefore seen as oligotrophic (which offer little to sustain life) ecosystems. Tropical soils are known to be poor in nutrients, but savanna soils contain even fewer nutrients than the soils of tropical forests (Sarmiento, 1984). PAN varies widely between the different savanna soils and depends on the different soil-forming factors (i.e., underlying geology, age, geomorphology, topography, climate, vegetation cover, drainage as well as insect and animal (biotic) activity (Sarmiento, 1984, Cole, 1986, Solbrig, 1996, Mistry, 2000)), which act over different scales of space and time. The physical and chemical properties of savanna soils are strongly dependent on underlying bedrock and the degree to which it has been exposed by weathering and erosion. Two main savanna soil types can be distinguished based on PAN (i.e., dystrophic and eutrophic savanna soils (Frost, *et al.*, 1986)). Dystrophic soils occur on old weathered surfaces which have been subject to soil-forming processes over prolonged periods of time and contain low levels of PAN as a result of relatively high precipitation rates and leaching whilst eutrophic soils occur on basic parent materials where precipitation rates are too low to promote extensive weathering, leaving relatively high levels of PAN. The presence of nutrients released from organic matter depends not only on the vegetative input but on the moisture regime of the soil and soil fertility. In the moist savannas (dystrophic soils), plant production and subsequent addition of organic matter to the soil is relatively high due to relatively high precipitation and a long wet season, after which nutrient release through microbial activity is favoured by the soil microclimate. In the dry savannas

(eutrophic soils), the addition of organic matter is seasonal and limited due to low rainfall and a short wet season, after which nutrient release by microbial activity is dependent on soil moisture (Frost, *et al.*, 1986).

A high sand content with concomitant low PAN may promote woody cover due to the advantage of greater percolation to deeper soil layers below grass rooting depths, which overrides the disadvantage of low PAN (Sankaran, *et al.*, 2005). This is the likely cause of the occurrence of pine woodlands with low density grass undercover on the sandy soils of the study site (see Chapter 4).

2.3.3.3. Fire

The occurrence of fire is characteristic of savannas. Although they can occur naturally by means of lightning, they are in recent times more likely to be human-induced. Humans set fire to savannas to clear areas for agriculture, to improve pastures, for hunting purposes and to keep animals, especially snakes, away from villages. The occurrence of human-induced fires has increased over time, typically occurring up to once a year, although they can sometimes be accidental or criminal (Mistry, 2000, Osborne, 2000). Savanna fires mostly occur in the dry season when moisture content of the plants is low and there is a higher presence of standing dead leaf biomass (Kellman and Tackaberry, 1997). Savanna vegetation has over time adapted to burning and is therefore maintained by frequent burning. Crown fires are rare and whilst only the foliage and smaller branches of larger woody vegetation are killed by fire, the stem and larger branches as well as subsurface xylopodia (tuberous roots) of woody shrubs (Solbrig, 1993) normally survive to resprout at a later stage. Grasses sprout to continue normal growth, many flowering shortly after fire, depending on the presence of adequate PAM and the level of pressure of herbivory. Tree and shrub species need substantial fire-free periods to successfully establish seedlings in the savanna. Studies have shown that fire suppression promotes the invasion of woody species, which grows gradually dense while the graminoid layer is gradually excluded (Kellman and Tackaberry, 1997, Sankaran, *et al.*, 2005).

It is believed that savanna fires can temporarily stimulate savanna productivity by deposition of nutrient elements in the form of ash. However, if these ashes are lost by means of wind and water, recurrent fires are believed to contribute to

impoverishment of savanna soils (Sarmiento, 1984, Kellman and Tackaberry, 1997). An additional indirect negative effect of fire is increased erosion due to exposed soil surface which makes it more susceptible to drying and subsequently more prone to erosion following precipitation (Osborne, 2000).

Fire, especially when woody species are severely affected, impacts on the carbon cycle by setting free into the atmosphere carbon stored in the trees as biomass. The carbon sequestration potential of the burnt savanna is consequently reduced (see 2.4). During a savanna fire carbon dioxide is the dominant emission from flame combustion together with nitric oxide (NO), nitrogen dioxide (N_2O), sulphur dioxide (SO_2) and water vapour (Seiler and Crutzen, 1980, Yokelson, *et al.*, 1996). Savanna burning is estimated to contribute 5-8 GtC/year to the atmosphere (Seiler and Crutzen, 1980), although it is not clear which definition of savanna is used to calculate this estimate.

2.3.3.4. Herbivory

African savannas are known for the presence of predominantly large vertebrate herbivores, while smaller vertebrates (such as armadillos) are present in savannas in other parts of the world (Kellman and Tackaberry, 1997). Vertebrate herbivores can be divided into grazers, which feed on grass and herbs, and browsers, which feed on woody vegetation. A small group fulfills both roles. Both groups can vary widely in size and their impact on the savanna vegetation. Browsers and mixed feeders tend to suppress woody cover, while grazers enhance it (Sankaran, *et al.*, 2005). Normally herbivores make use of the highly seasonal nature of the savannas by arriving soon after precipitation when primary productivity has increased and leaving as productivity and available biomass decline (Osborne, 2000). Apart from their pressure on the savanna vegetation, herbivores are thought to facilitate nutrient cycling through urination and excretion and to enhance species diversity by encouraging survival of fast growing vegetation species (Osborne, 2000). The presence of herbivores can thin tree densities and develop short grass of high nutritional quality (Kellman and Tackaberry, 1997). Domestic livestock can cause overgrazing and disturbance of the savanna ecosystem, where livestock numbers exceed the carrying capacity of an area (see also 2.3.3.5). Invertebrate herbivores that

frequently occur in savannas are grass-eating harvester termites, leaf-cutting ants and grasshoppers. These play an important role in depletion of biomass and seed predation (Mistry, 2000).

2.3.3.5. Human activities

Currently, human activities are thought to be a major source of disturbance to savannas worldwide (Frost, *et al.*, 1986, Sala, *et al.*, 2000). This is not surprising knowing that savannas are inhabited by 20% of the world's population (House and Hall, 2001). Pressure is directly related to the intensity of human activities and is caused by the need for food, fuel wood, fiber, building materials and a few specialist industries (e.g. collection of seeds) and also for recreation (Solbrig and Young, 1993, Young, 1993). Based on their physical conditions, savannas have potential for agricultural crop production and animal husbandry. Until approximately 60 years ago extensive cattle grazing and hunting were the main human activity in savannas; the American savannas are thought to have been inhabited by people for less than 30,000 years whereas African savannas are thought to have been used by pastoralists and shifting agriculturalists for more than a million years. In more recent years, humans have developed the capacity to cause rapid and considerable change in savannas through mechanical and chemical means (Frost, *et al.*, 1986). African savannas in particular are increasingly used for intensive agriculture (Solbrig and Young, 1993). This intensified human use has seriously degraded dry savannas. As water scarcity limits cropping agriculture in dry savannas, the most common land use in savanna areas worldwide is extensive ranching. The only threats to ranching are epidemics and predators in the very wet savannas. Traditional herding has proven to be more sustainable than modern ranching (Solbrig, 1993).

The largest cause of biodiversity loss in savannas is expected to be land use change, including deforestation. This in turn increases atmospheric CO_2 and climate change and can subsequently cause further land use change (Ribot, 1999, Sala, *et al.*, 2000). Removal of plant cover by deforestation, overgrazing or harvesting of agricultural crops can cause increased soil erosion, diminished biomass, loss of biodiversity and in the longer term, loss of soil nutrients (Frost, *et al.*, 1986). Degradation of savanna woodlands can take place when canopy cover and biomass are diminished through

human activities such as fuelwood collection (Ribot, 1999) and collection of non-timber forest products (NTFPs) (Schreckenberg, 1999); both of which can be exploited on a sustainable basis. The latter has shown to give some savannas added value for the local inhabitants, encouraging their conservation. Indirect effects of the removal of plant cover can lead to changes in surface hydrology elsewhere, such as increased flooding down-stream, changes in evapotranspiration and ultimately to species extinction (Solbrig and Young, 1993). Other effects can include invasion of thorn scrubs through grazing pressure (Dougill and Trodd, 1999).

Degradation by human activities is variable in time and space (Grainger, 1999) and can be coupled also to climatic effects (Fuller, 1999). It has also been argued (Fuller, 1999, Homewood and Brockington, 1999, Ribot, 1999) that the natural heterogeneity and continuing state of non-equilibrium of savanna ecosystems may have a greater effect than human disturbances. In most cases, the land use strategies adopted are influenced by national and international policy decisions, most of which are not specifically directed at savanna areas. Examples include international trade policy related to tariff and import quota arrangements, exchange rate policies, international aid policies, price support and subsidies influencing the demand for savanna products. These arrangements frequently under-price environmental attributes such as biomass, biodiversity and environmental quality (Young, 1993). As most savannas are situated in developing countries (see 2.3.2), the pressure of human disturbances has been significant in places. However, the future inclusion of savanna woodlands in forest conservation (e.g. under REDD) or carbon sequestration forestry projects under the Kyoto Protocol (see 2.2.3) is likely to accentuate the importance of sustainable management of savannas.

2.3.4. The morphology of savanna vegetation

The various savanna determinants and disturbances discussed above influence the morphology of savanna vegetation. Savannas are characterised by the co-dominance of grasses (graminoids) and trees (Solbrig, 1993, Sankaran, *et al.*, 2005). Apart from the main structural components of grasses and woody trees as discussed in this section, non-graminoid herbs or forbs and small woody plants (shrubs) also

commonly occur in smaller proportions. These are stratified in two main layers: grasses (together with sedges) and trees (together with shrubs), although tree cover may be very irregular. The equilibrium between grasses and woody vegetation is mainly determined by PAM, PAN, fire and herbivory (Furley and Newey, 1983), thereby causing a mosaic of various savanna vegetation assemblages such as grassland, woodland, shrubland and the occurrence of occasional marsh communities. Levels of PAM, PAN and the frequency of disturbance have a high spatial and temporal variability and contribute to the heterogeneity and complexity of savanna structure over short distances (Furley and Newey, 1983). This contributes to difficulties in defining savannas and separating them from other land cover classes such as forest (see 2.3.1)

Savanna communities can be considerably heterogeneous in composition and functioning. The amount of grass species in any savanna can number between 30 and 60, with 6 to 10 dominant species (Solbrig, 1996). Woody species composition varies between continents (Solbrig, 1996, Mistry, 2000) with variation along continental regions corresponding to PAM gradients and local changes occurring along physiographic gradients (Kellman and Tackaberry, 1997). The number of woody species varies widely, with Brazilian cerrados being most species rich (~10,000 species) and Australian savannas being the most species poor (Solbrig, 1996). It should be noted, however, that these differences in savanna tree species diversity is also related to the relative species richness of the different continents. In general, increasing latitudes show decreasing species diversity for both fauna and flora (Longman and Jenik, 1992).

2.3.4.1. Grasses (graminoids)

A distinctive morphological characteristic of savanna grasses is the absence of stem tissue. They are therefore relatively low-growing vegetation which, store their above-ground biomass in clusters of elongated leaves. Due to their height disadvantage, savanna grasses cannot compete with trees for light but are well adapted to withstand repeated destruction by fire and herbivory. This is made possible by protection of the embryonic tissue that enables regrowth either underground or at the base of the plant, often covered by a sheaf of dead leaf bases (Kellman and Tackaberry, 1997).

Savanna grasses are also well protected against the annual dry season; annuals through burying of seeds and perennials through dieback and dormancy (Mistry, 2000). Although some species require fire to complete their life cycle, the composition of the grasses in dry savannas seems to be more strongly affected by annual and inter-annual variations in precipitation. The effects of grazing or fire become more important in savannas with higher mean annual, and less variable, precipitation (Frost, *et al.*, 1986).

2.3.4.2. Woody vegetation (trees and shrubs)

Savanna trees and shrubs normally occur in relatively lower densities than grasses, although exceptions occur where woody vegetation cover forms a nearly closed canopy but allows enough light to penetrate to permit a nearly continuous layer of grass and sedges (Furley and Newey, 1983) (e.g., African miombo savannas). Trees are often relatively short with a gnarled branching pattern, although straight-boled trees occur (e.g., Caribbean pine; *Pinus caribaea*), which occurs in the study area (see 4.5.1). Most of the woody species are savanna specialists, but several species from local forests that can tolerate savanna conditions may occur (e.g., tropical oak; *Quercus oleoides*) from the dry forests of Central America that occurs in the study area (Kellman and Tackaberry, 1997). Other woody species that commonly occur in savannas are palms, which can grow in dense clumps or are interspersed within the woodland. These also occur in the study area. Woody vegetation have several strategies to survive the dry season. Most species are deciduous, shedding their leaves during the dry season and remaining leafless up to the beginning of the wet season. The time of leaf fall seems to be related to water stress but certain species only shed their leaves at the end of the dry season, making the period of leaflessness variable between years and species. Only high seasonal rainfall savannas, e.g. South American, can sustain evergreen savanna trees and shrubs, which replace their leaves during the middle of the dry season (Frost, *et al.*, 1986), which is often related to the level of the water table. This characteristic can cause seasonal changes in the canopy cover (Fuller, 1999) which, in turn, can complicate the place of savanna woodlands within the definition of *forest* as discussed in 2.2.3. Deep rooting systems and high root-to-shoot ratios are mechanisms for gathering nutrients in the nutrient-poor soils

of most savanna environments (Solbrig, *et al.*, 1996). Crown fires rarely affect tall trees, while trees and shrubs are generally protected from fire by their bark.

2.3.4.3. Interaction between grasses and woody vegetation

Trees and shrubs naturally occur dispersed amongst the more continuous grass layer. In savannas, the co-existence of grasses and woody species is less stable than in comparable temperate situations (Longman and Jenik, 1992), as in savannas species compete for light, water and nutrients. Solar radiation is not always a scarce resource for grasses in savannas, depending on the density of the tree canopy. PAM is shared between the grasses and trees by creating two separate layers of roots, a shallow grass root layer and a deeper tree root layer. In normal savanna conditions, grasses are therefore forced into dormancy in the dry season, while trees may be able to reach the ground water with their deep roots. Trees are therefore restricted to deep soils where the water table is within reach of their roots. In well-drained dry savanna areas, this restricts tree growth to depressions in which water can accumulate. In wet savannas with poor drainage, trees are restricted to elevations (Solbrig, 1993). The presence of trees can have a beneficial effect on the grasses in their vicinity by improving soil fertility and soil structure beneath the crown and improving water relations of shaded grasses. However, trees can also have a negative effect on grasses through competition for PAM and PAN (Osborne, 2000).

2.3.4.4. Savanna boundaries

Factors such as annual precipitation, duration of water stress, temperature, topography and soil conditions and their interrelations determine the ecosystem that neighbours a savanna (Cole, 1992, Longman and Jenik, 1992, Furley, 1992). Evergreen tropical forests appear at the high precipitation end and semi-deciduous forest and scrub appear at the lower precipitation end (Longman and Jenik, 1992). The boundaries of savannas with neighbouring ecosystems are normally abrupt; the transition from savanna to forest can occur within 50 m (Hopkins, 1992). The transition zone, or ecotone, frequently shows a characteristic abrupt change in morphology and species composition but generally contains woody species from both forest and savanna ecosystems with a lower grass density than in the neighbouring savanna (Cole, 1992, Hopkins, 1992).

The ecotone can be dynamic, showing signs of forest advancing into savanna, generally in protected areas, or savanna advancing into forest, generally in areas suffering human pressure through cultivation and fire (Furley and Newey, 1983, Cole, 1992, Hopkins, 1992) as well as herbivory (Hopkins, 1992). The forest-savanna boundary is also often irregular, and can include the presence of patches of savanna within the forest (savanna inliers) as well as patches and fringes of forest within the savanna (forest outliers). These patterns are normally determined by moisture availability (e.g. the extension of forests along streams as gallery forests, such as those occurring in the study area, see 4.5.2), the local influence of topography, drainage and fire (Furley and Newey, 1983). For example, forest outliers can occur due to the availability of soil water or exist as leftover patches of forest in the case of savanna advance. These can be large and numerous and normally occur closer to the forest-savanna boundary (Hopkins, 1992). Savanna inliers are normally associated with human pressure in forest-savanna boundary areas, but can also depend on local edaphic factors. These ecotones appear more abrupt and are thought to be more prevalent than previously believed (Hopkins, 1992). However, in places the ecotone can appear to be stable over the span of (several) centuries (Cole, 1992, Hopkins, 1992).

In cases of extreme human intervention, savannas have encroached entirely upon previously forested areas, thereby changing the land cover from forest to savanna. As neighbouring forest areas are normally resistant to fire, humans cause alteration by increasing the frequency of fires, sometimes in combination with extensive opening of forest canopy for cropping agriculture or ranging, whereby fire can more easily penetrate forest areas (Kellman and Tackaberry, 1997, Mistry, 2000).

2.4. Savannas and the global carbon cycle

Biomass distribution is not uniform between different sites and forest types (Cummings, *et al.*, 2002) and significant information gaps exist for forests occurring at the environmental extreme of the tropics, such as savanna woodlands (Brown and Lugo, 1982, House and Hall, 2001). Organic-matter storage and production in tropical forests and savannas are related to climatic factors, of which rainfall and temperature are most important (Brown and Lugo, 1982, Sankaran, *et al.*, 2005,

Grace, *et al.*, 2006). With savanna ecosystems encompassing a wide range of grass-tree mosaics, figures for net primary productivity and carbon stocks quoted in the literature vary widely. For savannas with woodland, these statistics are sometimes listed under forest or open woodland productivity rates, making it difficult to compare studies of individual savanna sites or to come up with a mean biomass stock or a mean productivity rate for savanna ecosystems.

Carbon makes up ~50% of vegetative biomass (Brown, 1997, Houghton, *et al.*, 2001, Snowdon, *et al.*, 2002) which can be defined as the dry weight of vegetal material expressed in mass units per unit area (Brown, 1997, Araújo, *et al.*, 1999). Carbon is stored in live or dead biomass, which occurs either above-ground (AG) or belowground (BG). Whilst above-ground dead biomass occurs as fine litter, dead wood or dead standing vegetation, live AG biomass occurs as living vegetation, of which the roots form BG live and dead biomass. Root biomass is cumbersome to measure but can be indirectly estimated by means of known root-to-shoot ratios, when the AG biomass is known (MacDicken, 1997, Chave, *et al.*, 2001). This carries with it a risk of error because it is difficult to distinguish live from dead roots. Soil forms a major source of BG carbon (Brown and Lugo, 1982). Savanna soil carbon is estimated at 200-300 Gt, which makes up 10-30% of the world's soil carbon (Grace, *et al.*, 2006).

Of the few studies that have estimated savanna biomass, very few have estimated both AG and BG biomass (House and Hall, 2001). Relative biomass contributions are variable between savanna types; Seiler and Crutzen (1980) report that BG biomass makes up 37% of the total biomass for dry savanna while this estimate is 29% for humid savanna, House and Hall (2001) list estimates ranging from 20% to 40% for BG biomass of different savanna types, but Grace *et al.* (2006) report a mean as high as 58% for savanna ecosystems worldwide[6].

Several authors give an extensive review of biomass carbon content and productivity rates for different savanna ecosystems based on literature studies, ranging from dry to tropical savanna (e.g. House and Hall (2001), Grace *et al.* (2006)). AG savanna

[6] Calculated from Table 1 in Grace et al. (2006), only considering studies that had estimates for both total AG and total BG biomass.

biomass carbon stocks vary widely according to the amount and extent of tree cover, for example from 1.8 t C/ha in the absence of trees to 30 t C/ha for areas with substantial tree cover (Grace, *et al.*, 2006). House and Hall (2001) give an average of ~20 t C/ha[7]. The study site is estimated to have 13.1±2.2 t C/ha (95% CI) (Brown, *et al.*, 2005) of which the respective contributions of the different savanna vegetation types are given in Fig. 4.13 (see also 4.5.3). In contrast, the global average total AG carbon density of tropical forests is estimated at 152±40 t C/ha (Grace, *et al.*, 2001).

Net primary productivity (NPP) rates for savannas vary between 1.4 and 22.8 tC/ha/year, with a mean and 95% CI at 7.2±2.0 t C/ha/year (Grace, *et al.*, 2006). The latter range approximates the average NPP rate of 5.4 t C/ha/year given by House and Hall (2001). In comparison, the mean NPP and 95% CI of tropical rain forests is given as 11.2±4.2 t C/ha/year by Grace, *et al.* (2001) and that of temperate forests 7.8 tC/ha/year[8] (Saugier, *et al.*, 2001). A factor that is thought to increase the carbon sequestration ability of savannas is the presence of plant species that are adapted to harsh environmental conditions or vegetation that can rapidly recover after unfavourable conditions, therefore maintaining elevated photosynthetic rates (Dias, *et al.*, 2006). More research is needed to understand the highly seasonal productivity rates and inter annual variations due to the effects of fire (Brown and Lugo, 1982, Grace, *et al.*, 2006). Although savannas contain lower biomass carbon stocks than tropical and temperate forests, the productivity rates are more similar, making savannas the third most productive biome (Saugier, *et al.*, 2001).

It should be noted that, although they have relatively low biomass compared to trees (Cummings, *et al.*, 2002), live woody 'non-tree' structures such as palms can form a relatively large component of the overall AG biomass in savanna woodlands (Cummings, *et al.*, 2002). This is noteworthy as palms are often omitted from biomass estimates and are in fact more likely to completely burn as opposed to the mild fire damage suffered by the taller savanna trees; contributing significantly to atmospheric carbon during savanna fire events. As outlined in 2.3.4 and 4.5, the

[7] Given as 4.02 kg DM/m^2 (House and Hall, 2001:374).
[8] Given as 1.55 kg DM/m^2/yr (Saugier, et al., 2001:545).

woody component of savannas encompasses savanna woodland trees, shrubs and tree-like palms.

2.5. Summary

Growing concern about the relationship between human-induced increases in greenhouse gases and an increasing average temperature led to international action in the form of the Kyoto Protocol. The international treaty aims to reduce the overall greenhouse gas emissions by at least 5% below existing 1990 levels in the commitment period 2008 to 2012. Reductions can be achieved not only by lowering greenhouse gas emissions, but by creating sinks to remove CO_2 from the atmosphere, e.g. through carbon sequestration in vegetation. The Clean Development Mechanism (CDM) initiative offers the opportunity for industrialised parties to create CO_2 sinks in developing countries in return for emission reduction credits (e.g., through forestry projects). A recent drive for the reduction of deforestation in developing countries (REDD) underlines the importance of savannas since the Kyoto Protocol definition of forests, based on a minimum canopy cover of as little as 10%, includes most savanna woodlands.

Traditionally seen as open areas of grassland, the term savanna now encompasses a wide variety of grass-tree mixtures. The defining characteristics are a continuous grass layer with the occurrence of a woody layer consisting of scattered to dense trees, shrubs and palms. Savannas occur in the warm (lowland) tropics and commonly experience alternating wet and dry seasons. Overlaps between the definitions of savannas and other land cover classes such as forest and sparse or open woodlands have occurred. These classification differences have led to an under-appreciation of their value, not only for their biodiversity, but also as important areas with potential for carbon sequestration. Little attention has been given to savannas in comparison to moist evergreen tropical forests, yet they have been shown to contain a higher biodiversity, greater productivity and therefore a larger impact on the global carbon cycle than previously appreciated. Savannas are productive ecosystems that cover approximately 20% of the Earth’s surface, with the third highest net primary productivity rate, after tropical and temperate forests.

Various savanna determinants and disturbances exist, which influence savanna vegetation morphology such as the tree-grass balance. Plant available moisture (PAM) and nutrients (PAN), fire, herbivory and human activities are interrelated to varying degrees and determine savanna functioning and morphology, giving rise to a mosaic of savanna vegetation assemblages such as grassland and woodland. They occur mostly in developing countries where they are especially prone to disturbances such as land cover change and fire, both which can potentially cause positive feedback to global warming.

Savanna structure can change significantly over short distances. This is related to changes in environmental determinants and disturbances, which contributes to the heterogeneity and complexity of savanna ecosystems. Their heterogeneity and often patchy vegetation structure limits the resolution at which savanna vegetation, and savanna biomass, can be effectively mapped and monitored using EO data and methods.

Under the Kyoto Protocol there is a clear need for accurate information on the spatial extent, biomass stock and growth potential of forests and woodlands, ranging from dense tropical forests to sparse woodlands with a canopy cover as low as 10%. This information should be readily available at regional and national scales. There is a need for accurate information on the vegetative biomass, how it interacts with the carbon cycle and how it ultimately impacts on the global climate. Moreover, there is a need for increased understanding of the dynamic nature of tropical biomass as it responds to fluctuations due to climate change and human pressure, especially in sensitive areas such as savannas and forest-savanna boundaries.

Obvious characteristics of the global forest resource, including savanna woodlands, which should be monitored are its extent and dynamics (due to afforestation, reforestation and deforestation activities as well as fire). However, monitoring of growing stock and carbon storage, or biomass accumulation is equally important (FAO, 2006). In order to monitor these characteristics globally, organisations such as FAO rely mainly on national inventories. Ideally, such inventories should include estimates of carbon emissions and removals caused by changes in forest biomass stocks due to forest management, harvesting and the establishment of plantations.

Chapter 3 discusses *in situ* and EO methods for estimating and mapping forest biomass as well as its subsequent monitoring. Such mapping is important not only to know where the carbon sequestration potential lies, but also to estimate the potential emissions that would arise from biomass burning, and is extremely important for input to, for example, carbon-climate models.

CHAPTER 3:
Biomass estimation using *in situ* and Earth observation (EO) methods

3.1. Introduction

Chapter 2 has highlighted the importance of measuring the biomass of savannas. A definition of biomass and its relation to carbon is given in 2.4. This research evaluates the use of SAR for estimating the above-ground (AG) biomass of savanna woodlands. Literature on biomass estimation in savanna areas is scarce (a few examples are Santos, *et al.* (2002), Barbosa and Fearnside (2004), Lucas, *et al.* (2004), Dias, *et al.* (2006), Salis, *et al.* (2006)), showing that the role of savannas in the global carbon cycle is still widely underestimated. By far more biomass estimation studies have been carried out in tropical forests (e.g. Brown (1997), Araújo, *et al.* (1999), Houghton, *et al.* (2001), Cummings, *et al.* (2002)), temperate forests (e.g. Brown (2002a), Tateno, *et al.* (2004)) and boreal forests (e.g. Fang and Wang (2001), Liski, *et al.* (2003)). Methods used for biomass estimation originated from *in situ* measurements requiring intensive field measurements. A sampling method is generally applied to destructive *in situ* measurements of which the results are extrapolated over a wider area. In contrast, Earth observation (EO) methods can provide repeatable observations over larger areas.

This chapter gives an overview of biomass estimation techniques. A discussion of *in situ* methods for biomass estimation is included (3.2) since EO methods are generally used in combination with *in situ* measurement methods, e.g. for validation as in the case of this research. An overview is then given of the main EO techniques that are applied to obtain above-ground (AG) biomass (3.3). Although a wide range of EO methods for biomass-related studies is discussed, more emphasis is placed on SAR and InSAR since they are used in this study. Throughout, the focus falls on the (potential) application of these methods in savanna woodland (sometimes referred to

in the literature as sparse or open woodland, see 2.3.1). Literature on EO of savannas is scarce but where relevant, examples are given.

3.2. *In situ* methods for biomass estimation

A crude approach to AG biomass estimation involves the complete harvesting of a plot, subsequent drying and weighing of the vegetation, followed by extrapolation to a larger area unit (Overman*, et al.*, 1994, Araújo*, et al.*, 1999). This direct measurement method is impractical, not only because it is laborious and destructive, but also due to its limitations for areas with spatially heterogeneous vegetation. In practice, two indirect methods are commonly applied for AG biomass estimation. The first involves the use of national forest inventory data, which is typically focused on the aerial extent of forest and merchantable timber volume. A biomass expansion factor (BEF) is applied per forest type to convert stem volume to AG biomass while taking into account non-commercial components such as branches, leaves and saplings (Fang and Wang, 2001, Brown, 2002a). Developed countries conduct regular inventories of their managed forest resource while many developing countries, mainly in the tropics, have a partial or full inventory of their forest resource, although this is normally more than 10 years old and few such inventories are repeated (FAO, 1993, Araújo*, et al.*, 1999). The second approach involves the use of allometric equations which apply functional mathematic relationships between tree measurements and tree biomass. Forest inventory data can be used if tree diameters and stand tables (i.e., number of trees per unit area) are reported. Allometric equations can be species-specific or generic (i.e., clumped by general species group) and exist for most forest types (Brown, 2002a). If allometric equations do not exist for the tree species of a study area, they can be developed based on the harvesting, measurement, drying and weighing of a carefully selected sample of trees representing all size classes and species in the study area (Overman*, et al.*, 1994, Brown, 1997, Chave*, et al.*, 2001, Cummings*, et al.*, 2002). Ideally, the establishment and periodical measurement of permanent plots laid out in a statistically sound design should be used for estimating live AG biomass and monitoring change over time (Brown, 2002a). Additional methods have, to a lesser extent, been applied for estimation of AG biomass (e.g., a canopy intercept method

for grasses and shrub-like vegetation (Jonasson, 1988, Frank and McNaughton, 1990)).

In the absence of existing woodland inventory data, this research relies on allometric equations developed by destructive sampling for the major tree species of the study area in Belize (see 4.5.3). The following subsections therefore elaborate only on methodological issues relating to the development of allometric equations.

3.2.1. Allometry for live above-ground biomass

Tree measurements or parameters most commonly investigated for the development of allometric equations are diameter at breast height (dbh), tree height, wood density, crown size and moisture content (i.e. mass of moisture per unit mass of fresh biomass) (Overman*, et al.*, 1994, Araújo*, et al.*, 1999, Chave*, et al.*, 2001). For practicality, tree parameters that can be measured with relative ease and accuracy are more likely to be included in an allometric function. For example, Overman *et al.* (1994) found that, although the addition of a parameter for wood density significantly increased the accuracy of their biomass estimation models, it was too time-consuming to measure, caused damage to trees and therefore was excluded. The most frequently used parameters for allometric functions estimating AG biomass are dbh and tree height. Dbh is often a standard inclusion in allometric biomass models since it is relatively easy to measure and included in many forest inventories, linked with the fact that it consistently shows good results as a predictor for biomass over a range of forest types (Brown, 1997, Araújo*, et al.*, 1999, Chave*, et al.*, 2001). There is, however, much debate on the value of tree height in allometric models. Although many models use only dbh, or a function of dbh (such as dbh^2 or ln(dbh)), it is also commonly added as a product with tree height. In forest environments, the inclusion of tree height is said to improve biomass estimations as it takes into consideration long thin saplings and emergent trees (Overman*, et al.*, 1994), whereas tree height is an impractical inclusion in tropical forests due to the heterogeneous range of tree architectures (Chave*, et al.*, 2001) and the difficulties in measuring tree height from the ground (Brown, 2002a). From an EO perspective, average tree height may be

more practically measured by, for example, InSAR, POLInSAR, SAR tomography, scatterometry and LiDAR; this is further discussed in 3.3.

Allometric equations can take on a range of different mathematical functions; whilst linear regression models were initially more frequently applied, the power-law function (i.e. $AGB = aD^b$, where D is dbh and a and b are scaling coefficients), is currently more widely accepted (Chave*, et al.*, 2001, Zianis and Mencuccini, 2004). This trend in allometric scaling is largely explained by the fractal-like volume-filling theory of West, Brown and Enquist (the WBE model, (West*, et al.*, 1997, Enquist*, et al.*, 1998), which predicts that the basal diameter (D) of a tree structure relates to its AG biomass through $AGB \propto D^b$, for a given scaling coefficient *b*. The value of *b* and whether it can be used as a universal constant applicable to all tree types is widely debated (e.g. Enquist, *et al.* (1998), Zianis and Mencuccini (2004), Li, *et al.* (2005), Hedin (2006), Woodhouse (2006b)).

Literature review shows that no single optimal allometric equation exists for determining AG biomass in the tropics. Selecting an optimal allometric equation from a suite of different functions and transformations including a range of independent parameters, or tree measurements, is usually based on a combination of the practicality of the parameters and the coefficient of determination (R^2). In the search for a general allometric equation for the estimation of biomass, several authors have resorted to generic groupings. Groupings according to general species, with an implicit ecological zoning (such as investigated by Brown and Lugo (1982)) yielded significant improvement of allometric biomass estimations using only dbh (Brown and Lugo, 1982, Brown, 2002a). The highly heterogeneous nature of tropical vegetation has also lead to groupings according to size class (Overman*, et al.*, 1994, Chave*, et al.*, 2001), applying different dbh size ranges. The use of generic allometric equations carries with it an advantage of including a larger sample of trees which tends to increase the precision and accuracy of the biomass estimations overall (Brown, 2002b).

3.2.2. Sources of error

The derivation of allometric models carries with it sources of error and associated error propagation for the estimation of AG biomass. Literature on this topic is scarce and the uncertainty associated with derived allometric models is rarely explicitly stated (Chave, *et al.*, 2004). The main sources of error are interrelated and are discussed below:

- **Tree measurement errors.** Errors in the measurement of sampled trees for the development of allometric models will propagate into the final allometric model (Chave, *et al.*, 2004), while measurement errors of standing trees for the application in allometric models will cause erroneous biomass estimates. The accuracy and precision of both dbh and tree height measurements depend on the measurement instrument used and the experience of the operator. Dbh measurement carries less risk of error than tree height because direct measurements are made compared to the indirect measurements for tree height. The most important sources of error for dbh measurement are irregularly shaped tree stems (Philip, 1994), inconsistent measurement technique (Husch, *et al.*, 2003) and large tree sizes (Phillips, *et al.*, 2000). Error sources for tree height measurements are discussed in section 5.3.2.2. An overall relative accuracy of up to ±10% is expected to be achieved for tree height measurements (Phillips, *et al.*, 2000, Chave, *et al.*, 2004). An additional effect of tree measurement errors during the development of allometric models is the subsequent erroneous exclusion or inclusion of trees that fall outside the dbh range of the sample (Chave, *et al.*, 2004).

- **Sampling errors** are related to sample size and representativeness of the sample plots across the landscape (Chave, *et al.*, 2004). Since savannas typically have spatially irregular occurrences of woodland, the latter is an important consideration. Many published allometric models are based on harvesting performed in a single forest, typically using <50 trees (Chave, *et al.*, 2004). The use of larger samples are encouraged to increase the accuracy of predictive allometric models (Overman, *et al.*, 1994, Araújo, *et al.*, 1999, Brown, 2002b), especially in tropical environments where the heterogeneity of tropical vegetation

decreases the likelihood of a representative sample (Cummings, *et al.*, 2002). It has been shown that the reliability of allometric models decreases with increasing dbh (Overman, *et al.*, 1994, Chave, *et al.*, 2001), possibly due to the under-representation of large trees during sampling. Although large trees (>70 cm dbh) do not occur abundantly, they are found to contribute considerably to the overall AG biomass, especially in savanna woodland. Small trees (<10 cm dbh) are not normally incorporated in forest inventories, causing an underestimation of 2-12% in total AG biomass (Chave, *et al.*, 2001, Cummings, *et al.*, 2002). As researchers tend to avoid disturbed forest and are more likely to select attractive forests, sample plots are unlikely to represent the heterogeneity of the landscape (Chave, *et al.*, 2004).

- **Errors relating to the allometric model** can be caused by errors in the allometric model, or an incorrect model choice. The first is intrinsically linked to measurement errors and sampling error during development of the model. The latter can be linked to the application of published allometric models across trees that fall outside the valid diameter range of the allometric model or incorrect species types (e.g., species with a dissimilar wood density) (Chave, *et al.*, 2004).

Any of these error sources or combinations of them can propagate into an erroneous final biomass estimate; upscaling of such estimates over a larger area can cause large differences in biomass estimates. Fang and Wang (2001) believe that global forest biomass is overestimated and that improved biomass estimation methods can account for the imbalance in the global carbon budget. Houghton, *et al.* (2001) compared seven previous biomass estimates for the Brazilian Amazon, of which three applied *in situ* techniques based on allometric models, two applied low resolution[1] optical EO techniques and two applied biomass modelling based on environmental gradients. They found that the mean biomass estimates varied by more than a factor of two, ranging from 100 t C/ha to 232 t C/ha. There was little agreement in the estimated spatial distribution of the biomass estimates for the Brazilian Amazon region, causing 60% of the variation of the estimated net carbon flux for the region.

[1] This refers to spatial resolution. Unless stated otherwise, all further use of the term *resolution* in this thesis refers to *spatial resolution*.

Although there is no true value with which to compare, it should be noted that the two estimates obtained with EO methods (196 t C/ha and 178 t C/ha), were the two estimates most similar to the mean of all seven estimates (177 t C/ha). A major advantage of EO methods over *in situ* methods based on sampling is that, depending on resolution, EO is better suited to detect differences in the spatial distribution of biomass density (e.g., the occurrence of forest gaps and land cover changes).

3.3. EO methods for biomass estimation

Its systematic observations at scales ranging from the local to global give EO technology potential to contribute to biomass mapping and monitoring initiatives under Kyoto the Protocol (Rosenqvist*, et al.*, 2003, DeFries*, et al.*, 2007). EO improves the ability to monitor inaccessible areas and can more accurately represent the spatial heterogeneity of the landscape. When the FAO Forest Resource Assessment of 2000 used an independent EO survey to supplement national reporting in the pan-tropical region, it led to a calibration of reported changes in forest area in Africa. The survey also provided important insight into differences in land use change patterns across the tropics (FAO, 2006).

Several EO methodologies exist for mapping forest or woodland extent and for quantifying the live AG biomass, but monitoring of forest degradation by EO is currently more technically challenging (DeFries*, et al.*, 2007). For inaccessible areas of developing nations where CDMs (see 2.2.3) will be set up, EO may be the only viable means to collect data as forest inventories are non-existent, old or incomplete (FAO, 2006). For such countries, the existence of data archives for a number of EO sensors extending back several decades also enables the estimation of a 1990 carbon stock baseline as required under the Protocol. EO can also be used for policing CDM project areas by monitoring past and present forest cover history or changes in surrounding land cover, specifically to detect leakage[2] through repetitive national observations (Peter, 2004, DeFries*, et al.*, 2007). EO-derived biomass estimates have

[2] 'Leakage' refers to the loss of carbon sequestration effect of an afforestation or reforestation project due to, e.g. the shift of activities that preceded the sequestration project elsewhere.

been effective for calibrating vegetation models that are used to predict global biomass and carbon flux (Le Toan, *et al.*, 2004). For successful carbon accounting to take place routinely, there is a need for accurate, reliable, cost-effective EO technology that can provide repeated biomass estimates at national and regional scales. Ease of repetition and the use of historic data as baseline datasets are especially important due to the dynamic nature of biomass through growth and external pressure and the requirements of the Kyoto Protocol (Houghton, *et al.*, 2001, Rosenqvist, *et al.*, 2003, DeFries, *et al.*, 2007).

Sensor resolution generally determines the scale and accuracy at which information can be retrieved. The minimum forest surface area (500-10,000 m^2) as set out in the Marrakesh Accords (see 2.2.3) will require a maximum ground resolution requirement for EO data between 22 and 32 m. This is relatively well covered by a number of spaceborne and airborne remote sensors; from medium resolution, providing data at forest level to very high resolution data from which data can be extracted at tree level. Spaceborne sensors generally offer more affordable data and have the advantage of repetitiveness which is needed for systematic observation of project areas. Airborne data have limited spatial coverage but can offer high to very high resolution data and the use of sensors that are not currently operational from space (e.g., P-band SAR) or of which only several operate from space (e.g., LiDAR). Active EO, such as radar, is more frequently used in the tropics as it is not as strongly affected by cloud cover as LiDAR and passive optical sensors. This is an important consideration as many developing countries are situated in the tropics. Radar and LiDAR can provide valuable structural information on the height and structure of vegetation, and the elevation of the underlying terrain. The combination of both active and passive EO data is likely to improve biomass estimation and forest extent mapping (Brown, 2002a). EO data should generally be used in conjunction with *in situ* data to calibrate data extraction and to test the accuracy of classification or biomass estimation outcomes. Data assimilation techniques, whereby carbon estimates from (e.g., EO data) are combined with *in situ* data such as flux observations and a dynamic model have improved ecosystem carbon modelling results (e.g. Williams, *et al.* (2005)).

3.3.1. Optical EO

Passive optical imagery is one of the most widely available sources of EO data which is used in various ways at a range of spatial and spectral resolutions for mapping and monitoring land cover such as forests (Hansen, *et al.*, 2005). Optical EO is especially useful for estimating forest biochemical attributes over large areas (Boyd and Danson, 2005) but has also been used for mapping forest attributes such as biodiversity (Foody and Cutler, 2003). Estimates of forest biomass and canopy cover are typically based on empirical relationships with vegetation indices such as the Normalised Difference Vegetation Index (NDVI) (Foody, *et al.*, 2001, Dong, *et al.*, 2003), with more success in deciduous and dry forests (Freitas, *et al.*, 2005) and even aged plantations where trees tend to be evenly spaced (Sader, *et al.*, 1989). The same counts for empirical relationships between forest height and infrared reflectance in even aged stands (Donoghue, *et al.*, 2004). In both cases sensitivity drops off upon canopy closure, causing the understorey and soils of the forest floor to be excluded from the spectral signature (Puhr and Donoghue, 2000). Other methods investigated for biomass mapping from optical EO in the tropics are neural networks (Foody, *et al.*, 2001, Foody, *et al.*, 2003) and Fourier-based textural ordination (Proisy, *et al.*, 2007).

Although optical sensors are mainly used to obtain horizontal information, it can be used for tree height retrieval using stereography from aerial photographs, for example Brown *et al.* (2005) used aerial stereo imagery to measure tree height and crown area in a savanna woodland of the study area, on which AG biomass estimates were based using allometric equations. Other applications of optical EO to savannas include savanna subtype (e.g savanna woodland) mapping from Landsat (Stuart, *et al.*, 2006, Palamuleni, *et al.*, 2007) and AVHRR vegetation indices (Ferreira and Huete, 2004), quantification of savanna vegetation types using imaging spectrometry and inverse modelling (Asner, *et al.*, 1998), fire risk mapping (Verbesselt, *et al.*, 2006), mapping of fire extent for fire emission estimation (Alleaume, *et al.*, 2005), and tree crown delineation and classification from high resolution hyperspectral data (Bunting and Lucas, 2006).

Optical EO is severely limited in the tropics due to frequent cloud cover, and shadowing on steep topography has been shown to hinder spectral correlations (Sader, *et al.*, 1989). Finally, where optical methods are used for height and biomass estimates, saturation is observed at very low levels of biomass (Kasischke, *et al.*, 1997).

3.3.2. LiDAR

Light Detection and Ranging (LiDAR) is an active instrument that transmits pulses in the visible or NIR region of the electromagnetic spectrum using a laser to generate highly collimated and coherent radiation (Wehr and Lohr, 1999, Aronoff and Petrie, 2005); it is commonly operated from an airborne platform but currently one spaceborne LiDAR instrument for surface and atmospheric studies exists aboard the ICESat[3] satellite (Zwally, *et al.*, 2002). The time difference for a transmitted laser pulse between transmitter and object is measured, but further data includes multiple returns from each pulse (Wehr and Lohr, 1999, Lovell, *et al.*, 2005). The returned signal containing multiple returns can be used to derive information on the vegetation canopy for forestry applications. Generally, the first return (from the part of the forest nearest to the sensor) will be returned from the (near) top of the canopy, while the rest of the forest vegetation causes several returns as the pulse makes its way through the canopy. The last return normally bounces off the ground surface and therefore causes a characteristic peak in the backscatter curve (Nilsson, 1996).

Two important LiDAR system characteristics are footprint size and point density. Footprint size is roughly characterised as either small-footprint (approximately 0.1 – 1 m) or large footprint (approximately 5-100 m) (Næsset, 2004, Andersen, *et al.*, 2005, Lovell, *et al.*, 2005). Point density is determined by the number of footprints per m^2. Together these characteristics determine the amount and resolution of the data retrieved and the accuracy of the retrieved parameters. Forestry applications commonly use small footprint LiDAR systems at both stand and single-tree level.

[3] The Geoscience Laser Altimeter System (GLAS) was originally designed to measure ice-sheet topography and cloud and atmospheric properties. It has a footprint of 70 m, spaced ~175 m apart along a track.

High point densities (e.g. 10 - 20 points/m^2) are preferable at the single-tree level (Hyyppä, *et al.*, 2001, Maltamo, *et al.*, 2005).

Small-footprint LiDAR has been used for forestry applications at the stand level for determining mean tree height (Næsset, 1997a, Hyyppä, *et al.*, 2000, Næsset and Økland, 2002, Holmgren, *et al.*, 2003), dominant tree height (Lim, *et al.*, 2003), basal area (Lim, *et al.*, 2003, Næsset, 2004), stand volume (Næsset, 1997b, Means, *et al.*, 2000, Næsset, 2004), and AG biomass (Patenaude, *et al.*, 2004). At the single-tree level, LiDAR has been used to delineate (through segmentation) separate trees (Hyyppä, *et al.*, 2001) to identify, locate, and relate tree characteristics to a single tree. Generally, LiDAR estimation of mean stand tree height is more accurate than height estimations of single trees (Næsset and Økland, 2002), but tree segmentation has a clear advantage over stand-level methods for heterogeneous forest areas. Large-footprint LiDAR, such as LVIS[4] (Drake, *et al.*, 2002) and SLICER[5] (Lefsky, *et al.*, 1999) have been used successfully to estimate AG biomass together with other forest parameters such as basal area in dense tropical and deciduous forest respectively and ICESat has been used for tree height estimation in temperate forest (Rosette, *et al.*, 2008).

Small-footprint LiDAR has been applied at woodland-level in savanna woodlands for characterising tree height and canopy cover (Tickle, *et al.*, 2006), and ultimately AG biomass (Lucas, *et al.*, 2006a), while at the tree-level, LiDAR data has been used to generate a three-dimensional model of the distribution of tree branches of individual trees (Lucas, *et al.*, 2006c).

The accuracy of parameter retrieval at both stand and single-tree level is determined by a combination of forest and LiDAR characteristics such as canopy density, crown shapes and the type of leaves, LiDAR footprint size and point density as well as underlying topography (Næsset, 1997b, 2004). For example, trees with a sharp top such as conifers require a very high point density to accurately detect the actual tree tops, and therefore have a greater probability of being underestimated (Nilsson,

[4] Laser Vegetation Imaging Sensor, operated at a footprint size of 25 m, spaced 25 m along-track and 9 m cross-track.

[5] Scanning LiDAR Imager of Canopies by Echo Recovery, operated at a footprint size of 10 m, spaced 10 m along-track and cross-track.

1996, Suárez, *et al.*, 2005). LiDAR-retrieved tree heights have been underestimated between 1% and 30% (McCombs, *et al.*, 2003, Wallington and Suárez, 2007). As most operational LiDAR systems are airborne and relatively expensive, LiDAR data is typically used as a high resolution data sample, which can be used in conjunction with another EO data source (e.g. Tickle, *et al.* (2006), Lucas, *et al.* (2006a), Lucas, *et al.* (2006c)).

3.3.3. Radar EO

Radio Detection and Ranging (RADAR, subsequently referred to as radar) is an active instrument that transmits pulses in the microwave region of the electromagnetic spectrum from an antenna (Woodhouse, 2006a); the time difference for a transmitted pulse between antenna and object is measured from which the range distance to the target is determined. Microwaves, unlike optical EO, are not impeded by daylight conditions nor by the atmosphere, e.g. haze, clouds and light rain (Trevett, 1986), therefore enabling radar EO data acquisitions at night time and in predominantly cloudy regions such as the tropics.

Radar altimetry is a practical application of this simplest form of active radar, operating at nadir to provide accurate altitude data. Radar scatterometry goes a step further to provide accurate measurements of the backscatter response as a function of depth into the target (Trevett, 1986, Woodhouse, 2006a)[6]. Although scatterometers are currently mainly used for observing wind and rain patterns over the oceans, scatterometry has been investigated for forestry applications. Altimeters and scatterometers are non-imaging radar as they tend to take isolated measurements, although this is not always strictly true for scatterometers. Imaging radar, on the other hand, provides a two-dimensional image that shows the spatial variability of targets measured on the Earth's surface by combining an oblique viewing angle with the effect of platform motion (see Fig. 3.1); effectively scanning the ground along the flight path. The resulting image is formed by combining signal strength (i.e. the

[6] Much of this section is synthesised from these two references.

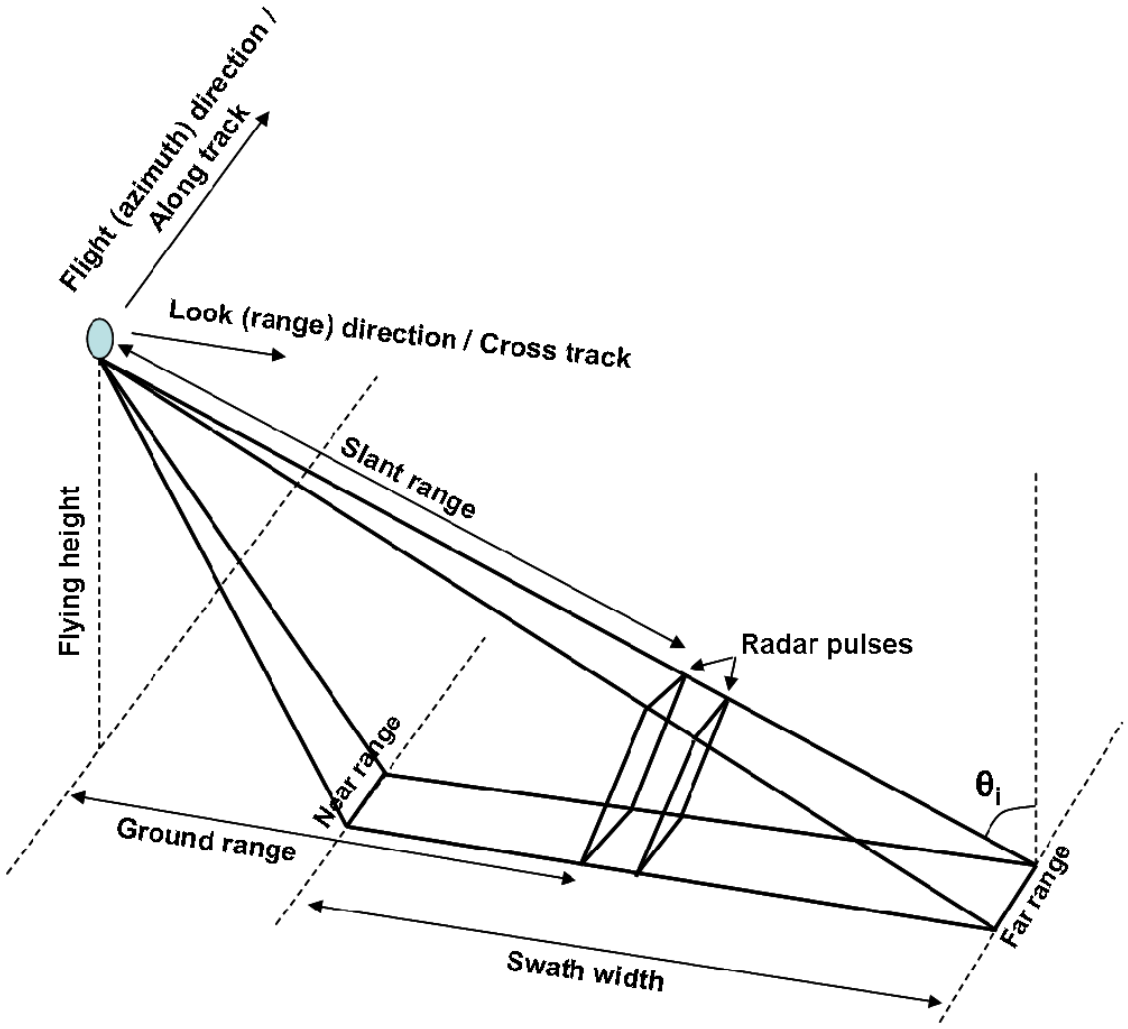

Figure 3.1: Diagrammatic representation of SAR viewing geometry. Incidence angle is indicated by θ_i (Compiled from: Trevett (1986) and Woodhouse (2006a))

strength of the radar backscatter) with range calculations (i.e. the distance of the reflecting target from the antenna) based on radar signal return time. The first example of this method was airborne Side-Looking Airborne Radar (SLAR) or Real Aperture Radar (RAR), but Synthetic Aperture Radar[7] (SAR) is now commonly used since the system geometry allows for higher azimuth resolution at longer range distances and therefore enables operation from space at high resolutions. Due to its

[7] SAR simulates a longer antenna by utilising the large range distance combined with the movement of the antenna along the flight path, giving the effect of a coherent combination of a collection of antennas; azimuthal resolution is improved as a result. Range resolution is determined by the bandwidth of the radar system (Woodhouse, 2006a).

viewing geometry, SAR data collection can be limited in areas with mountainous terrain as the topography causes shadowing and layover (see Woodhouse (2006a)). At a more localised level, layover can cause challenges e.g. at forest edges (Woodhouse, *et al.*, 2006) or due to emergent trees from a dense canopy (Hoekman and Varekamp, 2001).

For vegetation, the amount of microwave backscatter is affected by:

- "Roughness", determined mainly by roughness properties of the soil and vegetation such as leaf size and density, as well as the geometry of the vegetation such as branch size and orientation (Kasischke, *et al.*, 1997, Long, *et al.*, 2001)
- Dielectric properties, determined mostly by the moisture content and temperature and the phase state of water (e.g., whether vegetation is frozen or not) (Long, *et al.*, 2001, Le Toan, *et al.*, 2004).

In the case of SAR and side-looking scatterometry the local viewing geometry, governed by the local incidence angle, determines the amount of microwave backscatter returned from the ground target(s). This is also true for the wavelength (see Table 3.1) and polarisation (Le Toan, *et al.*, 1992, Patenaude, *et al.*, 2005, Woodhouse, 2006a). As a forest canopy contains structural components of different sizes, shapes, orientations, number densities and dielectric properties, the interaction of microwaves with the vegetation canopy is complex. Backscatter is strongest when the microwave wavelengths are of the same order as the structural components in the vegetation canopy (see also Fig. 3.2) (Le Toan, *et al.*, 1992, Kasischke, *et al.*, 1997, Le Toan, *et al.*, 2004, Woodhouse, 2006a, 2006b). In particular,

- X-band scatters strongly from twigs and leaves in the upper part of the canopy;
- C-band penetrates deeper into the canopy and scatters strongly from slightly larger twigs and small branches. Scattering mechanisms include direct scattering from the canopy elements as well as multiple scattering between the branches and trunk within the canopy with a minor contribution from the foliage;
- L- and P-band penetrate through the canopy and receive the greatest part of scattering from the trunk and the lower part of the canopy. Backscattering mechanisms that occur most frequently are direct backscattering from the

branches in the canopy, trunk-ground double bounce and direct scattering from the ground; the latter two are attenuated twice by the canopy as the microwaves propagate through the canopy;

- VHF receives virtually all backscatter from the underlying ground and the largest tree trunks.

Microwave polarisation is associated with the orientation of the electric field in the plane perpendicular to the propagation direction, of which the most commonly used are HH, VV and HV[8] (or VH). Polarisation in combination with the orientation of the targets affect backscatter (i.e., the response of a target normally changes with the polarisation thus enabling land cover classification) (Imhoff, 1995b). In general, HV polarisation causes highest backscatter from the canopy elements, HH polarisation causes highest backscatter from trunks (due to the interaction between ground and trunk), while VV polarisation causes highest backscatter from the ground (Woodhouse, 2006a). Due to their complexity and the way that microwaves interact with the different elements of the canopy, forest canopies are often modelled as a random volume (e.g., the Random Volume over Ground model; RVoG, Papathanassiou and Cloude (2001)), which assumes that all scatterers of different sizes are randomly orientated and distributed to represent the range of sizes and orientations within the forest; forming a statistically homogeneous medium.

Table 3.1 Microwave wavelengths commonly used for forestry applications (Sources: Woodhouse (2006a), Rosenqvist, *et al.* (2007))

Radar Band	Frequency (GHz)	Wavelength (cm)	Wavelengths of the data used in this study (see 5.2.1) (cm)
X	8 - 12	2.5 – 3.8	3 (Intermap STAR-3i)
C	4 - 8	3.8 – 7.5	5.6 (AIRSAR, SRTM)
L	1 – 2	15.0 – 30.0	24 (AIRSAR)
P (UHF)	0.3 - 1	30.0 – 100.0	68 (AIRSAR)
VHF	0.03 - 0.3	100.0 – 1,000.0	-

[8] H (Horizontal) and V (Vertical) indicate the orientation of the transmitter (second letter) and receiver (first letter) respectively. HV therefore indicates that vertical waves are transmitted while horizontal waves are received.

SAR, Interferometric SAR (InSAR), polarimetric InSAR (POLInSAR), SAR tomography and scatterometry are radar methods that have been applied to forest areas for biomass estimation or forest extent mapping. Although the use of radar for biomass estimation has been widely investigated for temperate forests (usually managed) (Le Toan, *et al.*, 1992, Kellndorfer, *et al.*, 2003, Walker, *et al.*, 2007b), boreal forests (Hagberg, *et al.*, 1995, Smith and Ulander, 2000) and tropical rainforests (Kasischke, *et al.*, 1995, Luckman, *et al.*, 1997, Ranson, *et al.*, 1997a, Hoekman and Varekamp, 2001), tropical savannas have been largely neglected in biomass estimates by EO (examples are cited in the sections below). This leaves a significant knowledge gap, as savannas cover approximately 20% of the Earth's surface and form the third most productive terrestrial ecosystem after tropical and temperate forests (see 2.4).

The remainder of this section discusses biomass estimation applications for the different radar EO methods, with more emphasis on SAR and InSAR methods and citing examples of applications in savannas where appropriate. For completeness, other methods such as POLInSAR, SAR tomography and scatterometry are included but are only briefly discussed.

3.3.3.1. SAR

One of the first large scale applications of radar land cover mapping was Projeto Radambrasil, which provided a comprehensive map of the whole of Brazil in the 1970s (Furley, 1986). This project relied on manual classification of SLAR images, using image grey tone and texture for vegetation mapping. Digital methods such as maximum-likelihood classification and knowledge-based techniques are now more commonly used (Kasischke, *et al.*, 1997). Image segmentation can utilise geometric, textural and topological characteristics to improve classification of the individual segments by overcoming radar speckle (e.g. Dong, *et al.* (2001)). Land cover types can be distinguished based on the fact that different wavelengths and polarisations react differently to the various components of the vegetation canopy (Kasischke, *et al.*, 1997, Hoekman and Quiñones, 2000, Dong, *et al.*, 2001, Santos, *et al.*, 2007) and the use of multi-temporal data can improve classification accuracies, especially as forest areas have a greater temporal stability compared to other land cover (Quegan,

et al., 2000). SAR has been shown to be especially effective for the differentiation of major structural differences in land cover such as forest/non-forest areas and the detection of inundation, especially under a vegetation canopy (Kasischke*, et al.*, 1997). The spatial resolution of spaceborne SAR, when used for land cover classification, can be a limiting factor as the minimum mapping unit of land cover patches should be considerably larger than the SAR spatial resolution. This is caused by the smoothing associated with speckle filtering which can reduce the spatial resolution by a factor of ~3 (Patenaude*, et al.*, 2005).

An advantage of radar EO over passive optical EO, is that radar backscatter can be related to forest stand parameters such as dominant height, basal area, branch dimensions and orientation, volume and biomass, particularly at HV polarization (Le Toan*, et al.*, 1992, Ranson and Sun, 1994, Ferrazzoli and Guerriero, 1995, Imhoff, 1995b, Kasischke*, et al.*, 1997, Kellndorfer*, et al.*, 2003). The existence of an empirical relationship between forest biomass and SAR backscatter has been increasingly used to estimate biomass over the past 10 years (Woodhouse, 2006a). However, the signal saturates with respect to biomass at a certain point, depending on wavelength, polarisation and study area; areas with higher biomass than the saturation level do not experience a concomitant increase in backscatter. Studies over different forest types, i.e. tropical, temperate and boreal, (Imhoff, 1995b, Luckman*, et al.*, 1997, Hoekman and Quiñones, 2000, Le Toan*, et al.*, 2004) have shown that C-band commonly saturates at biomass densities of ~20-30 t/ha, L-band at ~40-60 t/ha, P-band at ~100-200 t/ha and VHF at ~500 t/ha. Variations in saturation levels depend on the experimental conditions and the forest characteristics (Le Toan*, et al.*, 2004). The saturation level increases with wavelength, while HV polarisation yields a higher saturation level followed by HH and VV in differing orders (Le Toan*, et al.*, 1992, Kasischke*, et al.*, 1997, Kellndorfer*, et al.*, 2003). Longer wavelengths, preferably at HV polarisation, are therefore normally used for biomass-backscatter relationships. The contrast between HH and VV backscatter is greatest for a smaller amount of vegetation (Woodhouse, 2006a).

Due to the occurrence of saturation levels, forests at the high end of the biomass scale may present challenges for monitoring as they require longer wavelengths, of which P-band and VHF are currently not operational from space[9]. According to (Imhoff, 1995b), only 19% of the world's terrestrial biomass has biomass densities lower than the P-band saturation level[10]. The figures for L-band and C-band are 7.4% and 4% respectively. However, Kasischke *et al.* (1997) review alternative approaches based on the use of multi-channel radar data or multi-step approaches which considerably improve on the maximum biomass densities mapped by single frequency/polarisation methods. These are based on the premise that, apart from AG biomass density, radar backscatter is also related to various other forest characteristics related to biomass, such as basal area, tree height, tree number densities and the relationship between these components (Imhoff, 1995a, Kasischke*, et al.*, 1997, Lucas*, et al.*, 2004, Woodhouse, 2006b). The exclusion of high biomass forests through the occurrence of saturation levels has caused ongoing debate on the type of sensor to be included on a global biomass mapping satellite mission. At the time of writing ESA were planning a P-band BIOMASS[11] mission on the Earth Explorer series of satellites, although L-band was still considered an option. Those who favour P-band do so because of the higher saturation level, although operating a P-band sensor from space is particularly challenging and will therefore have a much lower spatial resolution compared to spaceborne L-band sensor capabilities. Currently, the newly launched ALOS PALSAR sensor (L-band) with a systematic observation strategy for acquiring near-global data (see Rosenqvist, *et al.* (2007)) over the first years of its lifespan is providing the opportunity to test fully polarimetric L-band data for global forest biomass estimation and monitoring (see 3.4).

There is a persistent assumption that backscatter intensity at long wavelengths will be sufficient to estimate biomass in savannas since they have biomass density that

---

[9] Due to the allocation of bandwidth and interference from the ionosphere, which becomes increasingly more of a problem with increasing wavelength (Woodhouse, 2007).

[10] Imhoff (1995b) cites a saturation level of 100 t/ha for P-band, 40 t/ha for L-band and 20 t/ha for C-band.

[11] See www.esa.int/esaLP/SEMFCJ9RR1F_LPfuturemis_0.html for more information.

generally falls under the saturation levels experienced for P-band in various studies. Savanna biomass density typically ranges from ~45 to ~130 t/ha (House and Hall, 2001), although lower biomass density has been reported (e.g. the study area of this research as estimated by Brown, *et al.* (2005)). However, this assumption has not been adequately validated. As the results of this research point out (see Chapter 6), the problems associated with SAR mapping of savannas are primarily related to the heterogeneous or patchy vegetation structure and low density of woodland in savanna areas. A further complication has been proposed (Woodhouse, 2006b) whereby a theoretical study implies that low density woodland will result in backscatter saturation at much lower biomass densities than is currently assumed. Current field data is insufficient[12] to evaluate SAR signal saturation for the savannas of the study area and should be pursued in future research.

The use of different (combinations of) wavelengths and polarisations of SAR has been investigated for savanna and savanna woodland classification (Hoekman and Quiñones, 2000, Lucas*, et al.*, 2006b, Lucas and Armston, 2007), biomass mapping (Santos*, et al.*, 2002, Lucas*, et al.*, 2004, Lucas*, et al.*, 2006a) and fire scar mapping (Menges*, et al.*, 2004). Interestingly, Lucas *et al.* (2006a) report non-typical saturation levels for their savanna woodlands; C-band HV saturated on average at 53 t/ha and L-band HV at 78 t/ha (both saturating at higher levels than studies in closed forests), while P-band HV saturated at an average of 62-72 t/ha which is a lower saturation level than reported for closed canopy forests.

3.3.3.2. InSAR

By combining two SAR measurements from antennas displaced in space and/or time, the phase difference between the two returned signals can be measured. This method is called interferometric SAR (InSAR, or IfSAR; Woodhouse (2006a)). Many InSAR viewing geometries exist, but the following discussion will focus only on single-pass interferometry as this study uses this type of data (see 5.2.1). Single-pass interferometry is achieved when two antennas on a platform are displaced in the

[12] The field data was collected specifically to evaluate, at a local level, SAR backscatter response and InSAR vegetation height retrieval based on detailed vegetation measurements (see 5.3). To evaluate SAR saturation for the savannas of the study area, field data is needed on woodland patch and forest plot biomass, covering a range of biomass densities.

across-track direction; the displacement between the two antennas is referred to as the *baseline*. By measuring the phase difference between the two radar signals for corresponding points in an image pair, an altitude can be calculated (Madsen and Zebker, 1998, Woodhouse, 2006a). This provides a three-dimensional model of the Earth's surface, commonly referred to as a Digital Elevation Model (DEM; Hoffman and Walter (2006), Rodríguez, *et al.* (2006)).

Combined with the typical interactions of SAR backscatter with forest environments (described above), InSAR can be used to estimate tree height[13]: single-pass shortwave InSAR such as X-band and C-band (see Table 3.1, Fig. 3.2) penetrate a full cover vegetation canopy by only a few wavelengths (Hofton*, et al.*, 2006, Woodhouse, 2006a). The retrieved three-dimensional surface model therefore approximates the near top of the vegetation canopy, hereafter referred to as a Digital Surface Model (DSM; Neeff*, et al.* (2005), Rowland and Balzter (2007)). A DSM is essentially a DEM with vegetation bias; the vegetation bias can be used to estimate vegetation height by subtracting the known ground surface under the forest, in the form of a ground survey-derived DEM, from the DSM (Hagberg*, et al.*, 1995, Askne*, et al.*, 1997). Alternatively, an InSAR-derived DSM created with longer wavelength InSAR such as P-band or L-band can be used when a survey-derived DEM is unavailable (Hagberg*, et al.*, 1995, Neeff*, et al.*, 2005, Balzter*, et al.*, 2007). This is possible because longer wavelength radar can penetrate the forest canopy up to the near-ground surface depending on the forest characteristics (e.g., density and homogeneity (see Fig. 3.2)). In contrast to LiDAR measurements which measure the actual top of the vegetation canopy (see Fig. 3.2), the vertical location of the InSAR retrieved height is determined by a combination of the relative scattering contributions of the vegetation stems, branches and leaves, and the ground surface combined with radar characteristics such as wavelength, polarisation and incidence angle which determine the vertical placement of the scattering phase centre (SPC) (Sarabandi and Lin, 2000, Woodhouse*, et al.*, 2006, Balzter*, et al.*, 2007, Dall, 2007).

[13] As discussed in 3.2, tree height is an important indicator of biomass (Overman, et al. (1994), Brown, (2002a), Patenaude, et al. (2004)). Allometric equations based on tree height, on occasion combined with tree species or generic grouping, can sometimes be used to estimate the above-ground biomass of a forest.

Volume scattering caused by the vegetation decreases the InSAR coherence, adds noise to the interferometric phase centre and displaces the SPC from the surface of the canopy (Dall, 2007); locating it anywhere between the canopy and the ground (Hofton, *et al.*, 2006, Simard, *et al.*, 2006). Due to characteristic interactions with the vegetation canopy, different SAR wavelengths produce different vertical locations of the mean SPC (see Fig. 3.2). Normally shorter wavelengths locate the SPC near the canopy top, while longer wavelengths locate the SPC near the ground surface. Due to this canopy penetration, underestimation of InSAR-derived vegetation height is typically expected to be (slightly) higher than for LiDAR height extraction methods (Wallington and Suárez, 2007), although this depends on the forest canopy characteristics (e.g., density and homogeneity) and the InSAR and LiDAR sensor characteristics (e.g., InSAR wavelength and polarisation and LiDAR footprint size and point density) (Carabajal and Harding, 2006, Woodhouse, *et al.*, 2006, Wallington and Suárez, 2007). Other factors that affect vegetation height retrieval from InSAR are crown shape, tree height, steep topography and the presence of emergent trees (Izzawati, *et al.*, 2006). Calibration of InSAR-derived DSMs and DEMs using ground reference data can improve tree height estimations (Hagberg, *et al.*, 1995, Izzawati, *et al.*, 2006, Wallington and Suárez, 2007) as consistent tree height underestimation can be accounted for and consistent bias with respect to the bare ground surface, normally quoted as a vertical accuracy range (e.g. see 5.2.1), can be adjusted for. Wallington *et al.* (submitted) give an overview of the accuracies obtained for canopy height retrieved by InSAR.

Unlike optical correlation methods, interferometric canopy height retrieval is not limited by the availability of light and canopy closure. In fact, the technique works best for full cover forest canopies (Hagberg, *et al.*, 1995, Izzawati, *et al.*, 2006). The use of InSAR for canopy height retrieval has been successfully applied in dense homogeneous forests such as temperate (Wallington, *et al.*, 2004, Walker, *et al.*, 2007b), tropical (Hoekman and Varekamp, 2001, Neeff, *et al.*, 2005) and boreal forests (Hagberg, *et al.*, 1995, Askne, *et al.*, 1997) as well as mangroves (Simard, *et al.*, 2006). Data fusion of InSAR with LiDAR and optical data has been investigated (Slatton, *et al.*, 2001, Walker, *et al.*, 2007a), as has the use of SRTM (see 5.2.1.3) data for national or global canopy height maps (Carabajal and Harding, 2006,

Hofton, *et al.*, 2006, Walker, *et al.*, 2007b). However, the use of InSAR for vegetation height retrieval has not been sufficiently tested in sparse heterogeneous forests. The heterogeneous structure and low vegetation density of savanna woodland may cause problems for InSAR-derived canopy height estimates (Hagberg, *et al.*, 1995, Izzawati, *et al.*, 2004, Mette, *et al.*, 2004). This study acknowledges this knowledge gap by investigating the application of InSAR for tree height retrieval in a sparse savanna woodland.

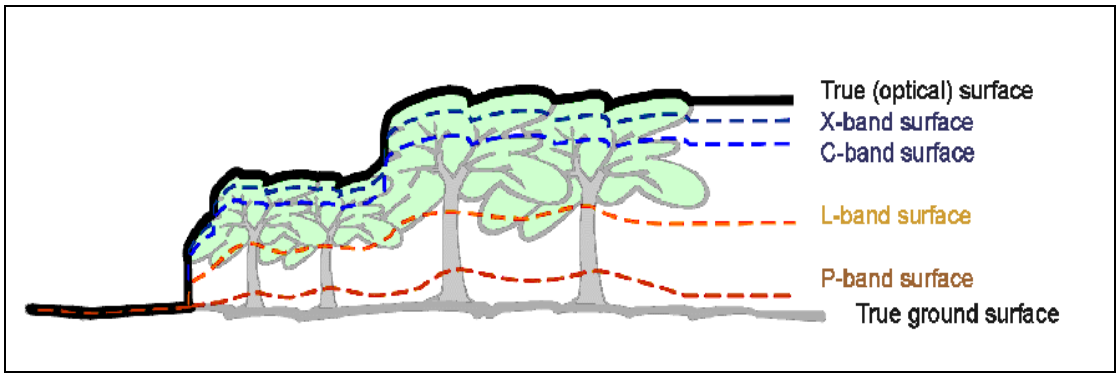

Figure 3.2: Comparison of true canopy surface with the typical scattering phase centres (SPCs) for different InSAR wavelengths (Woodhouse (2007) ©). The true (optical) surface can be seen as the level at which LiDAR measures canopy height.

An alternative way in which InSAR can be used for land cover classification is related to the occurrence of decorrelation in forests. The presence of a large vertical spread of scatterers cause increased (volume) decorrelation, which normally cause difficulties in the generation of an unambiguous DSM. In the case of repeat-pass InSAR, forests experience temporal decorrelation (Wegmüller and Werner, 1997, Woodhouse, 2006a). This decorrelation can be used for land cover classification (e.g. Wegmüller and Werner (1997)) if used in conjunction with SAR backscatter intensity and texture.

3.3.3.3. POLInSAR

Polarimetric SAR interferometry (POLInSAR; (Cloude and Papathanassiou, 1998, Papathanassiou and Cloude, 2001) uses the polarimetric information from single frequency InSAR to distinguish between canopy and ground. As this technique depends on SAR penetration to the ground surface to obtain, in an ideal situation, equal backscattering contributions from the canopy and the ground, fully

polarimetric L-band is usually most suitable (Cloude and Papathanassiou, 1998, Woodhouse*, et al.*, 2003). The canopy mainly consists of a combination of randomly orientated elements (leaves, twigs and branches) and therefore acts as a random scattering volume with no preference for a specific polarisation response. In contrast, the ground surface and trunk-ground interactions have a distinctive polarimetric response (Woodhouse, 2006a). This differentiation between crown and ground scattering enables forest height (DSM) and ground height (DEM) retrieval (Papathanassiou and Cloude, 2001, Woodhouse*, et al.*, 2003, Mette*, et al.*, 2004) by inverting a forest backscattering model, the Random Volume over Ground (RVoG) model (Papathanassiou and Cloude, 2001). RVoG models a forest with randomly oriented and distributed scattering elements in a canopy layer, thus forming a statistically homogeneous medium. The differences in coherence for the polarisations together with the extinction coefficient are input to the model. Various PolInSAR-based vegetation height estimation is an area of research that is still undergoing development. A review of canopy height retrieval studies using POLInSAR and their accuracies is given in Wallington, *et al.* (submitted).

3.3.3.4. SAR tomography

SAR tomography is a new, developing method whereby several (ideally more than 10) polarimetric data acquisitions are used together to retrieve fully volumetric data of a forest. This is achieved by the formation of an additional synthetic aperture in elevation by a coherent combination of data acquired in several flight paths (Guillaso and Reigber, 2005). The outcome is, in effect, a three-dimensional image (tomogram) of the land cover (e.g., forest) showing the variations in backscatter properties in the horizontal as well as the vertical (Reigber and Moreira, 2000, Guillaso and Reigber, 2005, Woodhouse, 2006a). The top of a volumetric scatterer such as a forest canopy and the ground surface can be identified from a tomogram, from which forest height can be retrieved, depending on the wavelength used (Guillaso and Reigber, 2005, Reigber*, et al.*, 2005). For forest, L- and P-band is more suitable (Reigber and Moreira, 2000) due to their ability to penetrate the forest volume. Theoretically, the accuracy of the height retrieval depends on the wavelength and polarisations of the microwave radiation and the resolution of the

tomogram. The latter depends on the maximum baseline between flight paths; a higher maximum baseline gives a higher resolution. The maximum baseline, in turn, is limited by the forest height (taller vegetation requires shorter baselines and therefore requires more flight paths to retain the height resolution), the flying height and the wavelength used (Reigber and Moreira, 2000).

Originally developed for medical applications, the first tomographic experiment over a forest was carried out with an airborne system (DLR's L-band E-SAR) (Reigber and Moreira, 2000). As airborne tomography presents several difficulties, the technique has been investigated using a C-band spaceborne dataset from ERS-1 (She, *et al.*, 2002, Fornaro, *et al.*, 2005). As resolution depends, amongst others, on the flying height, height retrieval from spaceborne tomography is expected to be less accurate. For forest height retrieval from spaceborne tomography, the use of L-band data needs investigation. A review of canopy height retrieval accuracies to date is given in Wallington *et al.* (submitted).

3.3.3.5. Scatterometry

Although scatterometers were originally designed and used for wind observations, they are increasingly applied for land applications such as monitoring of changes in soil moisture, detection of regional flooding, vegetation monitoring (Evans, *et al.*, 2005) and monitoring of ice (Long, *et al.*, 2001). The scatterometer transmits a microwave pulse at a range of incidence angles (Long and Hardin, 1994). By sacrificing range accuracy and spatial resolution scatterometers can very accurately measure the radar cross-section of a target (Woodhouse, 2006a), enabling the precise measurements of differences in backscatter as low as 1-2 dB (Long, *et al.*, 2001). As for SAR, the backscatter intensity depends on the roughness and dielectric properties of the surface target (see 3.3.3). These measurements can be particularly interesting for vegetation canopies since they allow microwaves to penetrate the canopy to a level which is determined by the microwave wavelength and the characteristics of the forest canopy, giving accurate measurements of the backscatter response of the forest as a function of the penetration depth (Woodhouse, 2006a).

As the first operational system was carried on the NASA Seasat mission from 1978 (Evans, *et al.*, 2005), relatively long records of spaceborne scatterometer data exist.

The wide swath provides near-daily coverage at resolutions of ~25-50 km over a range of incidence angles (20-55º) (Long, *et al.*, 2001). Consequently, scatterometry can supplement higher resolution instruments which often have narrow swaths with limited coverage and incidence angle diversity (Long and Hardin, 1994). Land studies using scatterometry have been primarily based on the changes related to soil and vegetation moisture content and the seasonal freeze-thaw cycle (Long, *et al.*, 2001). Spaceborne scatterometry is therefore potentially useful for investigating long-term changes in vegetation, such as drying or thawing, due to climate change. Several studies have linked scatterometry with vegetation parameters (Woodhouse, *et al.*, 1999, Woodhouse and Hoekman, 2000, Grippa and Woodhouse, 2002), low amounts of biomass (Macelloni, *et al.*, 2003), the detection of broadleaf growing season canopy dynamics (Frolking, *et al.*, 2006) and vegetation classification in the Amazon basin, including savanna vegetation formations (Long and Hardin, 1994) and savanna grass formation monitoring (Hardin and Jackson, 2003).

Airborne scatterometers, primarily from a helicopter platform (e.g. HUTSCAT (Hallikainen, *et al.*, 1993)), have been investigated for forest applications (Hyyppä and Hallikainen, 1993). The use of a helicopter platform provides the opportunity to allow longer integration time for measurements (Woodhouse, 2006a). Studies have shown good results for mean canopy height and dominant tree height retrieval using fully polarimetric X- and C-band at near-nadir over boreal forests (Hyyppä and Hallikainen, 1993, 1996) and even-aged homogeneous pine plantations (Martinez, *et al.*, 1998, Martinez, *et al.*, 2000). Reported precision of the retrieved heights (1-1.5 m) are in the same order as *in situ* measurements (Hyyppä and Hallikainen, 1996, Martinez, *et al.*, 1998, Martinez, *et al.*, 2000). Retrieved heights have, in turn, been correlated with stem volume, basal area and biomass. A recent study (Praks, *et al.*, 2007) used HUTSCAT-retrieved canopy height over boreal forest to validate airborne L- and X-band POLInSAR-retrieved canopy height and found a strong correlation ($R^2 \geq 0.75$). Coupling of a radiative transfer model with scatterometer data has increased understanding of backscatter mechanisms within a forest canopy (Martinez, *et al.*, 2000). Furthermore, using a principal component method, the radar return vs. range spectrum has been used to successfully identify tree species in the boreal forest (Hallikainen, *et al.*, 1990).

3.4. Global projects for biomass estimation

The recognition of biomass as one of the most important parameters of the global carbon cycle, and therefore an important determinant for global climate change modelling, has given rise to a number of global projects for biomass estimation over the past decades. A distinction can be made between projects that rely mainly on EO for global biomass estimates (see Table 3.3), and those that do not rely on EO or have an indirect link to EO-related biomass and carbon studies (see Table 3.2). Due to the strong spatial element in global biomass estimates, there are fewer of the latter.

The value of EO for global biomass projects is recognised for its spatially comprehensive data acquisition capabilities at repeated intervals. The biomass and carbon research community need mainly vegetation-related products with a known accuracy that are consistent and span the widest possible temporal range (Plummer, *et al.*, 2006). Most of the EO global biomass projects focus on mapping forest cover or land cover extent, which account for patterns of vegetation structure and activity (Hese, *et al.*, 2005). Based on this input, Dynamic Global Vegetation Models or global carbon-climate models can be used to simulate a full carbon account of entire ecosystems, including the surfaces that are not easily monitored by EO, such as the soils. Global biomass mapping projects that are based on EO have been mainly driven by space agencies such as the European Space Agency (ESA) and the Japanese Aerospace Exploration Agency (JAXA). Biomass and carbon projects initiated by ESA fall under either the Treaty Enforcement Services Using Earth Observation (TESEO) initiative, which focused on the use of EO for information provision to aid international treaties and conventions (e.g., Ramsar and UNFCCC or the Data User Element (DUE) programme) which promotes the development of EO services that fit the needs of end-user communities (ESA, 2007). Initiatives running under these flags include TESEO-Carbon, Kyoto Inventory, GlobCarbon, GlobColour (see Table 3.3), and use a combination of SAR and optical sensors. In contrast, the JAXA initiatives, Global Rain Forest and Global Boreal Forest Mapping project (GRFM/GBFM) and ALOS Kyoto & Carbon Initiative (see Table 3.3), are based solely on JERS-1 and ALOS PALSAR data respectively.

As a non-EO initiative, the Global Carbon Project (GCP) focuses on increased understanding of the natural and human elements of the global carbon cycle, primarily through the coordination and integration of research and modelling. An earlier initiative, FLUXNET, relies mainly on flux towers to measure CO_2, water vapor, and energy exchanges between vegetation canopies and the atmosphere (Baldocchi, *et al.*, 2001); improving the understanding of CO_2 exchanges between vegetation and the atmosphere. The limited sampling and lack of spatial element in flux measurements (Hese, *et al.*, 2005) is addressed by combining the numerous regional networks that together form FLUXNET (Baldocchi, *et al.*, 2001). Interestingly, one of the main aims of FLUXNET, later added after a funding contribution from NASA, is to provide data to validate EO-based estimations of net primary productivity, evaporation and energy absorption based on observations by NASA's EOS/Terra satellite. A new venture by NASA JPL, the Orbiting Carbon Observatory (OCO) which is planned for launch in 2008, aims to collect global measurements of carbon dioxide (CO_2) in the Earth's atmosphere. This will provide the first space-based CO_2 measurements. The Integrated Global Carbon Observation (IGCO) initiative also links with EO: it aims to set up a coordinated system of integrated global carbon cycle observations by combining global systematic *in situ* and EO-based observations of the carbon cycle. This will bring together observational strategies for terrestrial (through Global Terrestrial Observing System, GTOS), oceanic (through Global Ocean Observing System, GOOS) and atmospheric environments (through Global Climate Observing System, GCOS) and links with the modelling outcomes of the GCP. GTOS again links more directly with EO data products through one of its panels, Global Observation of Forest and Land Cover Dynamics (GOFC-GOLD), which forms a coordinated effort to provide ongoing EO-based and *in situ* observations of forests and other vegetation cover (see Table 3.3).

3.5. Summary

This chapter has given an overview of different methods for biomass estimation, culminating in an overview of past and current global biomass estimation projects using several of these methods. *In situ* biomass estimation methods involve laborious fieldwork based on sampling and sometimes require destructive techniques. The

development and use of allometric models for biomass estimation carries the risk of error propagation mainly through measurement and sampling errors. Sampling, especially, can lead to large errors in regional biomass estimates upon extrapolation. Due to the exclusion of mainly the largest and smallest trees and by avoiding disturbed forest, regional biomass estimates based on *in situ* methods are unlikely to accurately portray the heterogeneity of the landscape.

Under the Kyoto Protocol there is a clear need for accurate information on the spatial extent, biomass stock and growth potential of forests and woodlands ranging from dense tropical forests to sparse woodlands with a canopy cover as low as 10%. This information should be readily available at regional and national scales. Moreover, there is a need for increased understanding of the dynamic nature of tropical biomass caused by climate change and human pressure, especially in savannas and forest-savanna boundaries. A range of existing Earth observation (EO) techniques offer systematic observations at scales ranging from local to global, enabling frequently updatable biomass estimates which more accurately represent the spatial heterogeneity of the landscape. Moreover, EO improves the ability to monitor inaccessible areas.

Optical EO has been linked to canopy height and AG biomass, mainly through vegetation indices, but these methods have been shown to saturate at relatively low levels of biomass. Furthermore, optical EO is limited by cloud cover in the tropics. Active EO such as radar is therefore more practical for biomass studies in the tropics. Radar EO can be used for forest biomass estimation through known interactions of different radar wavelengths and polarisations with different parts of the vegetation canopy. Various radar techniques exist, providing different ways to estimate AG biomass. The existence of an empirical relationship between forest biomass density and SAR backscatter has been utilised to obtain estimates of AG biomass up to a saturation level, depending on the wavelength and polarisation used combined with forest characteristics. Based on these saturation levels, there is a persistent assumption that backscatter intensity at long wavelengths will be sufficient to estimate biomass in savannas since they have lower biomass levels. However, this has not been sufficiently investigated. InSAR, POLInSAR, SAR tomography and scatterometry can provide estimates of canopy height, which can be used in

conjunction with allometric equations to obtain estimates of AG biomass. A degree of underestimation is expected due to the penetration of microwaves into the forest canopy, the accuracy of which is dependant on a combination of radar characteristics (e.g. wavelength and polarisation) and forest characteristics (e.g. density and uniformity).

The recognition of biomass as one of the most important parameters of the global carbon cycle has given rise to a number of global biomass and carbon studies. A diversity of such projects exists of which most rely on EO data and methodologies due to its spatially comprehensive data acquisition capabilities at repeated intervals. The focus falls mainly on mapping forest cover or land cover extent to provide patterns of vegetation structure and change which can be input in global carbon-climate models. Unsurprisingly, these EO-based global biomass mapping projects have been largely driven by space agencies, primarily the European Space Agency (ESA) and the Japanese Aerospace Exploration Agency (JAXA). Most of these projects are short-lived and seem mostly for marketing purposes, but the JAXA initiatives based first on JERS-1 data and currently on ALOS PALSAR data is a first attempt to set up a near-global record of forest biomass monitoring by L-band SAR.

Table 3.2: A summary of major non-EO global biomass projects, in chronological order.

Project	Remit and Aim	Time frame	Main research themes	Project partners
FLUXNET	Promotes the synthesis and analysis of long-term carbon, water, and energy flux data acquired globally by various regional flux networks. Supports data sharing and calibration and flux intercomparison activities. A main goal is to provide data for validating estimations of net primary productivity, evaporation and energy absorption based on observations by NASA's EOS/Terra satellite (Baldocchi, *et al.*, 2001). See for more information: www.fluxnet.ornl.gov/fluxnet/index.cfm	1997, ongoing	Pattern identification Identification of global temporal and spatial patterns of carbon, water, and energy fluxes that may not be detectable by regional networks. Value-added products Production of value-added products on stand-scale CO_2, water, and energy fluxes by synthesizing data at the biome, cross-biome, continental, and global scales. Central database Supporting a central database for the archiving, documenting, and disseminating of flux data and supporting metadata on climate, site, vegetation, and soil characteristics EO and model validation FLUXNET data is used to support validation of EO land products and ecosystem models.	FLUXNET links the following regional flux networks: AmeriFlux (North and South America), CARBOEUROFLUX (Europe), OzFlux (Australia and New Zealand), Large-Scale Biosphere-Atmosphere Experiment (LBA) (South America), AsiaFlux (Japan, Korea, China, Malaysia, Thailand, Indonesia, Siberia), KoFlux (South Korea), Safari2000 (Southern Africa), TropiFlux (Panama), CARBOMONT (European mountain ecosystems), Fluxnet-Canada, TCOS-Siberia ChinaFlux
Global Carbon Project (GCP)	Aims to develop comprehensive understanding, relevant to policy, of the natural and human elements of the global carbon cycle and their interactions and feedbacks. To obtain this, an internationally consistent framework for the coordination and integration of research of the carbon-climate-human system is provided on regional and global scales. Model development and implementation is a primary activity (Plummer, *et al.*, 2006). See for more information: www.globalcarbonproject.org	2001, ongoing	Patterns and Variability Distribution over space and time of major regional and global pools and fluxes. Processes and Interactions Natural and human-driven carbon sources and sinks, emphasising links between cause and effect. Carbon Management Future dynamics of carbon-climate-human system and management opportunities.	Joint project of: the Earth System Science Partnership (ESSP) the International Geosphere-Biosphere Program (IGBP), the International Human Dimensions Program (IHDP), the World Climate Research Program (WCRP) DIVERSITAS

Integrated Global Carbon Observation (IGCO) A theme of the Integrated Global Observing Strategy Partnership (IGOS-P)	Aims to develop close collaboration with the international carbon cycle research community, e.g. by integrating its operational observations with GCP models. The main objectives are to provide long-term observations to improve understanding of the global carbon cycle, particularly the factors that control global atmospheric CO_2 levels and to monitor and assess the effectiveness of carbon sequestration and emission reduction activities on global atmospheric CO_2 levels (Ciais, *et al.*, 2007). See for more information: ioc.unesco.org/igospartners/Carbon.htm	Approved in 2003, ongoing Phase 1 (preparation): 2003-2006 Phase 2 (demonstration): 2006-2010 Planned to be operational in 2015	Improved knowledge base for better policy-making Working towards a coordinated international approach to provide improved understanding for the implementation of the Kyoto Protocol. Enhanced scientific understanding of the global carbon cycle Improving understanding of the current patterns of carbon stocks and flows and prediction of their changes in the future, to be done in close collaboration with IGBP and its partner global environmental change programmes, which have launched an international carbon research project that integrates multiple approaches, process studies, manipulative experiments, observations and models. Advanced Earth System observation capability Development of algorithms to map from EO satellites (e.g. Landsat, ALOS) the global distribution and temporal variability of forest cover and other land cover, biomass information, vegetation phenology and fires. Also, improvement of CO_2 distribution mapping from existing satellites, e.g. SCIAMACHY.	The Integrated Global Observing Strategy (IGOS) Partnership consists of the following members: Food and Agriculture Organization (FAO) Global Climate Observing System (GCOS) Global Ocean Observing System (GOOS) Global Terrestrial Observing System (GTOS) International Council for Science (ICSU) International Geosphere-Biosphere Programme (IGBP) (Lead) National Aeronautics and Space Administration (NASA/CEOS) United Nations Educational, Scientific and Cultural Organization (UNESCO)

Table 3.3: A summary of major EO global biomass projects, in chronological order.

Project	Remit and Aim	Time frame	Products and sensors	Contributors and End-users
Global Rain Forest and Global Boreal Forest Mapping project (GRFM/GBFM)	Aimed to develop operational forest monitoring techniques for tropical and boreal forests globally (Rosenqvist, *et al.*, 2000). See for more information: www.eorc.jaxa.jp/JERS-1	1996-1998 (last 3 years of JERS-1 operational life)	Spatially and temporally contiguous L-band SAR data were acquired for tropical and boreal forest areas, from which semi-continental scale, 100 m resolution, image mosaics were produced. The GRFM project is divided into geographical regions : South-East Asia, Australia, South and Central America, and Equatorial Africa. The GBFM project is divided into geographical regions : Boreal North America, Siberia, Europe Output data sets are available free of charge. JAXA satellite (and sensor) used: JERS-1 (SAR)	Lead by JAXA Earth Observation Research Center (EORC), in close collaboration with: NASA Jet Propulsion Laboratory (JPL) the Institute of Environment and Sustainability of the Joint Research Centre of the European Commission (JRC/IES) Japanese Ministry of International Trade and Industry (MITI) Alaska Satellite Facility (ASF) Swedish National Space Board (SNSB) Earth Remote Sensing Data Analysis Centre of Japan (ERSDAC) Remote Sensing Technology Centre of Japan (RESTEC) With scientific input from: University of California Santa Barbara (UCSB) Brazilian National Institute for Space Research (INPE) National Institute for Research of the Amazon (INPA) Swedish Land Survey office (LMV/METRIA)

TESEO-CARBON	An ESA TESEO initiative aiming to explore the potential of EO to support the implementation of the Kyoto protocol within the UNFCCC. See for more information: dup.esrin.esa.it/projects/summaryp54.asp	Completed in 2003	The project explored the potential contribution of EO for enforcing the UNFCCC and Kyoto Protocol. It took stock of potential users and developed prototype products, derived by different EO sensors, that could help to estimate the global terrestrial carbon storage of the reference year 1990 and monitor the changes in biomass and land cover at continental to global scales. European and US satellites (and sensors) used: Envisat (AATSR, ASAR, MERIS) ERS (SAR, Along Track Scanning Radiometer (ATSR)) SPOT-4/5 (VEGETATION, High Resolution Visible IR (HRVIR), High Geometric Resolution (HRG)) Aqua/Terra (MODIS, Advanced Spaceborne Thermal Emission and Reflection Radiometer (ASTER)), joint NASA and Japan Landsat 5/7 (TM /ETM), NASA Ikonos, US commercial Quickbird, US commercial	Contributed by a consortium of commercial companies and a national institute. End-users: Ministry of Environment, Italy UNFCCC Secretariat, Climate Change Secretariat, Germany

KYOTO INVENTORY	An ESA DUE project that built on the TESEO-CARBON project with the remit to develop an operational service to support national bodies in charge of reporting for the Kyoto Protocol or for trading resulting from the Protocol during the first commitment period 2008-2012. See for more information: dup.esrin.esa.it/projects/summaryp46.asp	Completed in 2006	Services include provision of monitoring with respect to afforestation, reforestation and deforestation (ARD) activities, or more generally land-use change activities. Mainly European satellites (and sensors) used: ERS (Active Microwave Instrument (AMI)) PROBA (Compact High Resolution Imaging Spectrometer (CHRIS)) SPOT 1-4 LANDSAT 5/7 (TM/ETM)	Contributed by a consortium of commercial companies, academic and national institutes. End-users: Dutch Ministry of Agriculture, Nature and Food Quality (LNV), Netherlands Finnish Forest Research Institute (METLA), Finland Ministry of Environment, Italy Ministry of Environment, Spain Norwegian Ministry of Agriculture, Institute of Land Inventory (NIJOS), Norway Swiss Agency for Environment, Forests and Landscape (SAEFL), Switzerland

GLOBCARBON	An ESA DUE project that aims to produce global terrestrial products to aid carbon model assimilation, which is intended to improve the accuracy of climate change forecasting (Plummer, *et al.*, 2006). See for more information: dup.esrin.esa.it/projects/summaryp43.asp	Started 2002. In progress, planned completion 2008	The focus is to create global estimates of the following aspects of terrestrial vegetation, for use in Dynamic Global Vegetation Models and as a contribution to the GCP: Burnt Area Estimates (BAE), Leaf Area Index (LAI), Fraction of Absorbed Photosynthetically Active Radiation (fAPAR) Vegetation Growth Cycle (VGC) Mainly European satellites (and sensors) used: SPOT-4 and SPOT-5 (VEGETATION instruments), ERS-2 (Along Track Scanning Radiometer-2 (ATSR-2)) Envisat (Advanced Along Track Radiometer (AATSR)) Envisat (Medium Resolution Imaging Spectrometer (MERIS)) Using data for 10 complete years, 1998-2007.	Contributed by a consortium of commercial companies and a national institute. End-users: Centre d'Etude Spatiale pour la BIOsphère (CESBIO), France Center for Terrestrial Carbon Dynamics (CTCD), UK International Geosphere-Biosphere Programme (IGBP), International Joint Research Center (JRC), International Laboratoire des sciences du Climat et de l'Environnement (LSCE), France Médias-France, France Max Planck Institute for Meteorology (MPI-Met), Germany Potsdam Institute for Climate Impact Research (PIK), Germany University of Toronto, Department of Geography and Program in Planning

GLOBCOLOUR	An ESA DUE project that aims to develop consistently calibrated global oceanic products for a period of 10 years in support of ocean carbon-cycle research. See for more information: dup.esrin.esa.it/projects/summaryp72.asp	In progress, planned completion 2008	Numerous ocean colour products for coastal zones and open waters at different time scales are to be produced, for example: Chlorophyll-a content Total suspended matter (TSM) Aerosol optical thickness (AOT) The focus falls on creating a merged dataset to ensure the output product is independent of the input data source. Mainly European satellites (and sensors) used: Envisat (MERIS) Parasol (Polarization and Directionality of the Earth's Reflectances (POLDER)) SeaStar (Sea-viewing Wide Field-of-view Sensor (SeaWiFS)), NASA Aqua (Moderate Resolution Imaging Spectroradiometer (MODIS)), joint NASA and Japan	Contributed by a consortium of commercial companies, academic and national institutes. End-users: International Ocean Colour Coordinating Group (IOCCG), International International Ocean Carbon Coordination Project (IOCCP), International

ALOS Kyoto & Carbon Initiative	Continues the GRFM/GBFM project using ALOS EO data. The focus falls on defining and optimising provision of data products and validated thematic information derived from *in situ* and EO-derived data required by international environmental conventions particularly UNFCCC, carbon cycle scientists and conservation programs (CCCs) (Rosenqvist, *et al.*, 2007). See for more information: www.eorc.jaxa.jp/en/index.html	In progress, ALOS launched Jan 2006	Development and validation of thematic products to be used by CCCs, mainly by fixed, systematic global L-band SAR (PALSAR) data observations to be acquired globally leading to the production of regional SAR mosaics at 50 m resolution. Biomes of special interest are forests; wetlands; deserts and semi-arid regions. JAXA satellite (and sensor) used: Advanced Land Observation Satellite (ALOS) Phased Array L-band Synthetic Aperture Radar (PALSAR)	Led by JAXA EORC, undertaken by an international Science Team consisting of scientists active in the fields of carbon modelling and biophysical parameter retrieval, SAR experts, and representatives from the Global Observation for Forest and Land Cover Dynamics (GOFC), Terrestrial Carbon Observations (TCO), Food and Agriculture Organization (FAO), several space agencies, universities and public research institutions. The Science Team will aim to assure the scientific relevance of the project outputs to other related international efforts such as Global Observation for Forest and Land Cover Dynamic (GOFC/GOLD), Integrated Global Observations for Land (IGOL), Global Terrestrial Observing System - Terrestrial Carbon Observations (GTOS/TCO).

Global Observation for Forest and Land Cover Dynamics (GOFC-GOLD)	GOFC-GOLD is a coordinated international effort to provide ongoing EO-based and *in situ* observations of forests and other vegetation cover, for the sustainable management of terrestrial resources and to obtain an accurate, reliable, quantitative understanding of the terrestrial carbon budget. Originally a pilot project under IGOS-P, it is currently a panel of GTOS. See for more information: www.fao.org/gtos/gofc-gold/	2004, ongoing	Objectives are to: Provide a forum for EO users and EO data producers Provide regional and global datasets containing information on forest cover, forest changes due to ARD, and forest biological functioning Promote globally consistent data processing and interpretation methods Promote international networks for data access, data sharing, and international collaboration Stimulate the production of improved products	Numerous agencies, organizations and institutions are involved as providers of data and information products, as users or as both users and providers. Examples are CEOS members and affiliates, universities and research institutions, NGOs, treaties and conventions such as UNFCCC, international organisations such as GCOS and FAO.
Orbiting Carbon Observatory (OCO)	The OCO mission will collect precise global measurements of carbon dioxide (CO_2) in the Earth's atmosphere. See for more information: oco. jpl.nasa.gov/	To be launched in 2008	The objective is to improve understanding of the natural processes and human activities that regulate the abundance and distribution of CO^2. OCO will provide the first space-based CO^2 measurements.	Funded under the ESSP Programme. NASA JPL leads and is partnered by Orbital Sciences Corporation and Hamilton Sundstrand Sensor Systems.

CHAPTER 4:
The study area: Rio Bravo Conservation and Management Area, Belize

4.1. Introduction

The study area lies in a lowland savanna tract in the Rio Bravo Conservation and Management Area (RBCMA) in Belize, Central America. At approximately 100,000 ha, the RBCMA is the second-largest protected area in Belize and is managed by the Programme for Belize (PfB), an NGO with the primary purpose to preserve the natural heritage and biological diversity of Belize. The area has been gradually built up through a succession of private land parcel purchases, of which the first was secured in 1989 and the latest was secured in 1997 (PfB, 2000). The main ecosystems of the RBCMA are evergreen broadleaf forest, savanna and aquatic/wetland systems (PfB, 2006). Apart from being representative of the Central American savannas (Bridgewater, *et al.*, 2002), the RBCMA savannas were chosen as field site for this research because of:

- the range of savanna vegetation types occurring in a limited area of low-lying, gradually varying relief,
- the recent completion of a detailed botanical inventory (Bridgewater, *et al.*, 2002) and land cover classification (Meerman and Sabido, 2001) for this area,
- the availability of a comprehensive set of EO data for this area, and
- the accessibility to the site from the Hill Bank Research Station.

After the location of the study area (4.2) is discussed, this chapter focuses on the physical properties and management aspects of the study area, emphasising how they are likely to affect the EO data used for this research. The section on climate (4.3) focuses on rainfall and temperature only as these mainly affect the dielectric properties of the surface; the presence of moisture in soil or vegetation increases the

dielectric properties, which generally leads to higher backscatter (Woodhouse, 2006a). The section on geology, topography and soils (4.4) gives information on the geometry and surface roughness of the land surface, which affects radar backscatter; the rougher the surface, the higher the backscatter. The above properties affect the type and structure of the savanna vegetation (4.5) that occurs in the RBCMA savannas which, in turn, determines volume structure and geometry that affects backscatter. The sections on land management (4.6) and fire (4.7) provide context for this research and give insight into the local conditions relevant for biomass studies.

4.2. Location

The Rio Bravo Conservation and Management Area (RBCMA) is situated in the Orange Walk District of north-western Belize in Central America (see Fig. 4.1). It is the second largest conservation area in Belize and forms a key area in the Meso-Central American Biological Corridor, ensuring connections between Belize and the rest of Central American conservation areas, for example the area is contiguous with the Aguas Turbias National Park on the Belizean side of the border which adjoins Quintana Roo on the Mexican side to the north, while the western boundaries link with the Rio Azul National Park in Guatemala and the Maya Biosphere Reserve. This, in turn, is linked with the Calakmul Biosphere Reserve in Mexico. Collectively, this forms part of a protected area complex covering 1.7 million ha, the largest conservation area and largest remaining tract of natural forest in Central America.

The main ecosystem within the RBCMA is evergreen broadleaf forest, but two large tracts of lowland savanna exist, occurring in two separate areas of approximately equal extent (see Fig. 4.1); the fieldwork area is situated within the Rancho Dolores savanna close to Hill Bank field station (17˚ 36'N, 88˚ 41'W) while the San Felipe savanna is situated to the north. According to the Central American Ecosystems Map for Belize (Meerman and Sabido, 2001) these savanna areas (shown in Fig. 4.1) cover ~87 km^2 and ~54 km^2 of the RBCMA respectively, amounting to ~14,100 ha. This covers ~14% of the total land area of the RBCMA as cited in the land titles (100,400 ha), but according to the PfB management plan (PfB, 2006) the savannas cover ~10% of the total RBCMA land area at 10,000 ha.

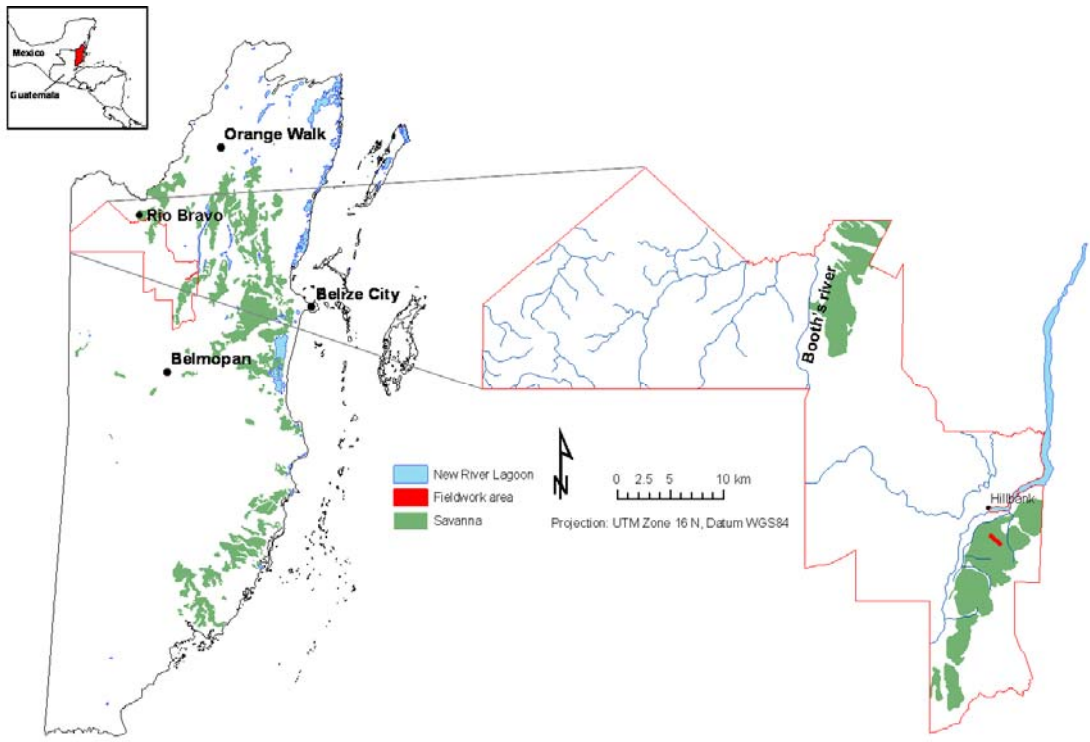

Figure 4.1: Map showing the location of the study area within the savannas of the Rio Bravo Conservation and Management Area (RBCMA) in Belize, Central America. The land cover classification is after Meerman and Sabido (2001): savannas are shown in green, the rest of the land cover in the RBCMA is mainly broadleaf evergreen forest. (Data source: SERVIR (2007))

4.3. Climate

Koeppen's classification categorises the northern Belizean climate as tropical wet-dry (Bridgewater, *et al.*, 2002). There is a distinct dry season lasting three months while the wet season lasts nine months. Total annual rainfall and seasonality varies greatly between years (PfB, 2000). Belize lies within the hurricane belt, and historically tropical storms and hurricanes have affected the country once in three years but usually don't cause much damage; the north being affected more frequently (BNMS, 2007). Although most hurricanes lose intensity inland, there are signs of storm damage in the larger broadleaf forest trees of the RBCMA caused by major hurricane events (PfB, 2000). Severe future hurricane damage in the savanna woodlands, which are vulnerable due to their sparse growth patterns, is therefore not ruled out.

The following sections focus on the rainfall and temperature of the study area. Knowledge of the rainfall regime is important for radar EO as the moisture content

of the soil and vegetation affects the dielectric properties of the surface scatterers, which determine the amount of backscatter returned to the radar sensor. Temperature and relative humidity affect the rate of evaporation of precipitation. Temperature records are shown in section 4.3.2 but relative humidity data were not available for the study area. The Belize NMS (2007) reports that relative humidity is approximately 80% during the year except during the dry season which experiences slightly lower humidity. When soil or vegetation increases in wetness, it scatters more SAR radiation back to the sensor (Woodhouse, 2006a).

For the period that this research was carried out, the closest functioning meteorological station to Hill Bank Field station, near the study area, was Rio Bravo in Orange Walk District (~27 km to the north) (BNMS, 2007). The rainfall and temperature records for this station were obtained from the Belize NMS and are given in the following sections.

4.3.1. Rainfall

Northern Belize has an annual rainfall of 1,500 mm. Clear wet and dry seasons occur, separated by a cool transitional period. The three-month dry season occurs between February and April/May, caused by strong anticyclones in the Atlantic that generate a persistent stable south-easterly airflow. Drought conditions regularly occur towards the end of the dry season. The wet season in Northern Belize starts in June and lasts until November, experiencing more than 60% of the annual precipitation (BNMS, 2007). Peaks normally occur in June and October (PfB, 2000) while August seems to be the driest month of the wet season. The cool transition period occurs from November through February, when rainfall declines and the country experiences frequent cold fronts (BNMS, 2007). King *et al.* (1992) and Belize NMS (2007) report variability in the total annual rainfall and average monthly rainfall between years for Northern Belizean meteorological stations.

Fig. 4.2 shows mean monthly rainfall graphs for Rio Bravo meteorological station, ~27 km from Hill Bank field station. The data were obtained from the Belize National Meteorological Service (BNMS). Historical rainfall records exist for a discontinued meteorological station at Hill Bank, listed in King *et al.* (1992), which

are included in Fig. 4.2. The trustworthiness of the latter data are unknown as it is uncertain how and when the station was sited and run. Rainfall data for the days preceding the acquisition of the radar data were also obtained from the BNMS and are shown in Table 4.1.

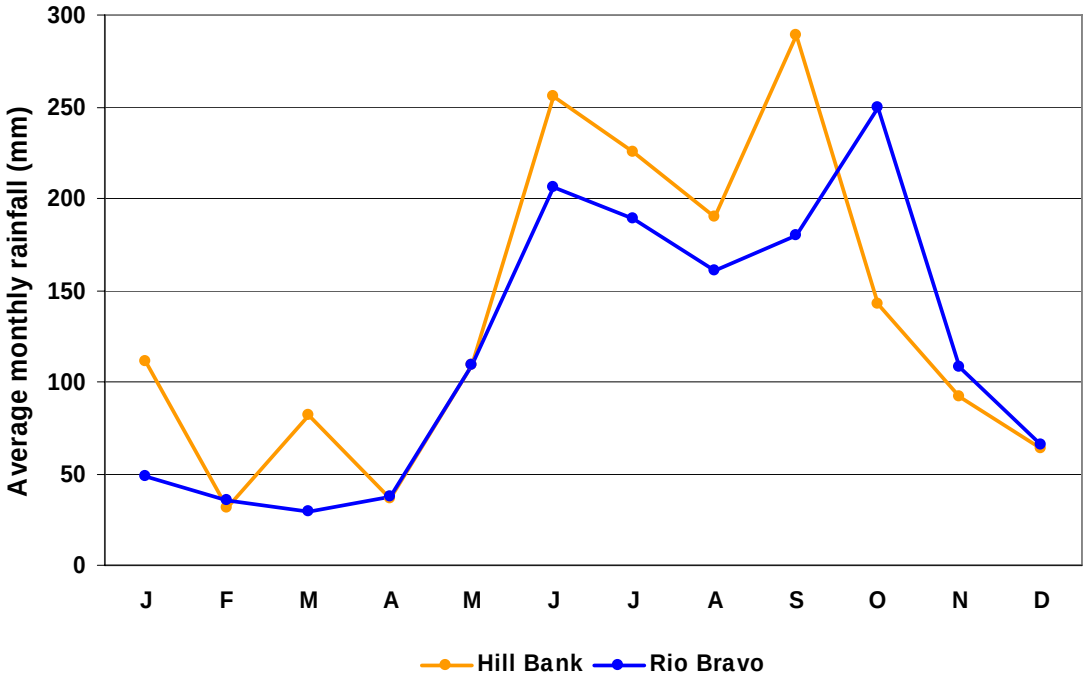

Figure 4.2: Mean monthly rainfall for Rio Bravo meteorological station (Data source: Belize National Meteorological Service). Historical rainfall records for a discontinued meteorological station at Hill Bank are also shown (Data source: King *et al.* (1992)).

4.3.2. Temperature

The subtropical climate causes only minor seasonal variations in temperature, with an approximate difference in seasonal temperatures of ~8 °C. The hottest period occurs in April and May, with temperatures remaining elevated up to September. The national mean maximum temperature is 31.5 °C. The highest temperature recorded at Rio Bravo was 38 °C (PfB, 2000). Temperatures in the savanna during fieldwork during April/May 2005 frequently exceeded 40 °C. The cooler period experiences frequent cold fronts and occurs from November to January, forming the cool transition period between the wet and dry seasons (PfB, 2000, BNMS, 2007). The mean maximum temperature for this period is 26.5 °C. The minimum temperature recorded at Rio Bravo was 9°C (PfB, 2000).

Fig. 4.3 shows mean monthly temperature graphs for the Rio Bravo meteorological station, obtained from the BNMS. Temperature data for the days preceding the acquisition of the radar data, provided by the BNMS, are shown in Table 4.1.

Table 4.1: Rainfall and temperature data for Rio Bravo meteorological station for the days preceding the acquisition of the radar data (Data source: Belize National Meteorological Service)

Intermap X-band, dates shown 22 March - 4 April 1999							
Date	**22**	**23**	**24**	**25**	**26**	**27**	**28**
Rainfall (mm)	0	0	0	0	0	0	0
Humidity (%)	-	89	90	87	97	92	85
Min. temperature	19	17.2	19.5	19.1	20.4	20.9	20.7
Date	**29**	**30**	**31**	**1**	**2**	**3**	**4**
Rainfall (mm)	0	9.2	2.0	0	0	0	0
Humidity (%)	89	94	96	89	86	86	86
Min. temperature	21	21.4	22.4	20.6	22.6	22.4	23.2
AIRSAR C-band, dates shown 4-7 March 2004							
Date	**1**	**2**	**3**	**4**	**5**	**6**	**7**
Rainfall (mm)	0	2.5	3.8	0	0	0	0
Average Temp. (ºC)	24	25.75	25	25.0	27.5	26.5	24.2
Humidity (%)	-	-	-	92	96	89	96
Min. temperature	17	21.5	21.5	20	24	22	16.5
Max. temperature	30	30	28.5	30	31	31	32

4.4. Geology, topography and soils

Geologically, northern Belize is considered part of the Yucatán Peninsula, forming part of the Yucatán Platform by means of a limestone plain that covers the northern half of Belize. The geology of this area is continuous with that of the southern part of the Yucatán and the northern Petén of Guatemala. Faulting on a NE-SW alignment gives rise to the main topographical features; a series of escarpments that determine the drainage of the main rivers in the RBCMA, such as the New River, Booth's River and Rio Bravo (PfB, 2000). The RBCMA consists mainly of the Northern Coastal Plain land region on the eastern half, on which the savannas are situated, and the Bravo Hills limestone karst land region to the west (King, *et al.*, 1992). The hilly landscape of the Bravo Hills, where altitudes range from 20 to 300 m, interlaces with the Northern Coastal Plain west of the Booth's River.

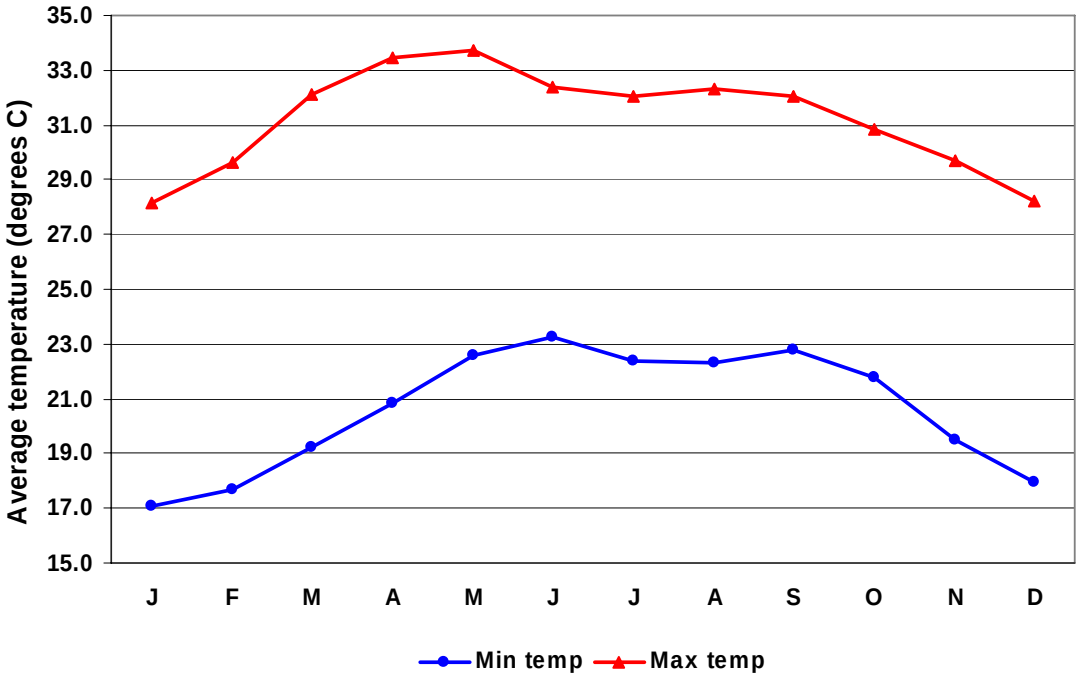

Figure 4.3: Graph showing the minimum and maximum monthly temperatures for Rio Bravo meteorological station (Data source: Belize National Meteorological Service).

The topography of the Northern Coastal Plain is flat undulating low-lying landscape which ranges between 0 and 20 m in altitude, but has local maxima up to 40 m (King, *et al.*, 1992). Underlain by limestone, it is covered over extensive areas by leached Pleistocene alluvia (PfB, 2006). The flat landscape of the study area enables the application of EO techniques without requiring complicated pre-processing. The EO data used for this research (see 5.2) do not contain distortions in the form of shadowing or layover effects due to strong topographical features. Geocorrection of EO data, depending on the specific EO sensor used, normally requires less special processing on flat terrain.

The main land systems that occur on the coastal plain of the RBCMA are the Crooked Tree and August Pine Plains containing pine savannas and the Hill Bank Plain with broadleaf forest (King, *et al.*, 1992). The savannas occur on deep deposits of leached Pleistocene alluvia and coarse-textured tertiary parent materials (Furley, *et al.*, 2001), of the Puletan suite soils. These soils are generally acid, nutrient deficient and subject to extreme dryness alternating with water-logging according to the season. Local rises in the landscape normally have Crooked Tree sub-suite soils,

which are moderately to excessively well-drained deep sandy soils, often carrying savanna woodland with pine and oak trees. The Boom soil sub-suite is very similar but is shallower and less well drained, and tends to have fewer species and smaller vegetation. Palmetto and wet open areas with grasses and sedges normally occur on the Haciapina sub-suite soils (King, *et al.*, 1992), which develop in depressions, that are wet for most of the year and have a higher humus content from down-wash (PfB, 2006). Broadleaf forest occurs on the Hill Bank Plain land system which consists of gently sloping land over hard Cretaceous and Tertiary limestone with generally well-drained soils that tend to wetness in low-lying areas (PfB, 2006).

4.5. Vegetation

Whereas Chapter 2 discusses global savanna morphology as determined by key ecological determinants and disturbances, this section focuses on the vegetation specific to the savannas that occur in the RBCMA. Under the Holdridge (1967) system, the RBCMA falls within a Subtropical Moist Forest Life Zone (King, *et al.*, 1992, PfB, 2000). The main ecosystems occurring within the RBCMA are broadleaf forest, savanna and aquatic/wetland systems (PfB, 2000, Furley, *et al.*, 2001, PfB, 2006), of which the savannas cover ~10% of the total area of the RBCMA (see also 4.2).

The vegetation of these savannas are characteristic of Central American and Caribbean savannas (Bridgewater, *et al.*, 2002) and consist of open grassland with palm and woody species that occur in places as pine and oak woodland. The species composition and further description of the dominant vegetation is given in 4.5.1, while the structure of the savanna subtypes are described in 4.5.2. A discussion is included on vegetation-specific characteristics that influence SAR backscatter in section 4.5.3.

4.5.1. Savanna species composition

A recent vegetation survey of the RBCMA savannas (Bridgewater, *et al.*, 2002) recorded a total of 258 savanna vegetation species, forming ~7% of the Belizean flora. The majority (57%) of the species are characteristic of drier savanna systems.

The woody species totalled 57, of which only 15 species were trees. Where there is an obvious woody component in the savanna vegetation the defining species are pine, oak and palmetto (Furley, *et al.*, 2001). The woody species occurring in the lowland RBCMA savannas, apart from a few exceptions, are identical to those of the upland Mountain Pine Ridge in Central Belize, as described by Johnson and Chaffey (1973) (Bridgewater, *et al.*, 2002).

Caribbean pine (*Pinus caribaea*) is the dominant tree species in the RBCMA savannas (Bridgewater, *et al.*, 2002). It can be found from sea level up to 470 m in elevation. It may reach 30 m tall but is commonly shorter (Horwich and Lyon, 1990), with larger trees reaching ~16 m in the study area (see Fig. 4.4).

(a) **(b)**

Figure 4.4: Examples of Caribbean pine (*Pinus caribaea*): (a) a single tree within pine-palmetto savanna, and (b) within denser savanna woodland

Oak (*Quercus oleoides* Schltdl and Cham.) grows in association with pine trees and can occur up to 500 m in elevation. While small groves of oak trees occur, it is more common to find individual oak trees interspersed with areas of less dense pine. It is a slow-growing tree that reaches 8 to 15 m in height and frequently has multiple trunks (see Fig. 4.5). It is sometimes more abundant in areas where fires occur frequently (Fournier, 2005).

Figure 4.5: An example of Oak (*Quercus oleoides* Schltdl and Cham.)

(a) **(b)**

Figure 4.6: Examples of woody shrubs: (a) Sandpaper tree, also known as Yaha (*Curatella americana L.*), and (b) Wild craboo (*Byrsonima crassifolia*)

Other main woody species that occur interspersed with pine and oak trees in the study area, commonly as shrubs or small trees, are the Sandpaper tree/Yaha (*Curatella americana* L.) rarely reaching 5 m in height, often with horizontally

spreading branches and Wild craboo (*Byrsonima crassifolia*) (Furley, *et al.*, 2001, Bridgewater, *et al.*, 2002) which can range from 1.5 – 10 m in height (Horwich and Lyon, 1990), but rarely exceeds 5 m in height in the study area. These two woody shrubs (see Fig. 4.6) are the most widely distributed woody species of the Neotropical savannas, and as such are seen as indicator species for Neotropical savannas (Bridgewater, *et al.*, 2002).

The palmetto/paurotis palm (*Acoelorraphe wrightii* H. Wendl. Ex Becc.) is a small palm which commonly reaches 3-6 m in height (see Fig. 4.7) (Horwich and Lyon, 1990). Palmetto is widespread and often grows in two forms (i.e., either as taller dense clumps interspersed with pine or as slightly sparser, shorter palmetto thicket) (Brown, *et al.*, 2005). As palmetto is most frequently associated with poorly drained soils (Bridgewater, *et al.*, 2002), the ground surface directly underneath palmetto thickets tends to be uneven and rough, forming drainage channels approximately 40 cm deep (see Fig. 4.8).

(a) **(b)**

Figure 4.7: Examples of palmetto/paurotis palm (*Acoelorraphe wrightii* H. Wendl. Ex Becc.): (a) a palmetto clump within a savanna woodland, and (b) slightly sparser, shorter palmetto thicket.

4.5.2. Savanna vegetation subtypes

Bridgewater *et al.* (2002) and Brokaw (2001) list various Belizean vegetation classification and mapping activities in the literature. Although various savanna vegetation classifications exist and have been applied to the RBCMA savannas (e.g.,

(a) **(b)**

Figure 4.8: The poorly drained soils under palmetto thicket form drainage channels which are uneven and rough: (a) the uneven ground is normally covered by grass but (b) is clearly visible after a savanna fire.

Meerman and Sabido (2001) for the Central American Ecosystems Map) the vegetation classification by Bridgewater *et al.* (2002) and Furley *et al.* (2001) are adapted for the purposes of this research; the savanna subtypes that do not occur in the field site, and have therefore not been included in the field data collections, are not included here, while *gallery forest* is added. The following savanna vegetation subtypes can be clearly distinguished in the study area of the Rancho Dolores savanna (refer to map in Fig. 4.1):

- **Pine-palmetto savanna** (Fig. 4.9)**:** Open grass-dominated area with scattered pines, palmetto clumps and woody shrubs. Only the pine trees reach tree stature (up to 20 m), while other woody species are present as shrubs. Palmetto occurs in dense clumps. The ground layer is dominated by tussock-forming grasses (up to 40 cm). Usually occurs on sandy soils.

- **Palmetto thicket** (Fig. 4.10)**:** Discrete large clumps or corridors of palmetto, normally ranging in height from 2 to 6 m. The ground layer can be open or closed, usually composed of tussock-forming grasses and sedges. Brown *et al.* (2005) distinguish palmetto thicket from palmetto clumps (described above) on the grounds that thickets are larger and generally less dense than the smaller palmetto clumps. Palmetto thicket usually occurs on wetter, poorly drained soils, most typically around wet depressions and in shallow valleys.

(a)

(b)

Figure 4.9: Two examples of pine-palmetto savanna: (a) open grass-dominated area with scattered pine trees, and (b) open grass-dominated area with scattered palmetto thickets.

- **Savanna woodland** (Fig. 4.11): Pine-dominated areas which form a broken canopy where the larger trees attain a height of ~16 m. Oak trees dominate in patches. The savanna woodlands, also called *pine ridges*, are reasonably dense groupings of pine trees that occur within the savannas and are similar in structure to larger tracts of Belizean pine forests, such as the Mountain Pine Ridge (Bridgewater, *et al.*, 2002). Scattered dense palmetto clumps and woody shrubs form an open understorey. These woodlands provide the major woody component of the savanna and usually occur on dry, very sandy soils.

Figure 4.10: Palmetto thicket

Figure 4.11: Savanna woodland

- **Gallery forest** (Fig. 4.12)**:** This is strictly a forest subtype (Furley, *et al.*, 2001), but is included here as gallery forest structures occur within the savanna and have been included in the vegetation height observations during the fieldwork campaign. As their occurrence is associated with water courses and streamlines,

they typically form narrow corridors along streamlines and sometimes exist as isolated forest patches within the savanna. The corridors, typically about 50 m wide, and patches of dense broadleaf forest vegetation have a rich species composition with a closed canopy and tall vegetation (10-20 m). They occur on sandy loams, reflecting colluvial or alluvial input to the soil.

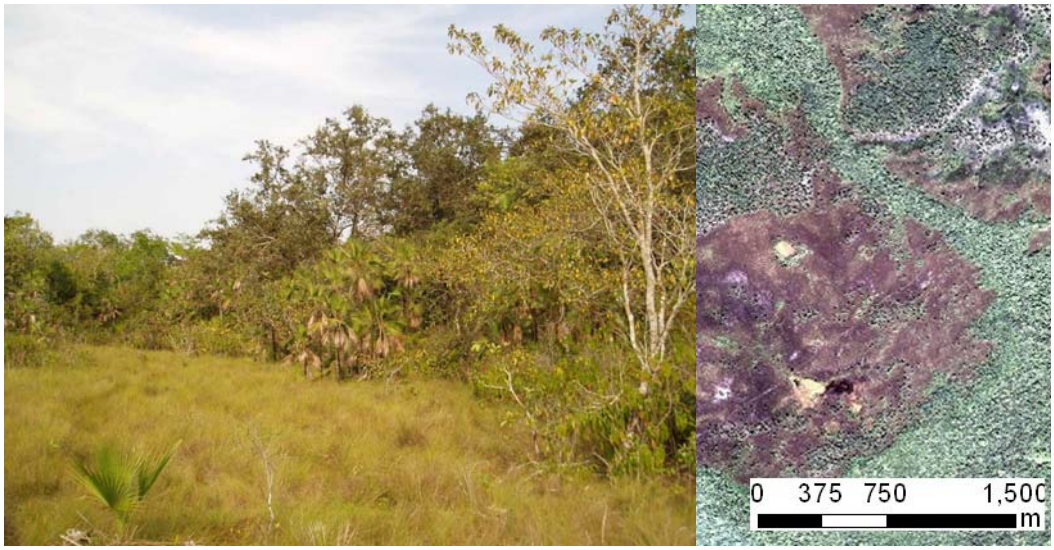

(a) **(b)**

Figure 4.12: Gallery forest (a) as it appears on the ground, and (b) a subset of an IKONOS satellite image (3-2-1, RGB) that shows the spatial pattern of gallery forests as they occur within the savanna.

For practical purposes the Programme for Belize distinguish between open grassland with scattered trees, pine woodland (with >10% canopy cover) and mixed pine-oak woodland in their management plan (PfB, 2006). Whichever way the savanna vegetation subtypes are classified, the different subtypes naturally occur as a mosaic within the savanna. As they form part of an ecological succession or part of an ecotone, the subtypes can not be considered as stable communities (Bridgewater, *et al.*, 2002).

4.5.3. Physical characteristics that influence SAR backscatter

Since different physical characteristics of the savanna vegetation such as above-ground biomass, canopy cover and stem number densities have an effect on SAR

backscatter (see 3.3.3), this section discusses these characteristics for the main woody species of the study area.

Using three-dimensional high resolution aerial videography, Brown *et al.* (2005) estimated the mean total above-ground biomass carbon stock of the RBCMA savannas as 13.1 t C/ha, with a 95% confidence interval of 2.2 t C/ha (which can be expressed as 1.31 kg C/m^2 ± 0.22 kg C/m^2). Contributions of the different vegetation types to the total carbon stock were found to be 51% trees, 25% grasses, 21% palmetto and 4% shrubs (see Fig 4.13). They developed allometric equations, based on destructive sampling in the Belizean savanna woodlands, for estimating the above-ground biomass for the main woody savanna vegetation (see Table 4.2). The allometric equation for oak is based on hardwoods in the US, verified as a reasonable estimate for the oaks of the RBCMA (Brown, 2006).

Table 4.2: Allometric equations to estimate above-ground biomass carbon for the main woody vegetation of the RBCMA savannas (Source: Brown (2006))

Species	Allometric equation	y units	x units	r^2
Pine	$y = 0.0407x^{2.8131}$	biomass, kg	dbh, cm	0.99
Oak	$y = 0.5 + \frac{25000x^{2.5}}{x^{2.5} + 246872}$	Carbon stock, kg	dbh, cm	0.99
Shrubs	$y = 2.547x - 2.6967$	Carbon stock, kg	total height, m	0.66
Palmetto	$y = 0.6341x - 0.0125$	Carbon stock, kg	total height, m	0.69

Stem number densities for pine trees in the savannas range from scattered trees to sparse woodlands. Bridgewater *et al.* (2002) reported pine number densities in the RBCMA savannas at 76.7 trees/ha, for oak at 11.6 trees/ha, and for yaha at 4.6 trees/ha. The average stem number density for the savanna woodlands of the study area was estimated at ~47 stems/ha, although this is probably an underestimation (see 5.6.2). Palmetto stem number densities vary widely between and within regions. Stem number densities up to 8,500 stems/ha, or 0.85 stems/m^2, have been recorded in Belize (Horwich and Lyon, 1990), whilst Faruggia (2002) recorded a maximum number density of 99 stems/ha around vernal pools in the Sapodilla coastal savanna in Stann Creek District and Woo (2002) counted 20.2 stems/ha in the savanna at Monkey Bay, Belize District. The latter two stem number densities are presumably for the respective study areas as a whole. The average stem number density for

palmetto clumps in the RBCMA study site was calculated as ~1.4 stems/m^2 (see 5.4.3). During the 2007 fieldwork campaign, Furley (2007) studied palmetto thicket stem number densities and counted between 1,000 and 4,875 stems/ha (0.1 and 0.5 stems/m^2) in the previously inaccessible main palmetto thicket occurring in the centre of the field data transect. This study showed that palmetto thickets are not only less dense than palmetto clumps, but also have spatially variable number densities.

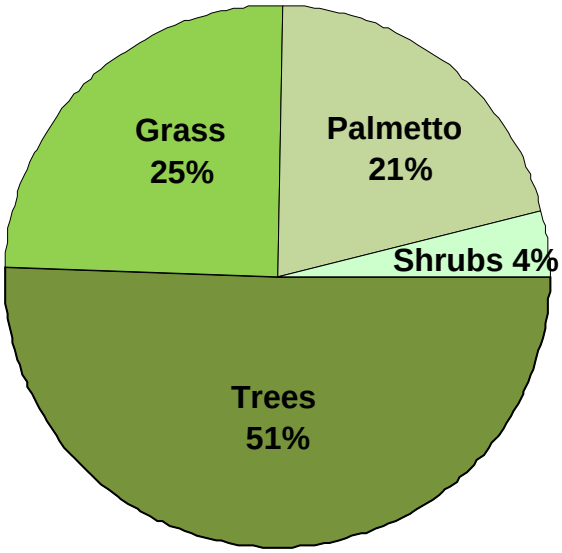

Figure 4.13: Diagrammatic presentation of the contributions of the vegetation types to the total above ground biomass in the study area (Source: Brown*, et al.*(2005))

The average canopy cover of the savanna woodlands of the study area was estimated at ~35% (see 5.6.2). Based on the combination of surface area, canopy cover and minimum tree height at maturity, the savanna woodland patches in the study area can be classified as *forest* under the FAO definition (see 2.2.3). Figs. 4.14(b) and 5.17 show the typical canopy cover of savanna woodlands in the study area, as seen on an IKONOS image (see also Figs. 5.7 and 5.9 for oblique aerial photography). Savanna woodland tree growth rates are believed to vary between age classes, with older trees maintaining a slow growth rate. This is further discussed in 5.4.5.

The ground cover is a more or less continuous cover of grasses (see Fig. 4.14), that can be thought of as long thin cylinders with a diameter of ~1 mm. The density of the grass cover clearly decreases in the savanna woodlands. Fig. 4.14(b) shows a subset

of IKONOS EO data (see 5.2.2.1) of the study area that shows the difference in density of the grass cover between open areas and savanna woodland. The image is a true-colour composite, showing the bright sandy soils that are visible through the grass cover under the savanna woodland.

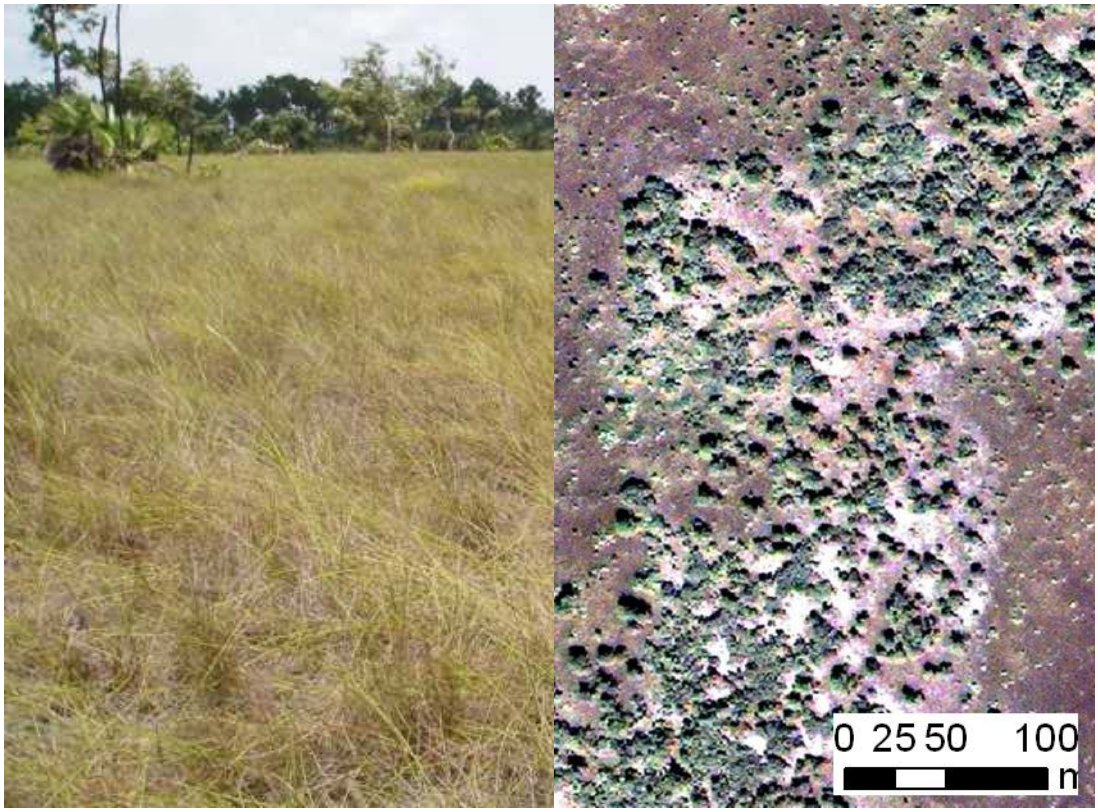

(a) **(b)**

Figure 4.14: Ground cover is a more or less continuous cover of grasses: (a) a close-up view of the tussock-forming grasses in an open area, and (b) a subset of an IKONOS satellite image (band combination 3-2-1, RGB) that shows the difference in grass cover density between open grassland areas an and savanna woodland; the sandy soils are clearly visible through the grasses in the savanna woodland.

4.6. Land management

As very few Central American savanna areas are conserved, the RBCMA forms an important conservation area (Bridgewater, *et al.*, 2002). It is an IUCN management category VI area (i.e., it has a protected core that is managed as a national park, buffered by a zone managed as a sustainable functional forest reserve and an outer area of engagement with surrounding communities). In their Management Plan for 2006-2010 (PfB, 2006), the PfB identify three main conservation targets

corresponding to the three main ecosystems of broadleaf forest, pine savanna and aquatic/wetland systems, of which the savanna is reported to be in the worst condition. Non-forest ecosystems only received conservation importance from 2001, when the savannas were identified as significant habitat for the endangered yellow-headed parrot. Unmanaged fire is the greatest single threat to the savannas, often linked to human activities such as hunting. Other illicit activities include timber theft and harvesting of plant parts, such as seeds and fruits. Land use change and deforestation in the wider landscape is also important as it causes loss of biological connectivity (PfB, 2006).

Future management of the RBCMA savanna ecosystem will emphasise fire management to maintain biodiversity and promote pine stocking and the control of invasive species. The sustainable use of certain savanna resources are envisaged, for example non-timber forest products (NTFPs) which include pine timber and seeds, fruits and conserves. The RBCMA management plan (PfB, 2006) describes the savanna ecosystem as degraded[1] but in 'good condition'. Current management is therefore primarily aimed at rehabilitation, which is a form of reforestation. This presents an opportunity for Kyoto-compliant carbon sequestration, pursued under the Rio Bravo Carbon Sequestration Pilot Project. At the same time these activities provide for a potential future timber resource. For these purposes, the savanna ecosystem vegetation subtypes distinguished in the management plan are open grassland with scattered trees, pine woodland (with >10% canopy cover) and mixed pine-oak woodland. Sustainable harvesting under licence of seeds, fruits and conserves of (e.g., palmetto seeds) is actively pursued. The woody stems of palmetto plants are also known to be used as building materials for lobster traps and fencing (Stuart, 2008).

4.7. Uncontrolled fire

Savannas are essentially fire-adapted landscapes, described in 2.3.3.3. Bridgewater *et al.* (2002) report apparent signs of fire in all savanna subtypes of the RBCMA while the Programme for Belize Management Plan (PfB, 2006) lists unmanaged fire as the

[1] The report is not clear which criteria is used for this classification.

most important threat to the savanna ecosystem, with the potential to affect significant areas of broadleaf forest. Savanna fires normally occur towards the end of the dry season when drought conditions regularly occur and the risk of fire in hardwood forest increases with exceptionally dry spells (PfB, 2000). Although Caribbean pine is not well adapted to resist fire, only protected by thick bark (Johnson and Chaffey, 1973), savanna fires are normally fast-moving at ground level and crown fires are rare.

Savanna fires have been suppressed in the study area in accordance with the PfB management plan. No local record is kept on the occurrence of fires, but the NASA Fire Information for Resource Management System[2] (FIRMS) (UoMaryland, 2007) shows that there have been occurrences of fires in the savannas of the RBCMA between 2000 and the time of writing this chapter (corresponding with the end of the 2007 dry season). Fig. 4.15 shows a map indicating the locations and years of the savanna fires in the RBCMA for this period. The Rancho Dolores savannas have experienced far less fires than the San Felipe savanna tract, but a succession of savanna fires spread through the Rancho Dolores savanna areas in April 2007, days before the second field visit; parts of the savanna were still burning during the first days of fieldwork (see Fig. 4.16). The fire suppression programme had caused fuel material to gradually build up, allowing the fire to easily spread over large areas of the Rancho Dolores savanna tract. Fig. 4.16(b) shows that the savanna fire damaged low vegetation such as the grass groundcover and palmetto. The crowns of large pines stayed mostly undamaged. Grass cover started regenerating within the first days after the fire and palmetto followed shortly after. Shrubs and pine seedlings were most severely damaged and might not all survive. This savanna fire in the study area has created an interesting new avenue for investigation into savanna regeneration.

[2] FIRMS processes active fire locations with the MODIS Rapid Response System using the standard MODIS MOD14 Fire and Thermal Anomalies Product. An active fire location is mapped at the centre of the 1 km MODIS pixel which is determined to contain a fire. High quality fire observations are available from November 2000.

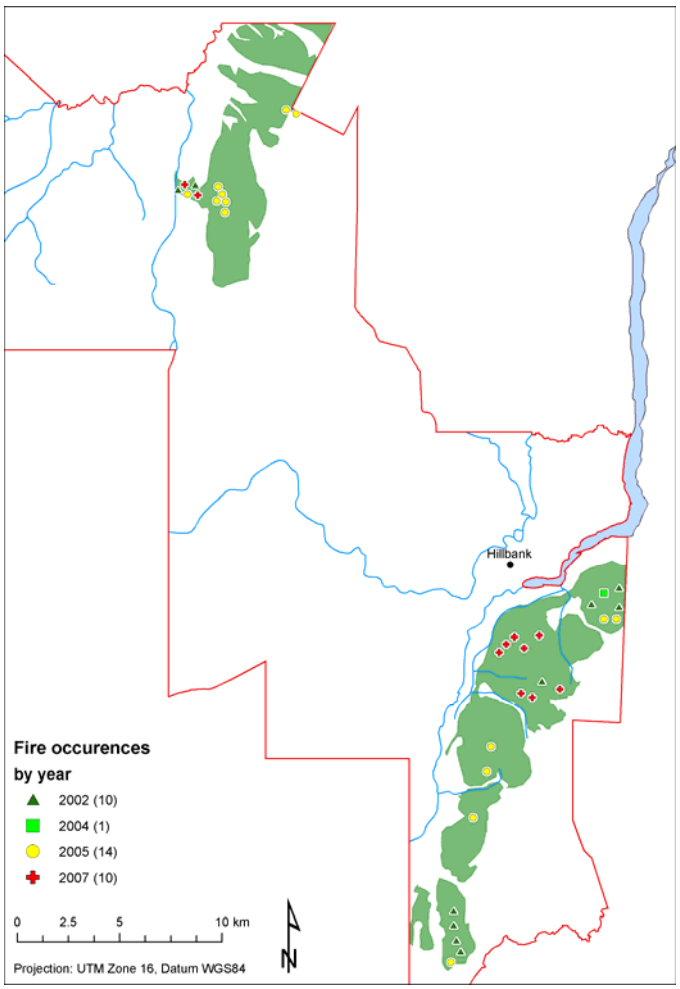

Figure 4.15: Map of savanna fire occurrences in the RBCMA savannas Jan 2000 - May 2007. Years that are not shown did not show fires on FIRMS. (Data source: UoMaryland (2007))

(a) **(b)**

Figure 4.16: (a) Savanna fire in progress, (b) effects of savanna fire, grass and small vegetation such as palmetto are burnt out while crowns of pine trees in the background are still largely undamaged.

4.8. Summary

This chapter has given an overview of the Rio Bravo Conservation and Management Area (RBCMA), emphasising the physical characteristics that are most likely to affect radar EO. Furthermore, management aspects that determine the need for specific EO applications were discussed. Of these, biomass estimation for Kyoto-compliant projects and savanna woodland mapping are the focus of this research.

The study area has a clear wet and dry season. To make the different datasets more compatible for comparison, all EO data and field data were acquired during the dry season over several years between 1999 and 2007. Rainfall and temperatures recorded at the nearest meteorological station to the field site have been reported for the days preceding the radar data acquisitions in 1999 and 2004. The small amount of rain received at Rio Bravo meteorological station 4 to 5 days prior to the acquisition dates of the Intermap STAR-3i and the AIRSAR data is not expected to have affected the radar data.

The topography of the study area is made up of flat undulating low-lying landscape which rules out distortion of radar data due to layover and shadowing from topographical features. The generally acid, nutrient deficient soils accommodate several savanna vegetation subtypes of which pine-palmetto savanna, palmetto thicket and savanna woodland are the most important in the study area. Although they are not strictly a savanna vegetation subtype, gallery forests have been included in the data acquisition and processing since they occur in the study area.

The mean total above-ground biomass of the study area (as determined in another study) is estimated at 13.1±2.2 t C/ha which is well within the SAR backscatter saturation points experienced in other studies (see 3.3.3.1). Of this, the savanna woodland trees were estimated to contribute 51%, followed by grasses (25%), palmetto (21%) and shrubs (4%). Furthermore, the average canopy cover of the savanna woodlands has been shown to be ~35%, making them potentially important areas for future carbon sequestration initiatives under the Kyoto Protocol. Stem number density is another physical characteristic that determines the amount of radar backscatter. Stem number density for trees in the savanna woodlands of the study area is estimated at >50 stems/ha. Palmetto stem number densities in the study area

are variable, but mostly high compared to other areas. Palmetto is therefore expected to have a strong effect on the SAR data.

Land management of the savanna ecosystem in the RBCMA focuses on fire management for biodiversity conservation and sustainable use of NTFPs such as pine timber and palmetto seeds. The rehabilitation of the pine resource in the savannas is an important component of possible Kyoto-compliant carbon sequestration programmes and provides a future pine timber resource. EO is useful for both these activities as it has potential to estimate the above-ground biomass of woody vegetation of the savanna woodlands. Timber volume and density have been operationally determined by SAR EO techniques in conventional forestry. The application of such techniques on sparse woodlands with a low biomass content relative to conventional managed forests has, however, not been adequately studied. This research therefore evaluates the use of SAR for estimating biomass of the sparse savanna woodlands of the study area. For their management of sustainable harvesting of other savanna vegetation such as palmetto seeds, EO techniques can be of use for mapping the locations and extent of the resources.

Uncontrolled fire is the single largest threat to the savannas. Although fire management is a management priority for the RBCMA, recent extensive fires in the study area have opened new opportunities for research; monitoring of savanna vegetation regeneration using EO data and methods could contribute to future management strategy as fire suppression, and the concomitant build-up of dry fuel material is still a debated topic.

Because they are representative of the savannas of Central America, the RBCMA savannas are a useful test site for savanna research. The availability of a comprehensive set of EO data and field data collected for this research during two fieldwork campaigns together with detailed botanical inventory data and a recent land cover classification provide a basis for future change detection and monitoring programmes.

Chapter 5:
Data description, (pre-) processing and data quality assessment

5.1. Introduction

This chapter describes the various Earth observation (EO) data sets, the collection of detailed *in situ* measurements, the manner in which the data was pre-processed and a discussion on the outcome of data quality assessment. Various EO data were used, both from SAR and optical sensors (5.2). The field data (5.3) were collected during two fieldwork campaigns in the dry season, of which the 2005 campaign formed the main data collection component by means of a detailed point-of-detail survey, which resulted in a set of positional (GPS) and vegetation inventory data consisting of measurements of savanna woodland vegetation. The 2007 campaign added wider coverage of land cover and ground elevation data beyond the 2005 survey area. This provided an opportunity to observe changes in the study area, including the rate of tree growth (5.4.5); an important factor for interpreting the EO data which have been acquired in the dry season over different years.

Since the analysis and interpretation of further analyses (discussed in Chapter 6) depend on the quality of the data used, this chapter describes the (pre-)processing of the various datasets (5.4 and 5.6) and then concludes with the outcome of data quality assessments (5.5 and 5.7). This is described in separate sections for the field data and the EO data. Processing of the field data entailed converting GPS observation files to a format using the same coordinate system and ellipsoid as the EO data. Subsequently, the ground surface data points were used to create a ground surface DEM for the fieldwork area. This is used later to derive tree heights from the InSAR data (see 6.6) The vegetation inventory data were used to derive palmetto stem number densities and to fill gaps in the field data by estimating crown diameters for tree crowns that were not measured during fieldwork. An analysis of tree growth rates in the study area is included since this forms part of the discussion of InSAR

analysis results in 6.6.2, which explores the effect of tree growth on the InSAR height retrieval results based on the difference in EO data acquisition dates.

Pre-processing of the EO data included vertical alignment of the InSAR data for direct comparison of tree height estimates (5.6.1 and 5.7.2). Further analysis of the EO data described in this chapter entails the extraction of woodland canopy cover from the high resolution optical EO data. The results of this analysis are used throughout discussions related to the minimum threshold for canopy cover for forest areas under the Kyoto Protocol. The accuracy of the positional field data (GPS measurements and survey network points) and the spatial alignment of the various EO data sets were determined to ascertain that all data were accurately co-registered. This is an important aspect for the data analyses and interpretation discussed in Chapter 6 due to the heterogeneity of the field area.

5.2. Earth Observation data

The data described here includes the EO data used for this project, both active and passive. The data have been acquired over different years, but always during the dry season, between March and May. The location and coverage of each is indicated in Fig. 5.6.

5.2.1. Synthetic Aperture Radar (SAR) data

5.2.1.1. AIRSAR

The primary SAR data set available to this research was NASA Jet Propulsion Laboratory (JPL) airborne AIRSAR data, consisting of C-band single-pass interferometry (VV polarization), fully polarimetric L- and P-band and C-VV backscatter data; the backscatter data was obtained as orthorectified radar images (ORI). Backscatter values were converted to dB[1]. The interferometric correlation and local incidence angle layers are included as additional data layers accompanying

[1] $\text{Backscatter}_{dB} = 10.\log_{10}(\text{backscatter}_{linear})$

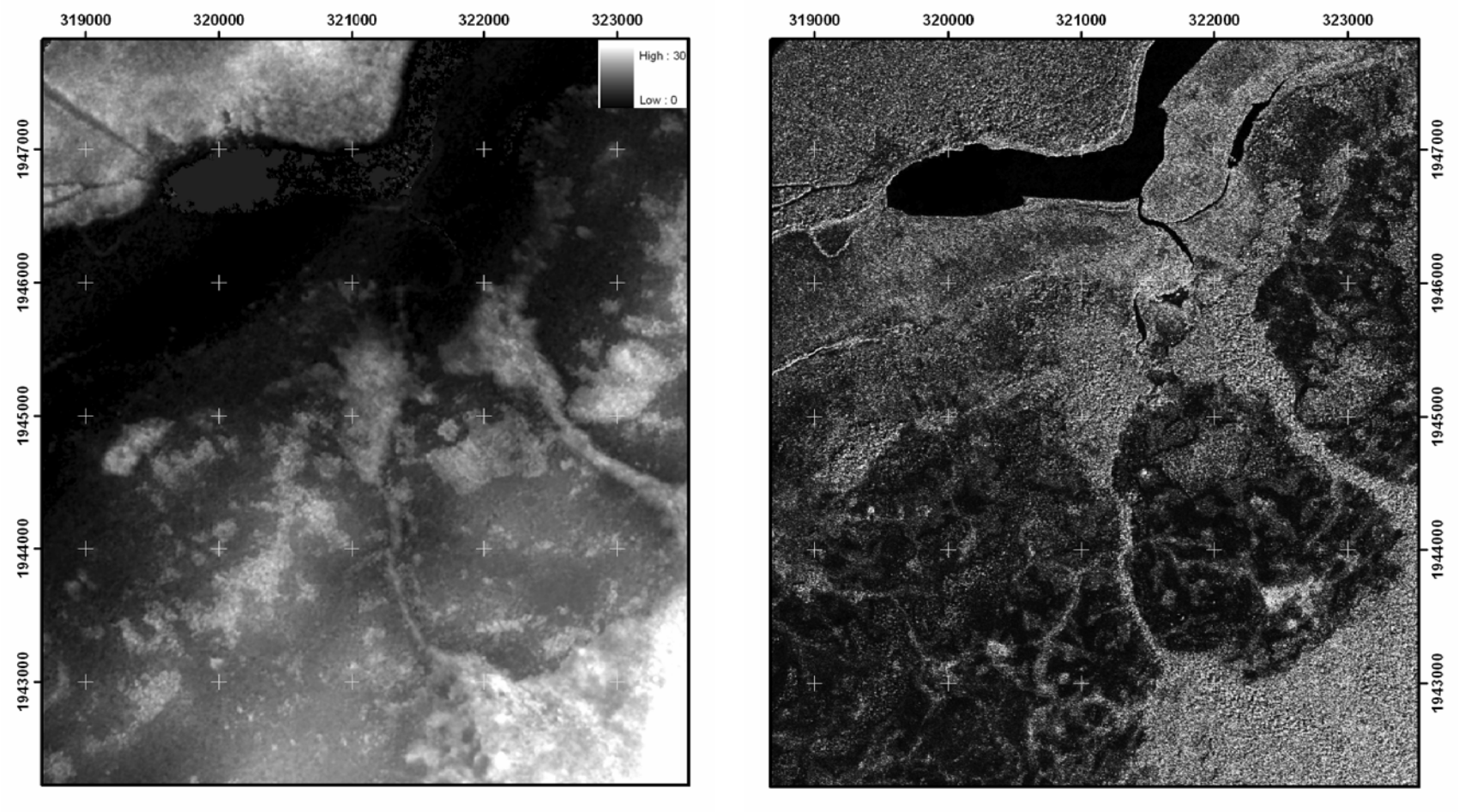

Figure 5.1: Subset of AIRSAR data: (a) C-band Digital Surface Model (DSM), (b) C-band backscatter.

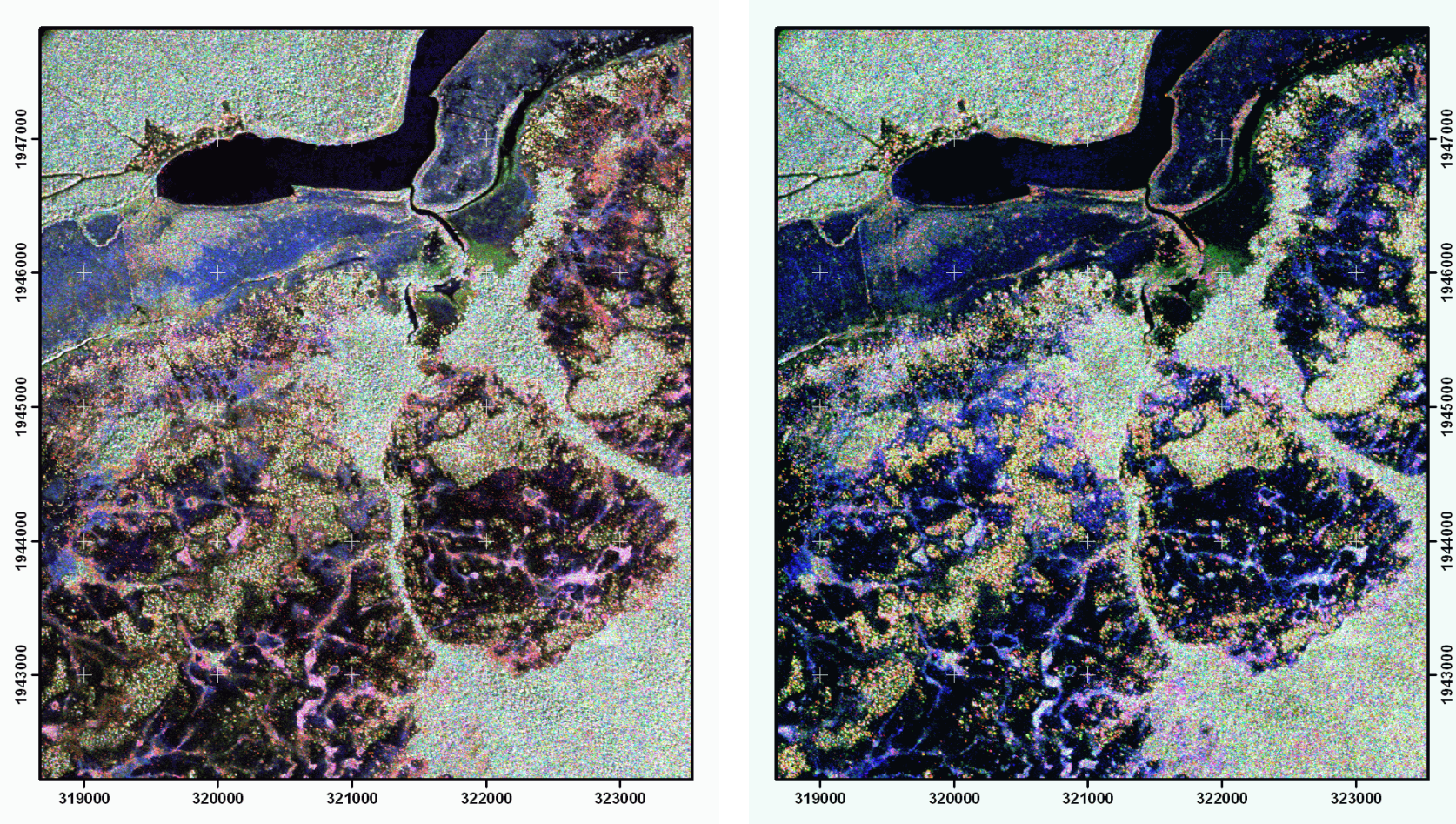

(a) **(b)**

Figure 5.2: Subset of AIRSAR data: (a) L-band POLSAR backscatter, HH-HV-VV (RGB), (b) P-band POLSAR backscatter, HH-HV-VV (RGB)

the C-band digital surface model (DSM). These data were acquired during the dry season, on 7 March 2004. The data characteristics are summarised in Table 5.1 and subsets of the datasets covering the study area are shown in Figs. 5.1 and 5.2.

Although it is not apparent upon visual inspection of the data, the C-band InSAR data suffers multipath error, resulting in a sinusoidal perturbation in the InSAR DSM (dealt with later in 5.7.3).

Table 5.1: AIRSAR data characteristics (source: AIRSAR data header files, (Lou, 2002))

Platform	NASA DC-8, airborne
Mode of operation	TOPSAR, or cross-track interferometry (XTI1)
Wavelengths	C-band, 5.6 cm, 5.3 Ghz L-band, 24 cm, 1.25 GHz P-band, 68 cm, 0.44 GHz
Polarisation	C-band: VV L-band: VV-VH-HH P-band: VV-VH-HH
Flying Height	8,200 m
Range direction	310°
Look angle (near, far, average at study site)	26.3°, 62.4°, 55.4°
InSAR baseline	5 m
Acquisition Date	07/03/2004
ORI and DSM posting	5 m
Horizontal RMSE	1 m
Vertical RMSE	1-3 m
Projection	UTM/WGS84
Datum	WGS84 (ellipsoidal)

5.2.1.2. Intermap

Additional radar data available for the study area is single-pass X-band interferometric SAR (HH polarization). The data were acquired for a commercial client by Intermap Technologies, a Canadian-based company. The data consist of an X-band DSM and an ORI for X-HH backscatter. Backscatter values

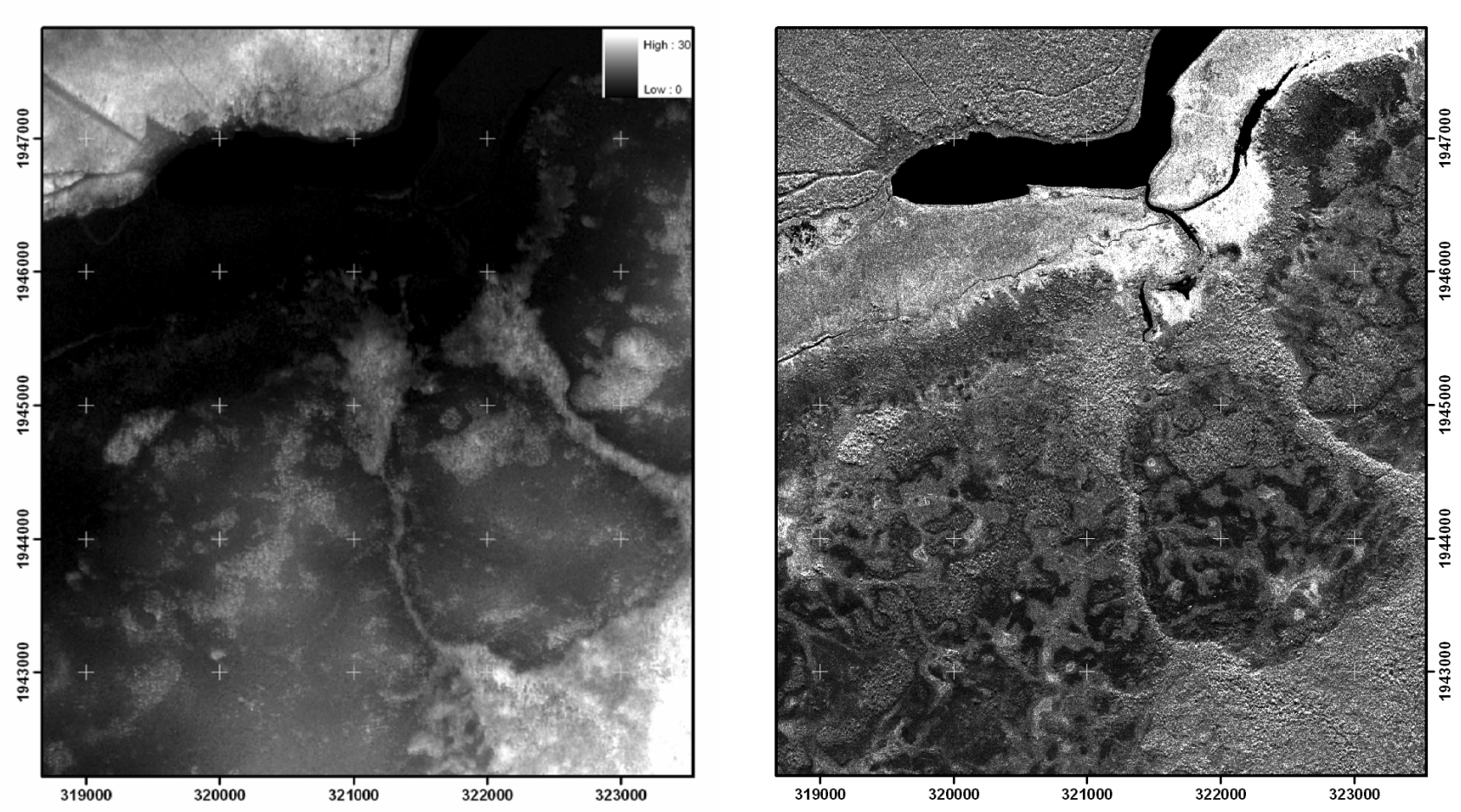

Figure 5.3: Subset of Intermap X-band data: (a) DSM, and (b) Orthorectified Image (ORI)

were in digital numbers[2]. The data were acquired over two days during the dry season in March/April 1999. The data characteristics are summarised in Table 5.2 and subsets of the datasets covering the study area are shown in Fig. 5.3.

Table 5.2: Intermap data characteristics (Source: Intermap data header files)

Platform	Learjet 36A, airborne
Sensor	STAR-3i
Wavelength	X-band, 3 cm, 9.5 Ghz
Polarisation	HH
Flying Height	9144 m
Range direction	180°
Look angle (near, far, ave. at study site)	Normally between 30° and 50°. Average at study site is unknown as data is made up of several different swaths.
InSAR baseline	1 m
Acquisition Dates[3]	28/03/1999, 04/04/1999 (majority acquired on 04/04/1999)
DSM posting **ORI posting**	5 m 2.5 m
Horizontal RMSE	2 m
Vertical RMSE	3 m
Projection	UTM/WGS84
Datum	EGM96 (geoidal), Mean Sea Level

5.2.1.3. SRTM

The Shuttle Radar Topography Mission (SRTM) is the first fixed baseline single-pass spaceborne InSAR system. It obtained single-pass spaceborne C-band elevation data from the Space Shuttle Endeavour during February 2000. The coverage is near-global, covering the Earth's surface between the latitudes of 60° N and 58° S. Spatial resolution over the study area is 3 arcseconds of latitude (~90 m). Higher resolution (1 arcsec, ~30 m) X-band InSAR data, developed by the German Aerospace Centre (DLR) was acquired concomitantly. The higher resolution data only covers a 50 km

[2] Intermap Technologies do not provide calibration constants with the data (Mercer, 2007). The ORI could therefore not be used for quantitative analysis and was only used for visual interpretation.

[3] The metadata listed the acquisition dates for the entire Intermap dataset for Orange Walk District as 26 March 1999 - 5 April 1999, but the specific dates on which the data was acquired over the study site have been confirmed by Bautts (2006).

sub-strip within the 225 km C-band InSAR data swath width and therefore unfortunately misses the study area. The C-band data was downloaded free of charge from the Global Land Cover Facility[4] (GLCF). The scene types downloaded are in WRS-2 format, prepared by the US Geological Survey (USGS). The data characteristics are summarised in Table 5.3 and a subset of the dataset covering the study area is shown in Fig. 5.4.

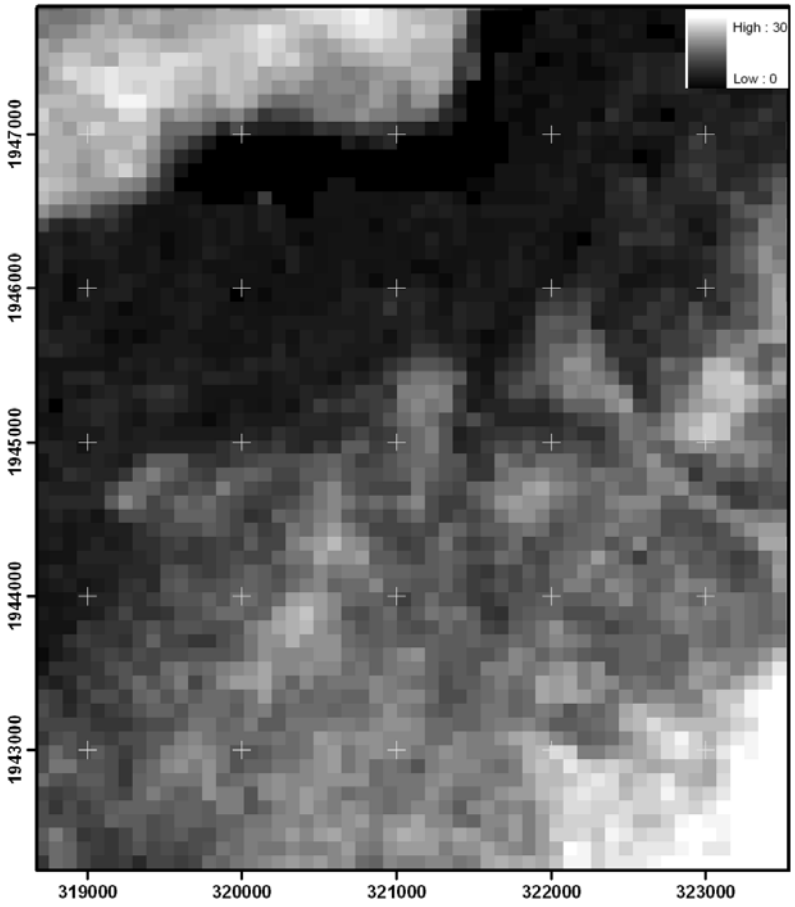

Figure 5.4: Subset of Shuttle Radar Topography Mission (SRTM) C-band DSM data

[4] http://glcf.umiacs.umd.edu/data/

Table 5.3: SRTM data characteristics (Source: Rodriguez, *et al.* (2006))

Platform	Space Shuttle Endeavour
Sensor	C-RADAR
Wavelength	C-band, 5.6 cm, 5.3 Ghz
Polarisation	Dual-polarisation capability: 4 subswaths transmit/receive H,V,V,H
Orbit height	233 km
Range direction	Varying
Look angle	15°-55°
InSAR baseline	60 m
Acquisition Date	11-22/02/2000
DSM posting	90 m
Absolute geolocation error	<20 m
Absolute height error for study area	5–10 m
Projection	Scene type WRS-2: UTM/WGS84
Datum	WGS84 (geoidal), Mean Sea Level

Table 5.4: IKONOS data characteristics (Source: GeoEye (2006))

Platform	IKONOS satellite
Operator	GeoEye
Spectral range	0.4450 - 0.516 μm (B) 0.506 - 0.595 μm (G) 0.632 - 0.698 μm (R) 0.757 - 0.853 μm (NIR) 0.526 - 0.929 μm (Panchromatic)
Orbit height	681 km
Orbit	98.1 degree, sun synchronous
Product	Georeferenced bundle product
Elevation angle from Earth's horizon	Typcally between 60 and 90°
Acquisition Date	07/03/2007, ~10:30 am local solar time
Resolution, nominal at 26° off-nadir	4 m (multispectral) 1 m (panchromatic)
Absolute geolocation error	< 50 m, without ground control
Datum/Projection	WGS84/UTM 16N

5.2.2. Optical data

5.2.2.1. IKONOS

A high resolution multispectral IKONOS image was acquired over the study area on the 7th of March 2007. The image consists of 4 bands, at 4 m-resolution, in the blue, green, red and near-infrared regions of the electromagnetic spectrum. The image was

georeferenced to the WGS84 datum and provided in a UTM 16N projection by the data provider. The image contains less than 10% cloud cover, which was specified with the order. The 1 m-resolution panchromatic band was used to pan-sharpen the multispectral bands using principle components analysis, which derives the spectral information from the multispectral bands and adds it to the panchromatic band. The data characteristics are summarised in Table 5.4 and a subset of the dataset covering the study area is shown in Fig. 5.5.

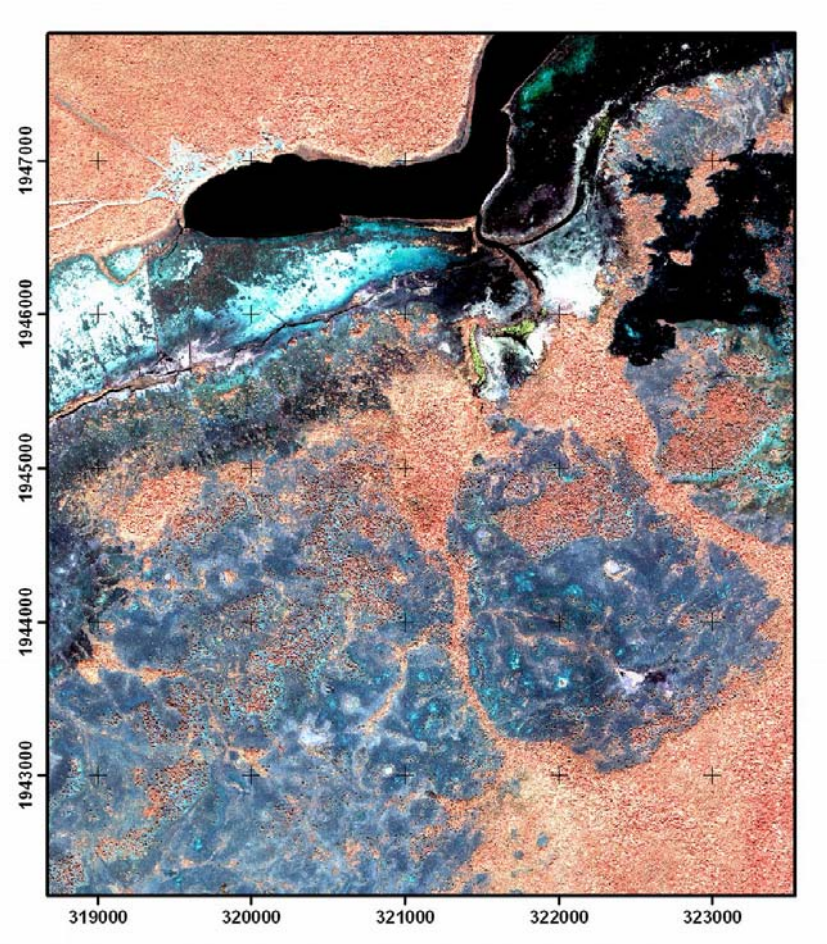

Figure 5.5: Subset of the IKONOS image, displayed as a false colour composite (4-2-3, RGB).The image has been pan-sharpened using the panchromatic channel.

5.2.2.2. Oblique aerial photography

A flight was made over the transect area during the 2005 fieldwork campaign, during which oblique digital aerial photos were made. The purpose of this additional imagery was to augment field data and to give a better understanding of the view that

a radar sensor would have. This assisted with the interpretation of unknown features in the radar data. Air marking was applied on both ends of the survey network that formed the backbone of the field data transect; this guided the capture of oblique digital photography. Examples are shown in Figs. 5.7 and 5.9.

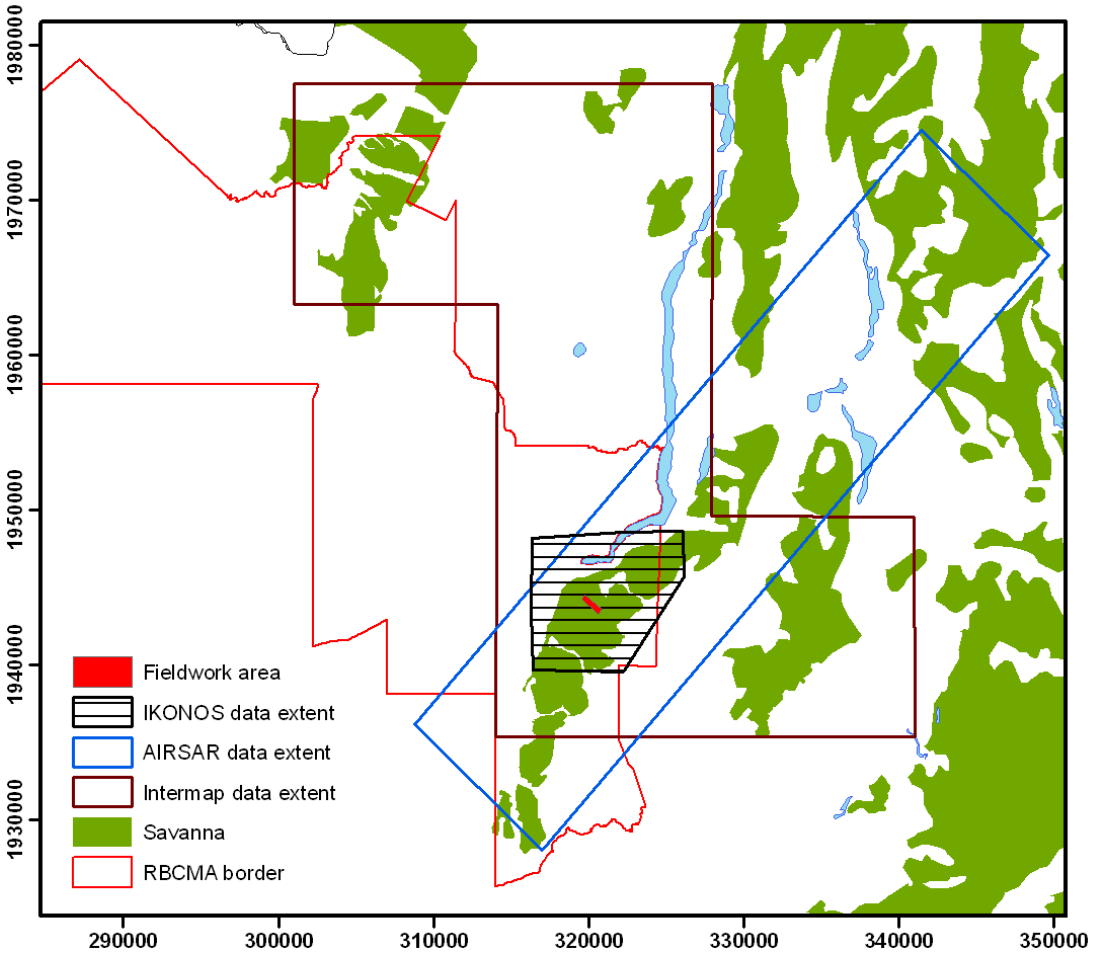

Figure 5.6: Map showing the location and coverage of all EO data in relation to the fieldwork area, for which detailed *in situ* data was collected in a transect in 2005. The SRTM data covers the whole map area. The oblique aerial photographs (section 5.2.2.2) are scattered over the study area and are not indicated on this map.

(a)

(b)

Figure 5.7: Two examples of oblique aerial photographs taken over the fieldwork area.

5.3. Field data

Field data was collected during two fieldwork campaigns. Detailed *in situ* measurements were made during the first fieldwork campaign, which formed the main field data collection element. This was conducted during a period of 6 weeks (4 April to 12 May 2005). The objective for this campaign was to collect accurate positional and dimensional data for the woody vegetation (trees, shrubs and palmetto) of the typical vegetation strata of the RBCMA savanna. A second fieldwork campaign lasting 8 days was conducted 5 to 12 April 2007. The main aim was collection of land cover data for two MSc projects (Jaas, 2007, Zisopoulis, 2007) and the opportunity was seized to obtain ancillary data for this research, including ground elevation data over a wider area and measurements for tree growth analyses. This section describes the field data and how it was collected.

5.3.1. Description of field data

The field data encompasses survey-grade positional data (comprising of x, y, z coordinates) and dimensional data for the woody vegetation within a transect area of approximately 800 m x 60 m crossing the typical vegetation strata of the RBCMA savannas. Data on the physical dimensions for each of the trees and shrubs comprise total height, diameter at breast height (dbh) and crown depth (from crown height measurements). Crown diameter measurements were made for a ~40% subset of the trees and shrubs, while the remainder of the crown measurement data are estimated based on regression analysis (see 5.4.4). Data for single palmettos comprise height and dbh, while height and dbh data on palmetto clumps exist for a representative sample for each clump. Additional data for each palmetto clump include a stem count. The data set consists of 1133 mapped points for pine (580), oak (125), shrubs (314), dead tree stems (25) and single palmetto (89) while polygons were mapped to represent palmetto thickets (75). Points for single palmetto may include multiple stems; most have <4 stems but several have up to 8 stems of which most are < 1.3 m tall. Additional ground points (2464) were collected in areas of open grass in the transect area. Fig. 5.8 shows a map of the transect field data.

Two years after the initial field work campaign, a ~10% subset of savanna woodland trees were re-measured for dbh, tree height and crown height to analyse the rate of tree growth in the savannas. This was done to take into account tree growth in the period in between InSAR data acquisitions (see 6.6.2 for further discussion). Additional data that were collected comprise average tree heights for a number of gallery forests (used for analysis discussed in 6.6.3) and ground elevation points over open grassland areas, spread over a wide area of the savanna to be used for quality assessment of the InSAR data (see 5.7.2).

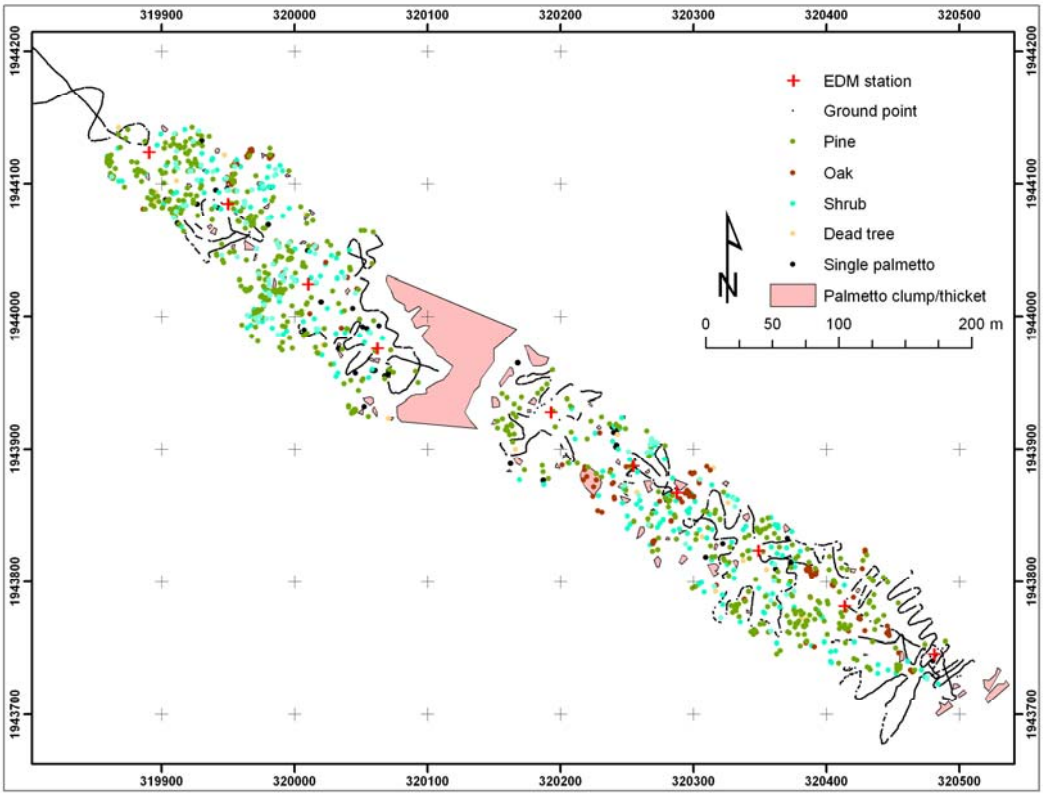

Figure 5.8: Map showing the transect field data. The locations of the six GPS stations at the far end of the transect are located outside the map area, but the positions of the total station electronic distance measurement (EDM) survey stations from which the vegetation was mapped are shown (see 5.3.2).

5.3.2. Field data collection methodology

Based on previous experience in the study area, when fieldwork was undertaken in plots (Cameron, *et al.*, 2006), it was decided to collect the main field data in a transect oriented in the range direction of the AIRSAR data (bearing 310°, see

5.2.1.1). This would allow for the identification of the effects of radar layover and shadowing during data interpretation. The Intermap range direction (180°, see 5.2.1.2) would then cross the transect at an angle of 50°. Although the SAR data ground resolution is at 5 m postings, it was decided that the field data should be collected at a higher spatial accuracy (mapped with a spatial accuracy < ~1 m) in order to allow for the possibility of future work to be undertaken in the savannas using very high resolution EO data (Moss, *et al.* (2006), included in Appendix I).

To obtain a field data transect at this level of spatial accuracy, a dual-frequency GPS receiver was used in combination with a total station to set up a linear survey network (see 5.3.2.1) along a transect line from which a point-of-detail survey (see 5.3.2.2) was conducted to map the woody vegetation. The fieldwork equipment is described in Appendix III. All trees, shrubs and palmetto taller than 1.3 m occurring within 30 m to both sides of the main transect line were included in the data collection. During the planning stages it was envisaged that the transect should have a width of at least 10 m and a length of approximately 400 m. The width dimension was based on the AIRSAR pixel size of 5 m, so that a 10 m-wide ground transect in the AIRSAR range direction would include sufficient ground data to compare to the SAR data. The length of the transect was based on the assumption that a ground transect spanning several savanna vegetation strata would have a considerable length. It was anticipated that a transect length of approximately 400 m would be feasible for collecting sufficient data in a 6-week period. However, due to uncertainties on the time needed for data collection, the fieldwork was planned with flexibility in mind.

A number of possible transect sites were identified during a desk-based study of the EO data before arrival at the field site. These were chosen based on the presence of vegetation strata typical of the savannas and accessibility from the field station. The candidate sites were visited during the first day in the field, upon which a suitable location was chosen approximately 2-3 km south of Hill Bank field station (Fig. 5.11 for location, Fig. 5.9 for site description). This site provided the potential for a transect to cross two pine ridges on both sides of a large palmetto ticket and had an area of open pine-palmetto savanna on either end, which were ideal for placing the GPS observation points needed for establishing the survey network. As these two end points would be connected by a number of survey stations in the survey network (see

5.3.2.1), flexibility was provided so that, in case of unforeseen constraints, data collection along the whole transect could be easily replaced by data collection along shorter, separate portions of the transect containing specific vegetation strata. The reasons for choosing this specific survey methodology is explained in Moss, *et al.* (2006:27-28), included in Appendix I.

Figure 5.9: An oblique aerial photo showing the centre line of the transect starting (from the far end) in an area of open pine-palmetto savanna, crossing a savanna woodland, passing through a local depression of palmetto thicket and then crossing through a second savanna woodland, ending in an area of open pine-palmetto savanna. The white cross visible in the foreground marks the position of the second traverse terminus (GPS2, see 5.3.2.1) and was placed for the purposes of air marking for the collection of oblique aerial photography (see 5.2.2.2)

During the second fieldwork campaign, a ~10% subset of savanna woodland trees were located by means of their coordinates and re-measured for dbh, tree height and crown height. The re-measured trees were permanently marked with numbered aluminium markers for future monitoring of tree growth rates in the savanna, a data need that was identified both by the Programme for Belize (Chuck, 2007) and the Belize Forest Department (Cho, 2007) upon enquiry on the existence of such data. Average tree heights were measured for a number of gallery forests (see 5.3.2.2) and

ground elevation for points on open grassland were extracted from land cover data collected by means of GPS (Jaas, 2007).

5.3.2.1. Establishing the survey network

The linear survey transect from which all other measurements (points-of-detail) were collected consisted of two traverse termini (GPS1, GPS2[5]), two reference objects at each terminus (1RO1, 1RO2, 2RO1, 2RO2) to provide opening and closing traverse bearings, and ten traverse/topographic detail stations (Stn 1 to Stn 10) which formed the main transect line from which all points of detail were collected (see Fig. 5.10). The linear survey network measured ~950 m in length between the two end points, each located in an open pine-palmetto savanna. GPS observations were carried out on each of the six traverse termini using the Trimble 4000SSi GPS receiver and the Trimble total station was used to observe the transect using the method of EDM reciprocal height traversing.

The survey network and point-of-detail survey were measured before the actual geographical coordinates of the traverse termini and reference objects of the linear survey network were known (section 5.4.1 describes post-processing of the GPS data). Therefore, arbitrary coordinates (5000, 5000, 100) were entered for the point of origin (GPS1) and an arbitrary azimuth angle (0°) was entered for the first measured angle (GPS1 to 1RO1). The survey network was initially mapped based on these arbitrary grid coordinates (in m), and then transformed into UTM grid coordinates (see 5.4.1).

Since the method chosen for post-processing the GPS data suggested a minimum of 6 hours observation time this was attempted for all GPS points, constrained by logistics only for GPS1. To enable evaluation of GPS positions obtained during post-processing of the GPS data (see 5.4.1), a known point (station 917) in the Belizean Geocentric Datum (ITRF 1994 epoch 1996.0), hereafter referred to as BGD96 point 917, was re-observed. As BGD96 point 917 was to be used for evaluation of the GPS data collection (see 5.5.1), it was logged for as long as possible. The maximum logging time possible given the 512 kb memory of the GPS data logger was 9 hours

[5] The position of GPS2 is shown on an oblique aerial photo in Fig. 5.9.

34 minutes. Fig. 5.11 shows the geographical location of all GPS observation points (the traverse termini, reference objects and BGD96 point 917) as well as the survey stations. The observation time for each of the GPS stations is shown in Table 1 in Viergever, *et al.* (2006:33) (included in Appendix II).

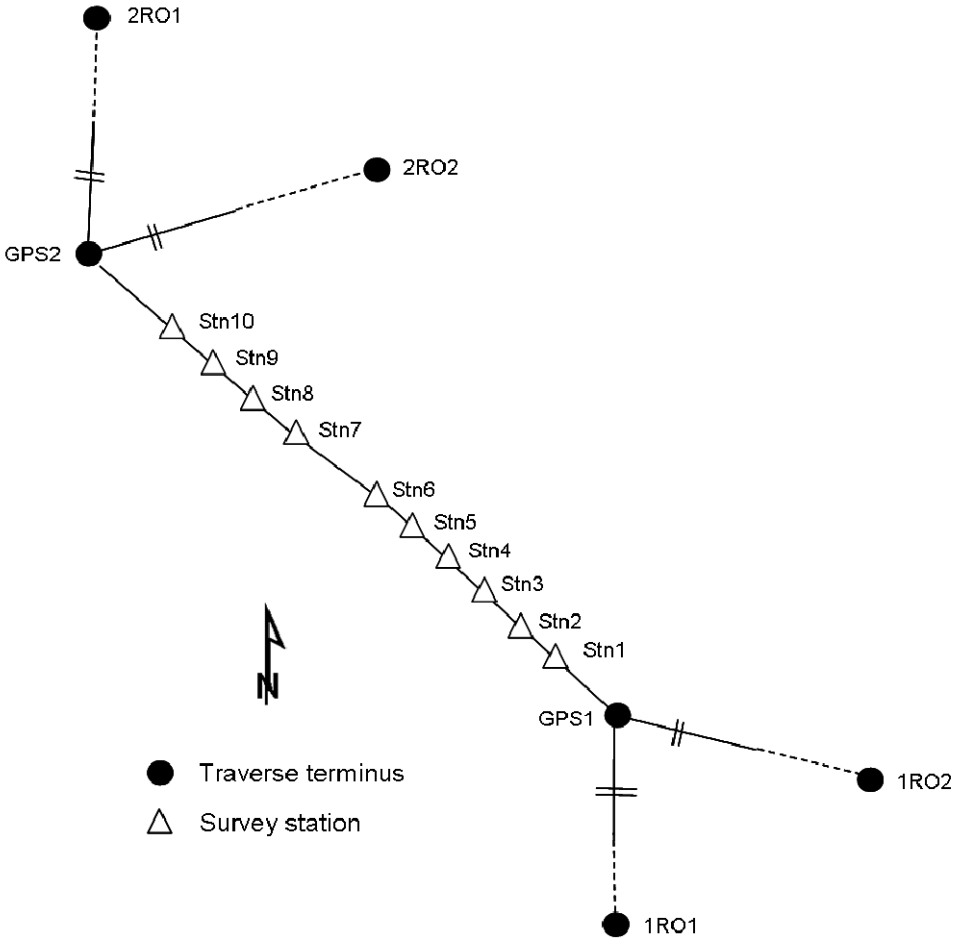

Figure 5.10: Traverse diagram showing traverse termini and reference objects observed by GPS as well as the 10 survey stations from which the point of detail survey was conducted

5.3.2.2. Point-of-detail survey

A detailed point-of-detail survey was undertaken from each of the ten traverse stations (Stn 1 to Stn 10) for all trees, shrubs and palmettos measuring > 1.3 m in height. This section describes the different positional and dimensional data collected as part of the survey.

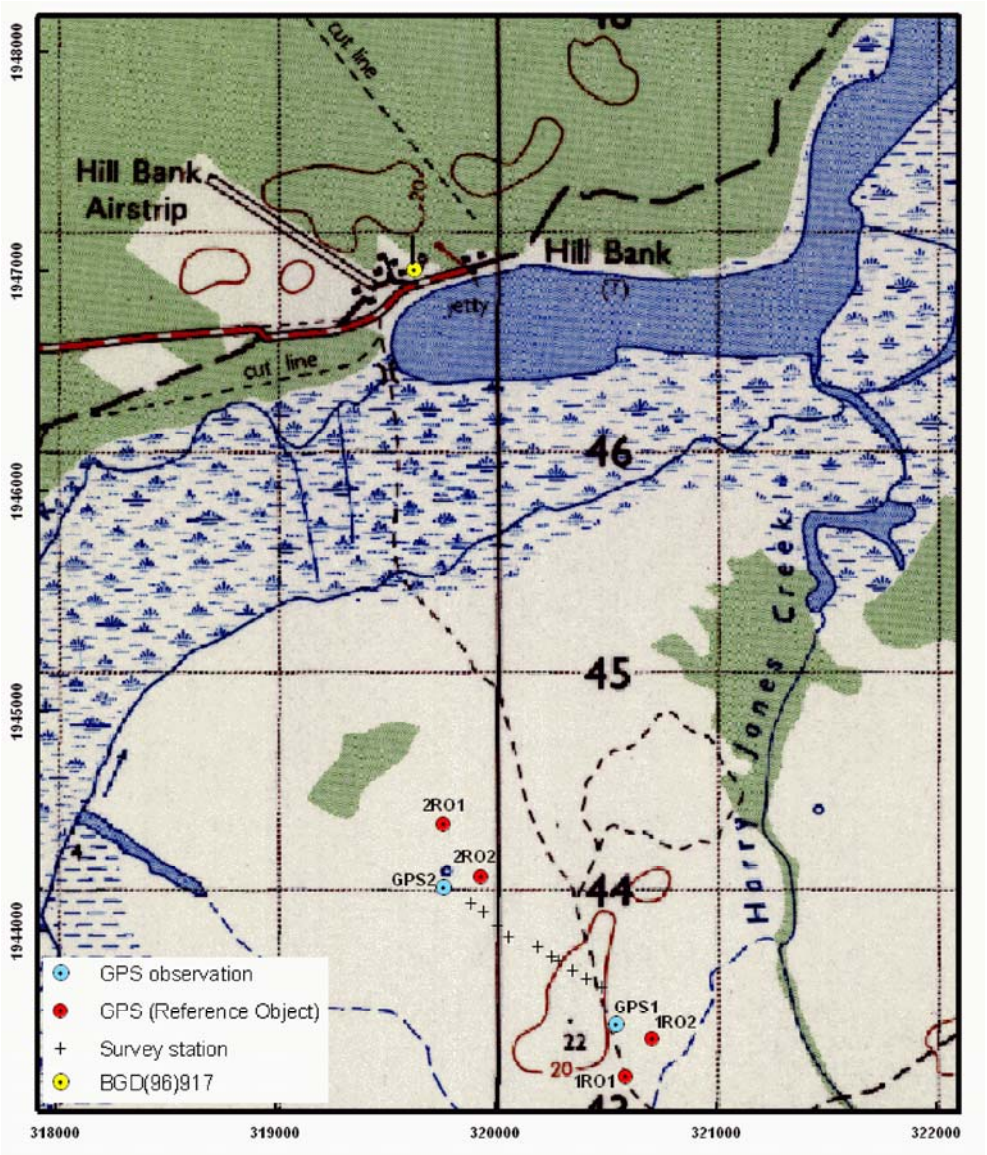

Figure 5.11: Geographical location of all GPS and traverse survey stations. Projection UTM 16 N, WGS84. Mapsheet reprojected to WGS84 from NAD27. Topographic map extract from 1:50,000 series (E555) by Military Survey, U.K. © Crown copyright 1993. Crown copyright map reproduced with the permission of the Controller of Her Majesty's Stationery Office.

Three-dimensional survey point coordinates

All woody vegetation included in the point-of-detail survey was first mapped with horizontal (x and y) coordinates and an elevation (z coordinate). Care was taken to follow a consistent method when mapping the x, y, z position of every tree, shrub and single palmetto in the transect as a point, and palmetto clumps and thickets as

polygons. Single points were mapped by placing a target prism pole as close as possible to the tree stem before recording the position with the total station. The target prism was always placed vertically according to surveying principles (Bannister*, et al.*, 1998), in the middle of the width of the tree stem as seen from the direction of the total station. The z position (ground elevation) was consistently recorded by placing the target prism pole lightly on the ground surface, taking care not to place the target on piles of dead litter or other obstructions. Since the target prism was at a known height, the ground elevation was calculated during post-processing (see 5.4.1). In some cases the target pole had to be placed slightly away from the stem, for example when the base of the tree was wide. In case of a leaning tree, the x, y, z position was mapped at the point where the stem grows out of the ground (see Fig. 5.12(a)). This occurred for < 1% of mapped trees. Where trees with multiple stems clearly formed a single tree, the target pole was placed on the ground surface in the centre of the multiple stems. This occurred mostly for oak trees, which tend to grow in clusters.

Following the above methodology, the x, y position of the centre of a single tree stem could be estimated for most cases based on the dbh measurement, by taking into account the stem radius. This was not done for the data set as the average maximum offset (in either x or y) for mapping the exact centre of every tree stem was calculated as ~0.08 m (based on an average dbh value of ~0.17 m), while the median maximum offset was ~0.06 m and the maximum offset was ~0.66 m. These offsets are within the ±1 m spatial accuracy which was aimed for in final field data accuracy.

Polygons delimiting palmetto clumps or thickets, were mapped as a collection of points containing a separate code for the start node and the end node. When mapping the points, the target prism pole was placed as close as possible to the edge of the palmetto clump or thicket before recording the position with the total station. A collection of points was recorded starting from one end and then moving systematically around the palmetto clump or thicket, placing points so as to best map the shape of the palmetto grouping.

Additional ground elevation points were collected in areas that were not covered by trees in order to produce an accurate ground surface digital elevation model (DEM, see 5.4.2). This was done by means of rapid ground point collection using the automatic-tracking mode of the EDM total station. During the 2007 fieldwork campaign, additional ground elevation data (2130 points in total) were collected in open grassland areas to assess the accuracy of the DSM data sets. Data were collected over a wider area in the savannas as opposed to the very localised and dense ground elevation data collected in 2005. The 2007 ground elevation data were collected by means of the two handheld Trimbles (see Appendix III).

Tree species

Every tree and shrub included in the data collection was assigned to one of the following tree species: Caribbean Pine (*Pinus caribaea*), Oak (*Quercus Oleoides Schltdl and Cham.*), Sandpaper tree/Yaha (*Curatella americana*), Wild Craboo (*Byrsonima crassifolia*) or Palmetto/Paurotis palm (*Acoelorraphe wrightii* (Griseb. & H. Wendl.)). For simplification, Yaha and Craboo were later combined into a separate *shrub* class as they both form shrub-like vegetation that mostly forms undergrowth in the savanna woodlands. Since they mostly form under-storey vegetation and have a relatively low biomass (Brown*, et al.*, 2005), it is expected that the results of this research will not be affected by not distinguishing between the shrub species.

Total height

Total height is defined as the vertical height of the tree, measured from the ground to the tip of the tree; not the length of the bole in case of a leaning tree (Philip, 1994, Husch*, et al.*, 2003). As the vegetation on the savanna woodland in the study area is sparse, the top part of the tree crowns were clearly visible. Where total height was measured for dense vegetation of the gallery forests, the height readings were made on the outer edges and through existing paths where the treetops were visible. This enabled measurement of total height by means of an indirect method, employing trigonometric principles. The use of a Vertex hypsometer ensured greater accuracy (see Appendix III) as horizontal distances are measured more precisely and potential

calculation errors are eliminated (see Fig 5.12(b)). Due to the nature of the trees in the study area, care was taken to avoid the two main possible sources of observational error:

- Errors due to non-linearity of the relationship of tree height and angle of sight (Philip, 1994). This occurred mostly for trees with round-shaped crowns of which the sides obscured the view of the tip of the tree. The tendency would be to overestimate the height of such trees when the hypsometer is pointed to the highest visible part of the tree crown. To avoid this error, care was taken to focus the hypsometer at the tip of the tree.
- Errors due to leaning trees occur because the hypsometer works on the assumption that measured trees are vertical. A tree leaning away from the observer is therefore underestimated, while trees leaning towards the observer are overestimated (Husch*, et al.*, 2003). Although a rare occurrence in the study site, observational error in such cases was avoided by taking measurements from a point where the lean was either to the left or the right of the observer.

For height measurements, an overall relative accuracy of ±10% is expected to be achieved from ground survey techniques (Phillips*, et al.*, 2000, Chave*, et al.*, 2004).

Crown height

Crown height is the vertical distance from the lower boundary of the crown to the ground level (Philip, 1994). The height of the lowest complete whorl of live branches, defining the lower margin of the tree crown, was measured with the Vertex hypsometer while measuring tree height. Crown depth, the vertical distance between the lower boundary of the crown to the tip of the tree, was later derived by subtracting crown height from total height.

Diameter at breast height (dbh)

Diameter at breast height (dbh) refers to the diameter of the tree bole, outside the bark, at a height of 1.3 m above ground level (Philip, 1994, Husch*, et al.*, 2003). This was measured directly with a dbh measuring tape (see Fig. 5.12(c)). Trees with special circumstances were measured according to standard procedures (Husch*, et*

al., 2003). Leaning trees were measured parallel to the lean on the high side of the tree, with dbh measured perpendicular to the longitudinal axis of the trunk. Trees that were crooked or had an abnormality at breast height, were measured just above the abnormality; trees of which the bole forked at or above breast height were measured as one tree just below the enlargement caused by the fork; trees of which the bole forked below breast height were measured as separate boles, adding up the separate dbh values during processing of the data.

(a) **(b)** **(c)**

Figure 5.12: Point-of-detail survey: (a) collection of three-dimensional survey point coordinates, (b) total height measurement, and (c) diameter at breast height measurement.

Crown diameter

Field measurements of tree crown diameter are complex due to the natural irregularity of tree crowns (Husch*, et al.*, 2003) and potential interlocking of tree crowns in dense tree patches (Philip, 1994). The average crown diameter may therefore be measured and calculated in a number of ways. Philip (1994) lists five methods, of which one was applied (i.e., measuring two diameters at right angles, oriented to a specific compass bearing). For practical purposes, the measurements were made as four separate radii from the tree bole outwards to the edge of the tree crown in the four main compass directions of 130º and 310º, coinciding with the range direction of the AIRSAR radar data and 40º and 220º, perpendicular to the AIRSAR range direction.

Where neighbouring trees had interlocking crowns in the direction of the radius to be measured, the distance between the two boles was measured and the average radius for the two interlocking crowns was calculated. Finally all crown radius data was converted into two perpendicular crown diameters. Although this does not always

give a true representation of crown shape, especially for oak and shrub, tree crowns are averaged to a circular shape for simplified visualisation.

Due to time constraint, crown diameter was only measured for a ~40% subset of the trees and shrubs, in a ~20 m wide strip towards the centre of the transect area. An amount of 412 trees and shrubs were measured out of the total of 1019 trees and shrubs in the transect: 270 out of 580 pine trees, 46 out of 125 oak trees and 96 out of 314 shrubs.

Palmetto clumps and thickets

The palmetto plants that occur within a clump tend to be uniform; therefore data collected for palmetto clumps comprise a ~5-10% sample of total height and dbh measurements as well as a complete stem count for the palmetto clump. The Vertex hypsometer and dbh measuring tape were used. As palmetto thickets were large, containing numerous palmetto plants of near-uniform height, a number of total height measurements were taken to characterise the average height of the thicket. Due to the density of the thickets, stem count was not possible. This data gap was filled during the 2007 fieldwork campaign, when Furley (2007) collected palmetto stem density data in palmetto thickets. This was made possible due to a fire in the study area which defoliated many of the palmettos (see Fig. 4.16(b)) and made the palmetto thickets accessible for stem counts.

5.4. Processing of field data

Various analyses were carried out on the field data for further use in the height retrieval and backscatter analyses of this research as described in Chapter 6. The GPS data were post-processed to obtain GPS solutions, which were then used to adjust the survey points to the UTM/WGS84 projection (5.4.1) to match the datum and projection of the EO data. A ground surface DEM was created for the survey transect using all adjusted data points (5.4.2). The point-of-detail vegetation survey data was further processed to calculate palmetto stem number densities for the transect area (5.4.3) and to estimate crown diameters for the trees that had not been measured for crown diameter (5.4.4). An analysis of tree growth in the study area,

based on tree height and dbh measurements during the two fieldwork campaigns in 2005 and 2007, forms an important part of the interpretation of the InSAR vegetation height retrieval analyses (see 6.6.2) and is discussed in 5.4.5.

5.4.1. Processing of positional data

During the 2005 fieldwork campaign, the GPS observation file was downloaded as DAT file from the Trimble 4000SSi receiver after each logging session. The DAT file was then converted into RINEX format and quality checked using TEQC GPS Toolkit freeware available from UNAVCO[6]. TEQC primarily provides translation, editing and quality check functions (UNAVCO, 2007). The RINEX files were then sent to two different web-based automated GPS data analysis services to determine the exact positions of each of the GPS stations. Two services were used to ensure a usable outcome in case one failed and for comparative purposes if both successfully delivered GPS point coordinates. These two services (AUSPOS[7] and Auto GIPSY[8]) are described in Viergever, *et al.* (2006:33) (included in Appendix II).

Horizontal coordinates (x and y) obtained from both web-based services were in precise ITRF geodetic latitude and longitude. In order to bring them in line with the projection of the EO data, these were converted to Universal Transverse Mercator (UTM) coordinates, UTM Zone 16 N, on the WGS84 ellipsoid using UTMS freeware available from the US National Geodetic Survey[9].

Elevations derived from GPS are relative to the GPS reference ellipsoid, WGS84 (Bannister, *et al.*, 1998). However, the reference surface for ground elevations is traditionally taken as Mean Sea Level (MSL), also known as elevation above the geoid (DMA, 1991). Both web-based services returned the elevation coordinates (z) in relation to the WGS84 ellipsoid (ellipsoidal height), while AUSPOS also provided the elevation coordinate as an above-geoid value. The separation between the geoid

6 http://facility.unavco.org/
7 http://www.ga.gov.au/geodesy/sgc/wwwgps/
8 http://milhouse.jpl.nasa.gov/ag/
9 http://www.ngs.noaa.gov/PC_PROD/UTMS/

and the ellipsoid is known as the geoid-ellipsoid separation (DMA, 1991) (see Fig. 5.13), calculated by equation 5.1:

$$N = h - H \qquad 5.1$$

where N is the geoid-ellipsoid separation,
h is elevation above ellipsoid,
H is elevation above geoid.

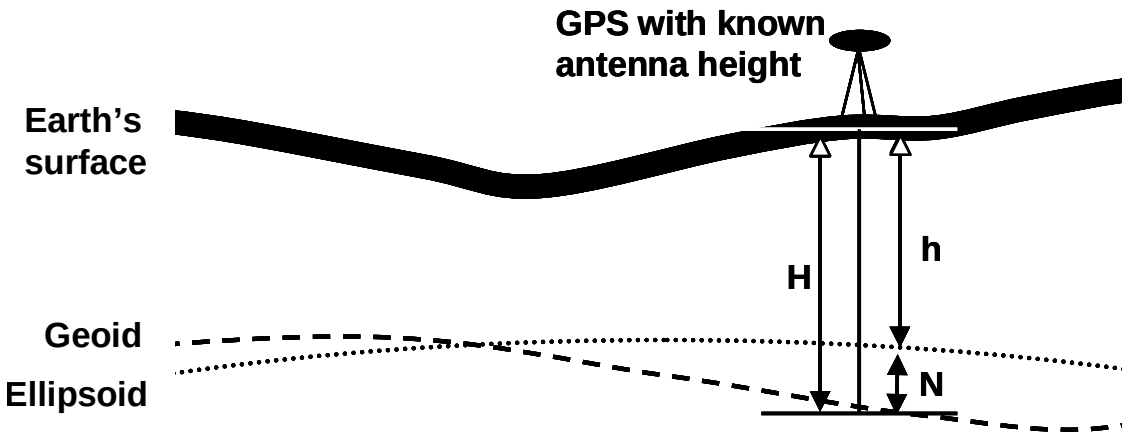

Figure 5.13: Diagrammatic representation of the geoid-ellipsoid separation, N

Based on the above-ellipsoid and above-geoid elevation coordinates returned by AUSPOS, the geoid-ellipsoid separation was calculated as ~-5.7 m for the study area. The above-ellipsoid elevation coordinates returned by Auto GIPSY were adjusted accordingly to calculate above-geoid elevation coordinates. Neither service took into account the offset caused by the GPS antenna height, which was adjusted for manually.

Since the survey network and point-of-detail survey were carried out before GPS solutions for the linear survey network were known, all survey points were recorded in an arbitrarily chosen coordinates (see 5.3.2.1). After GPS post-processing, Trimble Geomatics Office software was used to adjust the survey network and to transform all survey points to UTM grid coordinates by entering the known geographic coordinates of the traverse termini (GPS1, GPS2) and two reference objects (1RO1, 1RO2, 2RO1, 2RO2).

During the 2007 fieldwork campaign, GPS observations were taken in the field using the Trimble handheld GPS instruments while the 4000SSi GPS receiver (see Appendix III) was used as a base station (over known point BGD96 point 917) for differential correction. For the short period that our base station encountered errors, GPS data from the Belmopan Land Information Centre was used as substitute (Jaas, 2007).

5.4.2. Creation of a ground surface DEM

To obtain an estimation of the ground surface of the transect area under the trees, a Digital Terrain Model (DEM) of the ground surface was created by means of Inverse Distance Weighted (IDW) interpolation. The IDW interpolation method in ArcMap assumes that points closer to the prediction location have a larger influence than points further away. Although the output surface of this method is sensitive to clustering and the presence of outliers, this was not expected to be a problem on the gradual slopes of the study area. All mapped data points were used: the ground elevation height of all mapped trees and palmetto, GPS and EDM stations as well as mapped ground points over open areas including extra ground points outside the transect area, giving a total of 4176 ground elevation points for an area of 283,324.2 m^2, (28.33 ha); i.e. an average point density of 0.0147 points/m^2 or 1.47 points per 100 m^2 (147.4 points/ha). The resulting ground elevation DEM is shown in Fig. 5.14. The distribution of the data points used for the interpolation is superimposed on the DEM. Areas with higher point densities, such as the transect area, are expected to have the most accurate ground surface DEM interpolation. The DEM shows that the change in ground surface elevation is very gradual in the study area, with a slight decrease in elevation occurring in a north-westerly direction (i.e., in the range direction of the AIRSAR data). The total difference between the lowest and the highest points is 8.5 m. The gradual slope and low relief of the study area does not require special SAR processing or orthorectification of optical EO data to account for topography.

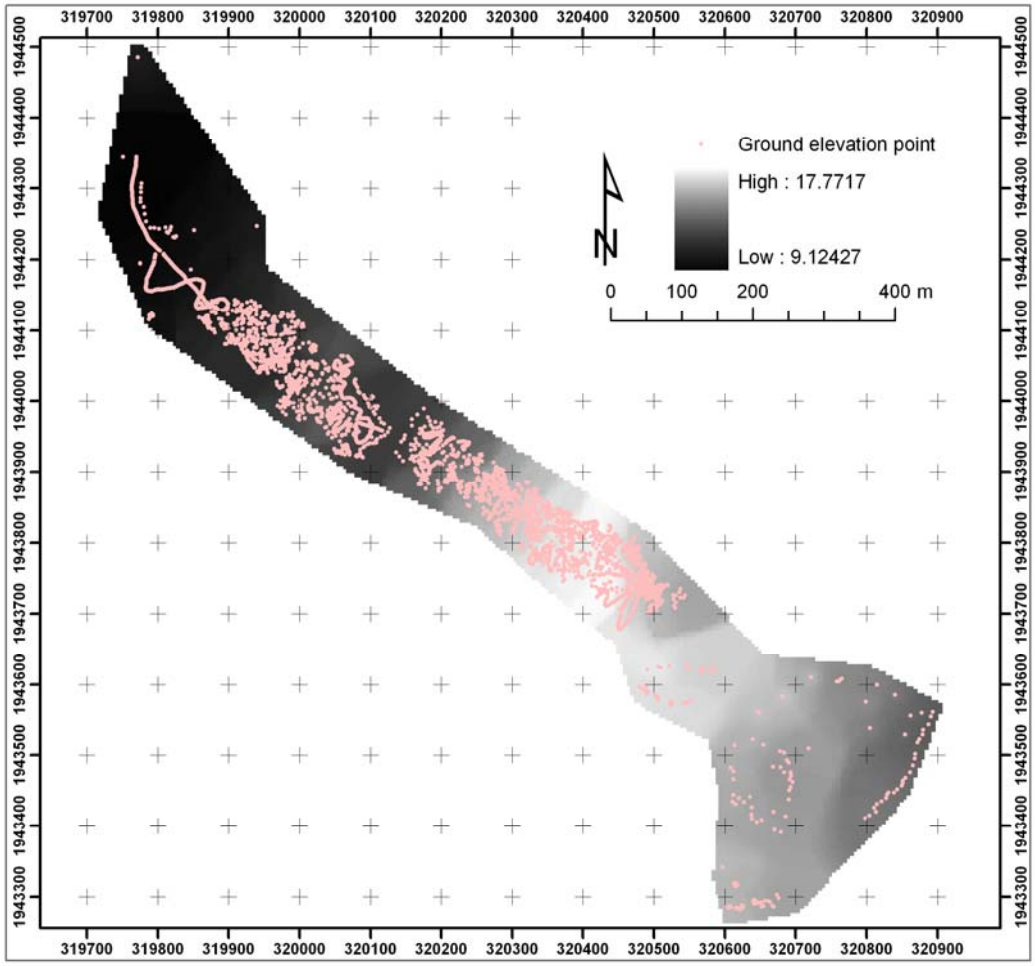

Figure 5.14: The IDW interpolated ground surface DEM with the ground elevation data points (4176) used for interpolation.

5.4.3. Calculation of palmetto stem number density

Average palmetto stem number density within palmetto clumps was calculated based on the stem counts for the palmetto clumps that were mapped as polygons. The number of palmetto stems was divided by the surface area for all mapped palmetto clumps having a stem count (63 clumps). The average stem number density for the 63 clumps was 1.4 stems/m^2. This was rounded down and used in further analyses as 1 stem/m^2, assuming a uniform distribution of palmetto stems across the study area. Palmetto number densities for the generally sparser palmetto thickets became available at a late stage in the research (see 4.5.3) and were therefore not

incorporated in the processing although it was taken into account during data interpretation.

5.4.4. Estimation of missing crown diameter measurements

Since only a 40% subset of all trees and shrubs had been measured for crown diameters during the 2005 fieldwork (see 5.3.2.2), crown diameter data for the rest of the trees was estimated using regression analysis. The data variables investigated as possible estimators for average crown diameter were dbh and tree height.

Initial visual tests for normality of the data (an assumption of the linear regression analysis model (Quinn and Keough, 2002)) showed that the histograms of all data variables were skewed. Visual inspection of scattergrams for the data with dbh and height as independent variables against average crown diameter as dependent variable showed a slightly curved relationship and heteroscedasticity (i.e., an uneven distribution of variances over the length of a fitted straight line). This suggested the need for transformation of one or both of the variables to normalise the data for regression analysis. The logarithmic transformation is one of the most frequently used transformations in biological applications and is appropriate where the standard deviation of y increases in proportion to the value of x (Zianis and Mencuccini, 2004). This is typical for growth data, of which the allometric growth curve is a well-known example (Sokal and Rohlf, 1995, Fowler, *et al.*, 1998).

Table 5.5 shows the r^2-values of the fitted linear regression model for each combination of (logarithmically transformed) dbh and tree height as independent variables and crown diameter as dependent variable for pine, oak and shrub. The values for Craboo and Yaha are also shown for comparison to the values for shrub. Logarithmic transformation of both dbh on the x-axis and average crown diameter on the y-axis was shown to be overall most suitable for linear regression analysis. The higher r^2-values for pine trees were expected as they are generally more uniform in shape than oak and shrub.

Table 5.5: Values for the coefficient of determination (r^2) for the linear regression model fitted for each combination of dbh and tree height as independent variable and crown diameter as dependent variable for pine, oak and shrub as well as Craboo and Yaha separately. The shaded cells represent the most suitable independent variables for linear regression analysis for pine, oak and shrub.

Pine	**crown diameter**	**log(crown diameter)**
dbh	0.78	0.83
log(dbh)	0.85	0.89
tree height	0.68	0.76
log(tree height)	0.6	0.73
Oak	**crown diameter**	**log(crown diameter)**
dbh	0.47	0.37
log(dbh)	0.51	0.5
tree height	0.44	0.41
log(tree height)	0.41	0.43
Shrub	**crown diameter**	**log(crown diameter)**
dbh	0.38	0.42
log(dbh)	0.39	0.46
tree height	0.28	0.29
log(tree height)	0.27	0.3
Craboo	**crown diameter**	**log(crown diameter)**
dbh	0.57	0.56
log(dbh)	0.49	0.54
tree height	0.57	0.47
log(tree height)	0.51	0.46
Yaha	**crown diameter**	**log(crown diameter)**
dbh	0.34	0.39
log(dbh)	0.37	0.44
tree height	0.21	0.24
log(tree height)	0.22	0.25

LabFit Curve Fitting Software[10] was used to fit a linear regression model to the logarithmically transformed dbh (as independent variable, x) and average crown diameter (as dependent variable, y). For the purposes of prediction, the linear regression model can be written in the format $y' = mx' + c'$, or $\log y = m(\log x) + \log c$, which can be back-transformed to derive a regression equation in the form $y = cx^m$. The back-transformed linear regression models used for estimation of the missing crown diameter data are listed in Table 5.6. The shaded cells indicate the regression models that were used to estimate missing average crown diameters, upon

[10] Version 7.2.33 was used. LabFit is freeware obtainable from www.labfit.net.

which further analyses are based. Since logarithmic transformation introduces a systematic bias into regression calculations, Sprugel (1983) and Zianis and Mencuccini (2004) suggest the application of a correction factor (see Appendix IV for further discussion on the correction factor suggested by Sprugel (1983)). The values for the correction factor for each of the regression equations are listed in Table 5.6.

Due to their relatively uniform appearance, palmetto crown dimensions were assumed identical for both crown diameter (120 cm) and crown depth (150 cm), based on field measurements.

Table 5.6: Back-transformed linear regression models and concommitant correction factors to estimate average crown diameter (*y* in cm) based on dbh (*x* in cm). Shaded cells indicate regression models used for this research.

Tree type	Coefficient of determination	Back-transformed regression equation (from log-transformed linear regression model)	Correction factor
Pine	$r^2 = 0.89$	$y=21.281x^{0.985}$	1.034
Oak	$r^2 = 0.5$	$y=56.624x^{0.695}$	1.134
Shrub	$r^2 = 0.46$	$y=71.285x^{0.469}$	1.048
Craboo	$r^2 = 0.54$	$y=69.984x^{0.482}$	1.042
Yaha	$r^2 = 0.44$	$y=71.779x^{0.465}$	1.051

5.4.5. Analysis of tree growth

Since part of this research evaluates vegetation height retrieval using EO data acquired in 1999 and 2004, combined with field data collected in 2005 (see 6.6), it is important to investigate growth rates of the main savanna tree species of pine, oak and shrub. Tree height and dbh measurements were re-observed for a subset of 97 trees and shrubs during the 2007 fieldwork campaign. These were compared to the 2005 observations for pine, oak and shrub respectively and investigated for significant growth over the 2-year period. Where growth was shown to be significant, the difference between the means of two samples was calculated to provide an estimate of average annual tree growth. A literature study on growth rates for the main species of the study area was carried out for comparison.

A t-test for matched pairs (Sokal and Rohlf, 1995, Fowler, *et al.*, 1998) was performed to ascertain whether there was a statistically significant difference between the means for total height and dbh measured in the two fieldwork campaigns[11]. A two-tailed test was carried out on all observations, including obviously incorrect measurements such as those that suggested a decrease in height or dbh over the two-year period. The results, which are shown in Table 5.7, showed only significant differences for the means of pine dbh and height as well as shrub height between the two measurements.

Table 5.7: Summary of results of the two-tailed t-test for matched pairs. Shaded cells indicate a statistically significant difference.

Tree measurement	t-statistic	Degrees of freedom	p-value
Pine height	-9.408	72	< 0.01
Pine dbh	-7.462	72	< 0.01
Oak height	-0.718	11	0.48
Oak dbh	0.767	11	0.46
Shrub height	-4.588	9	< 0.01
Shrub dbh	0.679	9	0.51

These significant differences were then quantified by calculating the difference between the means of the two samples based on the standard error of the mean (Fowler, *et al.*, 1998), shown in equation 5.2. This calculates the 95% confidence interval for the true population mean difference ($\mu_{2007} - \mu_{2005}$), giving the lower and upper limits within which we can be 95% confident the true population mean difference lies between.

$$\left(\bar{x}_{2007} - \bar{x}_{2005}\right) \pm 1.96 \times S.E._{diff} \qquad 5.2$$

where $S.E._{diff}$ is given by equation 5.3

$$S.E._{diff} = \sqrt{\frac{s_{2007}^2}{n_{2007}} + \frac{s_{2005}^2}{n_{2005}}} \qquad 5.3$$

[11] A test for the equality of variances, which is normally an assumption for the t-test (Sokal and Rohlf, 1995) was not done as the t-test is insensitive to heteroscedasticity when the two samples are of equal size (Marowski and Marowski (1990), cited by Sokal and Rohlf (1995)).

The 95% confidence intervals (CI) are shown in Table 5.8, indicating a relatively large range of possible mean growth in height and dbh for pine, and lower height increases for shrub. These differences show that some of the measurements contained errors, of which most were probably caused by observational error, including measurement errors and possible misidentification when revisiting the trees. This is shown especially by the presence of negative growth values. Based on these results, one could infer with 95% confidence that any of the pine trees measured in both fieldwork campaigns could have grown between 0.1 and 2.7 m in the two-year period (i.e., between 5 cm and 1.35 m per year). Pine dbh could have increased between 0 and 5.8 cm, or between 0 and 2.9 cm annually. Shrub height increase was shown to be lower, between 0 and 0.6 m annually.

Table 5.8: Lower and upper limits for 95% confidence interval for the true population mean difference, indicating lower and upper limits for height and dbh increase over 2 years between the 2005 and 2007 fieldwork campaigns (shaded cells). The 95% CI values for annual growth estimates are based on the 2-year CI values.

Tree measurement	Lower limit, 95% CI for growth: 2005-2007	Upper limit, 95% CI for growth: 2005-2007	Lower limit, 95% CI for annual growth	Upper limit, 95% CI for annual growth
Pine height (m)	0.1	2.7	0.05	1.35
Pine dbh (cm)	-1.2 (0)	5.8	0	2.9
Shrub height (m)	-0.2 (0)	1.2	0	0.6

Cumulative growth curves for trees of height or diameter over age generally show a sigmoid pattern, with an initial juvenile period followed by a long maturing period in which growth rates are nearly linear and a levelling off at old age (Husch, *et al.*, 2003). This is illustrated in Fig. 5.15, which shows a diagrammatic representation of cumulative growth related to tree age and the derived growth rate curve against age. Moreover, the pattern and amount of tree growth in different parts of the tree are affected to varying degrees by different stable and transient environmental factors. Stable factors are not likely to change within the lifetime of the tree and are related to soil texture, slope, aspect and soil nutrient levels, whilst transient factors are related to fluctuations in climate, surrounding vegetation structure and competition (Philip, 1994, Husch, *et al.*, 2003). In tropical areas with marked wet and dry seasons such as

the study area, growth may stop and restart several times per year (Philip, 1994). The large growth intervals derived for the trees of the study area indicate a need for further monitoring and re-observation of considerably larger samples of trees with a discrimination of age classes, over longer periods of time to understand tree growth rates in the study area.

Johnson and Chaffey (1973) identified the need for more research into the growth rate of pine trees in Belize. Data on growth related to tree height for the main species of the study area and similar parts of Belize was not available. Organisations such as the PfB and the Belize Forest Department primarily collect diametric growth rate because this is better suited for estimates of sheer volume increase (Cho, 2007, Chuck, 2007). Caribbean pine growth rates in Belize vary according to location. On the better sites of the coastal plain, Caribbean pine typically shows a mean annual dbh increase of approximately 1 cm (also reported in Johnson and Chaffey (1973)), while this decreases to as low as 0.4 cm increase per year at poorer sites (Cho, 2007). These reported dbh increases are lower than the 95% CI upper limit measured at the study site, which can be described as an environment with sub-optimal growth conditions (see Chapter 4). It has been noted that the lower growth rates reported could be a result of measuring older trees, which would have slowed in growth rate (Cho, 2007).

In literature, Caribbean pine growth on Nigerian savannas has been reported to stagnate at an early age, resulting in the production of sparse crowns (Kadeba, 1991). Examples of Caribbean pine growth rates reported for Nigeria are an average of 0.86 m in height per year (over 10 years between ages 5 and 15 years) with an associated 0.96 cm increase in dbh (Kadeba, 1991), whereas a study on the Atherton Tableland in Australia with conditions of high rainfall and sufficient fertility that are conducive to high Caribbean pine growth rates reports an average annual height increase of 1.95 m (over 2 years between ages 14 and 38 months) with an associated 2.1 cm increase in dbh (Applegate and Nicholson, 1988). Although it is difficult to compare these growth rates due to the differences in tree age, the pine height growth rate for the study area seems to lie in between these reported growth rates. It can be reasonably accepted that pine growth rates in the study area slow down with age. Since the older trees will have the largest impact on the vegetation height retrieval from DSM data

(see 6.6), it is believed that the growth rates towards the lower limit of the 95% CI are more realistic when taking into account tree height increase between data acquisition dates.

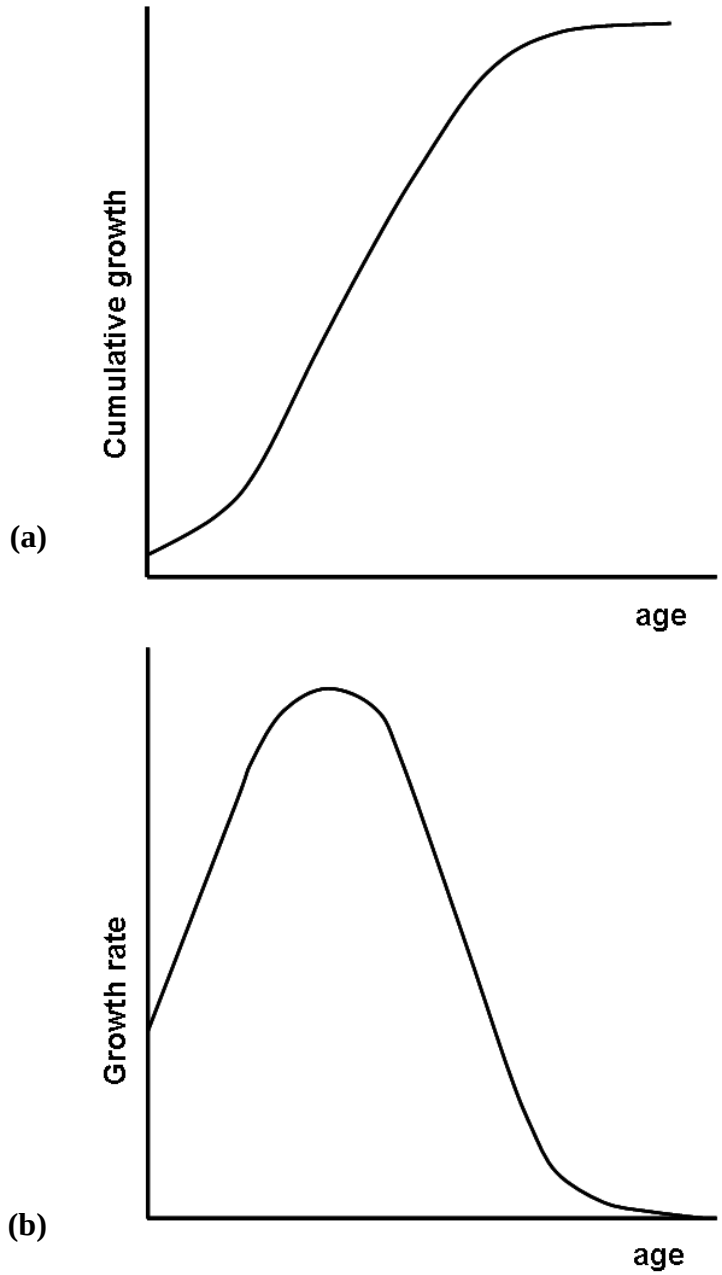

Figure 5.15: Diagrammatic representation of tree growth against age showing (a) cumulative growth, and (b) growth rate (Source: Husch, *et al.* (2003))

Growth data for palmetto was not available, but deemed negligible for this study as they form relatively low vegetation clumps, rarely exceeding 6 m in height and containing a relatively low amount of AG vegetative biomass compared to pine and oak (see 6.4). Further analyses will show that the presence of palmetto is not distinctly visible in InSAR-derived DSM data (see 6.6). Errors in height retrieval of palmetto due to palmetto height increase in between EO data acquisition dates can therefore be seen as negligible for the purposes of biomass estimation.

5.5. Quality assessment of field data

Since the interpretation of results for this research relies on accurate co-registration of the field data with the EO data, the GPS solutions (5.5.1) and the adjusted survey network (5.5.2) were assessed for spatial accuracy.

5.5.1. Accuracy assessment of GPS data

The accuracy of the 2005 fieldwork GPS observations was assessed in two ways. Firstly, the GPS solutions from Auto GIPSY and AUSPOS for the known point (BGD96 point 917) were compared over the full logging duration (9:34 hours, see Table 1 in Viergever *et al.* (2006), included in Appendix II). Apart from showing that it is not possible to comment whether AUSPOS or Auto GIPSY achieved greater absolute accuracy for horizontal coordinates, nor for ellipsoidal height coordinates[12], insight was gained on the effect of GPS logging duration on the GPS solutions of both online services. See Viergever, *et al.* (2006:34-35) for elaborate discussion on these results (included as Appendix II).

Secondly, as most GPS observation stations were logged for approximately 6 hours, the first 6 hours of logging data from the observations at BGD96 point 917 were used to obtain the expected level of accuracy for the rest of the (unknown) GPS points. The horizontal difference (2D) coordinates were calculated as the Euclidean distance, shown in equation 5.4:

[12] Based on the magnitude of uncertainty of absolute station confidence for BGD96 point 917 at the 95% level.

$$d = \sqrt{(x_2 - x_1)^2 + (y_2 - y_1)^2} \quad 5.4$$

where x_2 and y_2 are BGD96 point 917 published coordinates,
and x_1 and y_1 are coordinate solutions from AUSPOS and Auto GIPSY

To carry out these analyses, all coordinates for the AUSPOS and Auto GIPSY solutions were transformed to bring them into the same reference frame and epoch of BGD96 point 917 (i.e., ITRF1994 epoch 1996.0). See (Viergever, *et al.*, 2006:36) for an elaborate discussion of the methodology of these analyses. Table 5.9 shows the GPS solutions for 6 hours of GPS data logging at BGD96 point 917 from AUSPOS and Auto GIPSY compared to the published coordinates for BGD96 point 917. These results show that, barring unusual atmospheric disturbances on the observation days for any of the unknown points, we can assume that the GPS solutions returned from both AUSPOS and Auto GIPSY are probably accurate within ± 8 cm in horizontal coordinates and ± 15 cm in height coordinates. AUSPOS seems to provide the most accurate GPS solutions, although given the absolute station confidence at the 95% level for BGD96 point 917, this can not be certain.

Based mainly on the higher precision of the AUSPOS results over the entire logging duration, but also on the results in Table 5.9, the AUSPOS GPS solutions were used throughout the rest of the processing.

Table 5.9: GPS solutions for 6 hours of GPS data logging at BGD96 point 917 from AUSPOS and Auto GIPSY compared to the published coordinates for BGD96 point 917. Values are based on the BGD96 point 917 known coordinates minus solutions from AUSPOS and Auto GIPSY (see equation 5.4). The shaded cells indicate the web-based solutions on which the rest of the processing was based.

	Horizontal difference (2D) in m	**Ellipsoidal height difference error in m**
AUSPOS	0.068	-0.026
Auto GIPSY	0.076	-0.144

For the 2007 fieldwork campaign, differential correction of the GPS observations achieved <1 m precision when using BGD96 point 917 as a base station and <2 m for the few cases that the Belmopan Land Information Centre base station had to be used (Jaas, 2007).

5.5.2. Accuracy assessment of survey points

To test the accuracy of the adjusted survey points to the UTM/WGS84 projection, the traverse was computed for the AUSPOS GPS solutions by linear adjustment (Anderson and Mikhail, 1998, Bannister*, et al.*, 1998) over a traverse distance of 993 m. The horizontal misclosure over a traverse distance of 993 m was calculated[13] as 4.3 cm, while the vertical misclosure was calculated[14] as 0.7 cm. The horizontal misclosure of 4.3 cm is consistent with the results shown in Table 5.9 and the accuracy of a few centimetres per point suggested in the AUSPOS user guidance for 6 hours of continuous observations (Viergever*, et al.*, 2006). The vertical misclosure is surprisingly small at 7 mm and seems inconsistent with the predicted vertical accuracies for each of the traverse termini of ± ~3 cm per point, shown in Table 5.9. Given the observing conditions of 30˚ to 40˚ C with significant continuous heat haze, observation error due to refraction was likely to take place in pointing to the target prisms, leading to error in the vertical angles. The method of EDM heighting is also prone to observation error in measuring and reducing the instrument and target heights. Although the 7 mm vertical misclosure is within generally accepted standards for tertiary levelling, this unexpectedly small vertical misclosure in the height traverse could be the result of the cancelling out of errors in the GPS heights by errors of a similar magnitude in the terrestrial observations.

To test for significant trends in the survey points, the relative positioning of the AUSPOS GPS solutions was tested between GPS traverse termini and GPS reference objects (see Fig. 5.10). The figure shows that 1RO1 and 1RO2 serve as reference objects for GPS1, while 2RO1 and 2RO2 are reference objects for GPS2. The angles and distances between these points were measured in the field by EDM. Two GPS solutions (GPS and RO1) for each triplet of termini and ROs were used to calculate the expected horizontal and vertical position for the third (RO2), based on traverse calculations. Fig. 5.16 shows that, as expected from the absolute positioning results, relative positioning did not show any significant trends. Differences between

[13] The horizontal misclosure calculations are shown in Appendix V.

[14] The vertical misclosure calculations are shown in Appendix VI.

measured GPS horizontal and vertical position and calculated positions differed only slightly and did not show a consistent pattern.

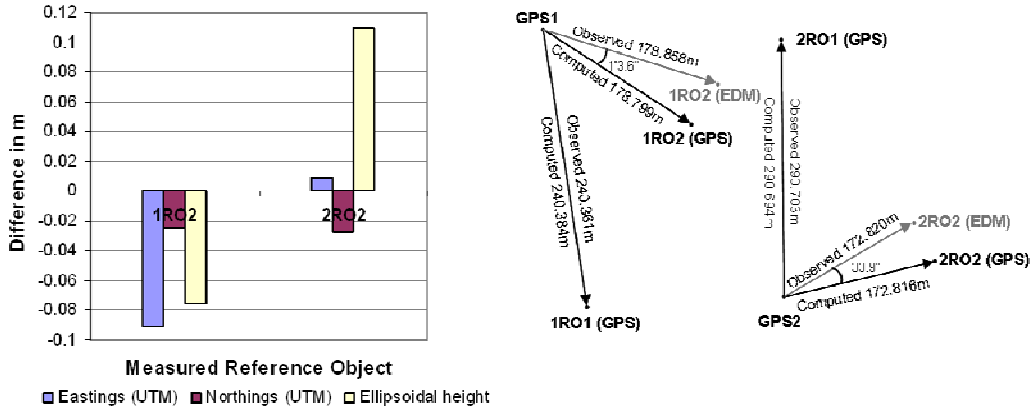

Figure 5.16: Difference between coordinates computed for RO2 (by GPS) and coordinates observed for RO2 (by EDM) using AUSPOS GPS solutions

5.6. EO data (pre-) processing

All EO data were delivered in georectified format and only required minor pre-processing for further processing. Before analysing the InSAR-derived DSMs for vegetation height retrieval, it was necessary to ensure that the DSM data were referenced to the same vertical datum (5.6.1), so that the different DSM elevation data would be directly comparable. Additionally, to place the woodlands of the study area within the context of the discussion on *forest*/*savanna* classification (see 2.3.1, also discussed throughout Chapter 2), the IKONOS and X-band DSM data were used to obtain an estimate of canopy cover for the woodlands of the study area (5.6.2)

5.6.1. Datum comparisons

To directly compare the elevation data obtained from the three DSMs, it was necessary to ensure that the different data measure elevation to the same vertical datum (elevation above mean sea level). Section 5.2.1 lists the vertical datum for each of the AIRSAR, Intermap and SRTM data. The Earth Gravity Model 96 (EGM96) was developed as an enhancement of the World Geodetic System (WGS84), reducing the uncertainties in the coordinates of the reference frame, the

gravitational model and the geoid undulations, but not changing the WGS 84; referred to as the WGS 84 EGM96 geoid (NIMA, 2004). The Intermap and SRTM geoids are therefore sufficiently comparable. The AIRSAR elevations, however, are referenced to the WGS84 ellipsoid. As described in 5.4.1, the geoid-ellipsoid separation for the study area was calculated as ~ -5.7 m. The AIRSAR DSM values were therefore adjusted to above geoid elevations by adding 5.7 m across all pixel values. The GPS field data was measured to the WGS84 geoid. This pre-processing ensured that all GPS data and all DSM data measured elevation to the same vertical datum (i.e., the WGS84 datum, or elevation above mean sea level (MSL)).

5.6.2. Extraction of woodland canopy cover and stem number density

To obtain canopy cover for the woodlands of the study area, eCognition software was used to segment the IKONOS optical EO data and the Intermap X-band DSM. By applying the optimal segmentation parameters for the IKONOS data derived by Zisopoulis (2007), tree crowns were delineated and subsequently classified using eCognition's nearest neighbour classification method (see Fig. 5.17). Segmentation of the X-band DSM (using scale factor 5) enabled delineation of the woodlands. The delineation results for both tree crowns and woodlands were evaluated by means of visual comparison with the IKONOS image (the rationale for relying on visual inspection is explained in Zisopoulis (2007)). Classification of woodland patches was carried out by applying eCognition's iterative nearest neighbour method using a combination of DSM values and the IKONOS near-infrared channel. Classified segments were then merged to form single polygons delineating the different woodland patches. ArcMap spatial queries and area calculations were then used to calculate the total area of tree crowns, woodland patches and the percentage canopy cover for three main woodland patches of the study area (see Fig. 5.17 and Table 5.10). Further discussion on the woodland canopy cover for the study area is given in 4.5.3.

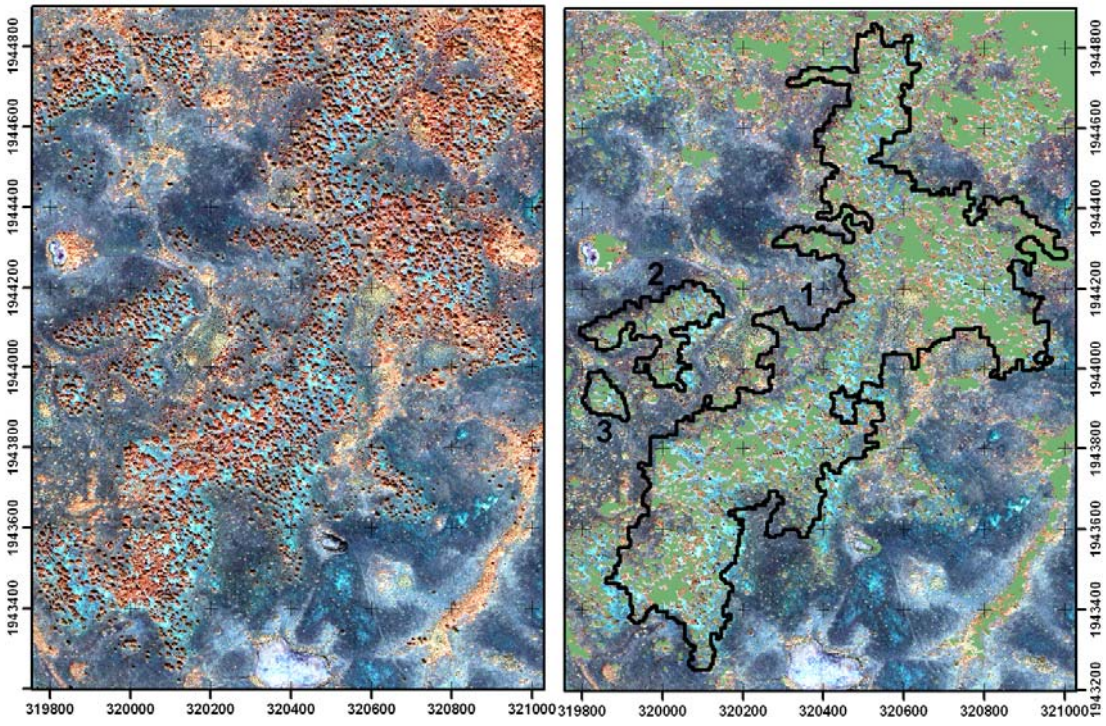

(a) Pan-sharpened IKONOS image shown in band combination 4-2-3 (RGB)

(b) Fig. (a) with delineated woodlands (black outlines) and tree crowns overlain (green)

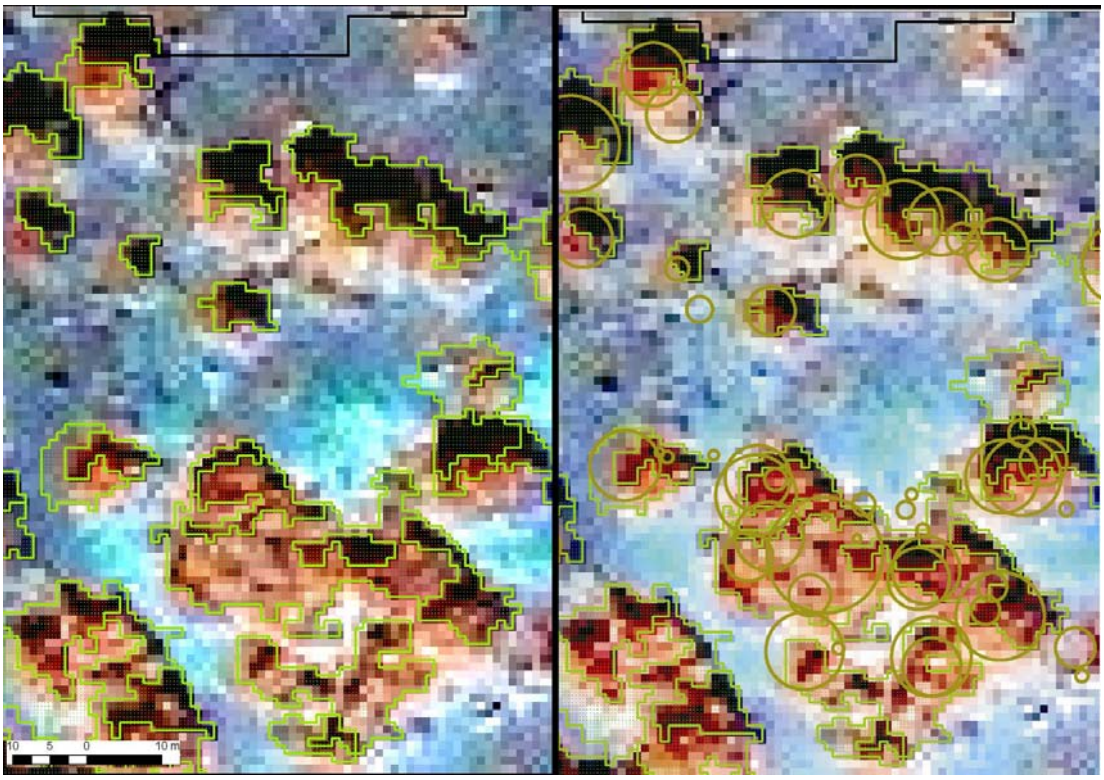

(c) Tree crowns as delineated by eCognition.

(d) Fig. (c) with tree crowns as estimated from field data (circles) overlain

Figure 5.17: A subset of the high resolution IKONOS satellite image showing savanna woodlands of the study area. Delineated woodlands and tree crowns are shown in (b) with a zoomed-in portion in (c) and (d). Figure (c) shows a zoomed-in section of the delineated crowns.

A canopy count is given, from which an estimate of stem number density was calculated (Table 5.10), giving an average stem number density of 47 stems/ha. It should be noted that these stem number densities are an underestimation caused by segmentation as one of interlocking or touching crowns.

Table 5.10: Woodland patch and crown areas with derived canopy cover. Woodland patch numbers are shown in Fig. 5.17 (b).

Woodland patch no.	Woodland area (m^2)	Total crown area (m^2)	Canopy cover (%)	No. of crown polygons	Stem no. density (stems/ha)
1	499,100	196,141	39.3	2,372	50
2	38,550	12,641	32.8	204	50
3	8,475	2,774	32.7	34	40

5.7. Quality assessment of EO data

Since the interpretation of results for this research relies on accurate co-registration of the field data with the EO data, first the horizontal alignment of the different DSM data was evaluated (5.7.1). Second, the vertical alignment of the DSMs with respect to the ground surface was checked and adjusted accordingly (5.7.2). This comparison was used to vertically adjust DSMs that contained an offset so that all DSMs could be directly compared for vegetation height retrieval, discussed in 6.6. Furthermore, during initial DSM data exploration a processing error was found in the AIRSAR C-band DSM data. Multipath error, as it is known, can result in erroneous elevation values and is further discussed in 5.7.3.

5.7.1. Horizontal alignment of DSM data

Horizontal alignment of the different DSM data sets was evaluated in two steps. First the cross-correlations between the three different DSMs were calculated and secondly, where the cross-correlations indicated that a shift was necessary, the root mean square (RMS) difference was calculated before and after the horizontal shift. Furthermore, the standard deviation was calculated to obtain the amount of variation within the elevation values of the DSMs.

All calculations were carried out using IDL scripts on subsets of ~7700 m x ~8000 m which included all savanna vegetation subtypes (see 4.5.2), access roads to Hill Bank and part of the New River Lagoon. First, all negative data values were assigned a zero-value. SRTM DSM 90 m pixels were resampled to (18 x 18) 5 m pixels using nearest neighbour resampling.

The RMS difference between the DSMs was calculated using equation 5.5, and the standard deviation (SD) was calculated using equation 5.6.

$$\text{RMS difference} = \sqrt{\frac{\sum d^2}{n}} \qquad 5.5$$

where *d* is the difference between the elevation value of the two DSMs compared, and *n* is the total number of pixels compared

$$\text{SD} = \sqrt{\frac{\sum (d - d_{mean})^2}{n}} \qquad 5.6$$

where d_{mean} is the mean difference between the two DSMs

Cross-correlation calculations confirmed what visual comparison of the DSM data showed: the Intermap and AIRSAR data were very well aligned, while a small shift was necessary to horizontally align the SRTM data with the other two DSMs. Consequently, the SRTM data was shifted 90 m west and 90 m north, which resulted in an improved alignment with the AIRSAR C-band and Intermap X-band DSMs.

Table 5.11 shows the RMS difference and SD values between the different DSMs. For comparisons with SRTM, values are shown before and after horizontal adjustment of the SRTM DSM. The results show that the Intermap X-band and AIRSAR C-band data are the most similarly matched digital elevation surfaces, with the lowest RMS difference and SD values. This is probably due to their identical spatial resolution of 5 m. The adjustment in both x and y for the SRTM data is shown to provide an improved match for both the Intermap X-band and AIRSAR C-band data (giving both lower RMS difference and SD values than before the shift). This 90 m shift in both x and y for the SRTM DSM is equivalent to one 3 arcsec SRTM pixel in both x and y, which may be explained by differences in coordinate assignment

between the data source and the image processing software used. A similar discrepancy was reported in Hofton, *et al.* (2006).

Table 5.11: RMS difference and standard deviation (SD) values for the different pairs of DSMs before and after horizontal adjustment of the SRTM DSM.

DSM 1	DSM 2	RMS difference (m)	SD
AIRSAR C-band	Intermap X-band	2.82	1.71
AIRSAR C-band	SRTM C-band uncorrected	4.15	3.99
Intermap X-band	SRTM C-band uncorrected	4.29	2.99
AIRSAR C-band	SRTM C-band after shift	3.02	2.33
Intermap X-band	SRTM C-band after shift	3.77	2.12

5.7.2. Vertical alignment of DSM data

In order to directly compare the retrieved vegetation heights from the different DSMs (discussed in 6.6), the vertical alignment of the DSMs with respect to the ground surface was checked. This was done by comparing the different DSM elevations over open grassland (i.e., areas in the DSM that do not contain vegetation bias) with GPS observations of ground surface elevation in these areas. DSMs that were found to contain a vertical offset with respect to the ground surface were adjusted accordingly.

The large collection of GPS field points collected during the 2007 fieldwork campaign for mapping vegetation features in the greater study area were used. Fig. 5.18 shows the spatial distribution of 2130 GPS points collected over open grassland. This analysis was two-fold. Firstly, to investigate the reliability of the 2007 GPS elevations data, the GPS ground elevations were compared to the transect area ground surface DEM[15] (see 5.4.2). Secondly, the GPS ground elevation data were compared to the respective DSM elevations over open grassland areas to test if the DSM data contained an offset with respect to the ground surface.

Fig. 5.19 shows a subset of 33 GPS field points that were collected over open grassland in the transect area. A two-tailed t-test for the equality of sample means was carried out (see discussion in 5.4.5) for the GPS observations and their

[15] Given that the transect area DEM was interpolated from a high point density of ground elevation data with an accuracy in the order of centimetres (see 5.5.1 and 5.5.2), it can be seen as ground truth for ground elevations in the transect area.

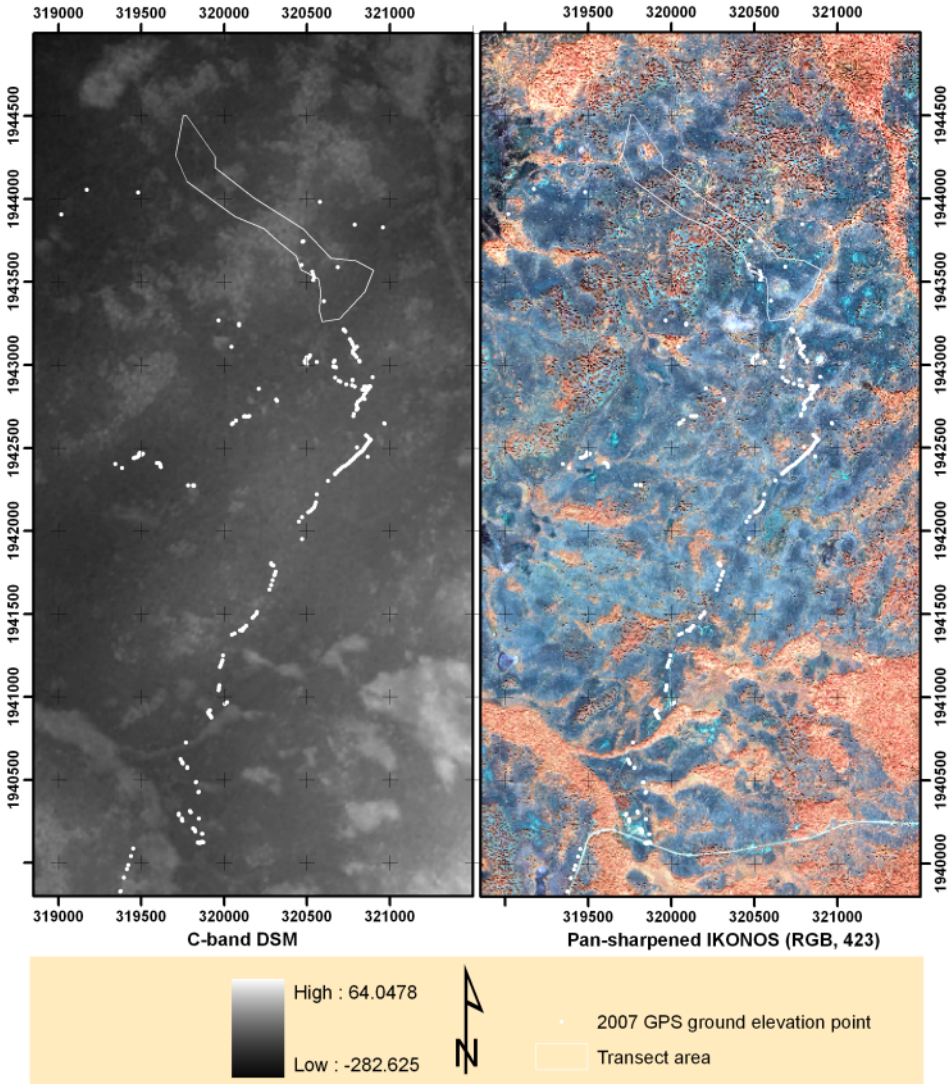

Figure 5.18: Map showing the location of the 2130 GPS points collected over open grassland during the 2007 fieldwork campaign. The location of the transect area DEM is shown. Map projection WGS84, UTM 16N. Several GPS point observations overlap slightly; the map therefore shows less than 2130 points.

corresponding DEM values. The results[16] proved that there is no significant difference in the mean of the 2007 GPS ground elevations and the 2005 ground surface DEM; the mean difference ($\mu_{DEM} - \mu_{GPS}$) was calculated as 0.1 m with the 95% confidence interval of the difference being (-0.18; 0.38). Although these results are based on only 33 GPS points, for the purposes of checking for offsets in the DSM

[16] t=0.75 (df=32, p=0.459). Pearson's correlation coefficient is r=0.593 (p<0.01)

data, the GPS ground elevations from the 2007 fieldwork are seen as an accurate representation of the true ground elevation.

For the second part of the analysis, the respective DSM and GPS ground elevation data were compared for the 2130 GPS points shown in Fig. 5.18. In the same way as above, a two-tailed t-test for the equality of sample means was carried out. Results, shown in Table 5.12, show that the elevations over open grassland for all three DSMs show significant differences to the GPS ground elevation values, although the absolute mean differences are <2 m. Based on these values, the X-band DSM seems to underestimate the ground surface by ~1.3 m, the AIRSAR C-band DSM seems to overestimate ground elevations by ~1.9 m and the SRTM C-band DSM seems to overestimate ground elevations by ~1.6 m. These differences fall well within the stated vertical accuracies of the different data sources (see 5.2.1). All DSMs show a significant modest correlation with the GPS ground elevation data. Based on these results, a correction factor was applied to the DSMs to improve direct comparisons between the DSMs and the field data: Intermap +1.3 m and SRTM C-band -1.6 m. Since the AIRSAR C-band suffers multipath error (discussed in 5.7.3), the difference calculated by means of the t-test does not represent the entire DSM, ruling out a uniform adjustment. It was therefore chosen not to apply a correction factor to the AIRSAR C-band DSM.

In summary, the two-fold analyses have shown firstly that the 2007 GPS ground elevations are a reliable representation of the ground surface of the transect area and secondly, that all DSM elevation data over open grassland differ significantly from the GPS field data, although the differences are < 2 m for all DSMs and fall within the respective vertical accuracies.

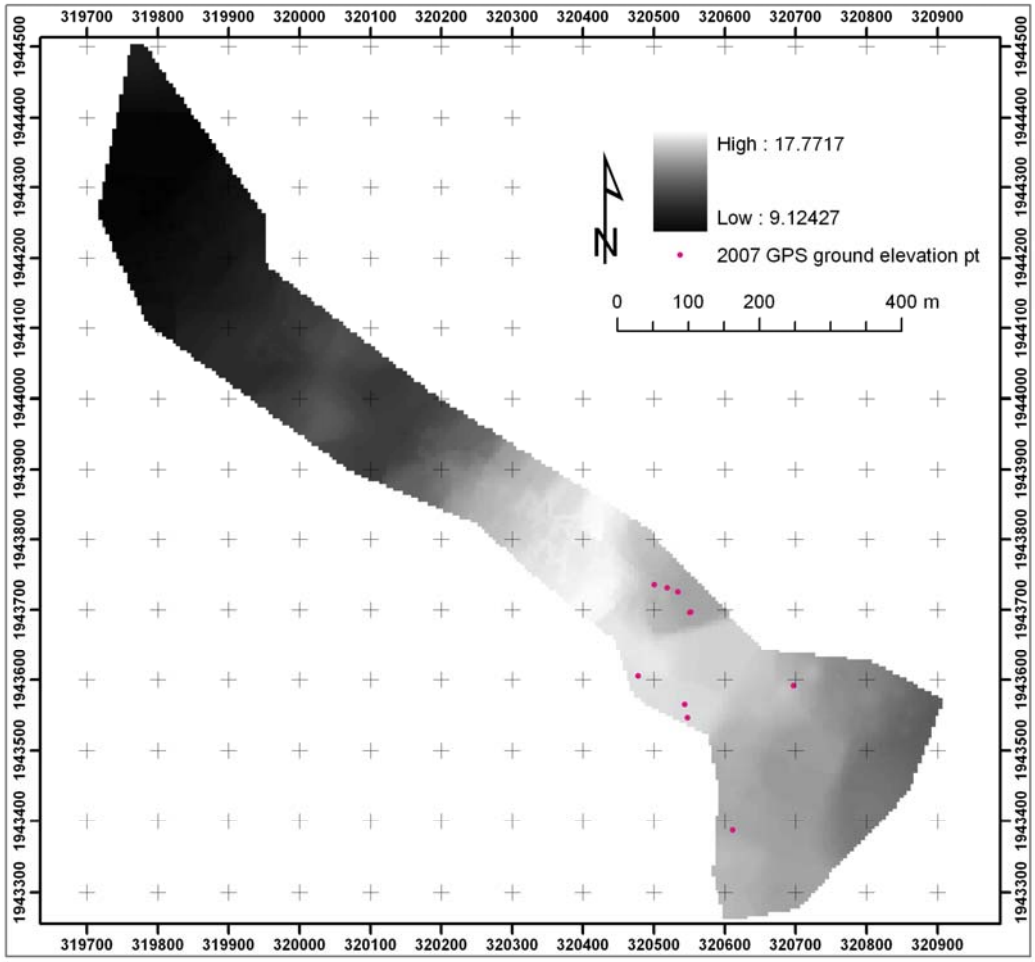

Figure 5.19: Map showing the location of the 33 GPS points collected over open grassland on the ground surface DEM for the transect area. Several GPS point observations overlap slightly; the map therefore shows less than 33 points.

Table 5.12: Results of a t-test for matched pairs between the 2007 GPS elevation data and the corresponding DSM data points for the X-band, AIRSAR and SRTM C-band DSMs; degrees of freedom 2130. The points represent ground elevation in areas without vegetation bias. All GPS and DSM elevation values refer to the WGS84 geoid.

Pair: (DSM – GPS)	t-statistic	Mean diff.	Std. dev.	p-value	95% CI for the population mean difference		Pearson's correlation coefficient (p-value)
					Lower boundary	Upper boundary	
X-band; GPS	-28.39	-1.30	2.12	<0.01	-1.39	-1.21	0.66 (<0.01)
AIRSAR C-band; GPS	33.03	1.92	2.68	<0.01	1.81	2.03	0.65 (<0.01)
SRTM C-band; GPS	26.89	1.57	2.70	<0.01	1.46	1.69	0.50 (<0.01)

5.7.3. Multipath error in the AIRSAR C-band DSM

During initial data exploration of the EO data, two non-random errors became apparent in the AIRSAR C-band DSM (TOPSAR) data. This became apparent upon subtracting the Intermap X-band DSM from the AIRSAR C-band DSM. Fig. 5.20(a) shows a fringe-like pattern in the azimuth direction, caused by multipath error, and a banding pattern perpendicular to the azimuth direction, caused by motion compensation errors. These are common non-random error sources in TOPSAR data (Madsen, *et al.*, 1995). Multipath error causes a sinusoidal perturbation that manifests itself as vertical errors as a function of incidence angle (i.e. range) and is caused by multiple reflections off the fuselage of the AIRSAR DC-8 platform during data acquisition (Imel, 2002). For the Belize TOPSAR data, the wavelike pattern is more clearly visible in the near range and the far range, while the middle section of the data suffers less because the Signal-to-noise ratio (SNR) is higher toward the centre of the scene (Chapman, 2007), minimising error. Note that the wavelength of the perturbation, of which a cross-track cross-section is depicted in Fig. 5.20(b), is not constant; a 500 m moving average much better represents the sinusoidal trend at the far range, while the perturbation at the near range appears erratic due to the much shorter wavelength of the perturbation. The outliers (due to large differences in C and X-band DSM elevations) on the cross-track cross section (Fig. 5.20(b)) at ~0.6 km and ~1.8 km are caused by patches of deforestation that have taken place in the 5-year period between acquisition of the 2 datasets (see 5.2.1); these appear as dark patches on Fig 5.20(a). The outliers (large C- band/X-band differences) on the cross-track cross section at ~ 2.7 km and ~ 3.1 km are probably caused by local (1 pixel) differences in DSM elevations caused by the difference in look direction of the two sensors (see 5.2.1). In general, the wavelength of the perturbation increases in the range direction which, although possibly a coincidence (Chapman, 2007), might be the result of the transformation of raw radar data from range resolution to ground resolution; raw data has a poorer ground range resolution at near range than at far

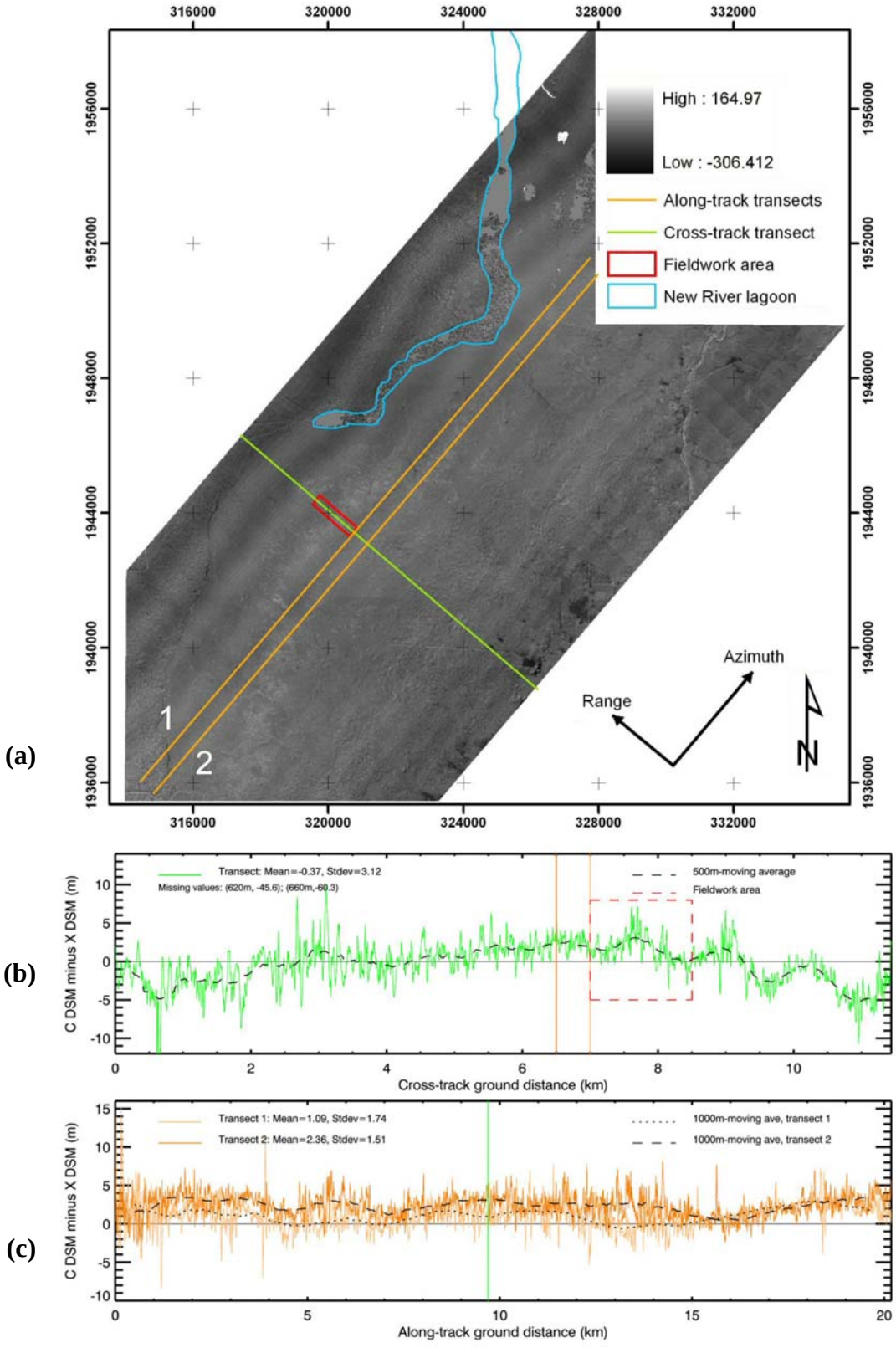

Figure 5.20: Illustration of AIRSAR C-band DSM multipath error: (a) Map showing pixel values for AIRSAR C-band DSM minus X-band DSM. The position of one cross-track cross-section (see also b) and two along-track cross-sections (see also c) as well as the fieldwork area are indicated. The image is in ground range.

range (Woodhouse, 2006a). Fig. 5.20(b) shows that the minimum and maximum perturbations, averaged by a 500 m moving average, are ~-5 m and ~3 m about the normal. Similar patterns have been reported (e.g. Kobayashi, *et al.* (2000) with height perturbations of ±5 m, and Prakoso (2006) with height perturbations of ±3 m). Fig 5.20(c) shows two along-track cross-sections, one that primarily coincides with a trough (transect 1) while the other primarily coincides with a peak (transect 2). As expected, transect 1 values are predominantly lower than those for transect 2. Neither of the graphs shows a consistent pattern. The apparent along-track banding caused by motion compensation errors therefore does not seem to significantly affect the DSM elevation values. The effect of the slight 'wiggle' in range, clearly visible north of the New River Lagoon, is visible at ~ 16 km along-track, from which point onwards both transects coincide with a peak in the sinusoidal perturbation. Motion compensation errors are associated with inaccuracies in measurement of aircraft motion, and can give rise to horizontal rubbersheet distortions (Madsen, *et al.*, 1995). At first sight one could expect the wiggle to be an effect of such rubbersheeting, but this is disproven by the perfect geographical overlay of the shapefile for the New River Lagoon in Fig 5.20(a). The wiggle is probably caused by changes in the roll and/or pitch of the aircraft during data acquisition.

In the literature, (Kobayashi, *et al.*, 2000) tried unsuccessfully to compensate for multipath error in their AIRSAR data firstly by modelling the expected multipath error based on the arrangement of the sensor antennas and secondly by applying a measured phase screen that is normally applied by JPL during TOPSAR processing. Two other possibilities existed for the removal of the multipath error of the Belize AIRSAR data: (i) reprocessing of the data using a newer JPL processor, Jurassic Prok (Chapman, 2006), and (ii) fitting a curve to the height data fluctuations to remove the wavelike pattern. The first option was continuously pursued for the duration of this research, but was unfortunately not possible due to an overfull schedule at JPL (Chapman, 2006, Hensley, 2007). Ongoing attempts are being made to have the data reprocessed by JPL. The second option was considered but not pursued because the sinusoidal perturbation does not occur evenly and also has a slight wiggle in range (see Fig 5.20(c)).

Figs. 5.20(a-b) show that the transect area is situated on a peak and a trough in the sinusoidal pattern, with deviations of ±1.5 m around the average. It should be noted that the values towards both ends of the transect area are ~0. The ends of the transect have areas of open grassland, for which one would expect the values for C-band DSM minus X-band DSM to approximate 0. Based on the values at the end points of the transect, there seems to be a slight tilt in the C-band DSM values, necessitating a slight (1-2 m) drop on the near-range end of the transect and a slight (~1m) lift at the far range end of the transect area. Over the entire transect area, the values are mostly >0, which although part of the multipath pattern, might also be partly attributed to the difference in mean scattering phase centre of the two DSMs over woodland (see discussion in 6.6.3).

The range, mean and standard deviation of the pixel values of the differenced grid (Fig 5.20(a)), were obtained to test for further trends in the data, based on the assumption that a mean value of ~0 would indicate the absence of a significant additional trend in the TOPSAR multipath error (see Table 5.13). Whilst the discussion will focus on the results for the adjusted (see 5.7.2) X-band DSM (shaded cells), results relating to the original X-band DSM are included for comparison. Although the range of the pixel values is large due to error values in the DSMs, mostly over water bodies, the mean is ~0, indicating the absence of a significant additional trend in the TOPSAR multipath error. In other words, the effect of the sinusoidal perturbation caused by the multipath error averages out over the entire TOPSAR image. The standard deviation of the mean is larger than the cross sections in Fig. 5.20(b-c) suggest and is caused by the occurrence of error values in the data. Note that the mean value when using the unadjusted X-band DSM is >0, indicating that the adjustment of the X-band DSM is an improvement of this dataset.

Table 5.13: Statistics for the pixel values of the AIRSAR C-band DSM minus the (adjusted) X-band DSM. Adjustment of the X-band DSM is discussed in 5.7.2

	No. of pixels	Minimum	Maximum	Range	Mean	Standard deviation
AIRSAR C-band minus X-band	9,158,579	-305.1	166.3	471.4	1.65	10.48
AIRSAR C-band minus adjusted X-band	9,158,579	-306.4	164.9	471.3	0.36	10.48

5.8. Summary

This chapter has given an overview of the various data sources used, including EO and field data. The EO data include SAR and optical data from various sources and acquisition dates ranging from 1999 to 2006. The field data were collected during two fieldwork campaigns. The 2005 campaign formed the main data collection in which woody vegetation >1.3 m were mapped and measured in a transect of ~800 m by ~ 60 m. The 3-dimensional coordinates (x, y and z) of the base of every tree, shrub and single palmetto was recorded using the total station (1133 points in total). Tree species, diameter at breast height (dbh), tree height and crown height were recorded and crown diameter was measured for a 40% subset. Palmetto clumps (75 in total) and thickets were mapped as polygons. Supplementary ground elevation points (2464 in total) were collected for the creation of a ground surface digital elevation model (DEM) for the transect area. The GPS observations and survey points were shown to have sub-decimetre accuracy, both horizontally and vertically. The second fieldwork campaign (2007) was used to collect additional data such as re-measurements of a subset of trees to estimate tree growth rates in the savanna. These were shown to be only significant for pine and shrub over the 2-year period between field work campaigns. However, with limited field data and without knowledge of the age class of the re-measured trees, it is difficult to assess actual annual tree height increase for the savanna. This shows the need for continued re-measurement of tree height over time and further analysis of tree growth rates for different species, height or age classes. Extra ground elevation data collected over a wide area were used test the vertical alignment of the different DSM datasets with respect to the ground surface so that they could be directly compared for vegetation height retrieval (discussed in 6.6).

A number of (pre-) processing steps were necessary to prepare the data for the main data analyses as discussed in Chapter 6. These include assessing the co-registration of the different EO datasets with the field data, which showed that, apart from the SRTM DSM needing a 1-pixel shift north and west, all datasets are accurately co-registered (i.e., they match up horizontally). Vertical alignment of the DSM data was undertaken by first matching reference geoids of the various datasets and second by

comparing DSM elevations over open grassland to GPS ground elevations. The latter resulted in a 1.3 m lift for the X-band DSM and a 1.6 m drop in the SRTM C-band DSM. DSM data exploration showed that the AIRSAR C-band DSM contains multipath error. The transect area occurs on a peak and a trough in the sinusoidal pattern, with deviations of ±1.5 m around the average for the transect area. There seems to be a slight tilt in the C-band DSM values, necessitating a slight (1-2 m) drop on the near-range end of the transect and a slight (~1m) lift at the far range end of the transect area.

The optical EO data have been used mainly for understanding and quantifying the canopy cover of the savanna woodlands, showing that mean canopy cover for the woodlands of the study area is >30%. The SAR data is further evaluated for its use in biomass estimation through vegetation height retrieval and backscatter relationships. This is further discussed in Chapter 6.

CHAPTER 6:
InSAR height retrieval and backscatter analysis results

6.1. Introduction

The processing and data quality assessment discussed in Chapter 5 were essential to prepare the data for evaluation of the main research aim (i.e., the evaluation of SAR for biomass estimation of tropical savanna woodlands). This chapter discusses the results of the backscatter analyses (6.5) and InSAR vegetation height retrieval (6.6). This is preceded by an assessment of the savanna woodland characteristics that are related to the occurrence of AG biomass (6.4). The discussion centres on woodland characteristics, such as vegetation height, that can be realistically retrieved using EO data and methods. L- and P-band SAR backscatter are then first evaluated for their relationship with biomass in the study area and secondly, the use of X-band and C-band InSAR-derived DSMs is evaluated for woodland vegetation height retrieval. Section 6.2 gives a summary of the data quality as determined in Chapter 5. This is followed by a description of the methodology that was followed for extracting the EO data (6.3) for comparison with the field data (6.3) on which analyses and interpretation are based.

6.2. Summary of data quality

The outcome of the pre-processing and data quality analyses described in 5.5 to 5.7 have shown that the field data are positioned at a three-dimensional accuracy well within the required ± 1 m because: (i) the GPS observations are accurate within ~7 cm horizontal and ~3 cm vertical (5.5.1), (ii) the survey points are accurate within ~5 cm horizontal and ~1 cm vertical (5.5.2), (iii) the points of detail were observed using a survey-grade total station instrument, and (iv) woody vegetation were mapped with only a small (< 0.66 m) offset caused by the method applied to map the points of detail (see 5.3.2.2). Furthermore, it was shown that the different EO data

were all co-registered (horizontally aligned) to within a 5 m pixel spacing (see 5.7.1; Table 5.11 gives RMS differences between the different DSMs). The accurate co-registration of all DSMs implies that the AIRSAR L- and P-band backscatter data are co-registered to the same degree of accuracy since they are linked to the AIRSAR DSM. All elevation data (GPS ground elevations, DSM and DEM) are referenced to the WGS84 geoid (all elevation therefore refer to elevations above mean sea level, MSL). Figs. 6.1 to 6.3 show 3-dimensional plots that demonstrate the vertical alignment of the DSM data with the field data collected in the 2005 fieldwork campaign and with the IKONOS optical imagery, showing good vertical alignment between all data sources. The AIRSAR C-band DSM contains multipath error which may affect vegetation height retrievals to different degrees over the whole image. Investigation has shown that the transect area occurs on a peak and a trough in the sinusoidal perturbation, with deviations of ±1.5 m around the average for the transect area. The multipath error therefore does not strongly affect the transect area.

6.3. Extraction and manipulation of EO and field data

Knowing that the field data and EO data are horizontally well aligned, it was possible to further analyse the EO data together with the field data by means of graphs comparing the SAR data values with physical measurements of the field data. SAR and InSAR data were extracted in the form of profiles in the exact range direction of the AIRSAR data (310º, see 5.3.2 for a discussion on the choice of field transect location and orientation). It should be noted that, although every effort was made to precisely orient the field data transect in a 310º/130º direction, the final orientation of the field data transect deviated by a few degrees. Fig. 6.4 shows the orientation of the field transect with 19 profile lines taken in the exact AIRSAR range direction. Profile lines were taken 10 m apart to suit the AIRSAR and Intermap data posting of 5 m. Fig. 6.5 shows how sub-transects were formed by means of buffering around each of the profile lines

Backscatter pixel values were extracted as sigma naught values in dB for the profile lines (see 5.2.1.1 for transformation from linear values of power). Except for the AIRSAR C-band DSM, all InSAR DSM values were first adjusted based on comparison of the DSM data with GPS data over open grassland (see 5.7.2).

Figure 6.1: Three-dimensional figure showing the IKONOS image (4-2-3, RGB) draped on the Intermap X-band DSM. Tree heights are shown as vertical green lines and average palmetto clump heights are shown in dark green polygons. The ground surface DEM is shown in brown.

Figure 6.2: Three-dimensional figure showing the IKONOS image (4-2-3, RGB) draped on the AIRSAR C-band DSM. Tree heights are shown as vertical green lines and average palmetto clump heights are shown in dark green polygons. The ground surface DEM is shown in brown.

Figure 6.3: Three-dimensional figure showing the IKONOS image (4-2-3, RGB) draped on the SRTM C-band DSM. Tree heights are shown as vertical green lines and average palmetto clump heights are shown in dark green polygons. The ground surface DEM is shown in brown.

Field data on trees, shrubs and palmetto occurring within each sub-transect (i.e. within a 5 m buffer to either side of the profile line) were extracted. The profile plots representing field data in this chapter represent trees shrubs and palmetto by their typical crown shape as observed in the field. The dense groupings of similarly sized trees in the graphs (e.g. Fig. 6.6) represent palmetto clumps and thicket. Dead trees, or trees without crown are represented as a trunk with the height measured in the field, e.g. profile 11 at ~225 m along the transect (e.g. see Fig. 6.7). Additionally, trees of which the trunk were not located within a certain sub-transect were also included if their (real or estimated) tree crown extended into the sub-transect by at least 4 m. These trees are plotted in dashed lines and all consequent plots based on field data (e.g. biomass and basal area moving averages) plotted in dashed lines include such trees in the calculations. Solid line plots represent the calculations excluding such trees (e.g. Fig. 6.6). Biomass was calculated for the field data as biomass carbon (in kg C/m^2) using allometric equations discussed and given in 4.5.3, using dbh for pine and oak and height for palmetto and shrubs. Note that carbon makes up approximately half of the total biomass (see 2.4) and that all graphs show carbon content. Basal area (in m^2/m^2). was calculated based on total dbh measurements. Moving averages of biomass carbon and basal area were calculated using a window size of 20 m in length for each 10 m wide sub-transect and a step size of 1 m, thereby calculating the average for each 20 x 10 m = 200 m^2 area within the sub-transects. The window is continuously moved 1 m along the sub-transect and the average biomass carbon (or basal area) value is plotted against the centre position of the moving window.

A narrow section of each graph shows the plan view at 1:1 scale, indicating the location of the vegetation within the 10 m-wide sub-transect and showing canopy cover and number density. Fig. 6.14(a) gives a tree and palmetto count for each sub-transect. The numbers for palmetto are partly based on stem counts (for the clumps), but largely estimated (see 4.5.3). Since not all tree crown diameters were measured, an indication is given as to how many tree crowns in the sub-transect have been estimated.

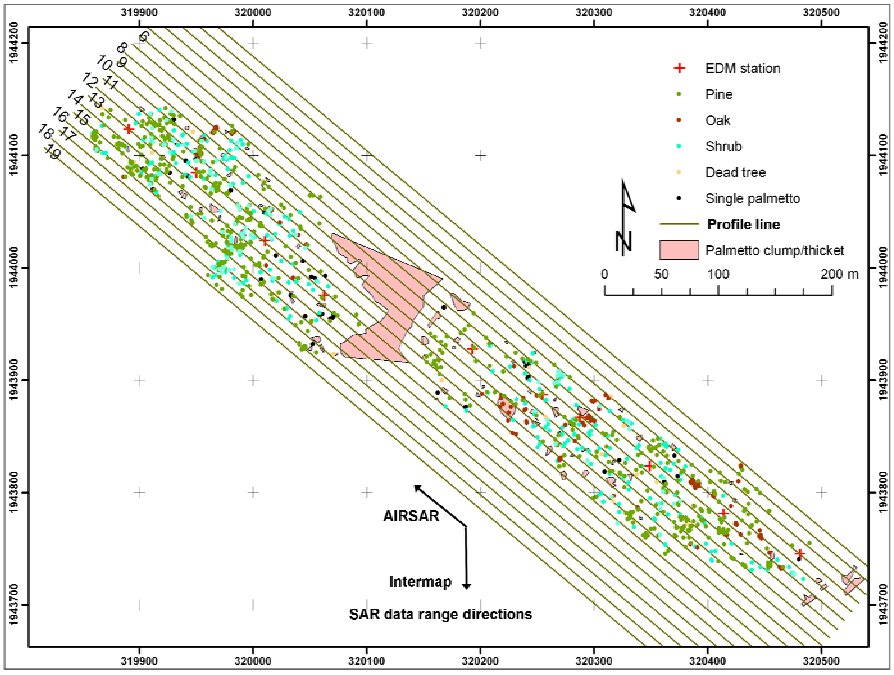

Figure 6.4: Map showing the location and orientation of 19 profile lines in the exact AIRSAR range direction with the field data transect. The offset in orientation of the field data transect is shown.

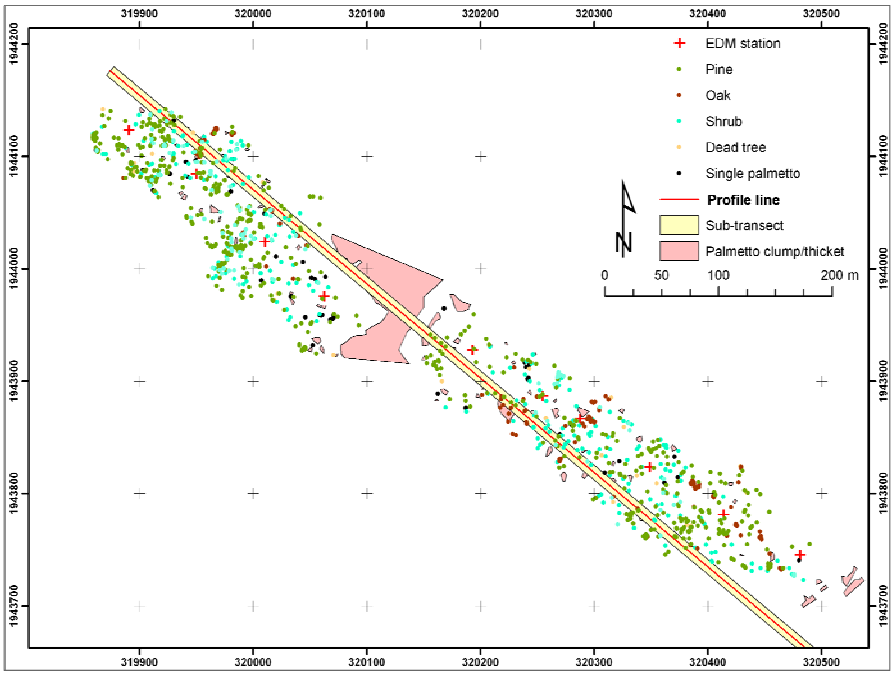

Figure 6.5: Map showing profile line 10 (middle line) and 5 m buffer to either side (in yellow).

Due to the offset between the field transect and the profile lines (see Fig.6.4), not all sub-transects contain the same length of field data. Since they contain similar lengths of field data and are located adjacent to each other, sub-transects 10 to 12 are used throughout this chapter. Adjacency of the sub-transects is important when investigating the DSM data from different EO data sources such as AIRSAR, Intermap and SRTM. As the profiles were taken in the exact range direction of the AIRSAR data, the effects of layover and shadowing will be apparent within the sub-transect. However, the Intermap and SRTM data have different range directions, therefore dominant vegetation structures within one sub-transect could influence the DSM surface in an adjacent sub-transect.

6.4. Savanna woodland characteristics that determine AG biomass

Before the use of SAR is evaluated for biomass estimation, an assessment is made on the relationship between savanna woodland characteristics and the amount and distribution of AG biomass carbon. The top graphs in Figs. 6.6 to 6.8 show schematic representations of savanna woodland characteristics such as measured tree height, crown depth and (measured and estimated) crown diameter. A plan view of the field data within the sub-transect shows the spatial distribution of the woody vegetation and gives an indication of the canopy cover and the stem number density. Biomass carbon and basal area are plotted as moving averages.

As discussed in 6.3, biomass carbon shown in the graphs was calculated from dbh measurements for pine and oak and from tree height measurements for shrubs and palmetto. Moreover, dbh and tree height are related in a power law function, shown especially clearly for pine and oak in Fig 6.9 (see also discussion in Woodhouse (2006b)). It can therefore be deduced that biomass is related to vegetation height on individual tree basis. On a wider scale such as at woodland patch level, vegetation height seems to be an indicator of AG biomass, although there does not seem to be a linear relationship between vegetation height and AG biomass. This is illustrated by 3 clumps of trees of similar height (~15 m) at 180 m, 670 m and 710 m along profile

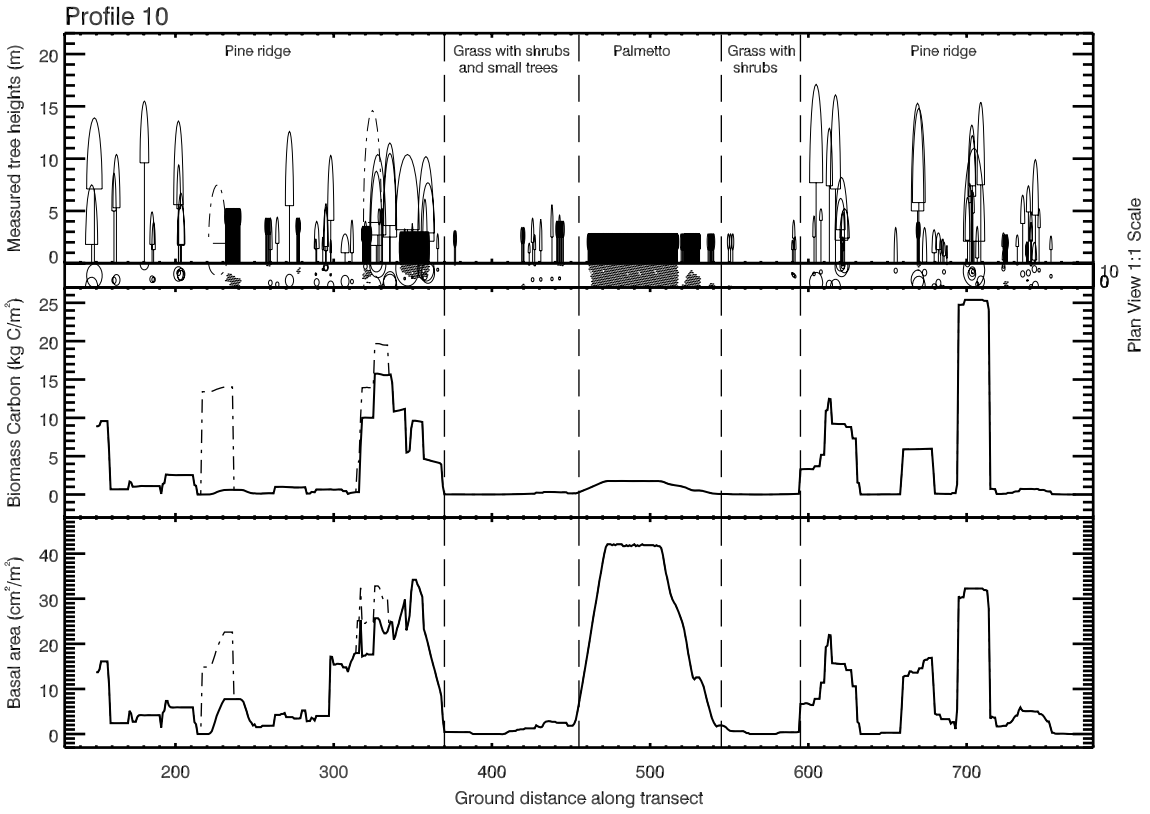

Figure 6.6: Schematic representation showing savanna woodland characteristics that determine AGW biomass – profile 10. Top part of the graph shows measured tree heights and crown dimensions, the plan view gives an indication of stem number density and spatial distribution within the 10-m wide profile. Biomass and basal area are plotted as moving averages using a window size of 20 m and a step size of 1 m. Trees of which the crown overhangs at least 4 m in the subtransect are shown in dashed lines. Moving averages for biomass and basal area are given for trees with trunks inside the sub-transect (solid line) and including trees of which the crown significantly extends into the transect (dotted lines).

10, which contain respectively 1, 6 and 25 kg C/m^2. These differences in biomass carbon are due to the heterogeneous nature of the vegetation distribution, which translate into differences in number densities and canopy cover.

Figs. 6.6 to 6.8 show a relationship between biomass and basal area. Except for areas of palmetto, this relationship is more linear than the relationship with vegetation height. This is related to the fact that AG biomass is calculated from dbh measurements for pine and oak. As crown diameter in general tends to be related to dbh, and because missing crown diameter measurements were estimated based on dbh measurements (see 5.4.4), canopy cover strongly corresponds with biomass carbon in the graph. For the same reason, biomass carbon corresponds to tree number

densities, except for areas of palmetto vegetation. It should be mentioned however that stem number density of the palmetto thickets was estimated based on stem number densities in the much denser but smaller palmetto clumps (see 4.5.3). The actual basal area of the palmetto thicket in the middle of the transect profile has therefore been overestimated in the graphs.

Certainly, for palmetto which forms generally low vegetation at high number densities and which has relatively low biomass, vegetation height is a suitable indicator for AG biomass. For the pine ridges of the savanna woodland, tree height gives a general indication of the occurrence and distribution of AG biomass. Based on this deduction, this chapter evaluates the use of shortwave InSAR-derived DSMs for vegetation height retrieval of the savanna woodlands. As discussed in 3.3.3.2, the use of InSAR for vegetation height retrieval has been successfully used for estimating AG biomass in dense homogeneous forests, but has as yet not been sufficiently tested in sparse heterogeneous woodland environments.

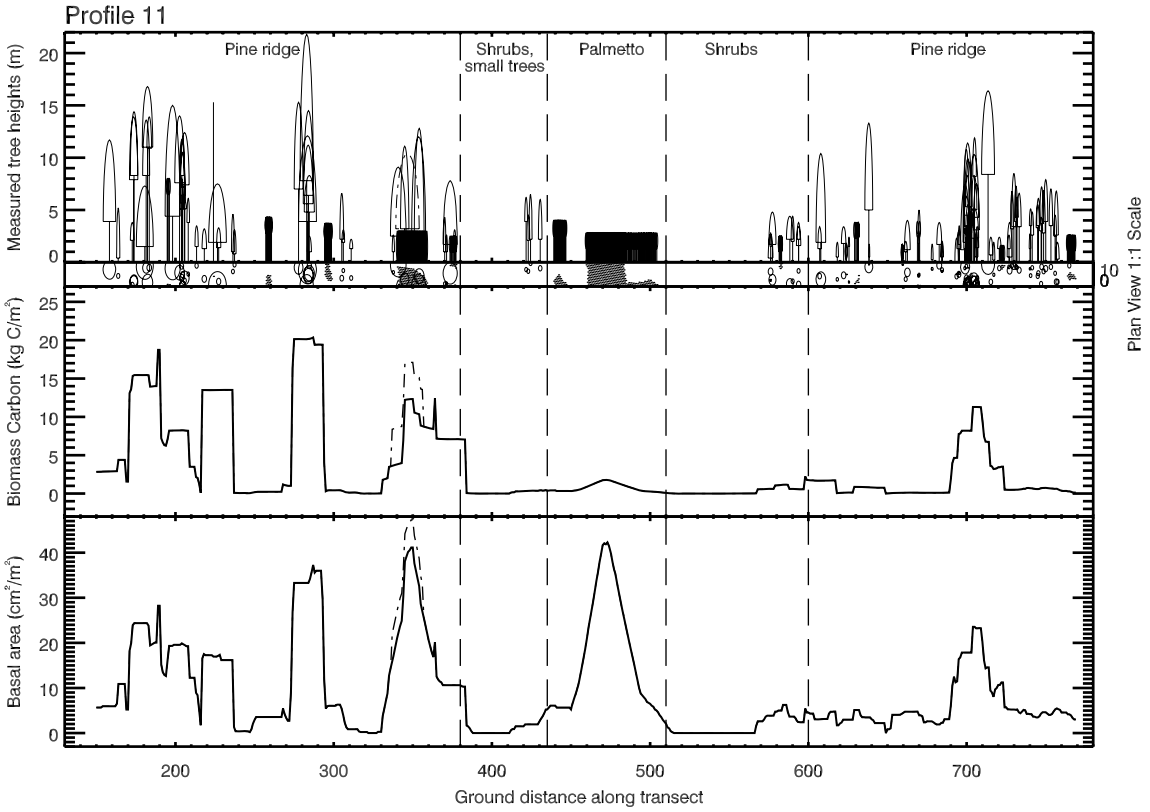

Figure 6.7: Schematic representation showing savanna woodland characteristics that determine AGW biomass – profile 11. See caption of Fig. 6.6 for further explanation.

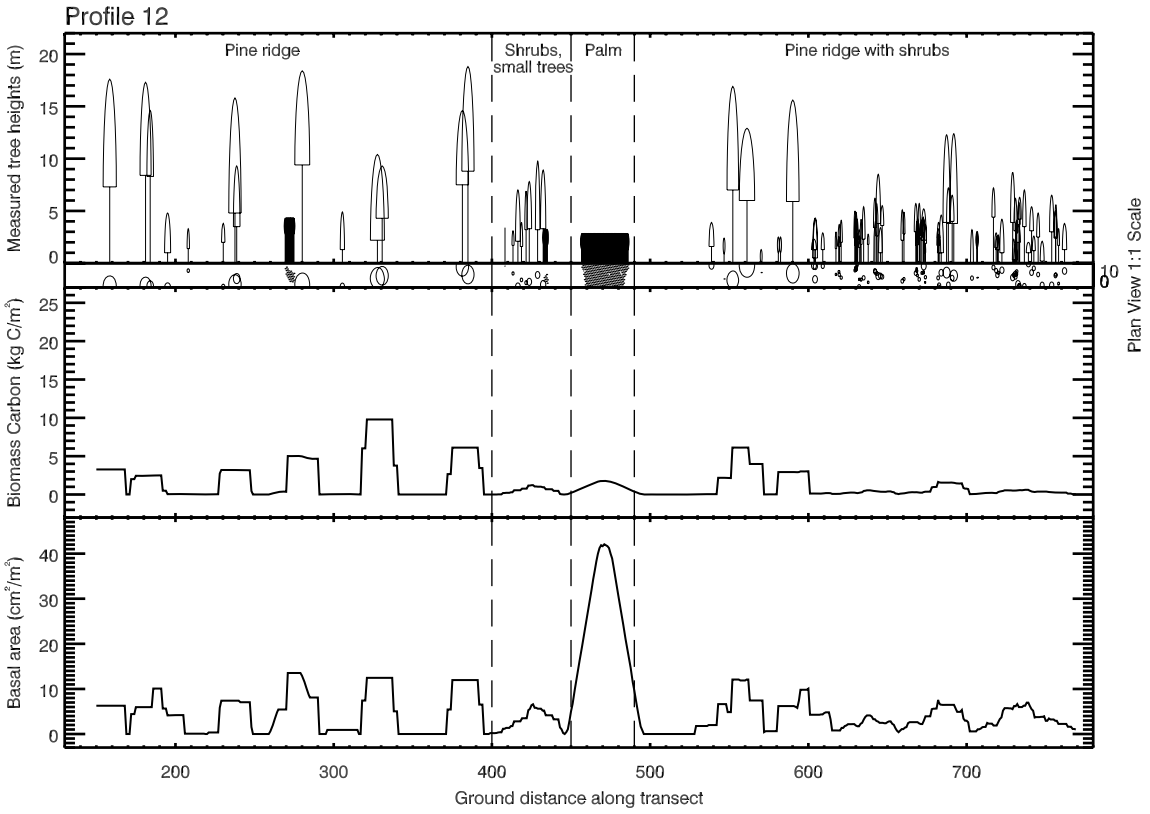

Figure 6.8: Schematic representation showing savanna woodland characteristics that determine AGW biomass – profile 12. See caption of Fig. 6.6 for further explanation.

Since this section shows that estimates of biomass distribution could be improved if vegetation height is used in conjunction with additional woodland characteristics such as canopy cover, tree number density, basal area or crown depth, the AIRSAR backscatter is first evaluated as an initial indicator of biomass distribution within the savanna woodlands. This is necessary as InSAR-derived tree height is affected not only by the height of the vegetation, but also factors such as crown characteristics such as shape and density (see 3.3.3).

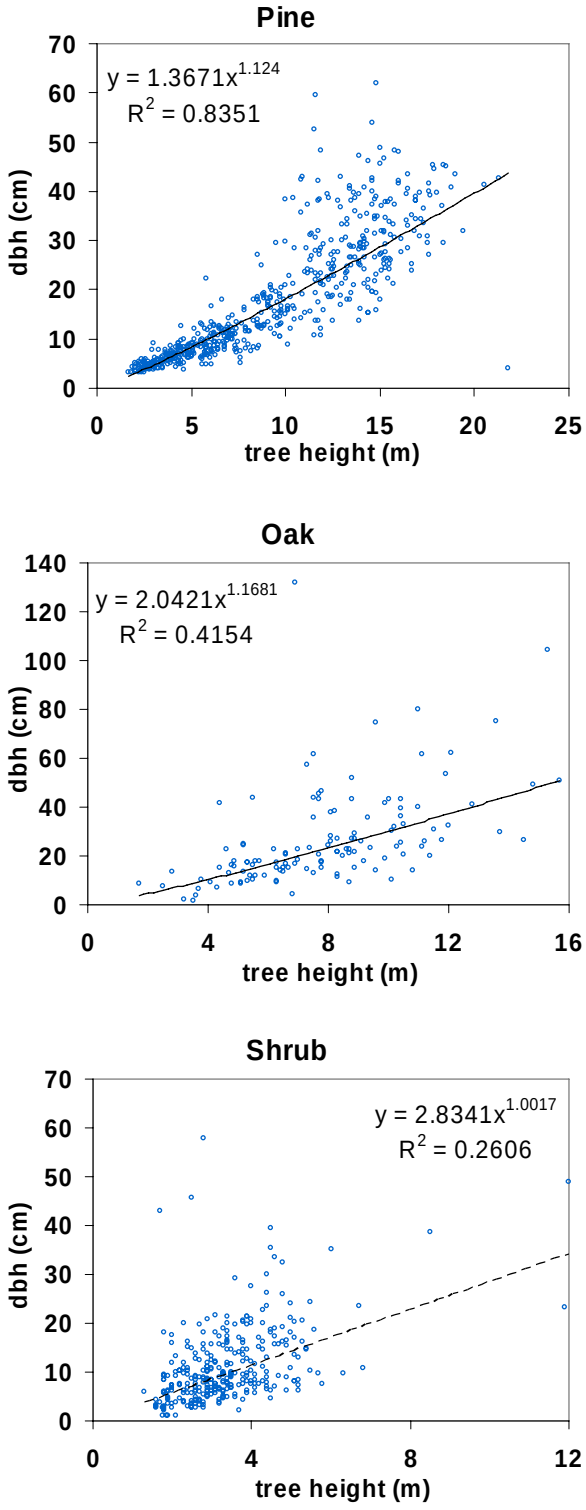

Figure 6.9: Scatterplots of tree height (in m) against dbh (in cm) as measured in the field for pine, oak and shrub. The powerlaw function with concommitant coefficient of determination is given for each.

6.5. Backscatter analysis

Figs. 6.10(a) to 6.10(c) show the AIRSAR polarimetric backscatter with the transect field data, biomass carbon and basal area for sub-transects 10 to 12 respectively. Fig. 6.11 compares the L- and P-band polarimetric backscatter for sub-transect 10. These graphs for sub-transects 11 and 12 can be found in Appendix VII. Figs. 6.12 and 6.13 show biomass-backscatter graphs for P-, L- and C-band at different polarisations based on plots of 2 different sizes (225 m^2 which is approximately equivalent to 9 AIRSAR pixels and 900 m^2 which is approximately equivalent to 36 AIRSAR pixels).

The figures show that, overall, C-band backscatter values are greatest, followed by L-band and P-band. These differences are expected (e.g., Imhoff (1995b), Lucas *et al.* (2006a)) and occur due to differences in canopy penetration combined with the differences in saturation levels for the different SAR bands. With a range in backscatter from -10 dB to -1 dB over the three profiles, C-VV backscatter varies very little. The biomass-backscatter plots in Figs. 6.12 and 6.13 show even less variation in backscatter for C-band. The small range in C-band backscatter values can be mainly attributed to the VV polarisation of the C-band which gives a higher backscatter return from the ground in the sparse woodland. This explains the low correlation coefficient between C-vv and biomass in Figs. 6.12 and 6.13. For the same reason P-vv and L-vv yield very weak correlation coefficients with biomass. The graphs in Figs. 6.12 and 6.13 do not show the presence of clear saturation levels for the various SAR bands, mainly caused by the overall low correlation coefficients for the various logarithmic trend lines. C-band typically saturates at approximately 20 t/ha biomass (although higher saturation levels have been reported for sparse woodlands, see the discussion in 3.3.3.1), which equates to 10 t C/ha (~1 kg C/m^2). L-band typically saturates at ~40-60 t/ha (~2-3 kg C/m^2) and P-band typically saturates at 100-200 t/ha (~5-10 kg C/m^2). Fig. 6.12 and 6.13 show that P-hh has the strongest correlation with biomass followed by P-hv and L-hv backscatter. This is unexpected as HV polarisation generally has a stronger correlation with biomass (e.g. Le Toan, *et al.* (1992)). The stronger correlation between P-hh backscatter and biomass can be explained by the sparse nature of the savanna woodland canopy that

lets through a considerable amount of the longer wavelength backscatter, which has a strong return from double bounces between stems and the ground. The moderate correlation between both P-hv and L-hv with biomass can be attributed to the greater part of this backscatter from these polarisations returning from tree crowns in the sparse canopy. Whilst the correlation coefficients quoted in literature for biomass-backcsatter correlations are generally higher than 0.65 (e.g. Le Toan, *et al.* (1992), Santos, *et al.* (2002), Le Toan, *et al.* (2004)), those in Figs. 6.12 and 6.13 are lower than 0.65. This is caused by the heterogeneous nature of the savanna woodland vegetation, including the presence of palmetto which has a high backscatter response for relatively low biomass.

When comparing the graphs in Figs. 6.12 and 6.13, it is clear that the choice of plot size is very important in a study area with a non-continuous canopy that has heterogeneous vegetation distribution. Fig. 6.13 shows weak correlations between biomass and backscatter throughout. This is caused by the heterogeneous nature of the vegetation distribution within the savanna woodlands. This effect is averaged when a larger plot size is used. Whilst plots of 15 × 15 m are acceptable for biomass-backscatter graphs in a closed canopy forest, they are not appropriate for non-continuous or sparse canopies.

In Figs. 6.10 to 6.11, peaks in C-, L- and P-band backscatter coincide with significant presence of trees, mostly in dense clumps or as sparse groupings of tall trees. Such conditions are generally associated with high biomass. Interestingly, high backscatter values correspond not only to areas of high biomass vegetation (i.e., single tall trees and dense groupings of tall trees) but also to palmetto clumps and thickets which have relatively low biomass. Even the presence of small palmetto clumps in between tree growth seems to cause a significant increase in backscatter values. For example, the palmetto clumps at ~235 m along the transect, profile 10 and at ~270 m along the transect, profile 12. Palmetto is very dense and leafy, but contains significantly less biomass carbon per unit area than trees that show similar L and P-band backscatter. During the dry season, when this data was acquired, palmetto vegetation does not contain excessive moisture in the stem. It is therefore hypothesized that the large

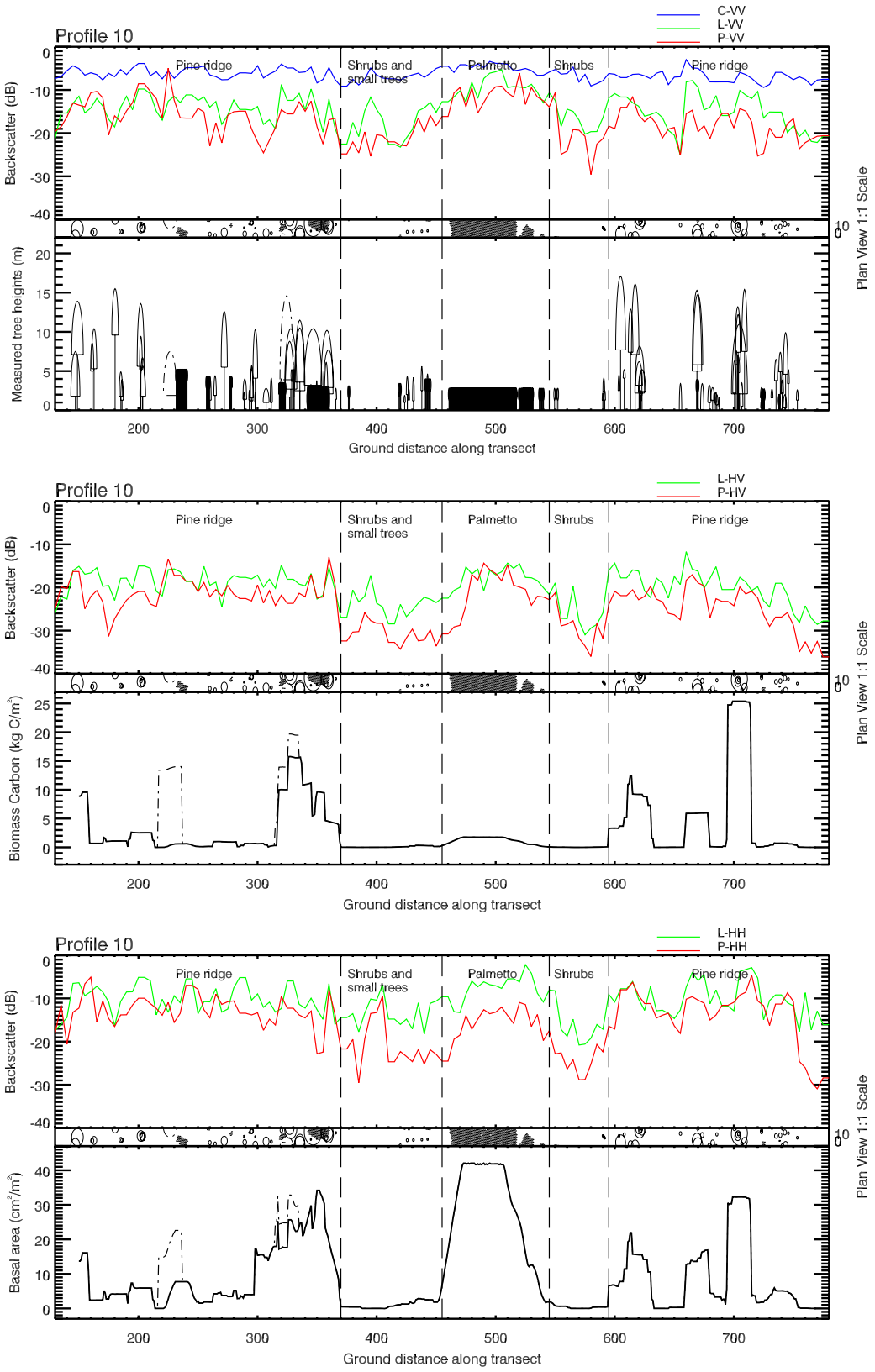

Figure 6.10(a): AIRSAR backscatter compared to field data: tree measurements, biomass carbon and basal area for profile 10. The latter two are graphed using a window of 20 m, moving in 1 m steps

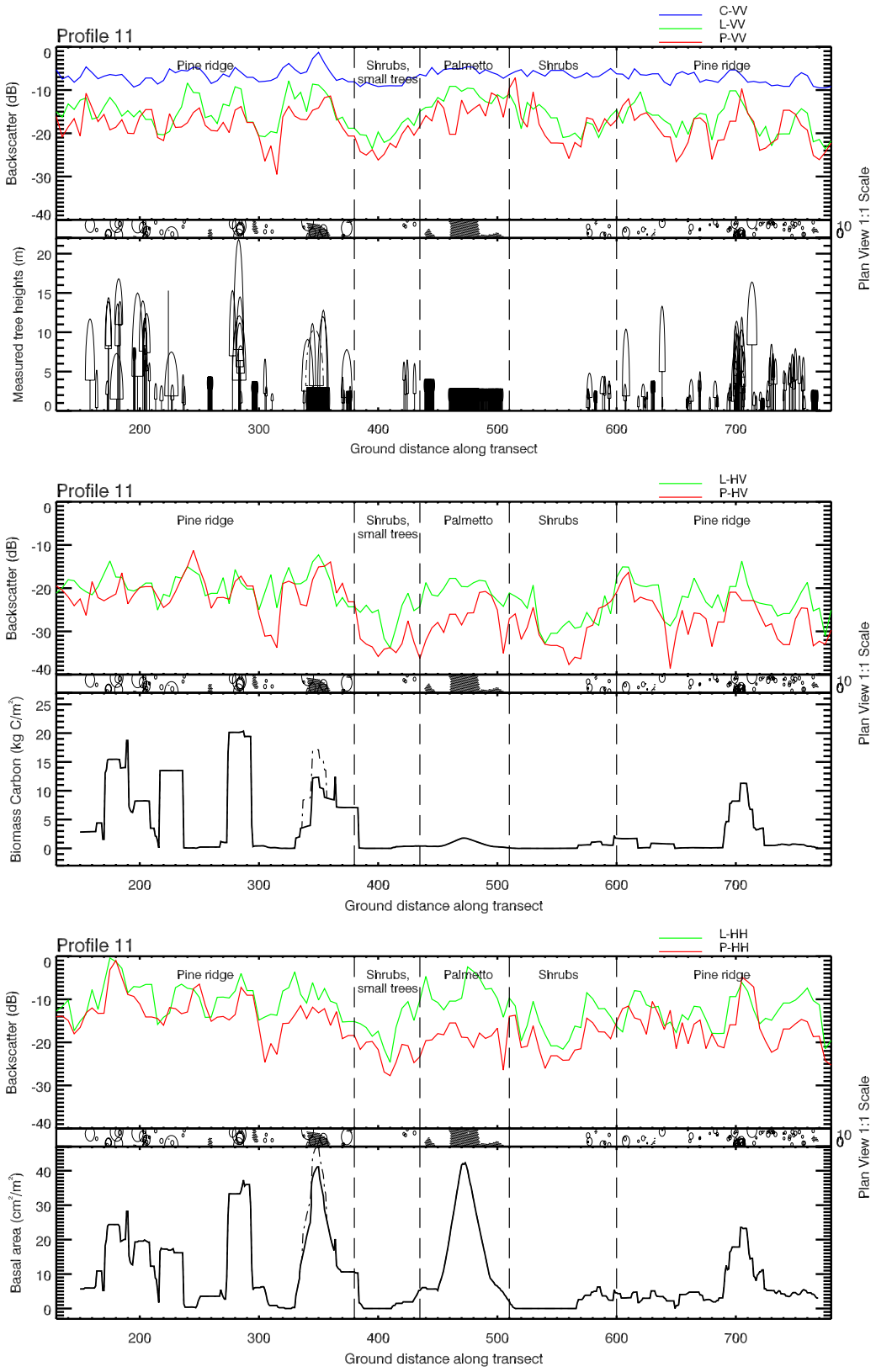

Figure 6.10(b): AIRSAR backscatter compared to field data: tree measurements, biomass carbon and basal area for profile 11. The latter two are graphed using a window of 20 m, moving in 1 m steps

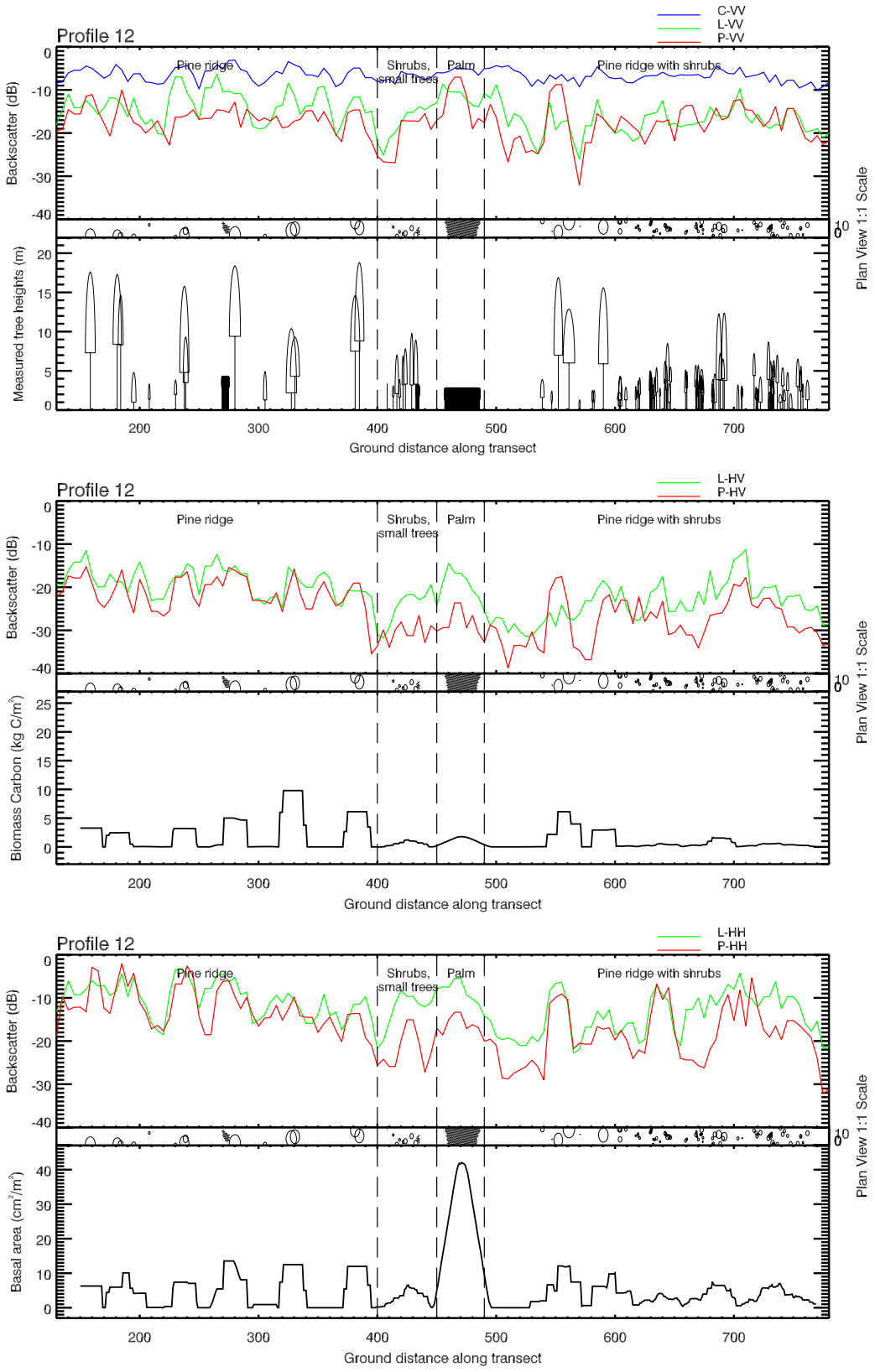

Figure 6.10(c): AIRSAR backscatter compared to field data: tree measurements, biomass carbon and basal area for profile 12. The latter two are graphed using a window of 20 m and 1 m steps

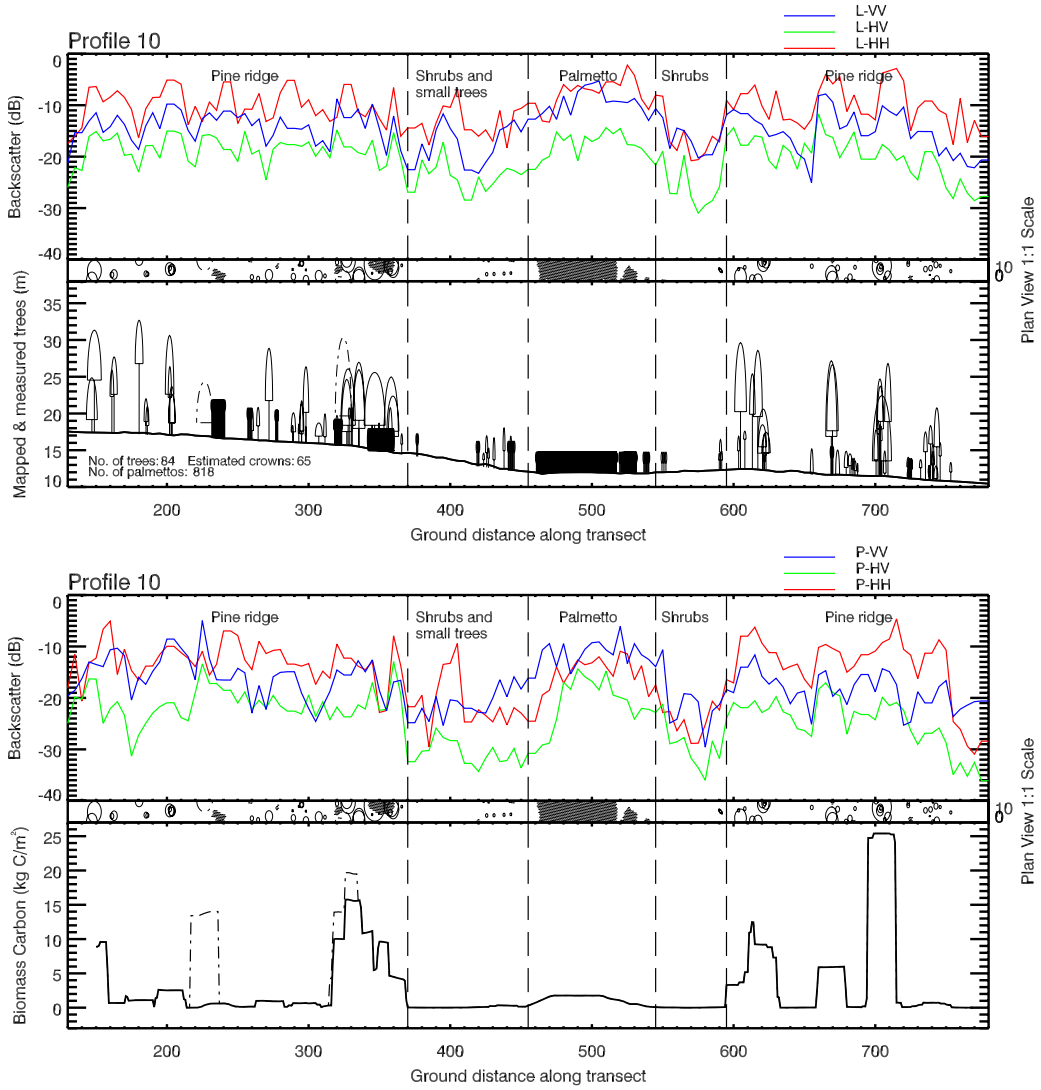

Figure 6.11: L- and P-band polarimetric SAR response, Profile 10. The graphs for profiles 11 and 12 are included in Appendix VII.

green leaves cause the high L- and P-band backscatter[1]. An alternative explanation is that the presence of multiple stems in dense groupings might cause high backscatter values for palmetto. Comparison of backscatter values to the basal area shows an overall stronger correspondence although here also, there is no consistent relationship between backscatter and basal area. Incidentally, banana plants are also known to give high backscatter values for relatively low biomass (Le Toan, 2007).

[1] An opportunity arose to test this when a fire in part of the study area destroyed all palmetto leaves in the large palmetto thicket towards the middle of the field transect area. It was hoped to compare ALOS L-band data over the study area after the fire to AIRSAR L-band backscatter values before the fire. Unfortunately this opportunity was missed due to sensor schedule conflicts.

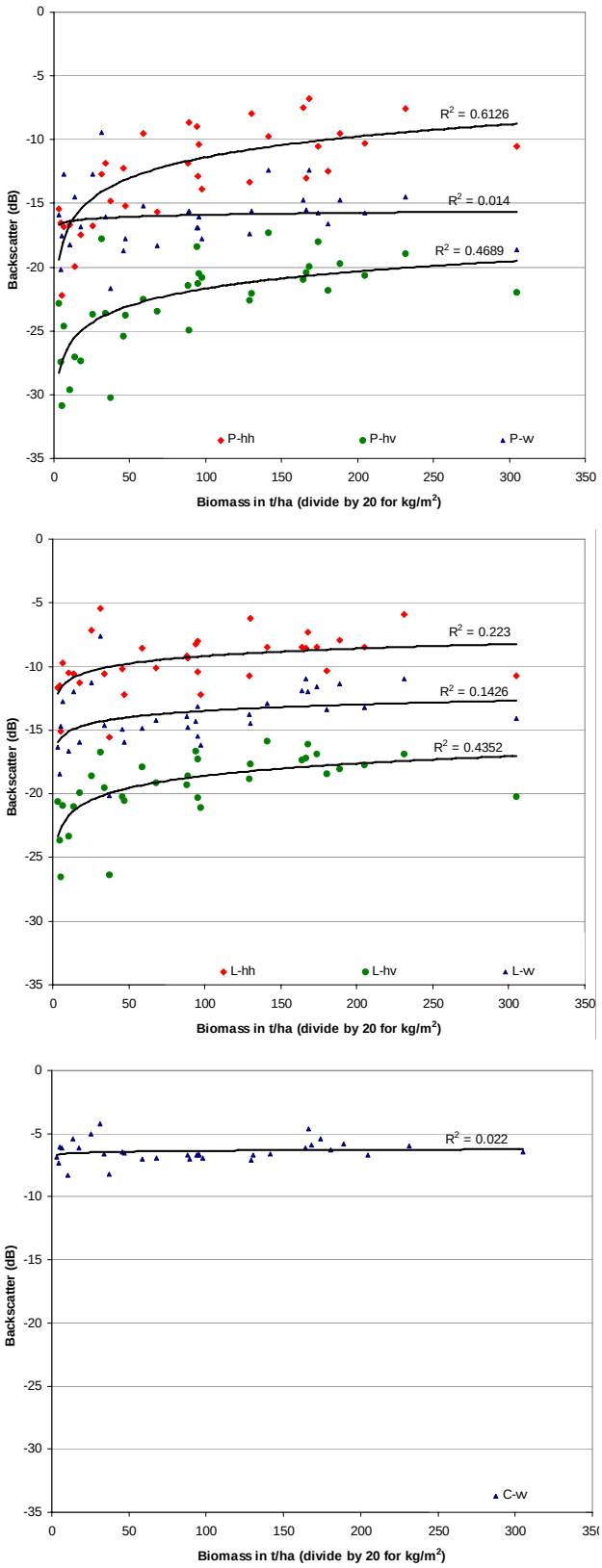

Figure 6.12: Biomass-backscatter plots for P-, L- and C-band at different polarisations for 33 plots of size 30x30 m (i.e., 900 m^2).

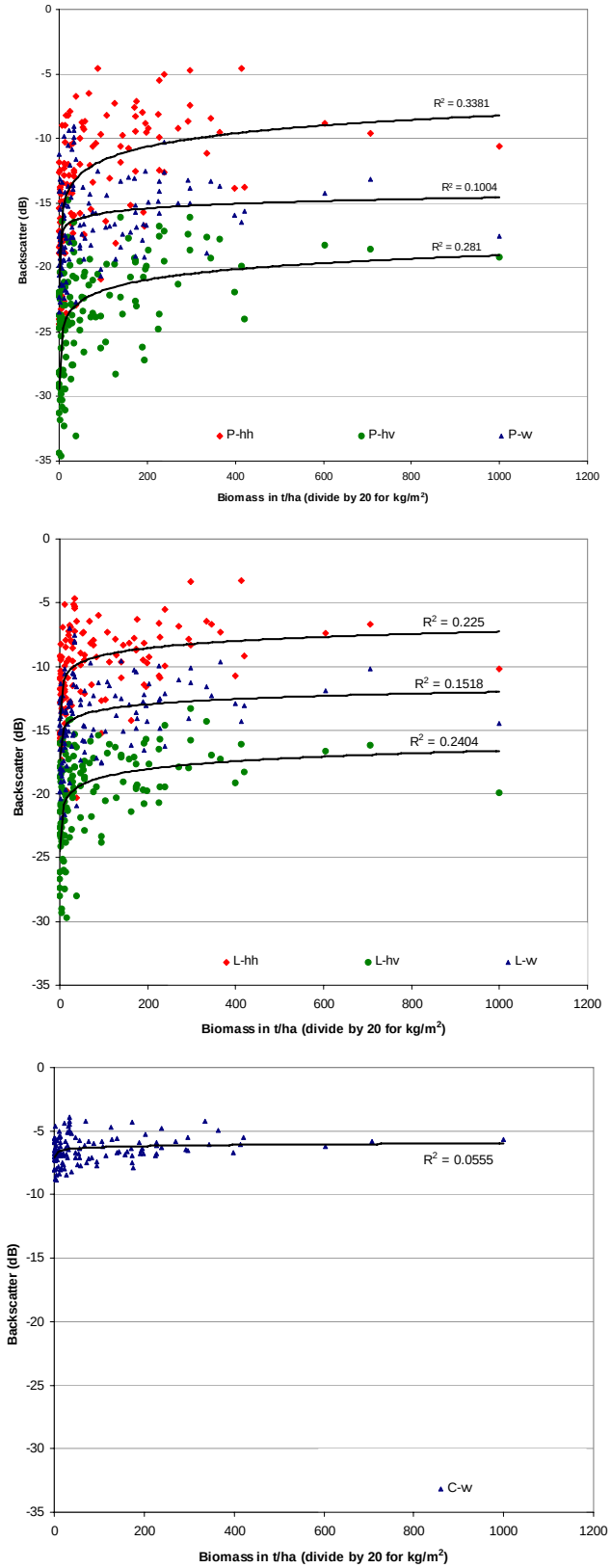

Figure 6.13: Biomass-backscatter plots for P-, L- and C-band at different polarisations for 132 plots of size 15x15 m (i.e., 225 m^2).

Fig. 6.11 shows L- and P- band polarimetric SAR backscatter for profile 10. This allows the direct comparison of the different polarisations with the field data. The figure shows that the difference in L and P band polarimetric response could be used to identify areas of palmetto as P-VV > P-HH whereas generally L- and P-band VV backscatter is lower than HH polarised backscatter.

Judging from all backscatter values in profile 11 (Fig. 6.10(b)), ~500 – 540 m along the transect suggests that fieldwork might have missed one or more small palmetto clumps at the edge of the palmetto thicket. This is further underlined by the fact that P-VV>P-HH for this area (see Appendix VII). It is common for smaller palmetto clumps to occur on the edges of large palmetto thickets. It is also possible that such clump(s) might have disappeared between field data collection and AIRSAR data acquisition (e.g. through burning). As the InSAR data does not suggest the presence of large trees, the higher backscatter values at this location are likely to have been caused by palmetto.

6.6. InSAR vegetation height retrieval

This section discusses the evaluation of the InSAR-derived DSMs for tree height retrieval as a means to estimate AG biomass in the savanna woodlands. Vegetation height retrieval is first discussed. As the results showed a surprising difference between the X-band and C-band DSMs. This is followed up in two subsequent sections which evaluate the effect of tree growth in between the data acquisition dates and differences in backscatter response for the X- and C-band in the study area.

6.6.1. Vegetation height profile plots

Figs. 6.14(a and b) and 6.15 show comparisons of the InSAR-derived DSM data with the field data for sub-transects 10-12. All DEM and DSM elevations are in m above Mean Sea Level (MSL). Fig. 6.14(a) shows the DSM profile plots together with the interpolated ground surface DEM (see 5.4.2) compared to field data plotted on the interpolated ground surface DEM. The bottom section of the graphs show

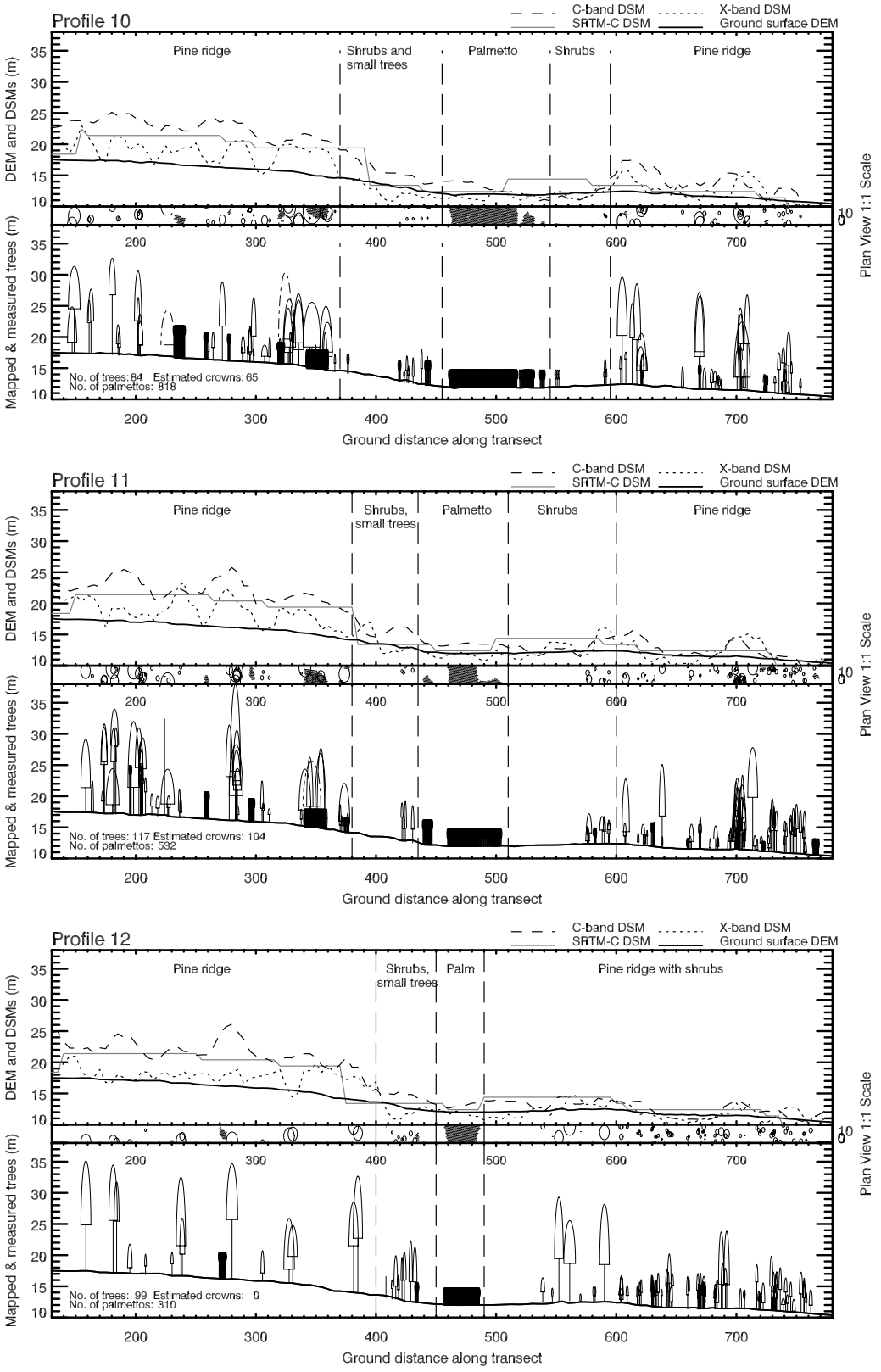

Figure Error! No text of specified style in document.**.1(a): Graphs showing DSMs with the ground surface DEM and actual tree measurements taken in the field. All elevations are in m above Mean Sea Level (MSL).**

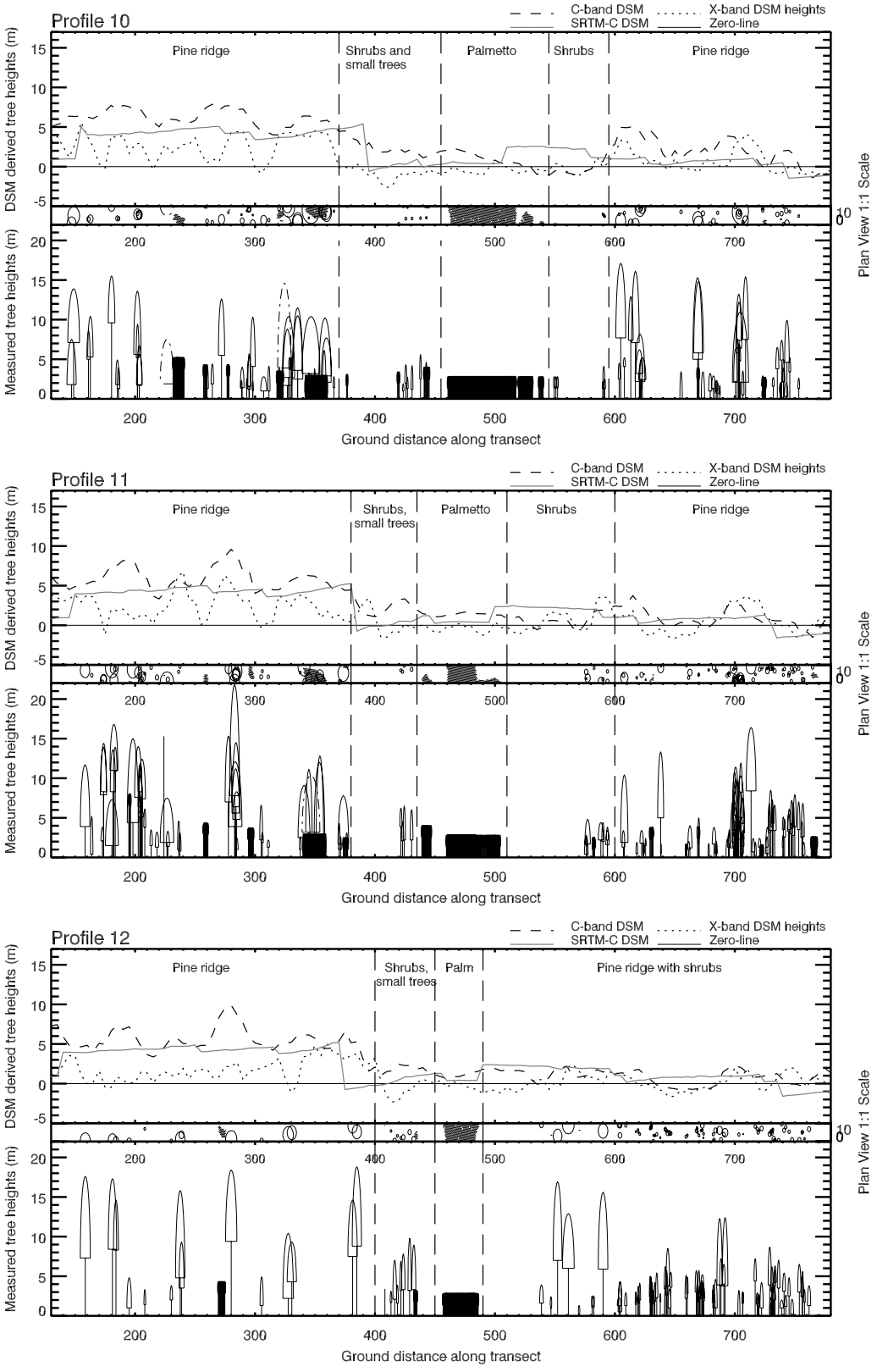

Figure 6.14(b): Graphs showing retrieved vegetation height from three DSMs with woody vegetation as measured in the field.

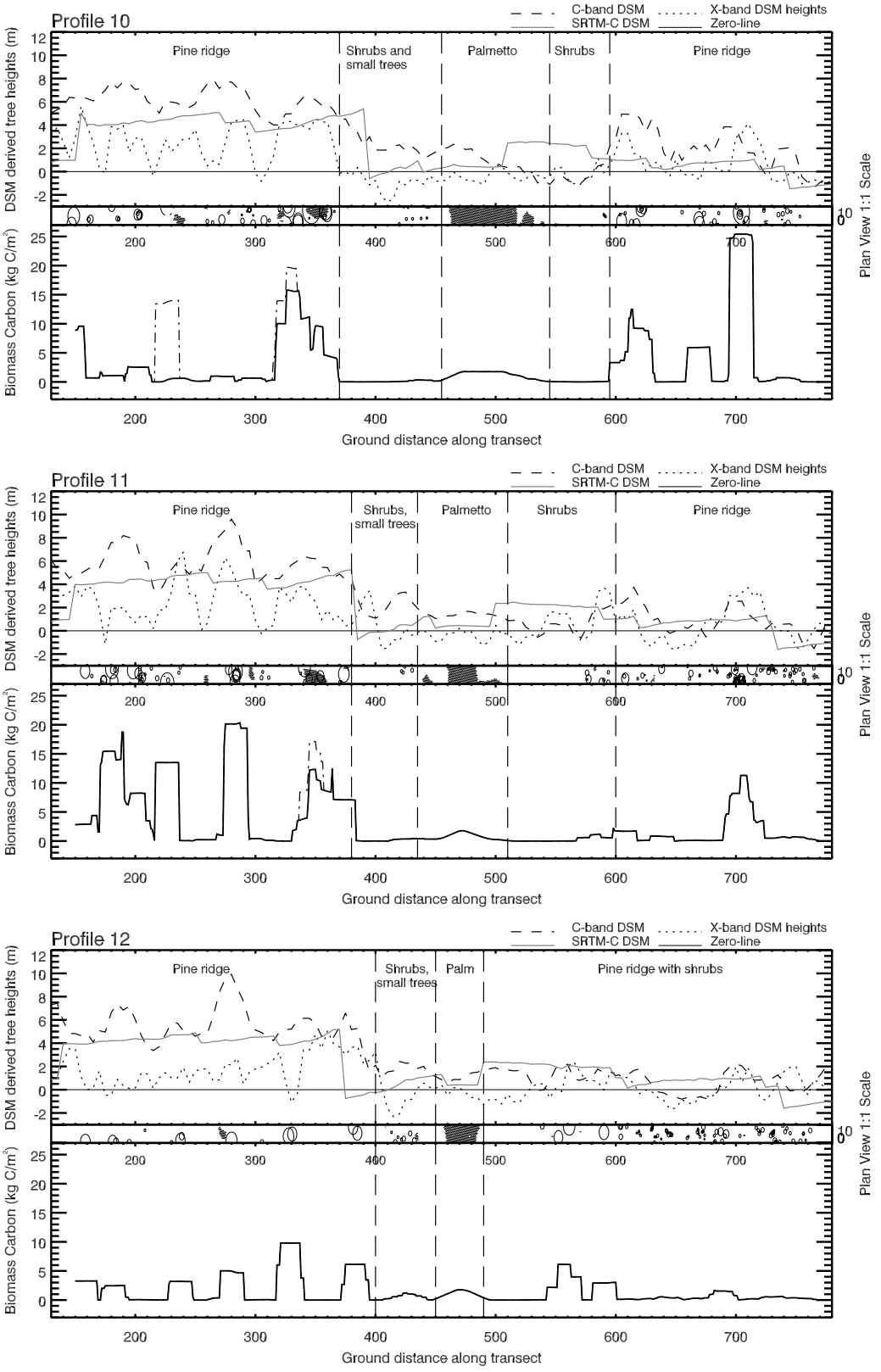

Figure Error! No text of specified style in document.**.2: Graphs showing retrieved vegetation height from three DSMs with moving average of biomass based on field data**

total height, crown depth and crown diameter for all trees and palmetto as measured in the field. The plan view gives an indication of canopy cover and stem number density. Fig. 6.15 shows retrieved tree heights, which were obtained by subtracting the DEM surface from the respective DSM surfaces. The biomass moving average is plotted for comparison. For extra reference, graphs showing DSM-retrieved vegetation heights together with the measured vegetation plotted on a zero line are included in Fig. 6.14(b).

Note that the AIRSAR range direction runs from left to right on the graph. The Intermap and SRTM range direction runs from the reader's right forming a 50º angle into the page. As a result, dominant vegetation features that occur in neighbouring sub-transects could influence Intermap and SRTM DSM patterns through radar layover and shadowing. Were this to occur, dominant vegetation structures in sub-transect 12 could influence DSM patterns in sub-transect 11 by means of layover and so forth, while dominant vegetation features in profile 10 could influence DSM patterns in profile 11 by shadowing and so forth (see Fig.6.4).

The effect of radar layover can be seen in places for the X-band DSM (e.g., the feature in the X-band DSM in profile 11, ~395 m along the transect could be partially caused by the pair of tall trees in profile 12, ~385 m along the transect). Similarly, the apparent mismatch in the X-band feature in profile 12, 350-370 m along the transect, which could be caused by the group of trees visible at ~360 m along profile 13[1] (see Fig. 6.4). As the profiles are oriented in the AIRSAR range direction, features in the AIRSAR DSM are in most cases very slightly displaced towards the near range end of the graph. Displacement is minimal and does not detract from visual interpretation of the graphs. This demonstrates clearly the advantage of collecting field data in the range direction in a heterogeneous woodland environment as opposed to using plots or transects which are not aligned with the range direction of radar data. Although it seems that layover has an only minor effect on the DSM elevations along the profiles, the fact that the X-band DSMs might in places be misinterpreted due to this effect should nevertheless be kept in mind.

[1] This profile was not plotted as the near range end of the profile falls off the edge of the field data.

Although all three DSMs show a clear trend in vegetation patterns, there are several notable differences. Since the SRTM C-band DSM has a much coarser resolution (90 m) than the other 2 DSMs (5 m), it shows the general vegetation height trend as opposed to local variations in vegetation height which is much more apparent in the higher resolution DSMs. In spite of its coarser resolution, it is notable that the SRTM C-band DSM elevations are generally more similar to the AIRSAR C-band DSM than the X-band DSM, probably due to similar C-band backscatter interactions with the vegetation giving similar scattering phase centres for SRTM and AIRSAR. This is especially clear for the pine ridge shown on the left-hand side of the graphs, where the SRTM DSM seems to consistently occur at approximately the minimum AIRSAR C-band DSM elevation. Considering the heterogeneous nature of the vegetation patterns and the relatively small woodland patches occurring in the study area, the SRTM DSM gives a surprisingly good representation of the broad vegetation patterns within the transect. This is also shown to be true for the greater study area (see Fig. 5.4). Perturbations such as the feature in the SRTM DSM around 550 m along the transect in all three profiles (Figs. 6.14 and 6.15) is probably caused by a patch of woodland occurring elsewhere within the 90 m pixel[2].

Fig. 6.15 shows comparisons of the retrieved tree heights with the moving averages for biomass. Visual comparison shows that there is a clear correspondence between the occurrence of peaks in the DSM-retrieved vegetation heights and peaks in biomass. However, this relationship is only based on the occurrence of a peak in biomass; the retrieved vegetation heights do not seem to bear any correlation with the amount of biomass on the ground. This is especially clearly illustrated in the peaks in DSM-retrieved vegetation heights in the pine ridge on the left in profiles 10 and 12 in Fig. 6.15.

There are several instances where DSM values estimate negative vegetation heights (see Fig. 6.15). This occurs mostly for the X-band DSM, notably in the area of dominant grass cover (i.e. mostly ground surface) with sparse shrubs and small trees ~415 m along the transect and over an area of sparse small trees within the pine ridge ~650 m along the transect. Inspection of the field data in neighbouring sub-transects

[2] This woodland patch is located at UTM 16N coordinates ~320050, 1943970m (see Fig. 6.4)

does not show dominant vegetation structures that might have caused this dip in the X-band DSM through radar shadowing. However, given the overall 1.3 m lift that was applied to the X-band DSM (see 5.7.2), most of the negative Intermap DSM surfaces still fall within the 3 m vertical RMSE of the Intermap data (see 5.2.1.2).

Comparison of the AIRSAR C-band DSM elevations with the X-band DSM elevations shows no consistent difference for retrieved vegetation heights. The X-band DSM values have a greater range, varying more widely between local minima and maxima (this can also be seen in Figs. 6.1 and 6.2). Since this is neither caused by differences in DSM resolution nor by differences in the DSM pre-processing[3], this difference could be caused by a difference in ground contributions from X- and C-band. This is further discussed in 6.6.3. The difference between the AIRSAR C-band and the X-band DSMs becomes smaller towards the right end of the graphs, with the AIRSAR DSM generally showing comparatively lower tree heights than for the left side of the graphs. This is caused by the effect of the multipath error discussed previously (see 5.7.3, Fig. 5.20). Fig. 5.20 shows that the far range end of the field transect coincides with a trough in the sinusoidal perturbation caused by the multipath error, while the near range end of the field transect coincides with a peak. When interpreting the graphs, one should keep in mind that the AIRSAR DSM should tilt slightly (1-2 m) upwards to the right end and slightly (1-2 m) downwards to the left end to give a locally corrected representation based on an averaged linear correction over the entire transect. The uncorrected AIRSAR DSM is shown in Figs 6.14 to 6.17 and 6.21.

Figs. 6.14 and 6.15 show that the DSMs generally underestimate tree heights for all DSMs. Tree height retrieval using InSAR in dense forest has been found to cause underestimation, mainly due to SAR penetration into the vegetation canopy (see 3.3.3.2 and Fig. 3.2). Since the field data transect includes savanna woodlands with a sparser canopy cover, tree height underestimation is much higher. Fig. 6.16 shows

[3] Intermap X-band has a transmit bandwidth of 67.5MHz, which gives a range resolution of 2.5m. During pre-processing a 7-8 m filter is used to smoothen the data before resampling to 5 m posting (B. Mercer, 2007). AIRSAR C-band has a transmit bandwidth of 40MHz, giving a range resolution of 3.3 m. No further filtering is done before resampling to 5 m posting (B. Chapman, 2007).

the under- and overestimation for all three DSMs along profiles 10-12. The degree to which the DSM-derived vegetation height is under- or overestimated was determined by dividing the sub-transect up into a number of bins and then comparing the tallest measured tree with the highest DSM value in each bin. Bins of 20 m long allowed for minor discrepancies between the field and DSM data due to radar layover and shadowing along the AIRSAR range direction, and in essence resulted in a number of consecutive 20 x 10 m plots. All DSMs were compared with the vegetation height data as measured in 2005. The bottom part of the graph shows the trees as measured in the field in 2005. The block outlines show the extent of the bins which were used to make comparisons between true vegetation height and DSM elevations. The height of each block shows the height of the tallest tree in each bin. The top part of the graph shows underestimation (<0%) or overestimation (>0%) of all three DSMs with respect to the vegetation height data as measured in 2005. Fig. 6.16 shows that vegetation height underestimation is generally lower for the pine ridge on the left side of the profile plots. Although the trees of the two pine ridges on both ends of the profile plots contain trees of approximately the same height for all three profile plots, the pine ridge on the left side has more tall trees and has an overall denser canopy cover. For the pine ridges, the X-band DSM shows vegetation height underestimation of 50-80% for the pine ridge on the left and 60-100% for the pine ridge on the right. The AIRSAR C-band shows slightly better results with 20-65% underestimation for the ridge on the left and 40-90% for the pine ridge on the right. SRTM C-band shows the highest range in underestimation, due to the much coarser spatial resolution. Values are 10-80% for the ridge on the left and 40-100% for the pine ridge on the right. Although the SRTM C-band DSM seems more comparable to the AIRSAR C-band DSM (Figs.6.14 and 6.15), the level of underestimation for SRTM is higher because of its coarser resolution which does not follow the local peaks and troughs in the vegetation canopy. Instances of overestimation of vegetation height occur for all three DSMs, but these generally exist where there is a gap of 40-50 m wide in between tall vegetation. The DSM then estimates a higher surface, mostly due to layover effects coupled with interpolation during pre-processing.

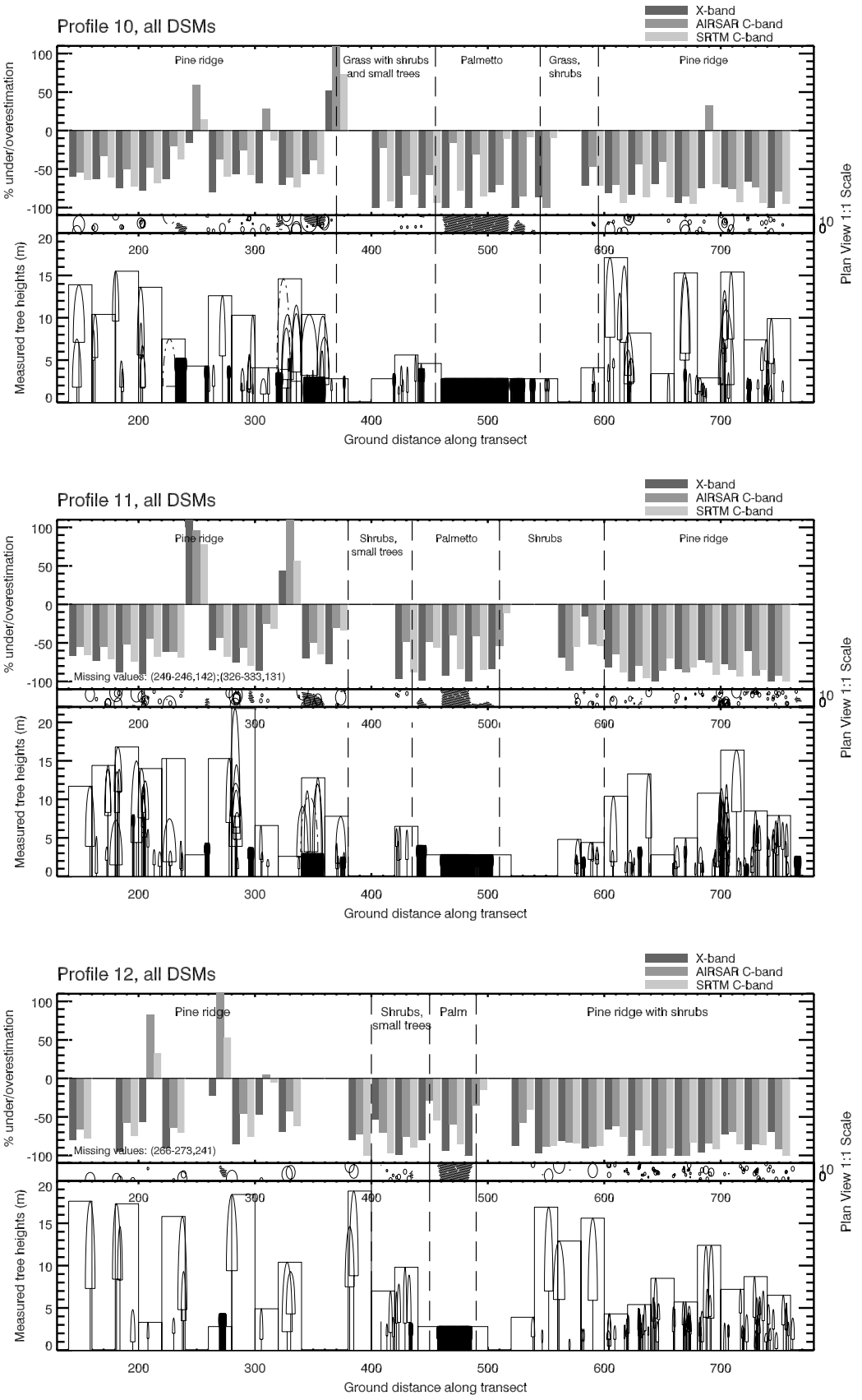

Figure Error! No text of specified style in document..**3: Graphs showing DSM-derived vegetation height underestimation (in %) for all three DSMs. Underestimations are calculated based on tree height measurements made in 2005.**

An unexpected result from Figs. 6.14 to 6.16 is that the X-band DSM retrieved predominantly lower vegetation heights than the C-band DSM for the sparse savanna woodlands. Based on the interaction of SAR backscatter of different wavelengths with forest environments (see 3.3.3, Fig. 3.2), the C-band DSM is expected to estimate lower tree heights than the X-band DSM. This unexpected difference was further explored for the effect of tree growth between the remote sensing data acquisition and field work dates (see 6.6.2) and for differences in backscatter response between X-band and C-band (see 6.6.3).

6.1.1. Evaluation of the effects of vegetation growth

An evaluation was done to assess whether tree growth between the data acquisition dates for the X-band and C-band DSM data (acquired in 1999 and 2004 respectively) and the field data (acquired in 2005) is responsible for the unexpected difference in the two DSM surfaces. This was done by comparing each DSM with the vegetation height as it might have been in the year of the DSM acquisition based on the 95% confidence interval for annual height increase for pine and shrub (see 5.4.5). Based on the lower and upper 95% CI limits, maximum and minimum growth over the period between field data collection and the different DSM data acquisitions were calculated for each bin and compared to the highest DSM value within the bin. Although the 95% CI limits give a large range of growth values, this method allowed for comparison of the levels of underestimation of the different DSMs.

X-band data was acquired 5 years prior to the AIRSAR C-band data and 1 year prior to the SRTM C-band data. An effect of the time difference between the X-band and AIRSAR C-band data acquisition is visible in Fig. 6.14, profile 11 at ~220 m along the transect, where a tall dead tree trunk (i.e. without a crown) was measured during the 2005 fieldwork campaign. It is clear that the C-band DSM acquired in 2004 was not as strongly affected by this tree as was the X-band DSM acquired in 1999. It is therefore believed that the tree lost its crown in between the data acquisition times in 1999 and 2004. Based on the minimum and maximum growth rates for pine and shrub (see 5.4.5), Fig. 6.17 shows X-band as well as AIRSAR and SRTM C-band DSM-derived vegetation height under/overestimation with respect to vegetation

heights as they might have been on the respective DSM acquisition dates. In other words, X-band is compared to vegetation heights as they might have been in 1999, SRTM C-band to vegetation heights as they might have been in 2000 and AIRSAR C-band to 2004 vegetation heights.

Fig. 6.17 shows the degree of under- or overestimation in DSM-retrieved tree heights for both maximum and minimum growth scenarios based on the upper and lower 95% CI boundaries. The bottom part of the graph shows the trees as measured in the field in 2005. The block outlines show the extent of the bins which were used to make comparisons between vegetation height and DSM elevations. The height of each block shows the height of the tallest tree in each bin as it might have been in the year of DSM data acquisition based on the lower boundary of the 95% CI for annual pine and shrub growth, giving the vegetation height based on minimum annual height increase. The horizontal line within each box gives the vegetation height as it might have been in the year of DSM acquisition based on maximum annual height increase, calculated using the upper boundary of the 95% CI for annual pine and shrub growth. Although these growth estimations are only based on limited field observations, the 95% CI gives an indication of the range of vegetation height increase that might have taken place over the years spanning the different DSM data acquisitions. This provides a way in which to directly compare the degree to which the different DSMs underestimate the vegetation heights. The top part of the graph shows underestimation (<0%) or overestimation (>0%) of each DSM with respect to the minimum and maximum vegetation height at data acquisition. Fig. 6.17 shows the results for profile 10; results for profiles 11 and 12 are included in Appendix IX. Comparison of the level of underestimation for the X-band with the AIRSAR C-band shows that X-band still has overall higher levels of underestimation for DSM-derived vegetation heights. This largely rules out tree growth as the reason for the C/X-band DSM difference over the sparse woodlands in the savanna.

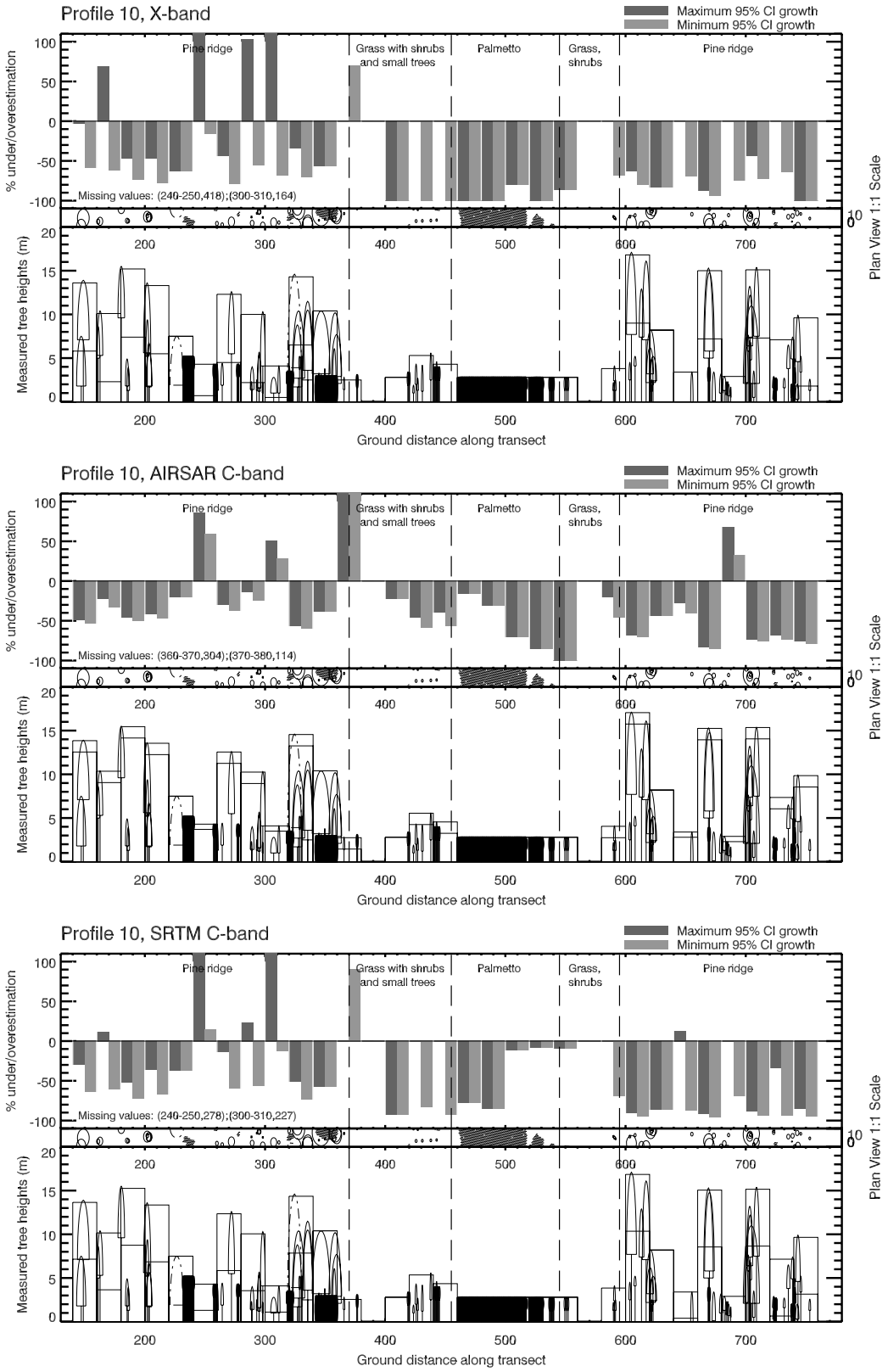

Figure Error! No text of specified style in document.**.4: Graphs showing DSM-derived vegetation height underestimation (in %) for all three DSMs, profile 10. Underestimations are calculated based on tree height as they might have been in the year of DSM acquisition based on 95% CI of pine and shrub growth. DSM acquisitions: X-band 1999, AIRSAR C-band 2004, SRTM C-band 2000, field data 2005.**

6.1.2. Modelling backscatter response for C- and X-band

As tree growth between InSAR data acquisition dates was largely ruled out as the cause for the unexpected difference in the X- and C-band DSMs, the polarimetric radar interferometry simulator (PRIS, Izzawati, *et al.*(2006)) was used to further investigate the differences in C- and X-band backscatter response as a possible cause. The model was run for sparse (Marino, *et al.*, 2008) and dense woodland (Marino, 2007) based on actual field measurements. Scattering phase centres (SPCs) were returned for X- (B/lambda = 159, extinction coefficient = 2.6) and C-band (B/lambda = 94, extinction coefficient = 1.87) at 5 m spatial resolution. The ground surface was modelled as intermediate rough dry soil. Equal ground contribution was assumed.

Fig. 6.18 shows the results of polarimetric radar interferometry modelling for a sparse and a dense grouping of trees. The green shapes represent tree crowns as measured in the field. The coloured dots show the modelled scattering phase centre (SPC, see 3.3.3.2) for the different polarisations. Red (HH) and blue (VV) points fall mostly in similar positions with blue plotted over the red, therefore showing more blue points. Green points (HV) return higher SPC values because HV polarisation

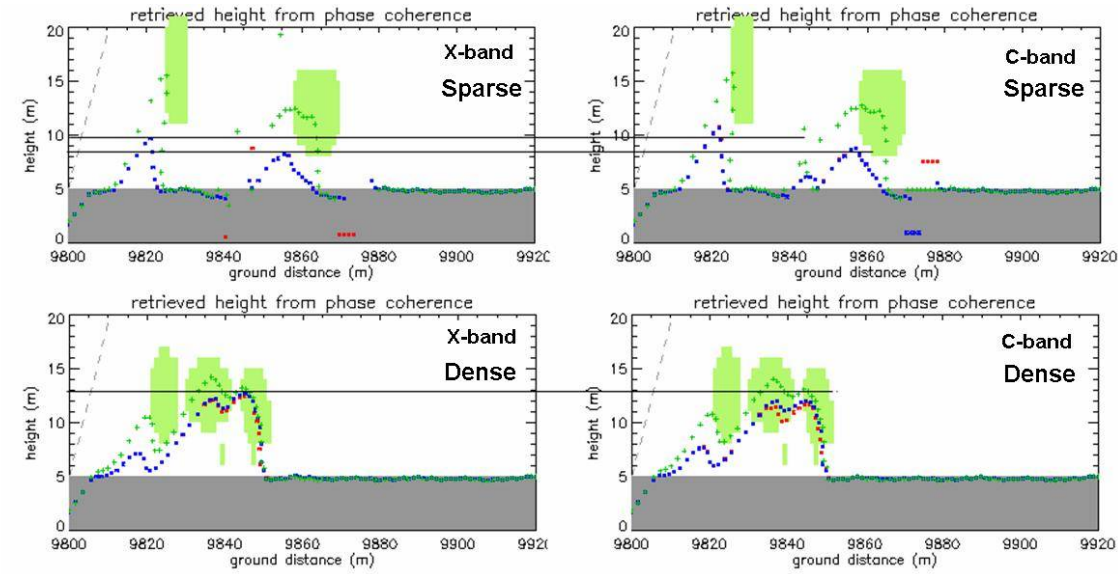

Figure Error! No text of specified style in document.**.5: PRIS modelling results, assuming equal ground contributions, showing returned scattering phase centres for X- and C-band for sparse and dense canopy. Green points represent HV polarisation, blue (VV) and red (HH) are mostly similar with blue plotted over the red. The horizontal lines compare the modelled SPCs for X- and C-band (Marino, 2007).**

reacts most strongly with tree crowns. The plots on the left represent X-band modelling results while C-band results are shown on the right. Horizontal lines compare the returned X-band SPCs with C-band SPCs. These results suggest that, for HH and VV polarisation, X-band provides slightly higher vegetation height estimates than C-band for dense canopies, while C-band performs slightly better for sparse canopies (in both cases the difference in absolute terms is ~1 m). This difference is not evident for HV polarisation, as it returns a much lower ground contribution.

These differences between C- and X-band returned SPCs can be explained for sparse canopies by differences in canopy extinction (i.e. penetration into the tree canopy) combined with ground return within the same slant range cell, as illustrated by Fig. 6.19. For the first slant range cell, the returned signal from the crown and the ground are equal for both C- and X-band. For subsequent slant range cells, however, extinction through the crown is greater for X-band, allowing the C-band signal to penetrate deeper into the crown. The second and third slant range cells in the figure therefore return a proportionally higher signal from the crown than from the ground

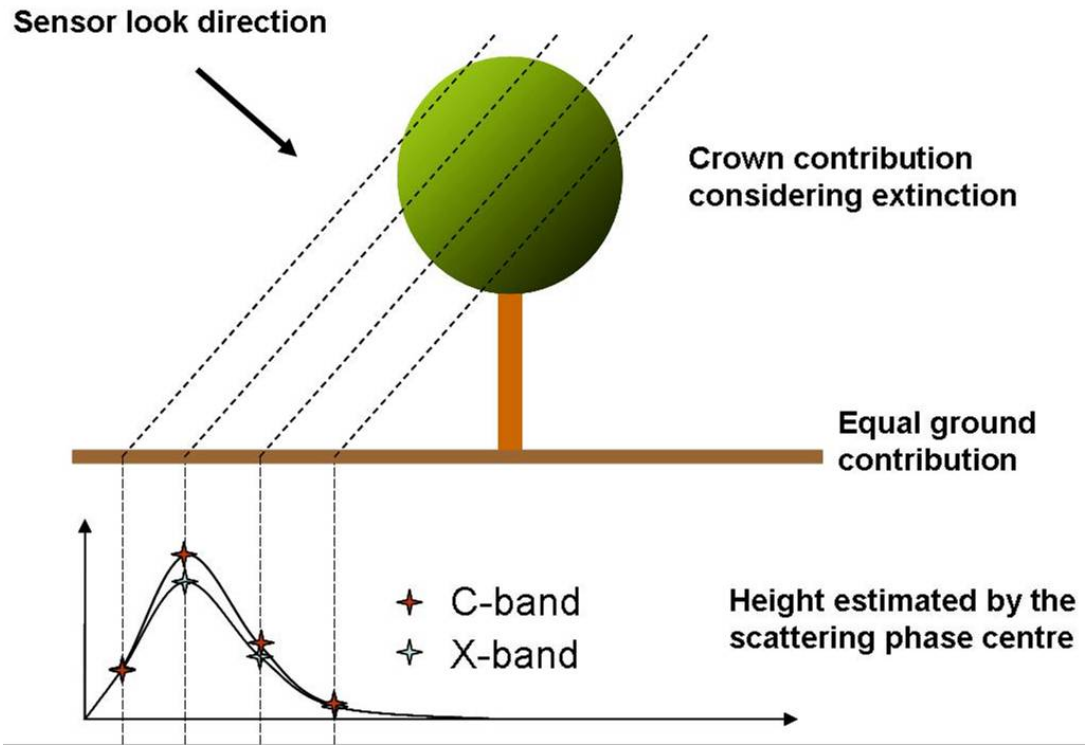

Figure Error! No text of specified style in document.**.6: Proportional crown and ground returns for C and X-band in a sparse woodland environment (adapted from Marino, *et al.* (2008)).**

for C-band whereas X-band receives a proportionally higher ground signal than crown signal. This combination causes a lower SPC for X-band than for C-band (Marino, 2007).

It should be noted that these modelling results are based on equal ground returns for X- and C-band. In reality, grass blades in the savanna fall well within the Rayleigh region for scattering for both the X- (3.5 cm) and C-band (5.7 cm) as the circumference of these long thin cylinders is ≈ 0.3 cm (based on a 1 mm diameter). Since backscatter drops off as a function of $\frac{1}{\lambda^4}$ in the Rayleigh region (Woodhouse, 2006a), the X-band backscatter from the grass undergrowth is theoretically a factor of ~7.4 (8.7 dB) higher than for the C-band backscatter. This causes a larger ground-level contribution for X-band, and therefore further lowering of the scattering phase centre for the X-band in comparison to the C-band DSM (Viergever, *et al.*, 2007).

Since the modelling outcome showed an interesting difference between the X- and C-band DSMs based on crown density, coupled with the effect of ground contribution, it was tested whether this difference was evident in the study area. Profile plots were created for the dense vegetation of the widest of the gallery forests in the study area (see Fig. 6.20). Data was collected during the 2007 fieldwork campaign; ground elevation was measured using a non-survey standard handheld GPS at an accuracy of ±5 m and tree heights were measured along a disused path that crosses the gallery forest. Profile lines were extracted in the direction of the field data, incidentally coinciding with the azimuth direction of the AIRSAR (Fig 6.20, profile 1) and in the range direction of the Intermap and SRTM data[4] (Fig 6.20, profile 2). Fig. 6.21 shows the DSM elevations along the two profiles of the dense gallery forest.

The instrumentation used to collect vegetation heights for the gallery forest was not as accurate as for the sparse woodlands. Nevertheless, tree heights can be estimated from the graphs by assuming that the true ground surface coincides with the

[4] A profile plot in the AIRSAR range direction would not allow for a cross-section because the gallery forest is oriented in the same direction.

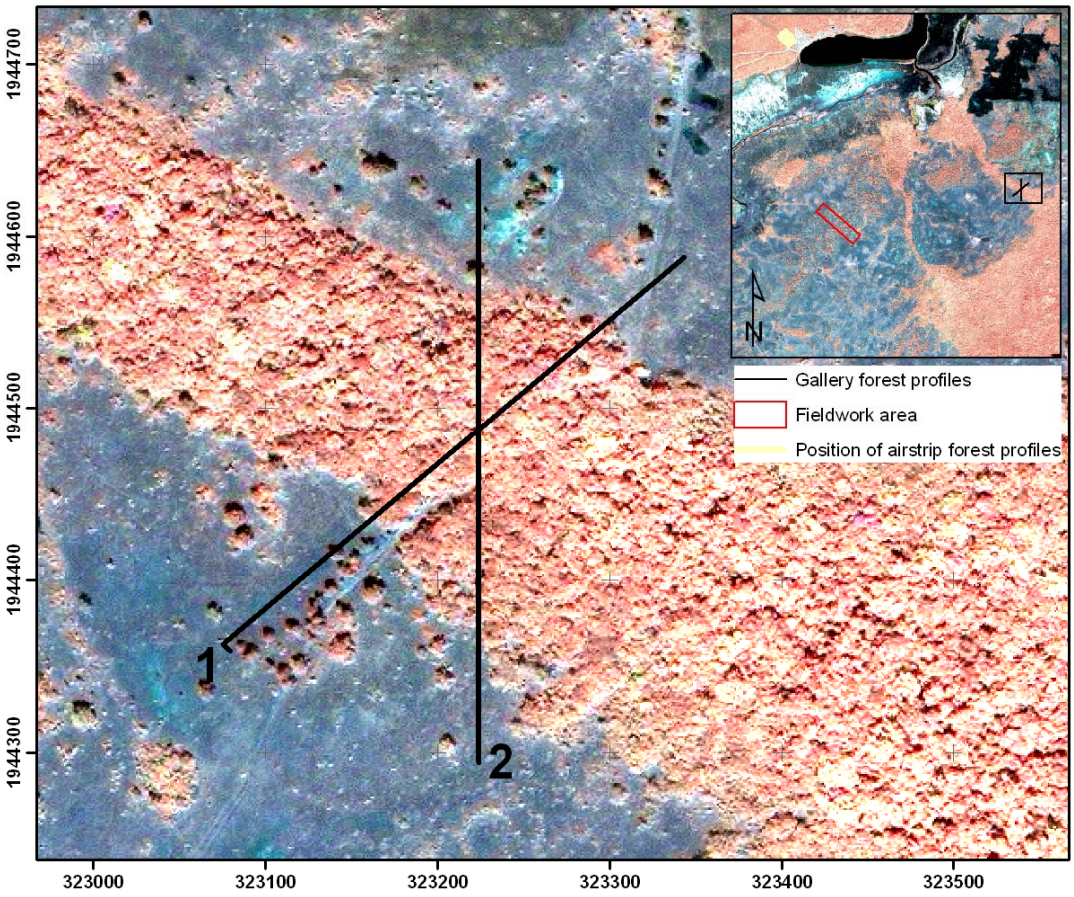

Figure Error! No text of specified style in document.**..7: Map showing the location of the profiles at a gallery forest in the study area and at the Hill Bank airstrip, the latter data were not used due to AIRSAR multipath error. The image backdrop and inset shows the Ikonos image at 1 m (RGB, 423). Profiles were taken in direction 210º (profile 1) and in 180º (profile 2).**

minimum DSM values on the left part of the graph for profiles 1 and 2. For profile 1, this is ~ 9 m which is marginally outside the GPS-measured ground surface elevation measurement of 15 m ± 5 m. If this estimated ground surface is subtracted from the maximum DSM values over the gallery forest, forest height estimates of 8-10 m (profile 1) to 8-11 m (profile 2) are obtained. As the tree heights for this gallery forest were measured between 10 and 17 m above the ground surface along profile 1, the approximate underestimation (~20-40%) in tree height estimation is smaller for the dense forest than for the sparse woodlands. This, however, needs more intensive investigation aided by accurate field measurements. In general, the three DSM surfaces represent much more similar elevations for dense forest than for the sparse woodlands, especially along profile 1. Again, the X-band DSM shows greater

variation than the AIRSAR C-band DSM even though the resolutions are identical. Considering the coarse SRTM resolution and the relatively narrow gallery forest structure (~170 m wide), this DSM gives a good estimation of the vegetation structure. Note that the SRTM DSM shows generally lower DSM elevations for the gallery forest due to averaging over the large pixels.

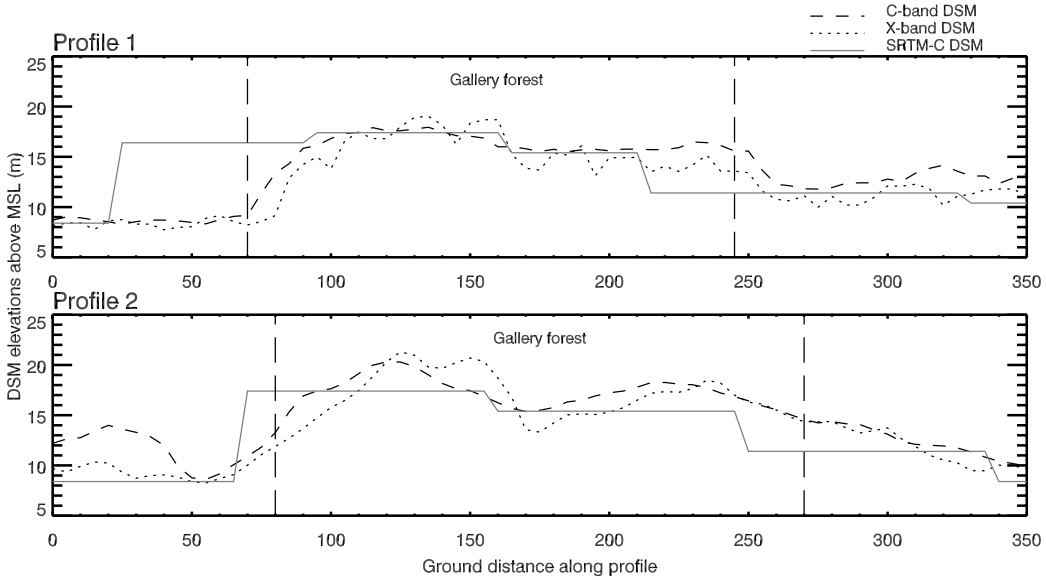

Figure Error! No text of specified style in document.**.8: Graph showing DSM elevations in m above Mean Sea Level (MSL) for two profiles of a dense gallery forest in the study area (see Fig. 6.20). The average ground surface elevation was measured at 15 m ± 5 m and the average tree height was measured at between 10 and 17 m above the ground surface along profile 1**

The 'dip' in the gallery forest surface visible in the AIRSAR C-band and X-band DSMs in profile 2 coincides with the disused path that crosses the gallery forest (also visible in Fig. 6.20). In both profiles, the X-band DSM is more similar to the C-band DSM than for the sparse woodlands shown in Fig. 6.14 and there are instances where the X-band DSM shows higher tree heights. It should be noted that the AIRSAR C-band DSM has not been adjusted in these profiles and could suffer minor effects of the multipath error[5] Analysis to further investigate the differences in C-band and X-

[5] This should be further investigated upon correction of the AIRSAR multipath error. Extensive survey-grade vegetation height field data was collected during the 2005 fieldwork campaign for the dense forest on both sides of the disused airstrip at Hill Bank station (see Fig 6.20, inset). Unfortunately these data could not be used as the AIRSAR multipath error caused a very large difference between the C-band and X-band DSMs in the far range region of the image (see Fig. 5.18).

band DSM values for sparse and dense forest over the wider study area suggests that C-band InSAR generally retrieves higher vegetation heights than X-band for sparse forest, and that the inverse occurs for dense forest (see Appendix X). Since these analyses have been carried out using the uncorrected C-band InSAR data, this should be repeated on the corrected AIRSAR data to obtain conclusive results.

6.2. Summary

Based on the relationship of several vegetation characteristics with AG biomass carbon content, vegetation height has been identified as a suitable indicator for AG biomass in the savanna woodlands. Since vegetation height can be practically measured from an EO perspective (through both active and passive EO methods as outlined in Chapter 3), this chapter evaluates the use of shortwave InSAR-derived DSMs for vegetation height retrieval of the savanna woodlands. It was also shown, based on field data and associated allometry, that biomass distribution could be linked to other woodland characteristics such as canopy cover, tree number density, basal area or crown depth. As the combination of these woodland characteristics determine SAR backscatter, this chapter first evaluated AIRSAR L- and P-band backscatter as an initial indicator of biomass distribution within the savanna woodlands. The main results are summarised in Fig. 6.22.

Based on the accurate co-registration of the field data and the EO data (discussed in Chapter 5 and summarised in 6.2), analyses were carried out based on visual comparisons of field data characteristics with SAR backscatter values and DSM elevations. These comparisons are shown in Figs. 6.10(a) to 6.17 and the results are discussed in sections 6.5 and 6.6. The main results of these evaluations are summarised in Fig. 6.22, showing the crown plan of the field data within the three sub-transects together with moving averages of AG biomass and basal area as a basis for comparison. Retrieved vegetation heights are shown for the X-band, AIRSAR and SRTM C-band DSMs. Backscatter for L- and P-band at HV polarisation are also shown. Since grey scale shading is used separately for each sub-transect in the various graphs, direct comparisons can be made based on relative differences within each sub-transect. For example, on a detailed level the brightest block in the plot for biomass in sub-transect 10 (~ 700 m along the transect) represents the highest

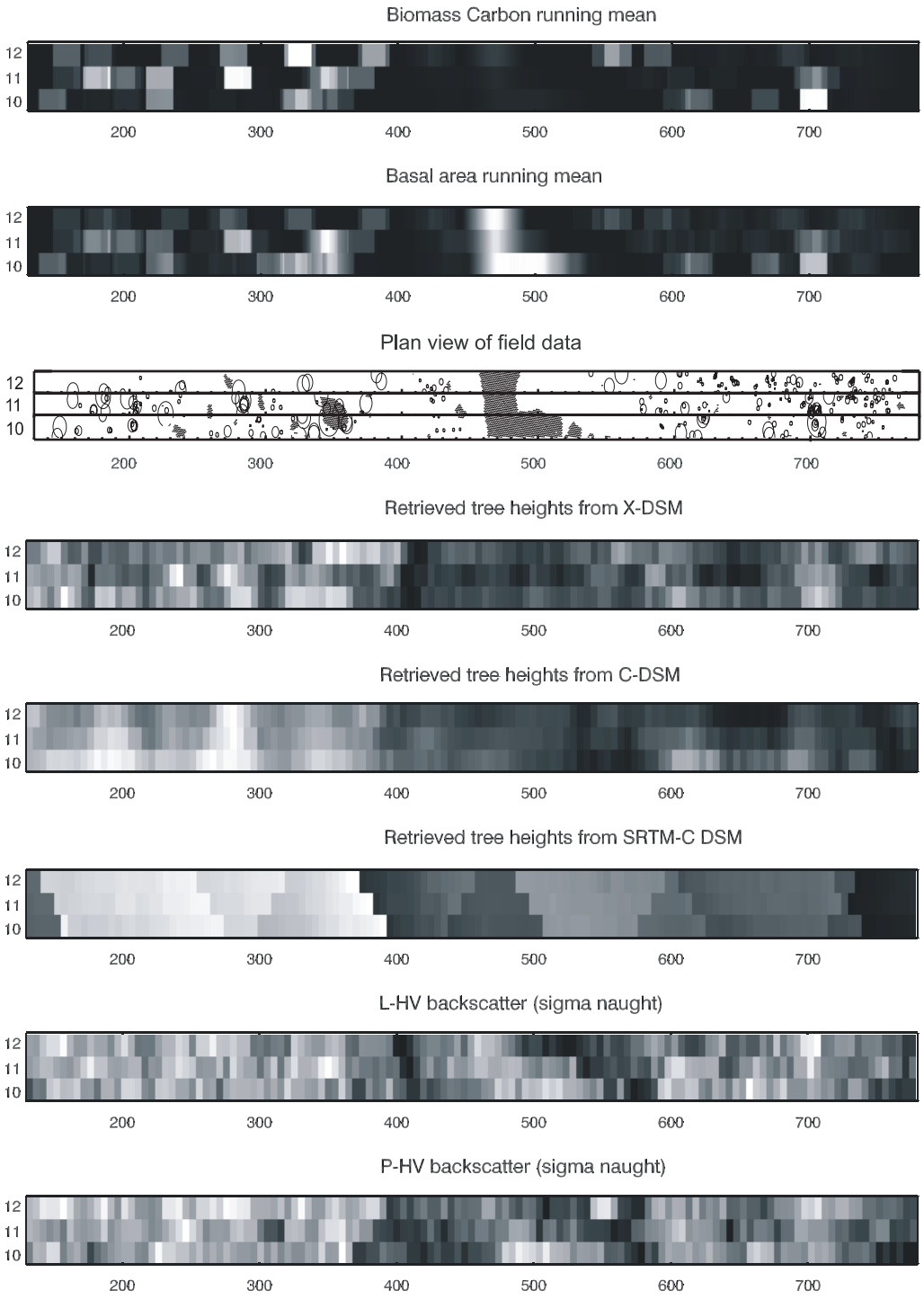

Figure Error! No text of specified style in document..**9: Summary of main results, showing the plan view of the field data, biomass carbon and basal area against retrieved vegetation heights from the Intermap (X-band), AIRSAR and SRTM (C-band) DSMs and AIRSAR L- and P-band backscatter at HV polarisation. Light shades represent high values (of biomass carbon, basal area, retrieved tree heights and backscatter) whilst darker shades represent lower values.**

amount of AG biomass in sub-transect 10. From the plan view of the field data, it is clear that this represents a dense patch of trees within a pine ridge. The actual heights can be obtained from a profile plot (e.g. Fig. 6.6) as ~15 m, which also shows that there are several other groups of trees of similar height within the sub-transect. These can be identified on the plot for X-band retrieved heights. The graph for C-band retrieved vegetation heights also identifies these patches of trees but the smoother surface more closely identifies the general trend in vegetation heights. This trend comes out even stronger in the very coarse resolution retrieved heights from SRTM C-band. Neither of the plots for backscatter show a particularly high backscatter for the patch of trees at ~700 m along the transect.

On a coarser scale, comparison of the plots shows that L- and P-band HV backscatter is strongly affected not only by areas of high biomass, but also by areas of high basal area (i.e. the large thicket of palmetto which has relatively low biomass). On comparing the DSM-retrieved vegetation heights with peaks in biomass, there is a strong correspondence between the occurrence of peaks in DSM-retrieved vegetation heights and peaks in biomass, although there doesn't seem to be a linear relationship. However, the pine ridge on the left of the transect contains overall higher biomass than the pine ridge to the right of the transect. This seems to be reflected in overall height retrieval for the two pine ridges in that all three DSMs retrieve overall shorter vegetation heights for the pine ridge on the right of the transect. The three plots for DSM-retrieved vegetation height generally show similar patterns in vegetation height. The X-band DSM shows more local variation, while the AIRSAR C-band, which has a similar data posting of 5 m, shows a smoother representation. The SRTM DSM gives a surprisingly good representation of the patterns of woodland vegetation, given the coarse spatial resolution of the SRTM data, with a data posting of 90 m.

Although the X-band DSM showed negative vegetation heights for some areas, these errors still fell within the reported 3 m vertical RMSE of the data. The fact that X-band data shows more troughs coinciding with areas between patches of trees, makes it potentially suitable for interpolating a ground surface DEM based on local minima. An unexpected result (see Figs 6.14 to 6.16) shows that X-band generally estimated lower tree heights than C-band. The effect of tree growth in between data acquisition

dates has been ruled out and subsequent modelling suggests that this difference is caused by differences in backscatter response due to the sparse and heterogeneous nature of the savanna woodland. As a comparison, DSM elevation transects for an area of dense forest suggests a more traditional distribution of SPCs so that X-band retrieves generally higher vegetation heights than C-band. Due to the occurrence of multipath error on the AIRSAR C-band data, which strongly affects parts of the image, this could not be tested with confidence on the greater image area and needs further investigation when the data has been corrected. Nevertheless, these results and the modelling discussed in 6.6.3 suggest that C-band InSAR might be more suitable than X-band InSAR for vegetation height retrieval in woodlands with sparse canopies and dominant grass undercover.

Interpretation of the sub-transects for DSM-retrieved vegetation heights has shown that it was advantageous to interpretation of the heterogeneous woodland environment to collect field data in the range direction of the AIRSAR data and subsequently to use neighbouring sub-transects to be able to take into account the effects of the Intermap range direction on apparent mismatches in the data.

CHAPTER 7:
Discussion, conclusions and recommendations

7.1. Introduction

This thesis has evaluated the capability of SAR for estimating the above-ground biomass of woody vegetation in heterogeneous tropical savanna woodland, by (i) investigating the effect of woody vegetation structure (AG biomass, canopy cover, basal area and height) on SAR backscatter and (ii) by using canopy height estimations from SAR interferometry. EO data used are fully polarimetric L- and P-band SAR backscatter (from AIRSAR) and single-pass C- and X-band InSAR (from AIRSAR and Intermap Technologies), all at 5m posting. Single-pass C-band SRTM InSAR data at 90 m posting was also used for comparison as this data has near-global coverage and is freely available. The study area, situated in Belize, contains vegetation typical of Central American savannas. Field data measurements relating to physical dimensions such as total height, crown height, diameter at breast height (dbh) and crown diameter of woody vegetation (mainly pine, oak and shrub) were acquired in a transect of 800 m x 60 m spanning the main savanna vegetation strata. Palmetto were measured for average height and stem number density. The field data encompasses 1133 mapped trees and single palmetto, 75 palmetto clumps and thickets, and an additional 2462 ground points. As the study area has a clear wet and dry season it was ensured that all EO and field data were acquired in the dry season to make them directly comparable.

This chapter first gives a summary of and discussion on the research results, linking the findings to that of others and discussing the implications of the main results for global savanna biomass mapping (7.2). Finally, recommendations are made for future research (7.3).

7.2. Discussion of results

The **field data (i.e., observations of trees, shrubs and palmetto vegetation within the field data transect) were shown to be spatially accurate to within 1 m in three dimensions** due to a combination of the following findings:

- the GPS observations were accurate within ~7 cm horizontally and ~3 cm vertically,
- the survey points were accurate within ~5 cm horizontally and ~1 cm vertically,
- the three-dimensional positions of field data were observed using a survey-grade total station instrument with mm accuracy,
- the method applied to map the points of detail caused a maximum offset of < 0.66 m horizontally.

Furthermore, it was shown that **the field data and the different EO data were horizontally well aligned (co-registered)**, while all elevation data (DSMs, ground surface DEM and GPS observations) were referenced to elevations above mean sea level. Minor vertical adjustments were made to the Intermap X-band and the SRTM C-band DSMs based on GPS measurements over areas of open grassland. Although the discrepancies fell within the reported vertical accuracies of the respective DSM data sets, the adjustments were done so that all the DSM data and the field data could be directly compared for the InSAR vegetation height retrieval. **All data were therefore also vertically aligned.** Although the AIRSAR C-band DSM contains multipath error, causing a sinusoidal perturbation of up to 5 m around the normal in the elevation data, it was shown that the field transect area was not strongly affected. The AIRSAR C-band DSM elevations show deviations of ±1.5 m around the average for the transect area. Over the entire image, deviations of up to 5 m are shown on a moving average plot of the perturbations. Similar patterns have been reported in other AIRSAR C-band DSM data with height perturbations of ±5 m (Kobayashi, *et al.*, 2000) and ±3 m (Prakoso, 2006).

Based on field data and associated allometry, the following deductions were made on the vegetation characteristics that determine AG biomass, both on an individual tree

basis and at woodland scale: **On an individual tree basis, there is a relationship between AG biomass and tree height, dbh, basal area and crown area.** This is based on the allometric equations used to calculate AG biomass (Brown, 2006), which use total height (for palmetto and shrubs) and dbh (for pine and oak) and on the relationship of dbh with tree height, basal area and crown diameter respectively. Similar relationships have been reported in Philip (1994) and Woodhouse (2006b). **At the woodland scale, vegetation height was shown to be an indicator of AG biomass, although there is no linear relationship between vegetation height and AG biomass.** This is caused by the heterogeneity within woodland patches, causing differences in tree number densities, basal area and canopy cover. A correspondence has also been shown between AG biomass and basal area, stem number density as well as canopy cover. However, palmetto vegetation forms an exception since it has relatively low biomass, even for areas with high basal area and stem number density.

Since woodland characteristics such as AG biomass density, tree height, canopy cover, basal area and stem number density determine SAR backscatter (Le Toan, *et al.*, 1992, Ranson and Sun, 1994, Ferrazzoli and Guerriero, 1995, Imhoff, 1995b, Kasischke, *et al.*, 1997, Kellndorfer, *et al.*, 2003, Woodhouse, 2006b), AIRSAR L- and P-band backscatter were evaluated as an initial indicator of biomass distribution within the savanna woodlands. Analysis of biomass-backscatter relationships for the study area demonstrates that apart from P-hh (and to a lesser extent P-hv and L-hv) backscatter which show a moderate relationship with AG biomass, **L- and P-band backscatter do not always have a strong correlation with AG biomass in savanna areas.** The graphs do not show the presence of clear saturation levels for the various SAR bands as have been reported in literature. This can be ascribed to the overall low correlation coefficients for the various logarithmic trend lines. Imhoff (1995b), Luckman, *et al.* (1997), Hoekman and Quiñones (2000), Le Toan, *et al.* (2004) have shown that C-band commonly saturates at biomass densities of ~20-30 t/ha, L-band at ~40-60 t/ha, P-band at ~100-200 t/ha and VHF at ~500 t/ha, with variations in the saturation levels determined by the experimental conditions and the forest characteristics such as dominant species, canopy structure and stem number densities (Le Toan, *et al.*, 2004, Woodhouse, 2006b). Because savannas typically have a biomass density lower than the reported saturation for L and P-band, there is a

persistent assumption that backscatter intensity at these wavelengths will be sufficient to estimate biomass in savannas. A further complication has been proposed (Woodhouse, 2006b) whereby a theoretical study implies that low density woodland will result in backscatter saturation at much lower biomass densities than is currently assumed. This is a likely explanation of the low biomass-backscatter relationships at L-band for the study area. This needs further study based on more data covering a wider range of biomass values, also in closed canopy forest.

Further analysis showed that both **L- and P-band backscatter were strongly affected not only by woodland areas of high biomass, but also by areas of palmetto having low biomass**. Although palmetto is characteristic of Central American savannas, these results underline the importance of considering the occurrence of similar palm-like vegetation in other savanna areas. A similar effect on SAR backscatter has been reported for banana plants, in which case it was suggested that banana plantations are masked out for the purposes of biomass estimation through backscatter relationships (Le Toan, 2007). **This is a problem in highly heterogeneous savanna areas such as the study area**, where palmetto occurs, not only in large thickets, but also as small clumps scattered in between the trees of the woodlands. The results show that the presence of palmetto clumps in woodlands cause a significant increase in backscatter values. Moreover, the presence of palmetto should not be entirely discounted through masking because they have been shown to contain 21% of the biomass in the study area (Brown, *et al.*, 2005).

Since vegetation height has been retrieved with relative success in closed canopy forest using InSAR methods (Hagberg, *et al.*, 1995, Wallington, *et al.*, 2004, Izzawati, *et al.*, 2006, Walker, *et al.*, 2007b), the use of shortwave InSAR-derived DSMs was evaluated for vegetation height retrieval for subsequent biomass estimation of the savanna woodlands. The results showed that **InSAR-derived DSMs provide an overview of the spatial distribution of woody biomass within the savanna** by accurately showing the location of forests and savanna woodlands. Unlike SAR backscatter, the DSMs do not clearly show the occurrence of low biomass palmetto which forms generally low vegetation within palmetto thickets. These results suggest that **InSAR-derived DSMs are a better indicator of the distribution of the bulk of the AG biomass of the woody vegetation in the**

savannas than SAR backscatter. However, the DSM-derived vegetation heights underestimate woodland vegetation heights: 50-100% for X-band and 20-90% for C-band. Underestimation of the InSAR-derived canopy height estimates is caused by the heterogeneous structure and low vegetation density of the savanna woodlands. This has also been reported by Hagberg, *et al.* (1995), Izzawati, *et al.* (2004) and Mette, *et al.* (2004). The degree of underestimation is not linearly related to tree height, but appears to be related to other factors such as tree number density, canopy cover and basal area. Results of the InSAR vegetation height retrieval analyses have shown that X–band retrieved generally lower vegetation heights than C-band for sparse woodland canopies. This is contrary to expectation based on the theory of interaction of SAR backscatter of different wavelengths with forest environments (Sarabandi and Lin, 2000, Woodhouse, *et al.*, 2006, Balzter, *et al.*, 2007, Dall, 2007). Analysis of tree growth in the study area has ruled out tree growth between the InSAR acquisition dates as a reason for this unexpected difference. Modelling results have shown that differences in canopy extinction for C- and X-band combined with differences in ground return may be the cause of this unexpected result in the sparse woodland canopies (Marino, *et al.*, 2008). This implies that **C-band InSAR might be a more suitable InSAR wavelength than X-band for vegetation height retrieval in sparse woodland canopies such as those found in savannas**. Similar results have not yet been reported in the literature.

SRTM C-band InSAR data was also evaluated for vegetation height retrieval in the savanna woodlands and found to **give a surprisingly accurate representation of the patterns of woodland vegetation**, given the coarse spatial resolution of the SRTM data at 90 m data posting combined with the sparse nature of the woodland canopy. SRTM has been used for the production of national and global canopy height maps for closed canopy forests (Carabajal and Harding, 2006, Hofton, *et al.*, 2006, Walker, *et al.*, 2007b) but there have been no reports on the use of SRTM for canopy height estimation in sparse or open woodlands. The results are encouraging as SRTM data has near-global coverage and is freely available, therefore having potential for global vegetation mapping and can also provide additional free data for developing countries who have limited funds for EO data acquisition. However, these data were only acquired in 2000 and are not frequently updated.

The results of both the backscatter analysis and the InSAR vegetation height retrieval show that it is not possible to use either method for estimating AG biomass in the savanna of the study area by itself. The heterogeneous character of the savanna vegetation and the uneven distribution of woodland characteristics such as vegetation heights and stem number densities within the woodlands complicate the application of both methods in isolation. For SAR backscatter, problems are caused by the occurrence of leafy palmetto vegetation which, although they have relatively low biomass, cause disproportionately high SAR backscatter compared to trees. This could cause an overestimation of savanna biomass. **Bearing in mind the heterogeneous nature of savannas in general, these results have implications for future EO missions for global biomass estimation** based on backscatter, especially at coarse resolutions such as the P-band BIOMASS mission currently planned by the European Space Agency. Furthermore, InSAR height retrieval was shown to strongly underestimate vegetation heights due to the low canopy cover of the savanna woodlands. The degree of underestimation is not consistent due to the heterogeneous nature of the woodlands related to uneven distribution of tree number densities, canopy cover and tree heights. As has been shown for closed canopy forests, height retrieval results are expected to improve for woodlands with a greater canopy cover. **The definition of *forest* under the Kyoto Protocol (see 2.2.3) therefore has direct implications for the accuracy of results for forest height retrieval using InSAR.** Although the height retrievals for forests and woodlands at the lower end of the canopy cover scale are highly underestimated, the **information derived from the InSAR data is nevertheless very useful for biomass mapping since it shows the distribution of woodlands which generally form areas of highest biomass concentration**. Results from this research suggest that in heterogeneous savanna environments, this data contains more information on the spatial distribution of biomass density than SAR backscatter.

An additional outcome of the research was the verification of the appropriateness and quality of the field data collection methodology. The **use of a transect oriented in the range direction of the main EO data (AIRSAR) for field data collection, instead of plots was shown to be advantageous**. The combination of the heterogeneous nature of the savanna vegetation and the nature of SAR viewing

geometry, which can cause slight displacement of data through layover and shadowing, could be accounted for during analysis and interpretation of the graphs showing the field data together with the SAR data along a narrow sub-transect. The use of a series of parallel sub-transects adjacent to each other enabled an explanation of the effects of SAR viewing geometry in the Intermap data. A series of plots of two different sizes (15 × 5 m and 30 × 30 m) were used to create biomass-backscatter plots for the study area. Comparison of the scatterplots based on these different plot sizes has shown that the choice of plot size is very important in an area with a non-continuous canopy and heterogeneous vegetation distribution. Whilst the use of plots in the order of 15 × 15 m is acceptable for biomass-backscatter graphs in a homogeneous closed canopy forest (e.g. Kelndorfer, *et al.* (2003), they are not appropriate for non-continuous or sparse canopies. Such areas require use of larger plots to average the effect of the heterogeneous vegetation distribution.

7.3. Recommendations

Based on the outcomes of this research, various recommendations are made for further research, not only towards improving the EO methods employed in this thesis for biomass estimation, but also for further research relevant to the study area.

Combining SAR and InSAR

The fact that neither SAR backscatter nor InSAR vegetation height retrieval can be used by itself for biomass estimation of the heterogeneous savanna vegetation structure, suggests further research into the combined use of these EO methods. For instance, SAR backscatter relationships with woodland characteristics such as basal area, stem number density and canopy cover could potentially be used in combination with woodland canopy height estimates to estimate AG biomass of the savanna woodlands. The combined information from InSAR and SAR backscatter could be used to make vegetation classifications, e.g. low InSAR-retrieved heights combined with high L- and P-band SAR backscatter values can be identified as palmetto thickets. An example is shown in Appendix XI. This would provide a step towards obtaining regional biomass estimates for the savannas. An attempt at regional biomass estimates was not made in this research because the field data was

not suited to this. Since the field data are detailed and localised, they do not encompass a range of biomass densities over a wide area within the savanna. Instead, the field data transect intersects the main savanna vegetation subtypes at one site and contains relatively detailed measurements of vegetation characteristics. This data was collected specifically to evaluate, at a local level, the effect of the savanna vegetation on SAR backscatter and InSAR-retrieved vegetation heights which has led to an increased understanding of the interaction of SAR with heterogeneous savanna vegetation.

Improving the use of InSAR for savanna woodland canopy height

It is advantageous to have an accurate representation of the ground surface in the form of a ground surveyed DEM for estimating vegetation height from InSAR data. However, developing countries seldom have such data for remote locations in savanna areas. Alternatives for estimating the ground surface are the use of longer wavelength InSAR or the interpolation of local minima of shortwave InSAR (e.g., the Intermap X-band data contained several minima that coincided with the ground surface, including areas within woodland). However, the existence of or opportunity for field observations to validate ground surface elevations derived by the above methods might be few. In the absence of *in situ* ground surface and vegetation height measurements for validation, the spaceborne GLAS LiDAR instrument on board ICESat could be useful if data is available. This was considered for this research, but data was not yet available for the study area. The existence of a “bald Earth” DEM, i.e. a global DEM without vegetation bias, would be a very useful data source for vegetation height retrieval using shortwave InSAR in remote locations.

Considering that the various shortwave InSAR DSMs used in this research had to be vertically adjusted, within their stated vertical RMSE, to match GPS field observations of the ground surface so that all DSMs and the field data were vertically aligned, the extraction of vegetation heights based on relative elevation differences between woodland areas and the surrounding open grassland is a more viable option for further exploration. Relative vegetation heights could be extracted by first delineating woodlands and using the DSM elevation values of the woodland patch relative to the ground surface of the surrounding open grassland. A segmentation

routine combined with an interpolation technique would be interesting paths for further research. There is also further scope for research into the use of three-dimensional models of the Earth's surface based on optical sensors for vegetation height retrieval, although the vegetation bias might be removed from such products.

X-band / C-band DSM inversion for sparse canopies

Since C-band InSAR was flagged up as a more suitable wavelength for vegetation height retrieval in sparse woodland as opposed to closed-canopy forest, a comparison of vegetation height retrieval of SRTM C-band and SRTM X-band for sparse heterogeneous woodland should be investigated. This was not possible for the study area since SRTM X-band only covers 45 km of the 225 km swath width of the C-band SRTM and therefore missed the study area. Such a comparison is hoped to be carried out on a savanna woodland in Australia, in collaboration with Richard Lucas. In order to conclusively prove the inversion of the C-band and X-band scattering phase centres over sparse woodland, processing should be repeated after correction of the AIRSAR C-band multipath error.

Contribution of other EO data

High resolution optical EO data was used to obtain canopy cover of the savanna woodlands in the study area. The use of segmentation and classification software such as eCognition™ provide the opportunity to automate the processing steps for tree crowns, and subsequent woodland delineation for the retrieval of canopy cover and tree number density. This was pursued by an MSc student (Michelakis, 2008). Since touching or interlocking tree crowns will be delineated as one crown, estimates for tree number densities will be inaccurate, requiring different strategies to overcome the problem.

The application of EO methods for the Kyoto Protocol

EO methods are likely to be used under the Kyoto Protocol as a monitoring tool for carbon stores. However, if EO methods such as the methods evaluated in this research, experience difficulties because of spatial heterogeneity caused by patchy vegetation structure, alternatives should be investigated. For example, the use of SAR and InSAR methods in combination with high resolution optical EO data to

obtain tree number densities or canopy cover for estimating AG biomass. An interesting issue arising from the use of EO data for biomass carbon estimation with respect to the 1990 base year is that Landsat is likely to be a popular data choice as it provides the opportunity for continuity due to its long history of global data acquisition. Since more accurate biomass estimation data and methods will develop in the near future, these methods should be combined with new Landsat data acquisitions to ensure accuracy and data continuity.

An important issue for future research is to evaluate to which degree canopy cover affects various EO data resolutions and EO methods for biomass estimation. If a cut-off point exists for minimum canopy cover, so that EO methods are unable to accurately estimate and monitor biomass for woodlands with a lower canopy cover, the Kyoto Protocol *forest* definition might need to be adapted to ensure more successful and robust monitoring methods in future.

Further research specific to the RBCMA study area

Further suggested research specific to the study area involves:

- Inclusion of savanna orchard and oak thicket vegetation subtypes in the savanna biomass estimations. These vegetation subtypes have not been studied in this research as they are situated far from the study site.
- Continued data collection and analysis on tree growth in the savanna woodlands. The subset of trees (97) that have been re-measured within the fieldwork transect, have been permanently marked for continued future monitoring. To obtain more accurate results on tree growth rates, (bi-)annualy repeated tree height measurements of the permanently marked trees in the study area are necessary. These data should preferably be sorted by age class. The Programme for Belize, the NGO who manages the study area, have also indicated that this data would be useful to them for pine woodland management.
- Savanna vegetation mapping can be greatly improved by using SAR data. In the past, the identification of especially palmetto has been problematic using optical EO data. The results of this research have shown that palmetto vegetation shows

up very clearly in AIRSAR polarimetric backscatter data. This is useful since in the region, palmetto is becoming a valued non-timber forest product (NTFP).

References

ALLEAUME, S., HÉLY, C., LE ROUX, J., KORONTZI, S., SWAP, R.J., SHUGART, H.H. and JUSTICE, C.O. (2005). Using MODIS to evaluate heterogeneity of biomass urning in southern African savannahs: a case study in Etosha. *International Journal of Remote Sensing,* 26(19): 4219-4237.

ANDERSEN, H.E., MCGAUGHEY, R.J. and REUTEBUCH, S.E. (2005). Forest measurement and monitoring using high-resolution airborne lidar. *USDA Forest Service - General Technical Report* PNW (642), USDA Forest Service.

ANDERSON, J.M. and MIKHAIL, E.M. (1998). *Surveying: Theory and Practice,* London, WCB McGraw-Hill.

APPLEGATE, G.B. and NICHOLSON, D.I. (1988). Caribbean pine in an agroforestry system on the Atherton Tableland in north east Australia. *Agroforestry Systems,* 7: 3-15.

ARAÚJO, T.M., HIGUCHI, N. and DE CARVALHO (JR.), J.A. (1999). Comparison of formulae for biomass content determination in a tropical rain forest site in the state of Pará, Brazil. *Forest Ecology and Management,* 117: 43-52.

ARONOFF, S. and PETRIE, G. (2005). Active sensors: Radar and lidar. IN Aronoff, S. (Ed.). *Remote Sensing for GIS Managers.* New York, ESRI Press.

ASHTEAD-TECHNOLOGY. (2005). Ashtead Technology Equipment Rental. www.ashtead-technology.com/ (Accessed 2 November, 2005).

ASKNE, J.I.H., DAMMERT, P.B.G., ULANDER, L.M.H. and SMITH, G. (1997). C-band repeat-pass interferometric SAR observations of the forest. *IEEE Transactions on Geoscience and remote sensing,* 35(1): 25-35.

ASNER, G.P., WESSMAN, C.A. and SCHIMEL, D.S. (1998). Heterogeneity of savanna canopy structure and function from imaging spectrometry and inverse modeling. *Ecological Applications,* 8(4): 1022-1036.

AUKLAND, L., MOURA COSTA, P., BASS, S., HUQ, S., LANDELL-MILLS, N., TIPPER, R. and CARR, R. (2002). Laying the Foundations for Clean Development: Preparing the Land Use Sector. A quick guide to the Clean Development Mechanism. *DFID Forestry Research Programme* ZF0167.

BALA, G., CALDEIRA, K., WICKETT, M., PHILLIPS, T.J., LOBELL, D.B., DELIRE, C. and MIRIN, A. (2007). Combined climate and carbon-cycle effects of large-scale deforestation. *Proceedings of the National Academy of Sciences,* 104(16): 6550–6555.

BALDOCCHI, D., FALGE, E., GU, L., OLSON, R., HOLLINGER, D., RUNNING, S., ANTHONI, P., BERNHOFER, C., DAVIS, K., EVANS, R., FUENTES, J., GOLSTEIN, A., KATUL, G., LAW, B., LEE, X., MALHI, Y., MEYERS, T., MUNGER, W., OECHEL, W., PAW, K.T., PILEGAARD, K., SCHMID, H.P., VALENTINI, R., VERMA, S., VESALA, T., WILSON, K. and WOFSY, S. (2001). FLUXNET: A new tool to study the temporal and spatial variability of ecosystem-scale carbon dioxide, water vapor, and energy flux densities. *Bulletin of the American Meteorological Society,* 82(11): 2415-2434.

BALZTER, H., ROWLAND, C.S. and SAICH, P. (2007). Forest canopy height and carbon estimation at Monks Wood National Nature Reserve, UK, using dual-wavelength SAR interferometry. *Remote Sensing of Environment,* 108: 224-239.

BANNISTER, A., RAYMOND, S. and BAKER, R. (1998). *Surveying, 7th edition*, Harlow, Longman.

BARBOSA, R.I. and FEARNSIDE, P.M. (2004). Wood density of trees in open savannas of the Brazilain Amazon. *Forest Ecology and Management*, 199: 115-123.

BARRON, R.J. (2001). Precision of three tree height measuring devices in forest conditions. *Research Note* No. 1 (2001), Northern Ireland Forest Service.

BAUTTS, D., Intermap Technologies (2006) [Intermap STAR 3i data acquisition dates] (Personal communication, 15 June 2006).

BNMS. (2007). Belize National Meteorological Service. www.hydromet.gov.bz/info.htm (Accessed 26 May, 2007).

BOLIN, B. and SUKUMAR, R. (2000). Global Perspective. IN Watson, R.T., Noble, I.R., Bolin, B., Ravindranath, N.H., Verardo, D.J. and Dokken, D.J. (Eds.). *Land Use, Land-use Change and Forestry. Special Report of the IPCC.* Cambridge, Cambridge University Press.

BOYD, D.S. and DANSON, F.M. (2005). Satellite remote sensing of forest resources: three decades of research development. *Progress in Physical Geography*, 29(1): 1-26.

BRIDGEWATER, S., IBÀÑEZ, A., RATTER, J.A. and FURLEY, P. (2002). Vegetation classification and floristics of the savannas and associated wetlands of the Rio Bravo Conservation and Management area, Belize. *Edinburgh Journal of Botany,* 59(3): 421-434.

BROKAW, N. (2001). A history of plant ecology in Belize. *Journal of Belizean Affairs*, 3(2): 1-39.

BROWN, S. (1997). Estimating biomass and biomass change of tropical forests: a primer. *FAO Forestry Paper* 134.

BROWN, S. (2002a). Measuring carbon in forests: current status and future challenges. *Environmental Pollution*, 116: 363-372.

BROWN, S. (2002b). Measuring, monitoring and verification of carbon benefits for forest-based projects. *Philosophical Transactions of the Royal Society,* 360: 1669-1683.

BROWN, S., Winrock International (2006) [Allometric equations, Belize savanna vegetation] (Personal communication, 8 June 2006).

BROWN, S. and LUGO, A.E. (1982). The storage and production of organic matter in tropical forests and their role in the global carbon cycle. *Biotropica,* 14(3): 161-187.

BROWN, S., PEARSON, T., SLAYMAKER, D., AMBAGIS, S., MOORE, N., NOVELLO, D. and SABIDO, W. (2005). Creating a virtual tropical forest from three-dimensional aerial imagery to estimate carbon stocks. *Ecological Applications*, 15(3): 1083-1095.

BUNTING, P. and LUCAS, R.M. (2006). The delineation of tree crowns in Australian mixed species forests using hyperspectral Compact Airborne Spectrographic Imager (CASI) data. *Remote Sensing of Environment*, 101: 230-248.

CAMERON, I.D., VIERGEVER, K.M., WALLINGTON, E.D., WOODHOUSE, I.H., MOSS, D. and STUART, N. (2006). Synthetic Aperture Radar for neo-tropical savanna inventory and vegetation height retrieval. IN Marçal, A. (Ed.). *Global Developments in Environmental Earth Observation from Space. Proceedings of the 25th EARSeL Symposium, Porto, Portugal, 6-11 June 2005.* Rotterdam, Millpress.

CARABAJAL, C.C. and HARDING, D.J. (2006). SRTM C-band and ICESat laser altimetry elevation comparisons as a function of tree cover and relief. *Photogrammetric Engineering and Remote Sensing,* 72(3): 287-298.

CHAPMAN, B., e-mail correspondence (2006) [TOPSAR C-band multipath error] (Personal communication, June 2006).

CHAPMAN, B., Telephone conversation (2007) [TOPSAR C-band pre-processing] (Personal communication, November 2007).

CHAVE, J., CONDIT, R., AGUILAR, S., HERNANDEZ, A., LAO, S. and PEREZ, R. (2004). Error propagation and scaling for tropical forest biomass estimates. *Philosophical Transactions of the Royal Society,* 359: 409-420.

CHAVE, J., RIÉRA, B. and DUBOIS, M.-A. (2001). Estimation of biomass in a neotropical forest of French Guiana: spatial and temporal variability. *Journal of Tropical Ecology,* 17: 79-96.

CHO, P., Belize Forestry Department (2007) [Caribbean pine growth rates in Belize] (Personal communication, April 2007).

CHUCK, D., Programme for Belize (2007) [Caribbean pine growth rates in Belize] (Personal communication, April 2007).

CIAIS, P., MOORE, B., STEFFEN, W., HOOD, M., QUEGAN, S., CIHLAR, J., RAUPACH, M., RASOOL, I., DONEY, S., HEINZE, C., SABINE, C., HIBBARD, K., SCHULZE, D., HEIMANN, M., CHÉDIN, A., MONFRAY, P., WATSON, A., LEQUÉRÉ, C., TANS, P., DOLMAN, H., VALENTINI, R., ARINO, O., TOWNSHEND, J., SEUFERT, G., FIELD, C., IGRASHI, T., GOODALE, C., NOBRE, A., INOUE, G., CRISP, D., BALDOCCHI, D., TSCHIRLEY, J., DENNING, S., CRAMER, W., FRANCEY, R. and WICKLAND, D. (2007). Integrated Global Carbon Observation Theme. A Strategy to Realize a Coordinated System of Integrated Global Carbon Cycle Observations. *(Obtained from ioc.unesco.org/igospartners/Carbon.htm, accessed 14/10/2007)*

CLOUDE, S.R. and PAPATHANASSIOU, K.P. (1998). Polarimetric SAR interferometry. *IEEE Transactions on Geoscience and remote sensing,* 36(5): 1551-1565.

COLE, M.M. (1986). *The savannas – biogeography and geobotany*, London, Academic Press Inc.

COLE, M.M. (1992). Influence of physical factors on the nature and dynamics of forest-savanna boundaries. IN Furley, P.A., Proctor, J. and Ratter, J.A. (Eds.). *Nature and Dynamics of Forest-Savanna Boundaries.* London, Chapman and Hall.

COX, P.M., BETTS, R.A., JONES, C.D., SPALL, S.A. and TOTTERDELL, I.J. (2000). Acceleration of global warming due to carbon-cycle feedbacks in a coupled climate model. *Nature,* 408: 184-187.

CUMMINGS, D.L., KAUFFMAN, J.B., PERRY, D.A. and HUGHES, R.F. (2002). Aboveground biomass and structure of rainforests in the southwestern Brazilian Amazon. *Forest Ecology and Management,* 163: 293-307.

CUNNINGHAM, W.P. and SAIGO, B.W. (2000). *Environmental Science: A Global Concern, sixth edition.,* London, McGraw Hill.

DALL, J. (2007). InSAR elevation bias caused by penetration into uniform volumes. *IEEE Transactions on Geoscience and remote sensing,* 45(7): 2319-2324.

DEFRA (2007). Draft Climate Change Bill. www.defra.gov.uk/corporate/consult/ climatechange-bill/ (Accessed 29 November 2007).

DEFRIES, R., ACHARD, F., BROWN, S., HEROLD, M., MURDIYARSO, D., SCHLAMADINGER, B. and DE SOUZA, C.J. (2007). Earth observations for estimating greenhouse gas emissions from deforestation in developing countries. *Envionmental Science and Policy,* 10: 385-394.

DIAS, A.T.C., DE MATTOS, E.A., VIEIRA, S.A., AZEREDO, J.V. and SCARANO, F.R. (2006). Aboveground biomass stock of native woodland on a Brazilian sandy coastal plain: Estimates based on the dominant tree species. *Forest Ecology and Management,* 226: 364-367.

DMA (1991). Department of Defense World Geodetic System 1984, it's definition and relationships with local geodetic systems. *Defense Mapping Agency Report* TR 8350.2, Second edition, Defense Mapping Agency, Fairfax, VA, USA.

DONG, J., KAUFMANN, R.K., MYNENI, R.B., TUCKER, C.J., KAUPPI, P.E., LISKI, J., BUERMANN, W., ALEXEYEV, V. and HUGHES, M.K. (2003). Remote sensing estimates of boreal and temperate forest woody biomass: carbon pools, sources and sinks. *Remote Sensing of Environment,* 84: 393-410.

DONG, Y., MILNE, A.K. and FORSTER, B.C. (2001). Segmentation and Classification of Vegetated Areas Using Polarimetric SAR Image Data. *IEEE Transactions on Geoscience and remote sensing,* 39(2): 321-329.

DONOGHUE, D.N.M., WATT, P.J., COX, N.J., DUNFORD, R.W., WILSON, J., STABLES, S. and SMITH, S. (2004). An evaluation of the use of satellite data for monitoring early development of young Sitka spruce plantation forest growth. *Forestry,* 77(5): 383-396.

DOUGILL, A. and TRODD, N. (1999). Monitoring and modelling open savannas using multisource information: analyses of Kalahari studies. *Global Ecology & Biogeography,* 8(3/4): 211-221.

DRAKE, J.B., DUBAYAH, R.O., CLARK, D.B., KNOX, R.G., BLAIR, J.B., HOFTON, M.A., CHAZDON, R.L., WEISHAMPEL, J.F. and PRINCE, S.D. (2002). Estimation of tropical forest structural characteristics using large-footprint lidar. *Remote Sensing of Environment,* 79: 305-319.

ENQUIST, B.J., BROWN, J.H. and WEST, G.B. (1998). Allometric scaling of plant energetics and population density. *Nature,* 395: 163-165.

ESA. (2007). ESA. www.esa.int (Accessed 14 October, 2007).

EVANS, D.L., ALPERS, W., CAZENAVE, A., ELACHI, C., FARR, T., GLACKIN, D., HOLT, B., JONES, L., LIU, W.T., MCCANDLESS, W., MENARD, Y., MOORE, R. and NJOKU, E. (2005). Seasat - A 25-year legacy of success. *Remote Sensing of Environment,* 94: 384-404.

FANG, J.-Y. and WANG, Z.M. (2001). Forest biomass estimation at regional and global levels, with special reference to China's forest biomass. *Ecological Research,* 16: 587-592.

FAO (1993). Forest Resources Assessment 1990 - Tropical Countries. *FAO Forestry Paper* 112.

FAO (2001). Global Forest Resources Assessment 2000. *FAO Forestry Paper* 140.

FAO (2006). Global Forest Resources Assessment 2005. *FAO Forestry Paper* 147.

FARUGGIA, F.T. (2002). *A floristic description of a neotropical coastal savanna in Belize.* Unpublished M.Sc. dissertation, Department of Botany, Miami University, Oxford, Ohio

FERRAZZOLI, P. and GUERRIERO, L. (1995). radar sensitivity to tree geometry and woody volume: a model analysis. *IEEE Transactions on Geoscience and remote sensing,* 33(2): 360-371.

FERREIRA, L.G. and HUETE, A.R. (2004). Assessing the seasonal dynamics of the Brazilian Cerrado vegetation through the use of spectral vegetation indices. *International Journal of Remote Sensing,* 25(10): 1837-1860.

FOODY, G.M., BOYD, D.S. and CUTLER, M.E.J. (2003). Predictive relations of tropical forest biomass from Landsat TM data and their transferability between regions. *Remote Sensing of Environment*, 85: 463-474.

FOODY, G.M. and CUTLER, M.E.J. (2003). Tree biodiversity in protected and logged Bornean tropical rain forests and its measurement by satellite remote sensing. *Journal of Biogeography*, 30: 1053-1066.

FOODY, G.M., CUTLER, M.E.J., MCMORROW, J., PELZ, D., TANGKI, H., BOYD, D.S. and DOUGLAS, I. (2001). Mapping biomass of Bornean tropical rain forest from remotely sensed data. *Global Ecology and Biogeography*, 10: 379-387.

FORNARO, G., LOMBARDINI, F. and SERAFINO, F. (2005). Three-dimensional multipass SAR focusing: experiments with long-term spaceborne data. *IEEE Transaction on Geoscience and Remote Sensing*, 43(4): 702-714.

FOURNIER, L.A. (2005). Tropical Tree Seed Manual Part II - Species Descriptions - Quercus oleoides Schltdl. & Cham. www.rngr.net/Publications/ttsm/Folder.2003-07-11.4726/PDF.2004-03-16.1058/file (Accessed 20 July, 2005).

FOWLER, J., COHEN, L. and JARVIS, P. (1998). *Practical statistics for field biology, 2nd edition*, Chichester, John Wiley and Sons.

FRANK, D.A. and MCNAUGHTON, S.J. (1990). Aboveground biomass estimation with the canopy intercept method: a plant growthform caveat. *Oikos*, 57(1): 57-60.

FREITAS, S.R., MELLO, M.C.S. and CRUZ, C.B.M. (2005). Relationships between forest structure and vegetation indices in Atlantic Rainforest. *Forest Ecology and Management*, 218(1-3): 353-362.

FROLKING, S., MILLIMAN, T., MCDONALD, K., KIMBALL, J., ZHAO, M. and FAHNESTOCK, M. (2006). Evaluation of the SeaWinds scatterometer for regional monitoring of vegetation phenology. *Journal of Geophysical Research*, 111(D17302): doi:10.1029/2005JD006588.

FROST, P.G., MEDINA, E., MENAUT, J.C., SOLBRIG, O.T., SWIFT, M. and WALKER, B. (1986). Responses of savannas to stress and disturbance. *Biology International Special Issue* 10.

FULLER, D.O. (1999). Canopy phenology of some mopane and miombo woodlands in eastern Zambia. *Global Ecology & Biogeography*, 8(3/4): 199-209.

FURLEY, P.A. (1986). Radar surveys for resource evaluation in Brazil: an illustration from Rondônia. IN Eden, M.J. and Parry, J.T. (Eds.). *Remote Sensing and Tropical Land Management*. London, John Wiley and Sons Ltd.

FURLEY, P.A. (1992). Edaphic changes at the forest-savanna boundary with particular reference to the neotropics. IN Furley, P.A., Proctor, J. and Ratter, J.A. (Eds.). *Nature and Dynamics of Forest-Savanna Boundaries.* London, Chapman and Hall.

FURLEY, P.A. (1999). The nature and diversity of neotropical savanna vegetation with particular reference to the Brazilian cerrados. *Global Ecology and Biogeography*, 8(3/4): 223-241.

FURLEY, P.A. (2007). Significance and biomass of the palmetto palm Acoelorraphe wrightii in Belizean lowland savannas. *Unpublished report to the Carnegie Trust for the Universities of Scotland*

FURLEY, P.A., BRIDGEWATER, S., IBÀÑEZ, A., MINTY, C., MURRAY, M., RATTER, J.A., STUART, N. and VASQUES, M. (2001). Savannas of the Rio Bravo Conservation Area: Vegetation and Soil-Plant Community Relationships. *Journal of Belizean Affairs*, 3(2): 64-105.

FURLEY, P.A. and NEWEY, W.W. (1983). *Geography of the Biosphere*, London, Butterworths.

GEOEYE. (2006). IKONOS imagery products guide. www.geoeye.com/whitepapers_pdfs/GeoEye_IKONOS_Product_Guide_v17.pdf (Accessed January, 2008).

GIBBARD, S., CALDEIRA, K., BALA, G., PHILLIPS, T.J. and WICKETT, M. (2005). Climate effects of global land cover change. *Geophysical Research Letters,* 32: L23705, doi:23710.21029/22005GL024550.

GRACE, J., JOSÉ, J.S., MEIR, P., MIRANDA, H.S. and MONTES, R.A. (2006). Productivity and carbon fluxes of tropical savannas. *Journal of Biogeography,* 33: 387-400.

GRACE, J., MALHI, Y., HIGUCHI, N. and MEIR, P. (2001). Productivity of tropical rain forests. IN Roy, J., Saugier, B. and Mooney, H.A. (Eds.). *Terrestrial Global Productivity*. London, Academic Press.

GRAINGER, A. (1999). Constraints on modelling the deforestation and degradation of tropical open woodlands. *Global Ecology and Biogeography,* 8(3/4): 179-190.

GRIPPA, M. and WOODHOUSE, I.H. (2002). Retrieval of bare soil and vegetation parameters from wind scatterometer measurements over three different climatic regions. *Remote Sensing of Environment,* 84: 16-24.

GUILLASO, S. and REIGBER, A. (2005). Polarimetric SAR tomography. *POLInSAR Conference, 17-21 January 2005, Frascati, Italy*.

GUILLASO, S. and REIGBER, A. (2005). Scatterer Characterisation Using Polarimetric SAR Tomography. *IGARSS Conference, 25-29 July 2005, Seoul, Korea*.

HAGBERG, J.O., ULANDER, L.M.H. and ASKNE, J. (1995). Repeat-pass SAR interferometry over forested terrain. *IEEE Transactions on Geoscience and Remote Sensing.*, 33(2): 331-340.

HAGLÖF (2005). User's Guide Vertex III and Transponder T3 v1.4. (Obtained from www.haglofsweden.com).

HALLIKAINEN, M.T., HYYPPÄ, J., HAAPENEN, J., TARES, T., AHOLA, P., PULLIAINEN, J. and TOIKKA, M. (1993). A helicopter-borne eight-channel ranging scatterometer for remote sensing. I. System description. *IEEE Transaction on Geoscience and Remote Sensing,* 31(1): 161-169.

HALLIKAINEN, M.T., TARES, T., HYYPPÄ, J., SOMERSALO, E., AHOLA, P., TOIKKA, M. and PULLIAINEN, J. (1990). Helicopter-borne measurements of radar backscatter from forests. *International Journal of Remote Sensing,* 11(7): 1179-1191.

HANSEN, M.C., TOWNSHEND, J.R.G., DEFRIES, S. and CARROLL, M. (2005). Estimation of tree cover using MODIS data at global, continental and regional/local scales. *International Journal of Remote Sensing,* 26(19): 4359-4380.

HARDIN, P.J. and JACKSON, M.W. (2003). Investigating SeaWinds terrestrial backscatter: equatorial savannas of South America. *Photogrammetric Engineering and Remote Sensing,* 69(11): 1243-1254.

HEDIN, L.O. (2006). Plants on a different scale. *Nature,* 439: 399-400.

HEFFERNAN, O. (2007). Climate deal agreed in Bali showdown. *Nature,* 450: 1136-1137.

HENSLEY, S., e-mail correspondence (2007) [TOPSAR C-band multipath error] (Personal communication, Augsut 2007).

HESE, S., LUCHT, W., SCHMULLIUS, C., BARNSLEY, M., DUBAYAH, R., KNORR, D., NEUMANN, K., RIEDEL, T. and SCHRÖTER, K. (2005). Global biomass mapping for an improved understanding of the CO2 balance - the Earth observation mission Carbon-3D. *Remote Sensing of Environment,* 94: 94-104.

HOEKMAN, D.H. and QUIÑONES, M.J. (2000). Land cover type and biomass classification using AirSAR data for evaluation of monitoring scenarios in the

Colombian Amazon. *IEEE Transactions on Geoscience and remote sensing,* 38(2): 685-696.

HOEKMAN, D.H. and VAREKAMP, C. (2001). Observation of tropical rain forest trees by airborne high-resolution interferometric radar. *IEEE Transactions on Geoscience and remote sensing,* 39(3): 584-594.

HOFFMAN, J. and WALTER, D. (2006). How complementary are SRTM-X and -C band digital elevation models? *Photogrammetric Engineering and Remote Sensing,* 72(3): 261-268.

HOFTON, M., DUBAYAH, R., BLAIR, J.B. and RABINE, D. (2006). Validation of SRTM elevations over vegetated and non-vegetated terrain using medium footprint lidar. *Photogrammetric Engineering and Remote Sensing,* 72(3): 279-285.

HOLMGREN, J., NILSSON, M. and OLSSON, H. (2003). Estimation of Tree Height and Stem Volume on Plots Using Airborne Laser Scanning. . *Forest Science,* 49(3): 419-428.

HOMEWOOD, K. and BROCKINGTON, D. (1999). Biodiversity, conservation and development in Mkomazi Game Reserve, Tanzania. *Global Ecology & Biogeography,* 8(3/4): 301-313.

HOPKINS, B. (1992). Nature and Dynamics of Forest-Savanna Boundaries. IN Furley, P.A., Proctor, J. and Ratter, J.A. (Eds.). *Ecological processes at the forest-savanna boundary.* London, Chapman and Hall.

HORWICH, R.H. and LYON, J. (1990). *A Belizean Rain Forest - The Community Baboon Sanctuary,* Gay Mills, Wisconsin, Orang-utan Press Community Conservation Consultants.

HOUGHTON, R.A., LAWRENCE, K.T., HACKLER, J.L. and BROWN, S. (2001). The spatial distribution of forest biomass in the Brazilian Amazon: a comparison of estimates. *Global Change Biology,* 7: 731-746.

HOUSE, J.I. and HALL, D.O. (2001). Productivity of tropical savannas and grasslands. IN Roy, J., Saugier, B. and Mooney, H.A. (Eds.). *Terrestrial Global Productivity.* London, Academic Press.

HUSCH, B., BEERS, T.W. and KERSHAW, J.A.J. (2003). *Forest Mensuration, 4th edition.,* Hoboken, New Jersey, John Wiley & Sons.

HYYPPÄ, J. and HALLIKAINEN, M. (1993). A helicopter-borne eight-channel ranging scatterometer for remote sensing. II. Forest inventory. *IEEE Transaction on Geoscience and Remote Sensing,* 31(1): 170-179.

HYYPPÄ, J. and HALLIKAINEN, M. (1996). Applicability of airborne profiling radar to forest inventory. *Remote Sensing of Environment,* 57: 39-57.

HYYPPÄ, J., HYYPPÄ, H., INKINEN, M., ENGDAHL, M., LINKO, S. and ZHU, Y.H. (2000). Accuracy comparison of various remote sensing data sources in the retrieval of forest stand attributes. . *Forest Ecology and Management,* 128(1-2): 109-120.

HYYPPÄ, J., KELLE, O., LEHIKOINEN, M. and INKINEN, M. (2001). A segmentation based method to retrieve stem volume estimates from 3-D tree height models produced by laser scanners. . *IEEE Transactions on Geoscience and remote sensing,* 39(5): 969-975.

IMEL, D.A. (2002). What's wrong with my AIRSAR data? *AIRSAR Earth Science and Applications Workshop, 4-6 March 2002, Pasadena, California, USA.*

IMHOFF, M.L. (1995a). A theoretical analysis of the effect of forest structure on Synthetic Aperture Radar backscatter and the remote sensing of biomass. *IEEE Transactions on Geoscience and remote sensing,* 33(2): 341-352.

IMHOFF, M.L. (1995b). Radar backscatter and biomass saturation: ramifications for global biomass inventory. *IEEE Transactions on Geoscience and Remote Sensing.,* 33(2): 511-518.

IZZAWATI, WALLINGTON, E.D. and WOODHOUSE, I.H. (2006). Forest height retrieval from commercial X-band SAR products. *IEEE Transactions on Geoscience and remote sensing,* 44(4): 863-870.

IZZAWATI, WOODHOUSE, I.H. and WALLINGTON, E.D. (2004). The impact of forest heterogeneity on the height retrieval using X-band inteferometry. *IGARSS Conference, 20-24 September 2004, Anchorage, Alaska, USA.*

JAAS, T. (2007). *Comparing semi-automated classification and visual interpretation methods of IKONOS imagery in the context of developing countries. A case study of Belizean savannas.* Unpublished MSc dissertation, Institute of Geography, The University of Edinburgh, Edinburgh (pp 99).

JOHNSON, M.S. and CHAFFEY, D.R. (1973). A Forest Inventory of Part of the Mountain Pine Ridge, Belize. *Land Resources Study Report* Foreign and Commonwealth Office, Overseas Development Administration, Land Resources Division.

JONASSON, S. (1988). Evaluation of the point intercept method for the estimation of plant biomass. *Oikos.,* 52(1): 101-106.

JRC. (2006). *Global Land Cover 2000*. www-gvm.jrc.it/glc2000/ (Accessed 1 November, 2007).

KADEBA, O. (1991). Above-ground biomass production and nutrient accumulation in an age sequence of *Pinus caribea* stands. *Forest Ecology and Management,* 41: 237-248.

KASISCHKE, E.S., CHRISTENSEN, N.L. and BOURGEAU-CHAVEZ, L.L. (1995). Correlating radar backscatter with components of biomass in Loblolly pine forests. *IEEE Transactions on Geoscience and remote sensing,* 33(3): 643-659.

KASISCHKE, E.S., MELACK, J.M. and DOBSON, M.C. (1997). The use of imaging radars for ecological applications - a review. *Remote Sensing of Environment,* 59: 141-156.

KELLMAN, M. and TACKABERRY, R. (1997). *Tropical Environments: The Functioning and Management of Tropical Ecosystems,* London, Routledge.

KELLNDORFER, J.M., DOBSON, C., VONA, J. and CLUTTER, M. (2003). Toward precision forestry: Plot-level parameter retrieval for Slash Pine plantations with JPL AirSAR. *IEEE Transactions on Geoscience and Remote Sensing.,* 41(7): 1571-1582.

KING, R.B., BAILLIE, I.C., ABELL, T.M.B., DUNSMORE, J.R., GRAY, D.A., PRATT, J.H., VERSEY, H.R., WRIGHT, A.C.S. and ZISMAN, S.A. (1992). Land Resource Assessment of Northern Belize. *National Resources Institute* Bulletin 43 (2 volumes).

KOBAYASHI, Y., SARABANDI, K., PIERCE, L. and DOBSON, M.C. (2000). An evaluation of the JPL TOPSAR for extracting tree heights. *IEEE Transactions on Geoscience and remote sensing,* 38(6): 2446-2454.

LE TOAN, T., ForestSAT Conference, Montpellier, France (2007) [Backscatter of banana plants] (Personal communication, November 2007).

LE TOAN, T., BEAUDOIN, A., RIOM, J. and GUYON, D. (1992). Relating forest biomass to SAR data. *IEEE Transactions on Geoscience and Remote Sensing.,* 30(2): 403-411.

LE TOAN, T., QUEGAN, S., WOODWARD, I., LOMAS, M., DELBART, N. and PICARD, G. (2004). Relating radar remote sensing of biomass to modelling of forest carbon budgets. *Climate Change,* 67: 379-402.

LEFSKY, M.A., HARDING, D., COHEN, W.B., PARKER, G. and SHUGART, H.H. (1999). Surface Lidar remote sensing of basal area and biomass in deciduous forests of Eastern Maryland, USA. *Remote Sensing of Environment,* 67: 83-98.

LI, H.-T., HAN, X.-G. and WU, J.-G. (2005). Lack of evidence for 3/4 scaling of metabolism in terrestrial plants. *Journal of Integrative Plant Biology,* 47(10): 1173-1183.

LIM, K., TREITZ, P., BALDWIN, K., MORRISON, I. and GREEN, J. (2003). Lidar remote sensing of biophysical properties of tolerant northern hardwood forests. *Canadian Journal of Remote Sensing,* 29(5): 658-678.

LISKI, J., KOROTKOV, A.V., PRINS, C.F., KARJALAINEN, T., VICTOR, D.G. and KAUPPI, P.E. (2003). Increased carbon sink in temperate and boreal forests. *Climatic Change,* 61: 89-99.

LONG, D.G., DRINKWATER, M.R., HOLT, B., SAATCHI, S. and BERTOIA, C. (2001). Global ice and land climate studies using scatterometer image data. *EOS Transcations, AGU,* 82(43): 503.

LONG, D.G. and HARDIN, P.J. (1994). Vegetation studies of the Amazon basin using enhanced resolution Seasat scatterometer data. *IEEE Transaction on Geoscience and Remote Sensing,* 32(2): 449-460.

LONGMAN, K.A. and JENIK, J. (1992). Forest-savanna boundaries: general considerations. . IN Furley, P.A., Proctor, J. and Ratter, J.A. (Eds.). *Nature and Dynamics of Forest-Savanna Boundaries.* London, Chapman and Hall.

LOU, Y. (2002). How accurate are my AIRSAR data? *AIRSAR Earth Science and Application Workshop, 4 - 6 March 2002, Pasadena, California, USA.*

LOVELL, J.L., JUPP, D.L.B., NEWNHAM, G.J., COOPS, N.C. and CULVENOR, D.S. (2005). Simulation study for finding optimal lidar acquisition parameters for forest height retrieval. *Forest Ecology and Management,* 214(1-3): 398-412.

LUCAS, R.M. and ARMSTON, J.D. (2007). ALOS PALSAR for characterizing wooded savannas in northern Australia. *IGARSS Conference, 23 – 27 July 2007, Barcelona, Spain*.

LUCAS, R.M., CRONIN, N., LEE, A., MOGHADDAM, M., WITTE, C. and TICKLE, P. (2006a). Empirical relationships between AIRSAR backscatter and LiDAR-derived forest biomass, Queensland, Australia. *Remote Sensing of Environment,* 100: 407-425.

LUCAS, R.M., CRONIN, N., MOGHADDAM, M., LEE, A., ARMSTON, J.D., BUNTING, P. and WITTE, C. (2006b). Integration of radar and Landsat-derived foliage projected cover for woody regrowth mapping, Queensland, Australia. *Remote Sensing of Environment,* 100: 388-406.

LUCAS, R.M., LEE, A.C. and WILLIAMS, M.L. (2006c). Enhanced simulation of radar backscatter from forests using LiDAR and optical data. *IEEE Transactions on Geoscience and remote sensing,* 44(10): 2736-2754.

LUCAS, R.M., MOGHADDAM, M. and CRONIN, N. (2004). Microwave scattering from mixed-species forests, Queensland, Australia. *IEEE Transactions on Geoscience and remote sensing,* 42(10): 2142-2159.

LUCKMAN, A., BAKER, J., KUPLICH, T.M., FREITAS-YANASSE, C.D.-C. and FRERY, A.C. (1997). A study of the relationship between radar backscatter and regenerating tropical forest biomass for spaceborne SAR instruments. *Remote Sensing of Environment,* 60: 1-13.

MACDICKEN, K.G. (1997). A Guide to Monitoring Carbon Storage in Forestry and Agroforestry Projects. *Forest Carbon Monitoring Program* Winrock International, Arlington, VA, USA.

MACELLONI, G., PALOSCIA, S., PAMPALONI, P. and SANTI, E. (2003). Global scale monitoring of soil and vegetation using SSM/I and ERS wind scatterometer. *International Journal of Remote Sensing,* 24(12): 2409-2425.

MADSEN, S.N. and ZEBKER, H.A. (1998). Imaging radar interferometry. IN Henderson, F.M. and Lewis, A.J. (Eds.). *Principles and applications of imaging radar. Manual of Remote Sensing Third edition, Volume 2*. New York, John Wiley and Sons.

MADSEN, S.N., MARTIN, J.M. and ZEBKER, H.A. (1995). Analysis and evaluation of the NASA/JPL TOPSAR across-track interferometric SAR system. *IEEE Transactions on Geoscience and remote sensing,* 33(2): 383-391.

MALHI, Y., MEIR, P. and BROWN, S. (2002). Forests, carbon and global climate. *Philosophical Transactions of the Royal Society A,* 360: 1567-1591.

MALTAMO, M., PACKALÉN, P., YU, X., EERIKÄINEN, K., HYYPPÄ, J. and PITKÄNEN, J. (2005). Identifying and quantifying structural characteristics of heterogeneous boreal forests using laser scanner data. *Forest Ecology and Management,* 216(1-3): 41-50.

MARINO, A., The University of Edinburgh (2007) [PRIS modelling results] (Personal communication, October 2007).

MARINO, A., HORN, R., VIERGEVER, K.M., WALKER, N. and WOODHOUSE, I.H. (2008). Foliage penetration effect on polarimetric SAR interferometry observation of forest. *EUSAR Conference, 2-5 June 2008, Friedrichshafen, Germany.*

MARTINEZ, J.M., BEAUDOIN, A., FLOURY, N., MÄKYNEN, M., LE TOAN, T., HALLIKAINEN, M.T. and UUSITALO, J. (1998). First results and analysis of HUTSCAT data over Austrian pine plantations. *International workshop on the retrieval of bio- and geo-physical parameters from SAR data, ESA ESTEC, Noordwijk, The Netherlands*.

MARTINEZ, J.M., FLOURY, N., LE TOAN, T., BEAUDOIN, A., HALLIKAINEN, M.T. and MÄKYNEN, M. (2000). Measurements and modeling of vertical backscatter distribution in forest canopy. *IEEE Transaction on Geoscience and Remote Sensing,* 38(2): 710-719.

MCCOMBS, J.W., ROBERTS, S.D. and EVANS, D.L. (2003). Influence of fusing Lidar and multispectral imagery on remotely sensed estimates of stand density and mean tree height in a managed Loblolly pine plantation. *Forest Science,* 49(3): 457-466.

MEANS, J.E., EMERSON, L., HENDRIX, C.J., ACKER, S.A., FITT, B.J. and M., R. (2000). Predicting forest stand characteristics with airborne scanning lidar. *Photogrammetric Engineering and Remote Sensing,* 66(11): 1367-1371.

MEERMAN, J.C. and SABIDO, W. (2001). Central American ecosystems map: Belize (Volume I). Programme for Belize, Belize City, Belize.

MENGES, C.H., BARTOLO, R.E., BELL, D. and HILL, G.J.E. (2004). The effect of savanna fires on SAR backscatter in northern Australia. *International Journal of Remote Sensing,* 25(22): 4857-4871.

MERCER, B., IGARSS conference, Barcelona, Spain (2007) [Intermap STAR 3i data pre-processing] (Personal communication, July 2007).

MERCER, B., Intermap Technologies (2007) [Intermap STAR 3i data quality] (Personal communication, July 2007).

METTE, T., PAPATHANASSIOU, K. and HAJNESK, I. (2004). Biomass estimation from polarimetric SAR interferometry over heterogeneous forest terrain. *IGARSS Conference, 20-24 September 2004, Anchorage, Alaska*.

MICHELAKIS, D. (2008). *Automated tree crown and woodland delineation from HR optical imagery in a savanna woodland.* Unpublished M.Sc. dissertation, Institute of Geography, The University of Edinburgh, Edinburgh

MIDDLETON, N. (1999). *The Global Casino: An Introduction to Environmental Issues, second edition,* London, Arnold.

MILLER, G.T. (1998). *Living in the Environment: Principles, Connections, and Solutions, tenth edition.,* Washington, Wadsworth Publishing Company.

MISTRY, J. (2000). *World Savannas,* Harlow, Pearson Education Limited.

MOSS, D., STUART, N., VIERGEVER, K. and WALLINGTON, E. (2006). SAR remote sensing for natural resource management – is there a role for ground survey? *Geomatics World,* 14(3): 24-28.

NÆSSET, E. (1997a). Determination of mean tree height of forest stands using airborne laser scanner data. *ISPRS Journal of Photogrammetry and Remote Sensing,* 52(2): 49-56.

NÆSSET, E. (1997b). Estimating timber volume of forest stands using airborne laser scanner data. *Remote Sensing of Environment,* 61(2): 246-253.

NÆSSET, E. (2004). Practical large-scale forest stand inventory using a small-footprint airborne scanning laser. *Scandinavian Journal of Forest Research,* 19(2): 164-179.

NÆSSET, E. and ØKLAND, T. (2002). Estimating tree height and tree crown properties using airborne scanning laser in a boreal nature reserve. *Remote Sensing of Environment,* 79(1): 105-115.

NEEFF, T., DE ALENCASTRO-GRAÇA, P.M., VIEIRA-DUTRA, L. and DA COSTA-FREITAS, C. (2005). Carbon budget estimation in Central Amazonia: Successional forest modeling from remote sensing data. *Remote Sensing of Environment,* 94: 508-522.

NILSSON, M. (1996). Estimation of tree heights and stand volume using an airborne lidar system. *Remote Sensing of Environment,* 56: 1-7.

NIMA (2004). Department of Defense World Geodetic System 1984, it's definition and relationships with local geodetic systems. *National Imagery and Mapping Agency Technical Report* 8350.2, Third edition, National Imagery and Mapping Agency, St. Louis, MO, USA.

OSBORNE, P.L. (2000). *Tropical Ecosystems and Ecological Concepts,* Cambridge, Cambridge University Press.

OVERMAN, J.P.M., WITTE, H.J.L. and SALDARRIAGA, J.G. (1994). Evaluation of regression models for above-ground biomass determination in Amazon Rainforest. *Journal of Tropical Ecology,* 10(2): 207-218.

PALAMULENI, L., ANNEGARN, H., KNEEN, M. and LANDMANN, T. (2007). Mapping rural savanna woodlands in Malawi: a comparison of maximum likelihood and fuzzy classifiers. *IGARSS Conference, 23 – 27 July 2007, Barcelona, Spain.*

PAPATHANASSIOU, K.P. and CLOUDE, S.R. (2001). Single-baseline polarimetric SAR interferometry. *IEEE Transactions on Geoscience and remote sensing,* 39(11): 2352-2363.

PATENAUDE, G., HILL, R.A., MILNE, R., GAVEAU, D.L.A., BRIGGS, B.B.J. and DAWSON, T.P. (2004). Quantifying forest above ground carbon content using LiDAR remote sensing. *Remote Sensing of Environment,* 93: 368-380.

PATENAUDE, G., MILNE, R. and DAWSON, T.P. (2005). Synthesis of remote sensing approaches for forest carbon estimation: reporting to the Kyoto Protocol. *Environmental Science and Policy,* 8: 161-178.

PETER, N. (2004). The use of remote sensing to support the application of multilateral environmental agreements. *Space Policy,* 20(3): 189-195.

PFB (2000). Rio Bravo Conservation and Management Area, Management Plan *Report to the Programme for Belize* December 2000.

PFB (2006). Forest Management Plan and Operational Guidelines 2006-2010. *Report to the Programme for Belize* 2006.

PHILIP, M.S. (1994). *Measuring Trees and Forests, 2nd edition,* Wallingford, CAB International.

PHILLIPS, D.L., BROWN, S.L., SCHROEDER, P.E. and BIRDSEY, R.A. (2000). Toward error analysis of large-scale forest carbon budgets. *Global Ecology & Biogeography,* 9: 305-313.

PLUMMER, S., ARINO, O., SIMON, M. and STEFFEN, W. (2006). Establishing a Earth Observation product service for the terrestrial carbon community: The GlobCarbon Initiative. *Mitigation and Adaptation Strategies for Global Change,* 11: 97-111.

PRAKOSO, K.U. (2006). *Tropical forest mapping using polarimetric and interferometric SAR data. A case study in Indonesia.* Unpublished Doctoral thesis, WIMEK-SENSE Research group Wageningen University, Wageningen (pp 141).

PRAKS, J., KUGLER, F., PAPATHANASSIOU, K.P., HAJNSEK, I. and HALLIKAINEN, M.T. (2007). Height estimation of boreal forest: interferometric model-based inversion at L- and X-band versus HUTSCAT profiling scatterometer. *IEEE Geoscience and remote sensing letters,* 4(3): 466-470.

PRENTICE, I.C., FARQUHAR, G.D., FASHAM, M.J.R., GOULDEN, M.L., HEIMANN, M., JARAMILLO, V.J., KHESHGI, H.S., LE QUÉRÉ, C., SCHOLES, R.J. and D.W.R., W. (2001). The Carbon cycle and atmospheric carbon dioxide. IN Houghton, J.T., Y. Ding, D.J. Griggs, M. Noguer, P.J. van der Linden, X. Dai, K.M. and Johnson, C.A. (Eds.). *Climate Change 2001: The Scientific Basis. Contribution of Working Group I to the Third Assessment Report of the Intergovernmental Panel on Climate Change.* Cambridge, Cambridge University Press.

PROISY, C., COUTERON, P. and FROMARD, F. (2007). Predicting and mapping mangrove biomass from canopy grain analysis using Fourier-based textural ordination of IKONOS images. *Remote Sensing of Environment,* 109(3): 379-392.

PUHR, C.B. and DONOGHUE, D.N.M. (2000). Remote sensing of upland conifer plantations using Landsat TM data: a case study from Galloway, south-west Scotland. *International Journal of Remote Sensing,* 21(4): 633-646.

QUEGAN, S., LE TOAN, T., YU, J.J., RIBBES, F. and FLOURY, N. (2000). Multitemporal ERS SAR analysis applied to forest mapping. *IEEE Transactions on Geoscience and remote sensing,* 38(2): 741-753.

QUINN, G.P. and KEOUGH, M.J. (2002). *Experimental Design and Data Analysis for Biologists,* Cambridge, Cambridge University Press.

RANSON, K.J. and SUN, G. (1994). Mapping biomass of a northern forest using multifrequency SAR data. *IEEE Transactions on Geoscience and Remote Sensing.,* 32(2): 388-396.

RANSON, K.J., SUN, G., LANG, R.H., CHAUHAN, N.S., CACCIOLA, R.J. and KILIC, O. (1997a). Mapping of boreal forest biomass from spaceborne synthetic aperture radar. *Journal of Geophysical Research,* 102(D24): 29599-29610.

REIGBER, A. and MOREIRA, A. (2000). First demonstration of airborne SAR tomography using multibaseline L-band data. *IEEE Transactions on Geoscience and remote sensing,* 38(5): 2142-2152.

REIGBER, A., NEUMANN, M., GUILLASO, S., SAUER, S. and FERRO-FAMIL, L. (2005). Evaluating PolInSAR parameter estimation using tomographic imaging results. *European Radar Conference (EURAD), 6-7 October 2005, Paris, France.*

RIBOT, J.C. (1999). A history of fear:imagining deforestation in the West African dryland forests. *Global Ecology & Biogeography,* 8(3/4): 291-300.

RODRÍGUEZ, E., MORRIS, C.S. and BELZ, J.E. (2006). A global assessment of the SRTM performance. *Photogrammetric Engineering and Remote Sensing,* 72(3): 249-260.

ROSENQVIST, A., MILNE, A., LUCAS, R., IMHOFF, M. and DOBSON, C. (2003). A review of remote sensing technology in support of the Kyoto Protocol. *Enviornmental Science & Policy,* 6: 441-455.

ROSENQVIST, A., SHIMADA, M., CHAPMAN, B., FREEMAN, A., DE GRANDI, G., SAATCHI, S. and RAUSTE, Y. (2000). The Global Rain Forest Mapping project - a review. *International Journal of Remote Sensing,* 21(6&7): 1375-1387.

ROSENQVIST, A., SHIMADA, M., ITO, N. and WATANABE, M. (2007). ALOS PALSAR: A pathfinder mission for global-scale monitoring of the environment. *IEEE Transactions on Geoscience and remote sensing,* 45(11): 3307-3316.

ROSENQVIST, A., SHIMADA, M. and MILNE, A.K. (2007). The ALOS Kyoto & Carbon Initiative. *IGARSS Conference, 23 – 27 July 2007, Barcelona, Spain*.

ROSETTE, J.A.B., NORTH, P.R.J. and SUAREZ , J.C. (2008). Vegetation height estimates for a mixed temperate forest using satellite laser altimetry. *International Journal of Remote Sensing,* 29(5): 1475 - 1493.

ROWLAND, C.S. and BALZTER, H. (2007). Data fusion for reconstruction of a DTM, under a woodland canopy, from airborne L-band InSAR. *IEEE Transactions on Geoscience and remote sensing,* 45(5): 1154-1163.

SADER, S.A., WAIDE, R.B., LAWRENCE, W.T. and JOYCE, A.T. (1989). Tropical forest biomass and successional age class relationships to a vegetation index derived from landsat TM data. *Remote Sensing of Environment,* 28: 143-157.

SALA, O.E., CHAPIN, F.S., ARMESTO, J.J., BERLOW, E., BLOOMFIELD, J., DIRZO, R., HUBER-SANWALD, E., HUENNEKE, L.F., JACKSON, R.B., KINZIG, A., LEEMANS, R., LODGE, D.M., MOONEY, H.A., OESTERHELD, M., POFF, N.L., SYKES, M.T., WALKER, B.H., WALKER, M. and WALL, D.H. (2000). Global biodiversity scenarios for the year 2100. *Science,* 287: 1770-1774.

SALIS, S.M., ASSIS, M.A., MATTOS, P.P. and PIÃO, A.C.S. (2006). Estimating the aboveground biomass and wood volume of savanna woodlands in Brazil's Pantanal wetlands based on allometric correlations. *Forest Ecology and Management,* 228: 61-68.

SANKARAN, M., HANAN, N.P., SCHOLES, R.J., RATNAM, J., AUGUSTINE, D.J., CADE, B.S., GIGNOUX, J., HIGGINS, S.I., LE ROUX, X., LUDWIG, F., ARDO, J., BANYIKWA, F., BRONN, A., BUCINI, G., CAYLOR, K.K., COUGHENOUR, M.B., DIOUF, A., EKAYA, W., FERAL, C.J., FEBRUARY, E.C., FROST, P.G.H., HIERNAUX, P., HRABAR, H., METZGER, K.L., PRINS, H.H.T., RINGROSE, S., SEA, W., TEWS, J., WORDEN, J. and ZAMBATIS, N. (2005). Determinants of woody cover in African savannas. *Nature,* 438: 846-849.

SANTOS, J.R., GONÇALVES, F.G., DUTRA, L.V., MURA, J.C. and PARADELLA, W.R. (2007). Analysis of airorne SAR data (L-band) for discrimination land use/land cover types in the Brazilian Amazon region. *IGARSS Conference, Barcelona, Spain, 23 – 27 July*.

SANTOS, J.R., LACRUZ, M.S.P., ARAUJO, L.S. and KEIL, M. (2002). Savanna and tropical rainforest biomass estimation and spatialization using JERS-1 data. *International Journal of Remote Sensing,* 23(7): 1217 -1229.

SARABANDI, K. and LIN, Y.-C. (2000). Simulation of interferometric SAR response for characterising the phase center statistics of forest canopies. *IEEE Transactions on Geoscience and remote sensing,* 38(1): 115-125.

SARMIENTO, G. (1984). *The Ecology of Neotropical Savannas*, Cambridge, Harvard University Press.

SAUGIER, B., ROY, J. and MOONEY, H.A. (2001). Estimations of global terrestrial productivity: Converging toward a single number? IN Roy, J., Saugier, B. and Mooney, H.A. (Eds.). *Terrestrial Global Productivity.* London, Academic Press.

SCHRECKENBERG, K. (1999). Products of a managed landscape: non-timber forest products in the parklands of the Bassila region, Benin. *Global Ecology & Biogeography,* 8(3/4): 279-289.

SCHULZE, E.D., VALENTINI, R. and SANZ, M.J. (2002). The long way from Kyoto to Marrakesh: Implications of the Kyoto Protocol negotiations for global ecology. *Global Change Biology,* 8: 505-518.

SEILER, W. and CRUTZEN, P.J. (1980). Estimates of gross and net fluxes of carbon between the biosphere and the atmosphere from biomass burning. *Climatic Change,* 2: 207-247.

SERVIR. (2007). *Mesostor*. servir.nsstc.nasa.gov/data/mesostor.html (Accessed 30 May, 2007).

SHE, Z., GRAY, D.A., BOGNER, R.E., HOMER, J. and LONGSTAFF, I.D. (2002). Three-dimensional space-borne synthetic aperture radar (SAR) imaging with multiple pass processing. *International Journal of Remote Sensing,* 23(20): 4357 – 4382.

SIMARD, M., ZHANG, K., RIVERA-MONROY, V.H., ROSS, M.S., RUIZ, P.L., CASTAÑEDA-MOYA, E., TWILLEY, R.R. and RORIGUEZ, E. (2006). Mapping height and biomass of mangrove forests in Everglades National Park with SRTM elevation data. *Photogrammetric Engineering and Remote Sensing,* 72(3): 299-311.

SLATTON, K.C., CRAWFORD, M.M. and EVANS, B.L. (2001). Fusing interferometric radar and laser altimeter data to estimate surface topography and vegetation heights. *IEEE Transactions on Geoscience and remote sensing,* 39(11): 2470-2482.

SMITH, G. and ULANDER, L.M.H. (2000). A model relating VHF-band backscatter to stem volume of coniferous boreal forest. *IEEE Transactions on Geoscience and remote sensing,* 38(2): 728-740.

SNOWDON, P., RAISON, J., KEITH, H., RITSON, P., GRIERSON, P., ADAMS, M., MONTAGU, K., BI, H.-Q., BURROWS, W. and EAMUS, D. (2002). Protocol for sampling tree and stand biomass. *National Carbon Accounting System Technical report* No. 31, Australian Greenhouse Office, Canberra.

SOKAL, R.R. and ROHLF, F.J. (1995). *Biometry, third edition,* New York, W.H. Freeman and Company.

SOLBRIG, O.T. (1993). Ecological constraints to savanna land use. IN Solbrig, O.T. and Young, M.D. (Eds.). *The World's Savannas: Economic Driving Forces, Ecological Constraints and Policy Options for Sustainable Land Use. Man and the Biosphere Series, Volume 12.* Paris, UNESCO.

SOLBRIG, O.T. (1996). The diversity of the savanna ecosystem IN Solbrig, O.T., Medina, E. and Silva, J.F. (Eds.). *Biodiversity and Savanna Ecosystem Processes: A Global Perspective.* Heidelberg, Springer-Verlag.

SOLBRIG, O.T., MEDINA, E. and SILVA, J.F. (1996). Determinants of tropical savannas. IN Solbrig, O.T., Medina, E. and Silva, J.F. (Eds.). *Biodiversity and Savanna Ecosystem Processes: A Global Perspective.* Heidelberg, Springer-Verlag.

SOLBRIG, O.T. and YOUNG, M.D. (1993). The World's Savannas: Economic Driving Forces, Ecological Constraints and Policy Options for Sustainable Land Use. Man and the Biosphere Series, Volume 12. IN Solbrig, O.T. and Young, M.D. (Eds.). *Economic and ecological driving forces affecting tropical savannas.* Paris, UNESCO.

SOLOMON, S., QIN, D., MANNING, M., ALLEY, R.B., BERNTSEN, T., BINDOFF, N.L., CHEN, Z., CHIDTHAISONG, A., GREGORY, J.M., HEGERL, G.C., HEIMANN, M., HEWITSON, B., HOSKINS, B.J., JOOS, F., JOUZEL, J., KATTSOV, V., LOHMANN, U., MATSUNO, T., MOLINA, M., NICHOLLS, N., OVERPECK, J., RAGA, G., RAMASWAMY, V., REN, J., RUSTICUCCI, M., SOMERVILLE, R., STOCKER, T.F., WHETTON, P., WOOD, R.A. and WRATT, D. (2007). Technical Summary. IN Solomon, S., Qin, D., Manning, M., Chen, Z., Marquis, M., Averyt, K.B., Tignor, M. and Miller, H.L. (Eds.). *Climate Change 2007: The Physical Science Basis. Contribution of Working Group I to the Fourth Assessment Report of the Intergovernmental Panel on Climate Change.* Cambridge, Cambridge University Press.

SPRUGEL, D.G. (1982). Correcting for bias in log-transformed allometric equations. *Ecology*, 64: 209-210.

SPRUGEL, D.G. (1983). Correcting for bias in log-transformed allometric equations. *Ecology*, 64(1): 209-210.

STUART, N., BARRAT, T. and PLACE, C. (2006). Classifying the Neotropical savannas of Belize using remote sensing and ground survey. *Journal of Biogepgraphy,* 33: 476-490.

STUART, N., Institute of Geography, The University of Geography (2008) [Commercial value of palmetto in Belize] (Personal communication, March 2008).

SUÁREZ, J.C., SNAPE, S., ONTIVEROS, C. and S., S. (2005). Use of airborne LiDAR and aerial photography in the estimation of individual tree heights in forestry. *Computers and Geosciences,* 31(2): 253-262.

TATENO, R., HISHI, T. and HIROSHI, T. (2004). Above- and belowground biomass and net primary production in a cool-temperate deciduous forest in relation to topographical changes in soil nitrogen. *Forest eEcology and Management,* 193: 297-306.

TICKLE, P.K., LEE, A., LUCAS, R.M., AUSTIN, J. and WITTE, C. (2006). Quantifying Australian forest floristics and structure using small footprint LiDAR and large scale aerial photography. *Forest Ecology and Management,* 223: 379-394.

TREVETT, J.W. (1986). *Imaging radar for resource surveys*, London, Chapman and Hall.

TRIMBLE. (2005). All about GPS. www.trimble.com/gps/ (Accessed 2 November, 2005).

UNAVCO. (2007). *TEQC, The Toolkit for GPS/GLONASS/SBAS Data*. facility. unavco.org/software/teqc/teqc.html (Accessed 11 May, 2007).

UNFCCC. (2007). *United Nations Framework Convention on Climate Change.* unfccc.int (Accessed 7 September, 2007).

UNFCCC. (2008). *United Nations Framework Convention on Climate Change*. (Accessed 17 January, 2008).

UOMARYLAND. (2007). Fire Information for Resource Management System. http://maps.geog.umd.edu/firms/ (Accessed 28 May, 2007).

USGS. (2007). *Global Land Cover Characterization*. edc2.usgs.gov/glcc/glcc.php (Accessed 1 November, 2007).

VERBESSELT, J., JÖNSSON, P., LHERMITTE, S., VAN AARDT, J. and COPPIN, P. (2006). Evaluating satellite and climate data-derived indices as fire risk indicators in savanna ecosystems. *IEEE Transaction on Geoscience and Remote Sensing,* 44(6): 1622-1632.

VIERGEVER, K., MOSS, D., STUART, N. and WALLINGTON, E. (2006). SAR remote sensing for natural resource management – using online GPS services as control for detailed ground truthing. *Geomatics World,* 14(4): 32-37.

VIERGEVER, K.M., WOODHOUSE, I.H. and STUART, N. (2007). Backscatter and Interferometry for Estimating Above-ground Biomass in Tropical Savanna Woodland. *IGARSS Conference Proceedings, 23 – 27 July, Barcelona, Spain, pp 2346-2349*.

VREUGDENHIL, D., MEERMAN, J., MEYRAT, A., GÓMEZ, L.D. and GRAHAM, D.J. (2002). Map of the Ecosystems of Central America: Final Report. World Bank, Washington, D.C., USA.

WALKER, W.S., KELLNDORFER, J.M., LAPOINT, E., HOPPUS, M. and WESTFALL, J. (2007a). An empirical InSAR-optical fusion approach to mapping vegetation canopy height. *Remote Sensing of Environment,* 109: 482-499.

WALKER, W.S., KELLNDORFER, J.M. and PIERCE, L. (2007b). Quality assessment of SRTM C- and X-band interferometric data: Implications for the retrieval of vegetation canopy height. *Remote Sensing of Environment,* 106: 428-448.

WALLINGTON, E.D., IZZAWATI and WOODHOUSE, I.H. (2004). Forest height estimation from X-band SAR. *IGARSS Conference, 20-24 September 2004, Anchorage, Alaska, USA.*

WALLINGTON, E.D. and SUÁREZ, J.C. (2007). Evaluation of commercial airborne LiDAR and SAR products to estimate top height and associated parameters in production forests in Britain. IN Reynolds, K.M., Thomson, A.J., Köhl, M., Shannon, M.A., Ray, D. and Rennolls, K. (Eds.). *Sustainable Forestry.* Wallingford, CABI.

WALLINGTON, E.D., WOODHOUSE, I.H., PATENAUDE, G., VIERGEVER, K.M. and MARINO, A. (submitted). A review of forest height estimation using active remote sensing. *Forestry,*

WEGMÜLLER, U. and WERNER, C. (1997). Retrieval of vegetation parameters with SAR interferometry. *IEEE Transactions on Geoscience and remote sensing,* 35(1): 18-24.

WEHR, A. and LOHR, U. (1999). Airborne laser scanning - an introduction and overview. . *ISPRS Journal of Photogrammetry and Remote Sensing,* 54(2-3): 68-82.

WEST, G.B., BROWN, J.H. and ENQUIST, B.J. (1997). A general model for the origin of allometric scaling laws in biology. *Science,* 276: 122-126.

WHYTE, W. and PAUL, R. (1997). *Basic surveying,* Oxford, Laxton.

WILLIAMS, M., SCHWARZ, P.A., LAW, B.E., IRVINE, J. and KURPIUS, M.R. (2005). An improved analysis of forest carbon dynamics using data assimilation. *Global Change Biology,* 11(1): 89-105.

WOO, J.J.E. (2002). *Flora and vegetation of a lowland savanna in northern Belize.* Unpublished M.Sc. dissertation, Department of Botany, Miami University, Oxford, Ohio

WOODGET, A.S. (2007). *An assessment of the use of airborne LiDAR for estimating growth of Sitka spruce (Picea sitchensis) plantation forestry at Kielder Forest, UK.* Unpublished M.Sc. dissertation, Geography Department, Durham University, Durham

WOODHOUSE, I.H. (2006a). *Introduction to Microwave Remote Sensing,* London, Taylor and Francis.

WOODHOUSE, I.H. (2006b). Predicting backscatter-biomass and height-biomass trends using a macroecology model. *IEEE Transactions on Geoscience and remote sensing,* 44(4): 871-877.

WOODHOUSE, I.H., The University of Edinburgh, Institute of Geography (2007) [P-band SAR from space] (Personal communication, December 2007).

WOODHOUSE, I.H., The University of Edinburgh, Institute of Geography (2007) [Use of figure showing SPCs from different wavelengths] (Personal communication, December 2007).

WOODHOUSE, I.H., CLOUDE, S.R., HUTCHINSON, C. and PAPATHANASSIOU, K.P. (2003). Evaluating PolInSAR tree height and topography retrievals in Glen Affric. *Workshop on Applications of SAR Polarimetry and Polarimetric Interferometry (POLinSAR), 14-16 January 2003, ESA-ESRIN, Frascati, Italy*.

WOODHOUSE, I.H. and HOEKMAN, D.H. (2000). Determining land-surface parameters from the ERS wind scatterometer. *IEEE Transaction on Geoscience and Remote Sensing*, 38(1): 126-140.

WOODHOUSE, I.H., IZZAWATI, WALLINGTON, E.D. and TURNER, D. (2006). Edge effects on tree height retrieval using X-band interferometry. *IEEE Geoscience and remote sensing letters*, 3(3): 344-348.

WOODHOUSE, I.H., VAN DER SANDEN, J.J. and HOEKMAN, D.H. (1999). Scatterometer Observations of Seasonal Backscatter Variation Over Tropical Rain Forest. *IEEE Transaction on Geoscience and Remote Sensing*, 37(2): 859-861.

YOKELSON, R.J., GRIFFITH, D.W.T. and WARD, D.E. (1996). Open-path Fourier-transform infrared studies of large scale laboratory biomass fires. *Journal of Geophysical Research-Atmospheres.*, 101(D15): 21067-21080.

YOUNG, M.D. (1993). National and international influences that drive savanna land use. IN Solbrig, O.T. and Young, M.D. (Eds.). *The World's Savannas: Economic Driving Forces, Ecological Constraints and Policy Options for Sustainable Land Use. Man and the Biosphere Series, Volume 12.* Paris, UNESCO

ZIANIS, D. and MENCUCCINI, M. (2004). On simplifying allometric analyses of forest biomass. *Forest Ecology and Management*, 187: 311-332.

ZISOPOULIS, I. (2007). *Comparing object-oriented land cover classification of airborne SAR and IKONOS data: A case study of a Belizean savanna.* Unpublished MSc dissertation, Institute of Geography, The University of Edinburgh, Edinburgh (pp 81).

ZWALLY, H.J., SCHUTZ, B., ABDALATI, W., ABSHIRE, J., BENTLEY, C., BRENNER, A., BUFTON, J., DEZIO, J., HANCOCK, D., HARDING, D., HERRING, T., MINSTER, B., QUINN, K., PALM, S., SPINHIRNE, J. and THOMAS, R. (2002). ICESat's laser measurements of polar ice, atmosphere, ocean, and land. *Journal of Geodynamics*, 34(3-4): 405-445.

APPENDICES

Appendix I: Moss D., Stuart, N., Viergever, K. and Wallington, E. IV. SAR remote sensing for natural resource management – is there a role for ground survey? Geomatics World, 14(3): 24-28.

Paper follows on next page
(Reproduced with permission of PV Publications Ltd)

Appendix II: Viergever, K. Moss D., Stuart, N. and Wallington, E. (2006). SAR remote sensing for natural resource management – using online GPS services as control for detailed ground truthing. Geomatics World, 14(4): 32-37.

Paper follows on next page
(Reproduced with permission of PV Publications Ltd)

Appendix III: Fieldwork equipment

GPS equipment

During the 2005 fieldwork campaign, a Trimble 4000SSi GPS receiver with a micro-centred L1/L2 antenna and ground plane was used (see Fig. 1(a)). This equipment provides high-precision positioning using dual frequency GPS, L1 (1575.42 MHz) and L2 (1227.60 MHz) channels, with carrier phase processing and P-code processing on both L1 and L2 frequencies. The reported accuracy of this instrument is ±1 cm + 2ppm horizontal and ±2 cm + 2 ppm vertical (Ashtead-Technology, 2005).
During the 2007 fieldwork campaign, the objective was to collect accurate landcover data in the form of polygons and points. For this purpose, the Trimble 4000SSi was used as base station, while two Trimble handhelds (GeoXH™ and GeoXT™) were used as rovers to collect data in the field (see Fig. 1(c)). Both these handheld GPS instruments employ integrated groundplane EVEREST™ multipath rejection technology and have internal single frequency receivers with 12 channels for tracking L1 code and carrier signals. The reported accuracy, both real-time and postprocessed for the GPSs are sub-metre for the GeoXT™ and subfoot (30 cm) for the GeoXH™ (Trimble, 2005). Trimble TerraSync™ software was used to collect field data while ESRI ArcPad software was used to locate trees measured and mapped during the 2005 fieldwork campaign for re-measuring in 2007.

Reflectorless EDM total station

The total station instrument used during the 2005 fieldwork campaign is a Trimble 5600 DR200+ (Model 5605, see Fig. 1(b)) with a reflectorless electronic distance measurement (EDM). The EDM system transmits a number of very short optical pulses which are reflected off a target and received back at the instrument. The instrument then calculates the distance based on the average total travel time of the pulses. The DR200+ model increases range and accuracy by measuring the shape of the pulses before calculating the transmit time, thereby minimising the influence of noise. The range, using a single prism, is 5500 m with an accuracy of ±(3 mm + 3 ppm) (Trimble, 2005).

Vertex hypsometer

A Vertex III hypsometer and Transponder T3 were used for measuring tree heights. The device can be used to measure heights, distance, angle, inclination and air temperature. The transponder is held to the tree trunk at breast height (1.3m) so that the Vertex can determine the exact distance from the tree by means of ultrasonic signal pulses. Upon pointing the Vertex hand unit to the top of the tree, the height of the tree is trigonometrically calculated using an angle reading device and a simple computer chip (Haglöf, 2005). As the accuracy of the instrument is affected by humidity, air pressure, surrounding noise and, above all, ambient temperature, the vertex was calibrated every day before use. The reported maximum temperature is 45 °C, while the reported error on distance measurement when calibrated regularly is 1% for distances up to approximately 30 m, depending on ambient conditions

(Haglöf, 2005). Two studies (Barron, 2001, Woodget, 2007) compare the accuracy and precision of absolute tree height measurements of three different instruments: both test the Haglöf Vertex III hypsometer and a clinometer. As a third instrument Barron (2001) tests an altimeter while Woodget (2007) tests a reflectorless hypsometer. Both studies show that the Vertex III hypsometer consistently measures heights more precisely and accurately compared to the other instruments over a range of tree heights. Tree height readings do not differ significantly from the actual tree height and showed a maximum mean deviation from true height of ±0.6 m and ±1.5 m respectively. The Vertex III hypsometer is also shown to be easier to use by non-expert users.

(a) (b) (c)

Figure 1: Equipment used for fieldwork: (a)Trimble 4000SSi GPS antenna, (b) Trimble 5600 DR200+ total station, and (c) Trimble GeoXH handheld GPS used together with a fieldwork map

Measuring tape

A specially calibrated tape measure, or diameter tape, was used to directly measure the diameter at breast height (dbh) of tree trunks, instead of calculating diameter from circumference measurements made by conventional tape measure. To directly read off measured diameter, the tape is graduated at intervals of π units (cm #156). This provides a simple method, both saving post-processing time and ruling out the possibility of errors in converting stem circumference to diameter. This method is accurate only for trees with a circular trunk (Husch, *et al.*, 2003) and therefore suitable for the study area due to the nature of the trees. Crown diameter was recorded by means of a conventional 25 m tape measure.

Appendix IV: Correction factor for logarithmic transformations

Logarithmic transformation introduces a systematic bias into regression calculations. Therefore, Sprugel (1982) suggests a correction factor to be applied to such logarithmic functions. The equations for calculating the correction factor (CF) based on the standard error of estimate (SEE) of the regression are given by (Sprugel, 1982):

$$SEE = \sqrt{\sum (\log y_i - \log \hat{y}_i)^2 / (N-2)}$$

where $\log y_i$ are the values of the independent variable in the log-transformed linear regression model and $\log \hat{y}_i$ are the corresponding predicted values calculated from the regression model. As the correction factor is calculated to base-*e* logs, the value for SEE should be multiplied by $\log_e 10 = 2.303$ to convert to base *e*. This corrected SEE value is then used to calculate the correction factor:

$$CF = \exp(SEE^2 / 2)$$

Appendix V: Traverse calculations: horizontal misclosure

Traverse route GPS1-stn1-stn2-stn3-stn4-stn5-stn6-stn7-stn8-stn9 -stn10-GPS2

Input data:

AUSPOS coordinates for opening and closing bearings

	Easting (x)	Northing (y)
GPS1	320544.066	1943578.238
1RO1	320588.085	1943341.919
1RO2	320709.376	1943510.108
GPS2	319766.525	1944195.076
2RO1	319763.107	1944485.75
2RO2	319931.135	1944247.695

Observed angles

	Dec. degr.
1ro1-gps1-stn1	169.8336
gps1-stn1-stn2	138.5711
stn1-stn2-stn3	185.2469
stn2-stn3-stn4	182.1605
stn3-stn4-stn5	176.5013
stn4-stn5-stn6	181.5869
stn5-stn6-stn7	166.7277
stn6-stn7-stn8	202.9477
stn7-stn8-stn9	182.1697
stn8-stn9-stn10	167.7669
stn9-stn10-gps2	177.2244
stn10-gps2-2ro1	239.1408

Slope distances

	m
1ro1-gps1	240.363
gps1-stn1	178.657
stn1-stn2	76.204
stn2-stn3	77.463
stn3-stn4	75.186
stn4-stn5	38.477
stn5-stn6	74.014
stn6-stn7	139.032
stn7-stn8	71.297
stn8-stn9	85.378
stn9-stn10	71.087
stn10-gps2	143.081
gps2-2ro1	290.705

Step 1: Calculated opening and closing bearings based on coordinates above

	Degr from true N	Dec degr
GPS1-1RO1	-79.448	169.44847306
GPS1-1RO2	-22.398	112.39826232
GPS2-2RO1	-89.326	359.32629699
GPS2-2RO2	17.727	72.27307462

Step 2: Calculate the angular correction to be applied through traverse

known bearing alpha-gps1-1ro1	169.448
sum theta	2169.8775
no. of stns	12
deduct	2160

apparent bearing alpha-gps2-2ro1	179.325973
given bearing gps2-2ro1	179.326297

angular error	-0.000324	dec degrees
angular error	1.17	seconds
therefore correct through traverse with	2.69944E-05	dec degrees per station

Step 3: Calculate traverse

				Back bearing (starting from 1RO1-GPS1)					
	observed (incl) angle	corrected (incl) angle	corrected incl angle (RIGHT)	349.4484731	Slope distance to next station	Horizontal distance to next station	difference E	Difference N	
gps1	169.8336	169.833627	190.166373	339.2821001	178.657	178.654611	63.202119	167.1016525	
stn1	138.5711	138.571127	221.428873	297.8532270	76.204	76.19505085	67.36765	35.59895281	
stn2	185.2469	185.246927	174.753073	303.1001540	77.463	77.46172217	64.891021	42.30217284	
stn3	182.1605	182.160527	177.839473	305.2606810	75.186	75.1814275	61.388188	43.40204395	
stn4	176.5013	176.501327	183.498673	301.7620080	38.477	38.47150881	32.71009	20.25109941	
stn5	181.5869	181.586927	178.413073	303.3489350	74.014	73.97982155	61.798167	40.66940534	
stn6	166.7277	166.727727	193.272273	290.0766620	139.032	139.0306892	130.58237	47.72605873	
stn7	202.9477	202.947727	157.052273	313.0243890	71.297	71.29607981	52.12195	48.64600059	
stn8	182.1697	182.169727	177.830273	315.1941160	85.378	85.37288951	60.162879	60.57192598	
stn9	167.7669	167.766927	192.233073	302.9610430	71.087	71.08358155	59.642017	38.67434993	
stn10	177.2244	177.224427	182.775573	300.1854700	143.081	143.0732564	123.67286	71.93734113	
gps2	239.1408	239.140827	120.859173	359.3262970	290.705	290.7026634	3.4181007	290.6825676	
							777.53931	616.8810032	
Step 4: Calculate closing bearing and horizontal misclosure					Calculated GPS2:		319766.53	1944195.119	
					Observed GPS2:		319766.53	1944195.076	
					Difference with observed GPS2:		0.0016901	0.043003189	
					Horizontal misclosure[1]:				0.0430364

[1] Traverse horizontal misclosure $= \sqrt{(\text{Diff Eastings})^2 + (\textit{Diff Northings})^2}$

Appendix VI: Traverse calculations: vertical misclosure

Traverse route GPS1-stn1-stn2-stn3-stn4-stn5-stn6-stn7-stn8-stn9 -stn10-GPS2

Using the observed vertical angles and slope distances, together with the measured station heights the elevation of the final traverse point (GPS2) was calculated based on the elevation of the first point (GPS1). This is then compared to the AUSPOS elevation (Anderson and Mikhail, 1998). As the legs of the traverse were short, the curvature and refraction of the earth were not accounted for; a simple trigonometric equation was used to calculate the height from one station to the next. Equation 1 gives the formula for calculating the difference in height between 2 stations as shown in Fig. 2.

$$H_{AB} = D.Sin(VA) + HI_A - HI_B \qquad 1$$

Where:
H_{AB} = Height difference from station A to station B
D = slope distance (m)
VA or θ = Vertical angle
HI_A = Instrument height of station A
HI_B = Instrument height of station B

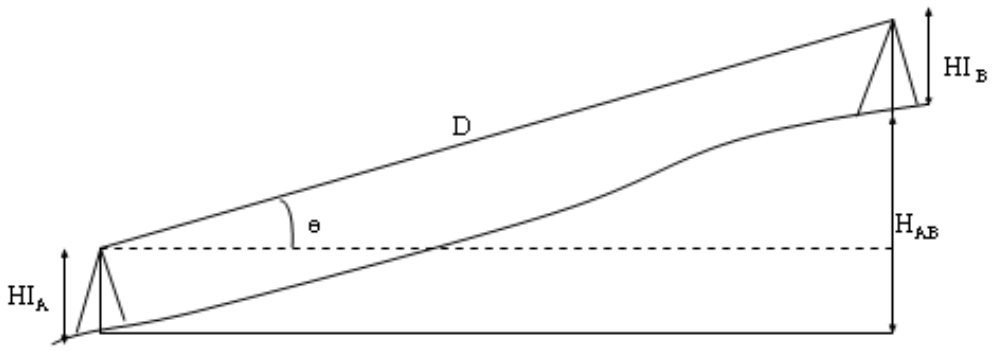

Figure 2: Calculation of the height difference between two stations in a traverse (based on Whyte and Paul (1997). Theta in the figure represents the vertical angle (VA)

Leg	Slope dist. D (m)	Vert. angle (VA)	VA (dec degr)	90-VA (dec degr)	HI A	HI B	H_{AB}	Ave H_{AB}
GPS1-STN1	178.657	90°17'47"	90.2963	-0.30	1.564	1.148	-0.508	-0.507
STN1-GPS1	178.653	89°52'17"	89.8713	0.13	1.56	1.456	0.505	
STN1-STN2	76.204	89°07'19"	89.1219	0.88	1.56	1.556	1.172	1.170
STN2-STN1	76.247	91°00'59"	91.0163	-1.02	1.392	1.207	-1.167	
STN2-STN3	77.463	90°19'45"	90.3291	-0.33	1.392	1.51	-0.563	-0.566
STN3-STN2	77.481	89°47'41"	89.7947	0.21	1.562	1.27	0.570	
STN3-STN4	75.186	90°37'55"	90.6319	-0.63	1.562	1.511	-0.778	-0.779
STN4-STN3	75.214	89°26'47"	89.4463	0.55	1.51	1.458	0.779	
STN4-STN5	38.477	90°58'05"	90.968	-0.97	1.51	1.51	-0.650	-0.651
STN5-STN4	38.511	89°24'49"	89.4136	0.59	1.49	1.233	0.651	
STN5-STN6	74.014	91°44'29"	91.7413	-1.74	1.49	1.507	-2.266	-2.267
STN6-STN5	74.043	88°28'18"	88.4716	1.53	1.567	1.274	2.268	
STN6-STN7	139.032	90°14'56"	90.2488	-0.25	1.567	1.515	-0.552	-0.552
STN7-STN6	139.064	89°53'49"	89.8969	0.10	1.579	1.277	0.552	
STN7-STN8	71.297	90°17'28"	90.2911	-0.29	1.579	1.505	-0.288	-0.288
STN8-STN7	71.321	89°56'19"	89.9386	0.06	1.526	1.314	0.288	
STN8-STN9	85.378	90°37'37"	90.6269	-0.63	1.526	1.511	-0.919	-0.921
STN9-STN8	85.403	89°31'04"	89.5177	0.48	1.53	1.327	0.922	
STN9-STN10	71.087	90°33'43"	90.5619	-0.56	1.53	1.51	-0.677	-0.679
STN10-STN9	71.11	89°34'37"	89.5769	0.42	1.536	1.38	0.681	
STN10-GPS2	143.081	90°35'46"	90.5961	-0.60	1.536	1.507	-1.460	-1.461
GPS2-STN10	143.103	89°29'33"	89.4925	0.51	1.555	1.36	1.463	

Based on calculations shown in table above, the final vertical misclosure was calculated

total traverse length (slope distance)	1029.876
Known height of GPS1	16.7871
Calculated Ave H_{AB}	-7.500
Calculated height of GPS2	9.287
Known height of GPS2	9.2801
Vertical misclosure (m)	0.007

Appendix VII: Backscatter figures for profiles 11 and 12

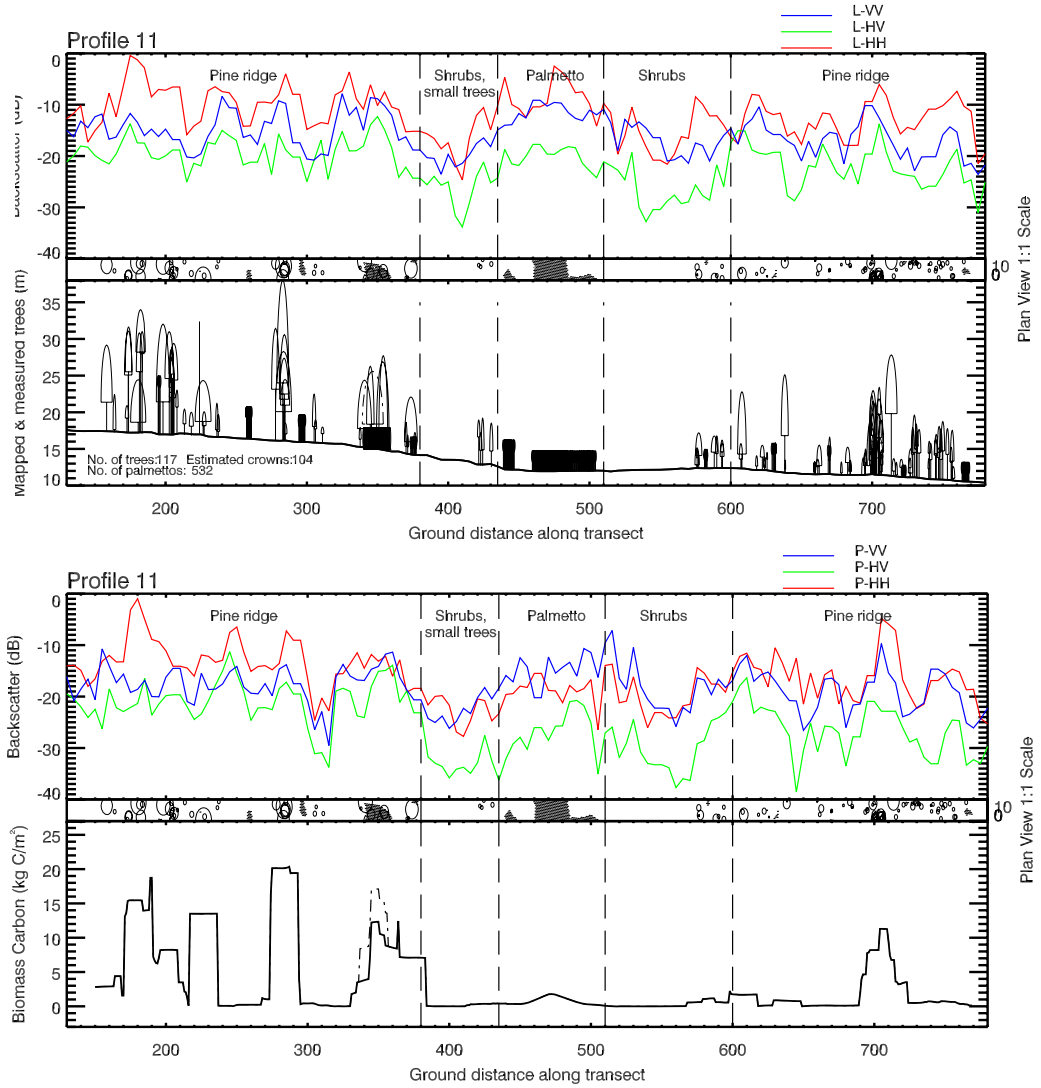

Figure 3: L- and P-band polarimetric SAR response, Profile 11

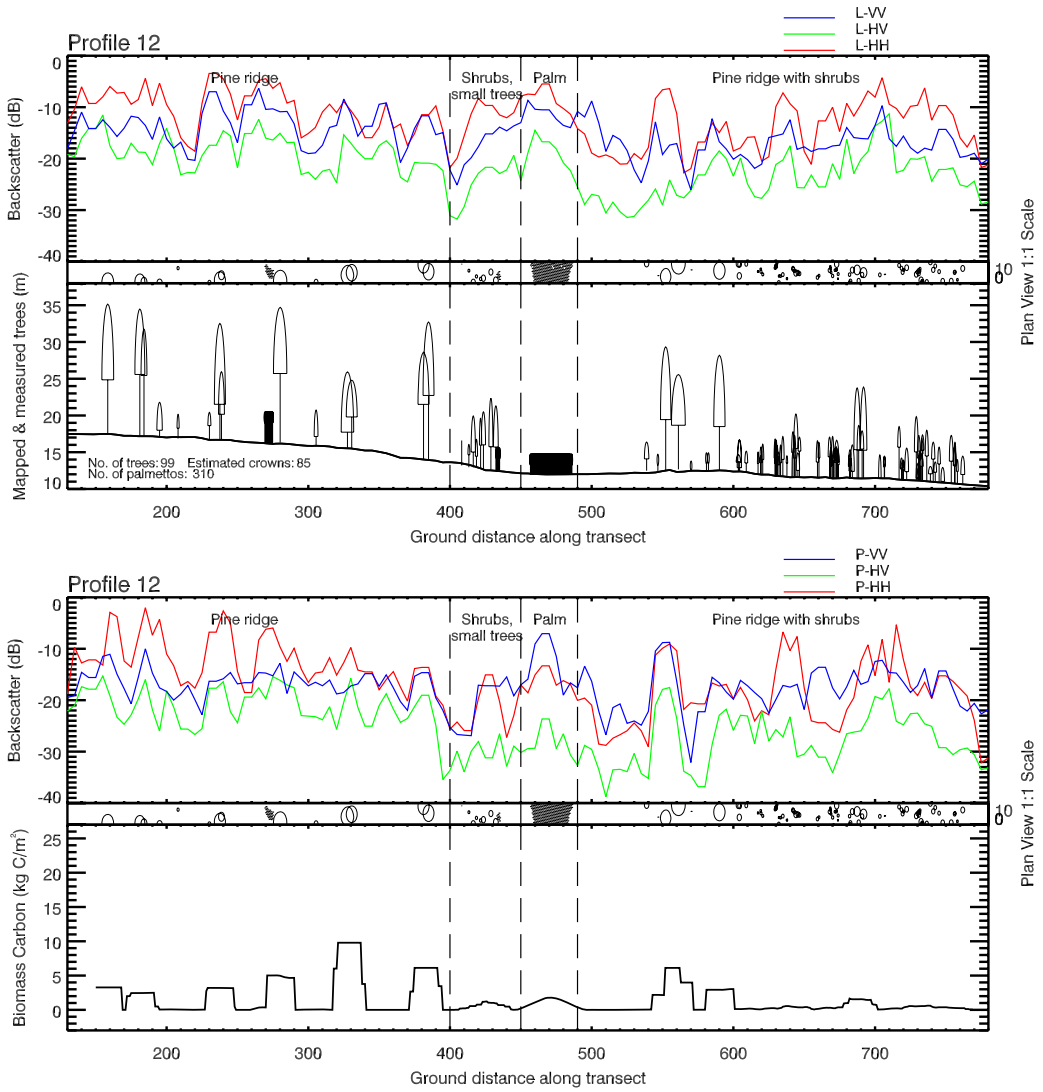

Figure 4: L- and P-band polarimetric SAR response, Profile 12.

Appendix IX: Figures showing underestimation of DSM-retrieved vegetation heights

Figures follow on next page

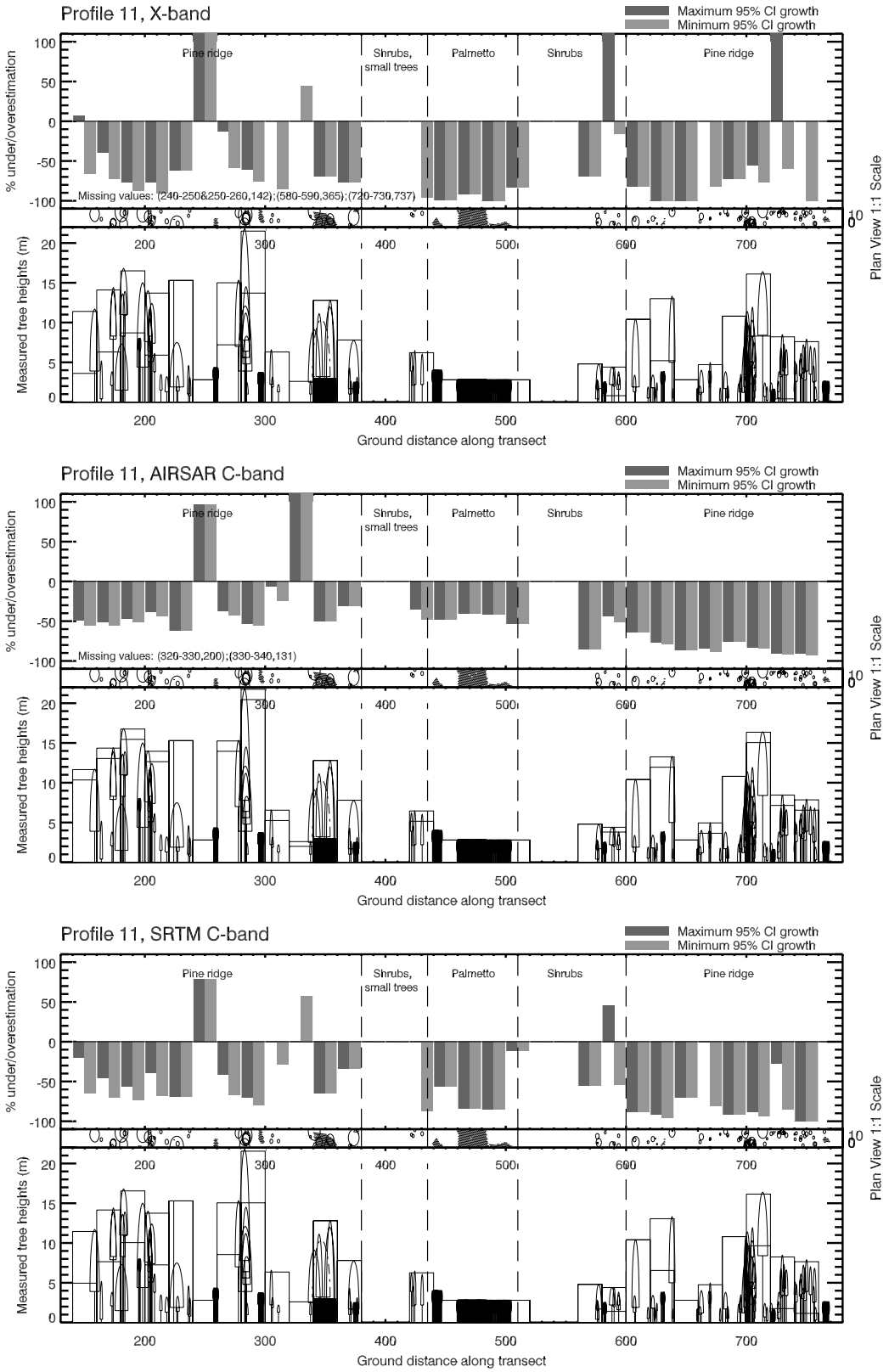

Figure 5: Graphs showing DSM-derived vegetation height underestimation (in %) for all three DSMs, profile 11. Underestimations are calculated based on tree height as they might have been in the year of DSM acquisition based on 95% CI of pine and shrub growth.

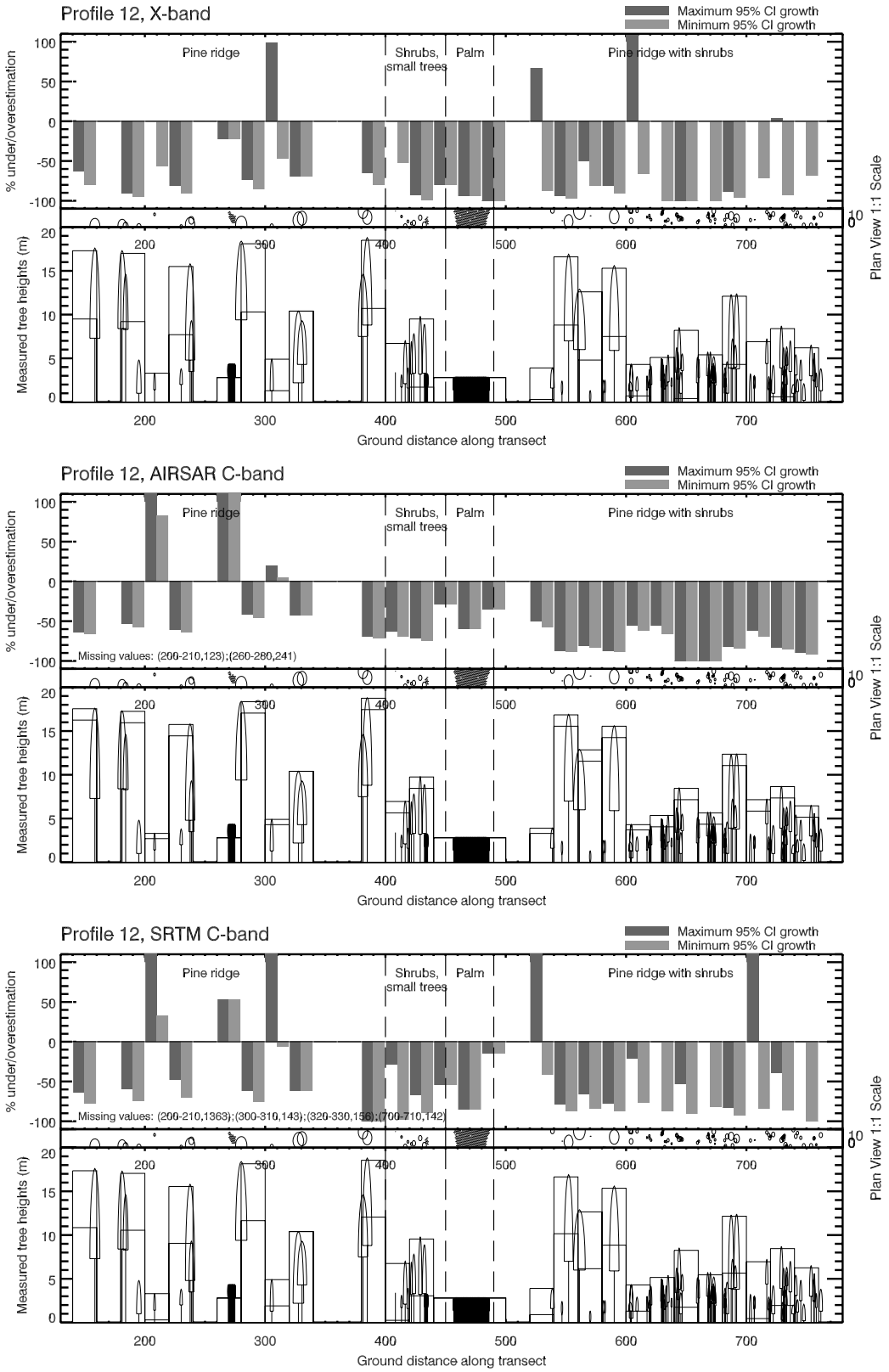

Figure 6: Graphs showing DSM-derived vegetation height underestimation (in %) for all three DSMs, profile 12. Underestimations are calculated based on tree height as they might have been in the year of DSM acquisition based on 95% CI of pine and shrub growth.

Appendix X: Analysis of C-band minus X-band DSM values

To further investigate the modelling results which suggest that C- and X-band SPCs were different for sparse and dense forest, DSM values were compared for dense forest, sparse woodland and open grassland throughout the study area. Several polygons were digitised for these three land cover classes, evenly spread to account for the effect of the AIRSAR multipath error (see Fig. 8). Pixel values were extracted (see Table 1) and statistically tested for significant differences. Since the samples were of largely varying size, the t-test was unsuitable to test for significant differences between the samples. The GT2-method for comparing means based on unequal sample sizes was therefore applied (Sokal and Rohlf, 1995). The results (Table 2) show that the mean pixel values for the dense tropical forest, sparse savanna woodland and open grassland are significantly different at the 99% confidence level.

Table 1: Sample statistics for the three land cover classes, based on the difference between the C-band DSM and the X-band DSM

	Dense tropical forest	**Sparse savanna woodland**	**Open grassland**
Mean ($\bar{Y}$)	0.34	2.80	1.28
No. of pixels (n_i)	107,712	37,508	25,015
s^2	2.26	2.05	1.31

Table 2: GT2-method test statistic values are shown above the diagonal while the differences between pairs of means appear below the diagonal, shaded cells are significant at the 0.01 level

	Dense tropical forest	**Sparse savanna woodland**	**Open grassland**
Dense tropical forest	-	0.025	0.029
Sparse savanna woodland	2.47	-	0.034
Open grassland	0.95	1.52	-

Fig. 9 shows the means and the 95% CI around the means for the extracted pixel values of the three land cover classes. Although the graph shows that both dense forest and sparse woodland have a positive mean, it is notable that the values lie to either side of the mean for open grassland, which forms a reference point. The 95% CI for dense tropical forest has a similar range than the savanna woodland, but contains mostly negative values, while the 95% CI for savanna woodland values are mostly positive. This shows that, C-band DSM values are generally higher than X-band DSM values over sparse woodland and that X-band DSM values are generally higher than C-band DSM values over dense forest for the data of this study area. This should be repeated on the corrected AIRSAR data.

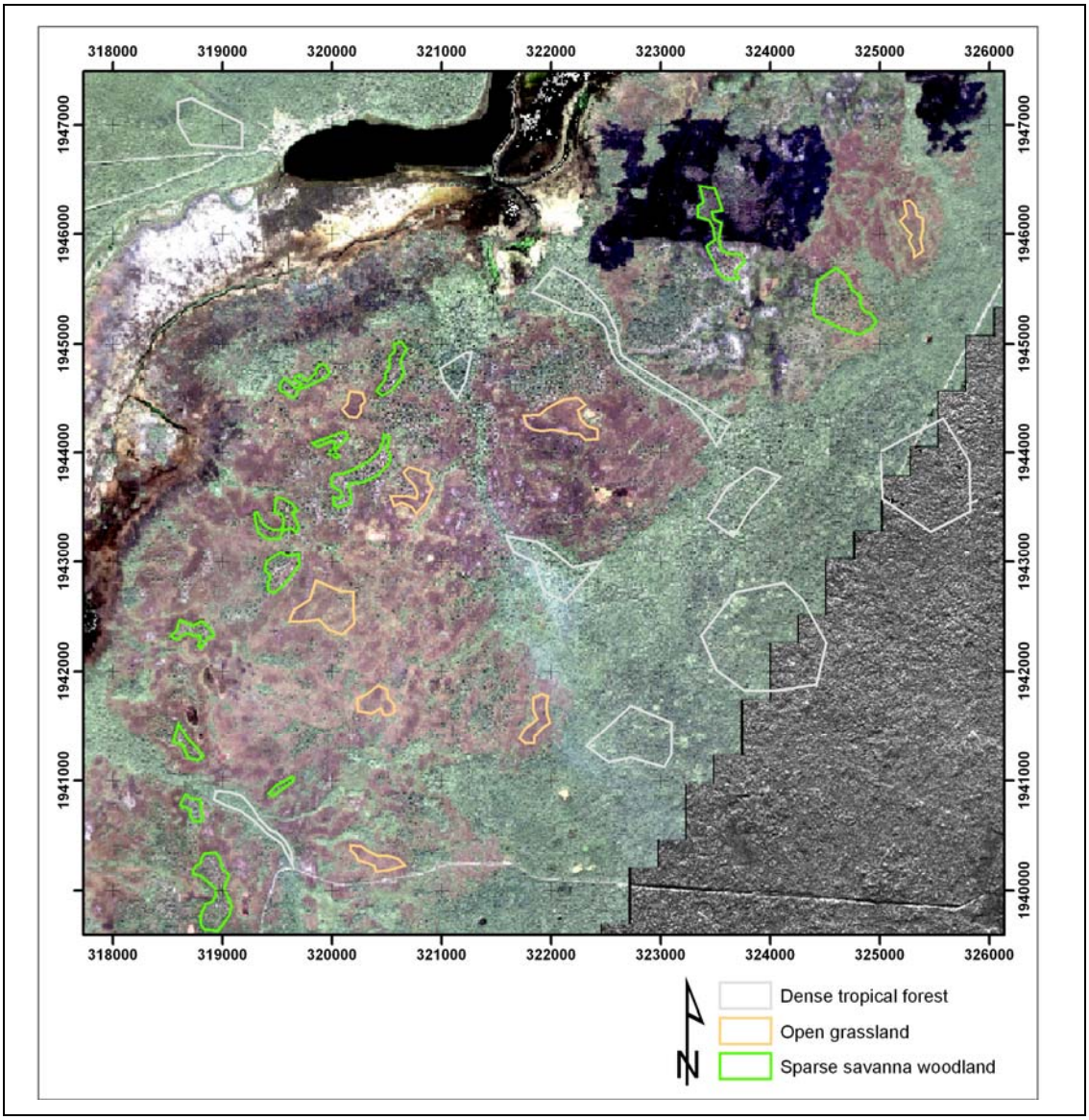

Figure 7: Map showing the digitised polygons for each of the three land cover classes: dense tropical forest, sparse savanna woodland and open grassland. The image backdrop is an Ikonos image at 1 m (RGB, 3-2-1); the bottom-right corner, not covered by the Ikonos image, is filled in with the Intermap X-HH backscatter image at 2.5 m spatial resolution.

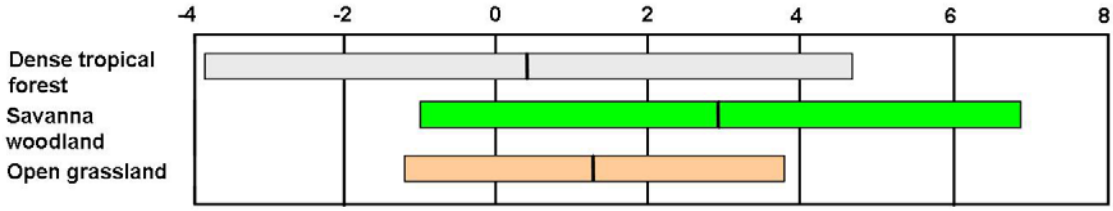

Figure 8: Graph showing the means and 95% CI around the mean for the C-band minus X-band image pixel values for the three main land cover classes.

Appendix XI: Combining InSAR with SAR backscatter

Fig. 10 (on next page) shows an example of the combined use of InSAR data and SAR backscatter for vegetation classification in the savannas of the study area: the higher elevations in the AIRSAR DSM indicate the presence of savanna woodlands and low values of the C-band DSM combined with high P-VV SAR backscatter values can be identified as palmetto thickets. It is notable that, due to the varying density and clump size of palmetto vegetation, palmetto is sometimes difficult to distinguish using the optical EO data. This is especially true for coarser resolution optical data as shown by Stuart (2006).

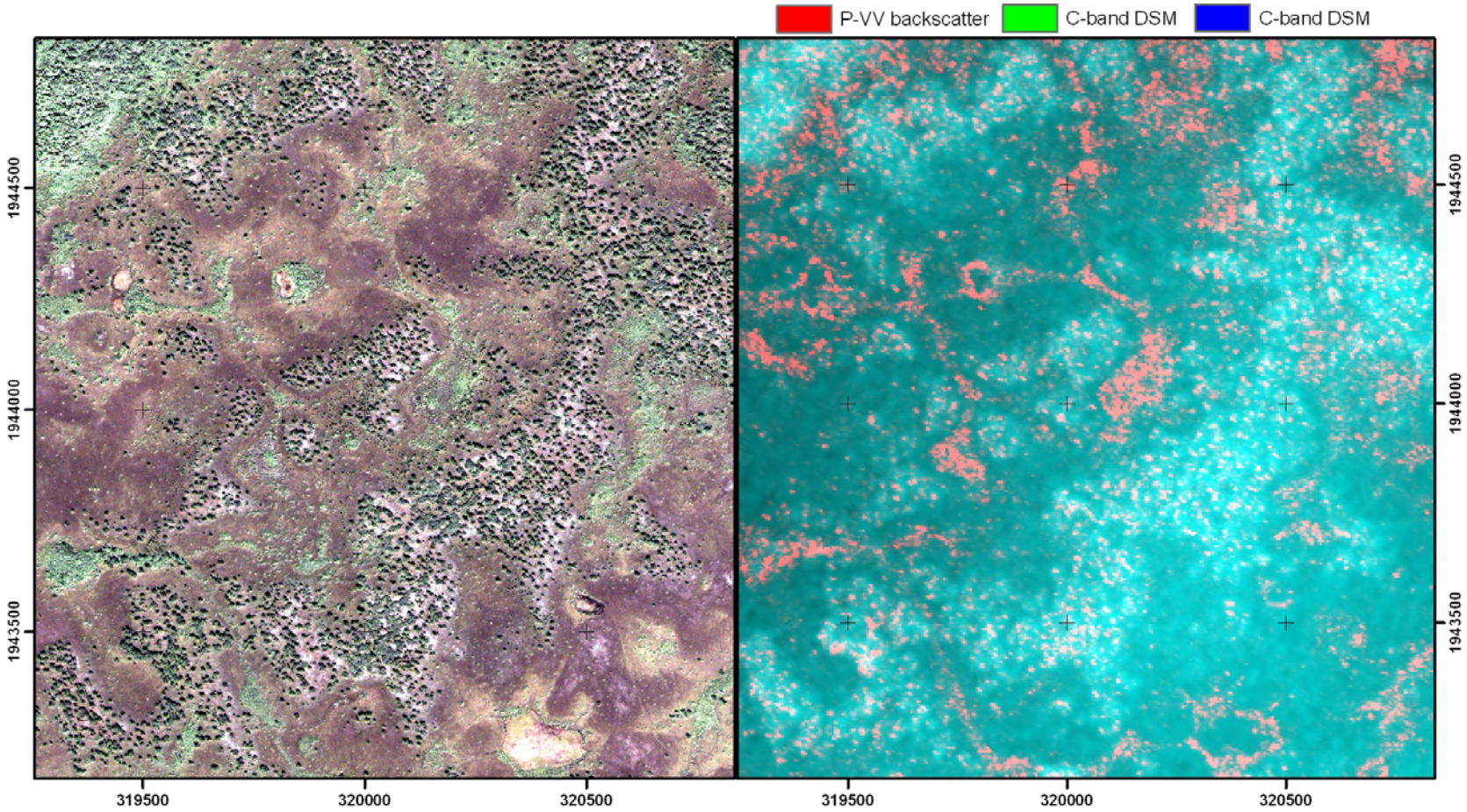

Figure 9: Left is a true colour IKONOS image of the savannas, showing clearly the distribution of savanna woodlands and palmetto vegetation in between open grassland with a patch of dense forest in the upper left corner of the image. Right is a colour composite combining InSAR (C-band DSM in green and blue: lighter shades of cyan indicate areas of relatively higher elevations, i.e. woodlands and forest) with SAR backscatter (P-VV backscatter in red).